Changes in the morphology, mass balance, and dynamics of Brown Glacier, Heard Island, with comparison to the surrounding sub-Antarctic islands

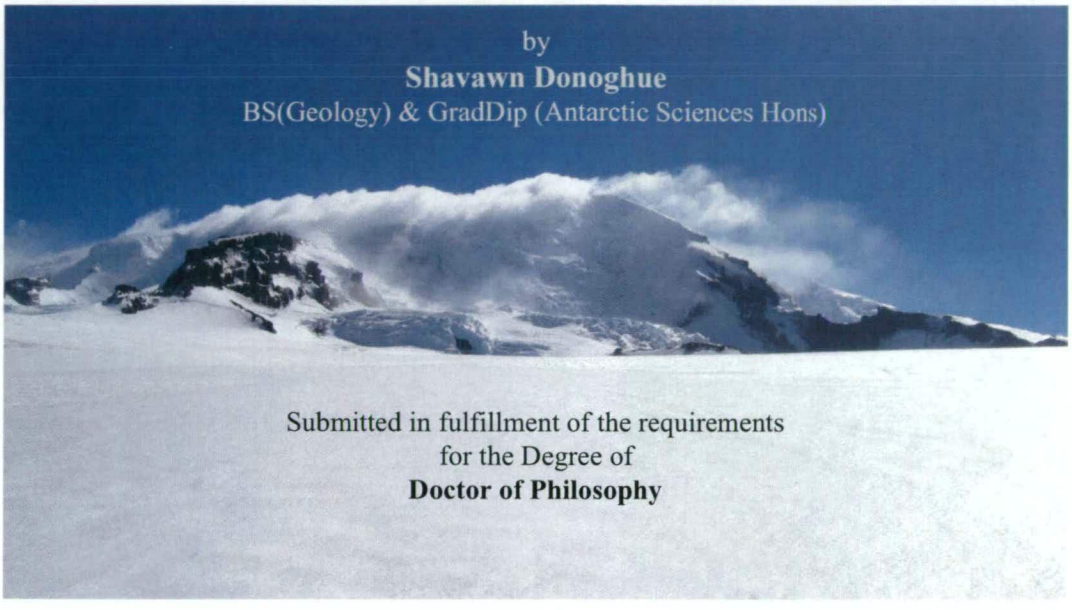

by
Shavawn Donoghue
BS(Geology) & GradDip (Antarctic Sciences Hons)

Submitted in fulfillment of the requirements
for the Degree of
Doctor of Philosophy

UTAS
University of Tasmania
School of Math & Physics

2nd October 2009

Declaration

This thesis contains no material which has been accepted for a degree or diploma by the University of Tasmania or any other institution. To the best of my knowledge and belief this thesis contains no material previously published or written by another person except where due acknowledgement is made in the text.

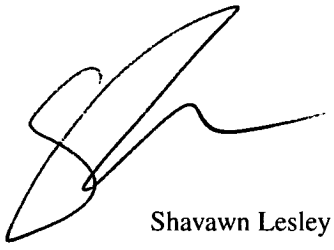

Shavawn Lesley Donoghue

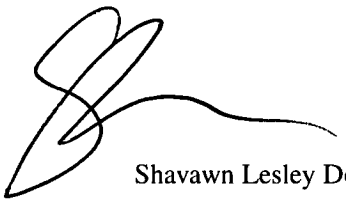

Shavawn Lesley Donoghue

Acknowledgements

With the completion of this thesis of study I would like to thank the following people:

To my supervisor, Ian Allison, for finding a project that kept me fascinated for the last five years, for endless hours staring at excel sheets and reading chapters on plane trip after plane trip.

To the Soggy Bottom Boys, Doug Thost and Martin Truffer, for a great field season, some very long hours in a water tank waiting out the weather and for all of the help along the way to finishing. Especially to Doug who always seemed to find all the 'little' things that I kept requesting.

To the Australian Antarctic Division for funding the two Heard Island expeditions and to the members of the 2000/01 and 2003/04 ANARE expeditions to Heard Island, who assisted with the Brown Glacier surveys. This thesis draws heavily on the team efforts led by Doug Thost, Martin Truffer and Andrew Ruddell, all who participated in the survey work.

To my other supervisors, Mark Curran, for trying to make me a into a chemist, Rob Massom, for always giving encouragement, and Kelvin Michael for making sure everything actually got in on time, thank you, thank you, thank you.

To Adam Trevarrow, it has been fun sharing an office with you for the last five years. Thanks for discovering LyX, being a good thesaurus, fixing my bike, and even making the odd birthday cake.

To Jo Jacka for encouraging me to continue with my interests in glaciology through my Honours degree and providing the opportunity to manage the ice mechanics laboratory for several years until I started my PhD. I would also like to thanks Jo for giving me a long list of contacts in order to obtain the necessary temperature and precipitation data for this study. In turn I appreciate the timely efforts of P. Pettre, C. de Villiers, L. Testut, S. Pendlebury, and I. Barnes-Keoghan in my requests for meteorological data for Crozet, Marion, New Amsterdam, Kerguelen and Heard islands.

I'd also like to say thank you to the several other people who have helped me acquire additional data sets. Including P. Mayewski for the glaciochemical data from Big Ben, J. Roberts for providing the sea surface temperature data for the Southern Indian Ocean, A. Vrana for providing his notes from the first mass balance measurements on Brown Glacier in 1992 and J. Shaw and J. Scott for information on the vegetation changes across Heard Island.

To Susan, John, Jemery, the Naomis, Andrew, Mark and Jen for making me laugh, eat well, paddling and bushwalking trips and generally keeping my sanity. And to all the frisbee players from Bush, Southside and Tiggers and to the soccer girls for helping me escape from being in front of this computer to run around on a field over the last few years.

And finally to my family, who despite living on the other side of the world, gave me much need support in finishing this "paper".

Abstract

Heard Island is located in one of the more isolated regions of the southern Indian Ocean at 53°06' S 73°30' E. There are 29 glacerised basins on Heard Island, which cover 70% of this 367 km^2 island. Changes in the positions of Heard Island's glaciers, and by inference, changes in the region's climate, have been recorded only intermittently since the establishment of the first Australian base in 1947. In the 1950s the majority of these glaciers were stable or slightly thinning until a marked retreat began in the early 1960s. The retreat from the 1960s has continued through the last recorded observation in 2004. As of 1997, the glaciers on Heard Island had a total area of 257 km^2 and an estimated volume of 14.2 km^3.

The limited climate records for the southern Indian Ocean have shown that there has been a +0.9° C (or +1.7° C $100a^{-1}$) change in temperature on Heard Island between 1947 and 2006, with similar increases in temperatures on the other sub-Antarctic islands (e. g., +2.7° C $100a^{-1}$ at Marion, +1.0° C $100a^{-1}$ at Kerguelen and +1.4° C $100a^{-1}$ at New Amsterdam islands). Additionally there has been a decrease in precipitation at Marion Island and Kerguelen since the late 1960s.

The changes in air temperature and precipitation in the southern Indian Ocean over the last 60 years has had a significant effect of the glacier coverage on the region's islands. There have been dramatic changes in the extent of several glaciers observed on Marion, Crozet, Bouvetøya, and Kerguelen. The glaciers and semi-permanent snow cover on the more northern Marion and Crozet islands have disappeared completely since these islands were first discovered. Kerguelen Island glaciers have decreased in extent, with one of the original five regions disappearing completely. The limited observations on Bouvetøya indicates there has been only minor changes in it's glacier fronts.

There are few observations of glacier front changes and even fewer glacier mass balance measurements on Heard Island. The changes in glacier front and climate for Brown Glacier, located on the northeastern coast of Heard Island, was determined by combining the climatic and physical characteristics that are measured on Heard Island, from 1950 to present.

Ice core and crevasse samples were collected on Brown Glacier, on the northeast coast, in 2004 to determine the net balance from stratigraphic data and glaciochemical analysis. Oxygen isotope and trace ion were measured from ice cores and crevasses to observe any seasonal signals present in the ice and thereby determining the net balance. Although meltwater affected some of the sample sites a comparison with a low melt location, at 2450 m asl, reveals that melt effects are very site specific. Two non-melt affected sites, at elevations of 756 m and 920 m, provide an estimated net balance of 1.5 m w.e.

Ablation was estimated from a combination of stake networks, downward looking sonars and a degree day model. A twenty stake central flowline network and downward looking sonars were deployed on Brown Glacier during the summers of 2000/01 and 2003/04 to measure the changes in the surface height. These measurements were compared to a degree day model for

the ablation over the same period. The results indicated that in remote areas, degree day models can provide good estimates of the ablation when limited energy balance variables are available.

The mass balance models for Brown Glacier indicate that an increase in temperature of 0.9° C between 1950 and 2001, and possibly a decrease in precipitation, has resulted in the retreat of the glacier. The steady state mass flux for 2001 indicates that if all of the current parameters remained constant then the terminus of Brown Glacier will retreat to an elevation of 350 m.

IPCC projections for 2090 were used to predict the changes that would occur on Brown Glacier if there was a further increase of temperature of 1.8 and 3.4° C. In both of these models Brown Glacier would cease to exist or possibly retreat to a small, semi-permanent snow field.

This has similar implications for the other glaciers on Heard Island. Further increases in temperature and a continuation of the decreasing precipitation trends observed on the neighbouring sub-Antarctic islands implies that the smaller glaciers on Heard Island would also begin to retreat at a more rapid rate over the next 90 years. Glacier such as the Mary Powell, Nares, and Deacock that do not originate from high on the Big Ben Plateau are likely to retreat to elevation above ~1000 m asl and the glaciers on the Laurens Peninsula will have disappeared completely.

Contents

List of Figures

List of Tables

1. Introduction to Heard Island Glaciers

1.1. Introduction

Heard Island is a sub-Antarctic island located at 53°06' S 73°30' E in the southern Indian Ocean. This isolated island is 4,100 km south west of Perth, Australia, 4,850 km south east of South Africa and 1,500 km north of the Antarctic continent (Figure 1.1). There are several other sub-Antarctic island groups nearby (Figure 1.1). The two closest to Heard Island are the McDonald Islands, 45 km to the west, and the Kerguelen Archipelago, 440 km to the north. Heard, McDonald, and Kerguelen islands are each aerial landforms of the Kerguelen Plateau, a large submarine plateau extending from 45° to 60° S.

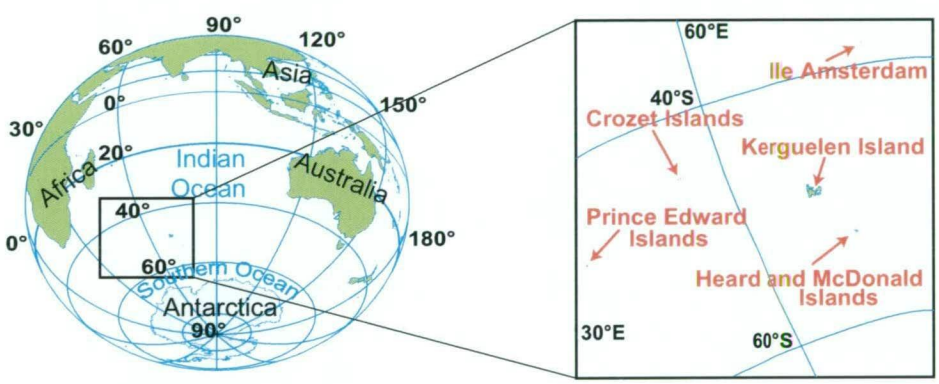

Figure 1.1.: Location of Heard, McDonald, Kerguelen, Crozet, Prince Edward and Amsterdam islands in the Southern Indian Ocean. Adapted from Australian Antarctic Division (AAD) map catalogue.

Heard Island's position south of the Polar Front is unique among the islands of the southern Indian Ocean (e. g., Kerguelen, Crozet, and Marion). This high elevation, 2745 m above sea level (asl), roughly circular island is 70% (in 1988) covered in glaciers. The physiography and orographic effects of the island have resulted in the glaciers on the lee and windward sides reacting differently to changes in the climate. Heard Island is also unique in that it supports some of the few long term but intermittent meteorological records in the southern Indian Ocean. These longer records, compared to recently deployed buoys, are used to measure changes in the temperature on the islands and can be compared to records from Kerguelen, Crozet, and Marion islands. These 60 years of intermittent meteorological records combined with the 100+ years of photographic and historical narratives provide a sporadic yet informative record of the climatic and glaciological changes on Heard Island.

The temperate glaciers of Heard Island were first systematically observed in the early 1900s. The majority of these glaciers were stable or slightly thinning until a marked retreat began in

the early 1960s. The retreat from the 1960s has continued through the last recorded observation in 2006. As of 1997, there were 29 glacerised basins (41 termini) and 3 glaciated basins (that may have been glaciated during the Last Glacial Maximum (LGM)) on Heard Island with a total area of 257 km^2 and with an estimated volume of 14.2 km^3 (Ruddell, 2006).

The isolation and uniqueness of Heard Island has lead to this mass balance study on one of the islands temperate glacier. Brown Glacier was chosen because it is a small accessible glacier on the eastern coast. It is here on the eastern, leeward side of the mountain that the glaciers have been observed to have the most recent and highest rate of retreat on the island.

Limited visits, incomplete meteorological records and few cloud free satellite images of the island means that several methods were necessary to estimate the mass balance of Brown Glacier and its changes. These include:

- Compilation of photographic, historical narratives and published reports to provide an indication of the relative changes in the mass balance (Chapter 2),
- Analysis of meteorological records from Heard Island (Chapter 4) and the surrounding sub-Antarctic islands (e. g., Kerguelen, Marion, and Crozet) (Chapter 3) to determine local and regional changes in temperature and precipitation,
- Surveys of Brown Glacier, conducted during two summer field seasons in 2000/01 and 2003/04 (Chapter 5), to measure mass balance variables,
- Collection of samples for glaciochemical analysis to estimate an annual net balance of Brown and Stephenson glaciers (Chapter 6),
- And development of a simple mass balance model (Chapter 7) to quantify the changes in Brown Glacier between 1950 and 2000 and to predict future changes,

Due to the limited data available from Heard Island, I found that it was only with a combination of all of these methods that the best estimation of Brown Glacier's mass balance could be established.

1.2. Why study temperate glaciers?

Glaciers currently cover 10% of the Earth's land surface (Lemke et al., 2007). The majority of these permanent ice covered areas are found in Antarctica and Greenland. The rest of the Earth's glaciers and ice caps, many of which are temperate glaciers, are found in alpine or high latitude regions. These make excellent climatic indicators because these warm, steep sloped, fast flowing glaciers have a quicker response time to climate change than larger, colder ice masses such as those in Antarctica and Greenland (Lemke et al., 2007).

Observed glacier fluctuations contribute important information for detecting climate change (Oerlemans et al., 1998). These permanent ice covered regions incorporate climatic change and variation information over various time scales. Glaciers are among the clearest signals of ongoing warming trends existing in nature and good visible expressions of climate change (Lemke et al., 2007).

There are various reasons to study glaciers including the following.

1. As a hydrological and economic resource. Glacier melt has been used for centuries to provide potable water, irrigation and electricity among other social benefits. Himalayan glaciers feed many of the largest river systems in the world (e. g., Yangtze and Brahmaputra). Meltwater from these mountain glaciers flood the lowlands of India, China, and Bangladesh providing irrigation. One of the most important irrigation factors is timing of the high flow periods (Chen and Zhang, 2002). Winter precipitation is stored in the glacier and released by melt in spring and summer, which are the important growing seasons. Changes in the amount of meltwater in these rivers could possibly destroy crops by over-flooding or result in drought-like condition (Chen and Zhang, 2002).

2. The interaction between glaciers and the oceans is significant due to glacial meltwater's influence on sea level. At present glaciers are retreating worldwide, as in general, glaciers currently experience more annual melt than snow accumulation (a negative mass balance) (Lemke et al., 2007). If the mass balance continues to be negative there will be increased water input into rivers and oceans causing sea levels to rise significantly in years to come. Recent estimates indicate that non-polar glaciers, which are very sensitive to changes in climatic conditions, have contributed $0.50 \pm 0.18\,\mathrm{mm\,a^{-1}}$ in sea level equivalent between 1961 and 2004, and $0.77 \pm 0.22\,\mathrm{mm\,a^{-1}}$ between 1991 and 2004 (Lemke et al., 2007). In comparison, the Greenland ice sheet has contributed an estimated -0.07 to $0.17\,\mathrm{mm\,a^{-1}}$ sea level equivalent between 1961 and 2003, and 0.14 to $0.28\,\mathrm{mm\,a^{-1}}$ between 1993 to 2003, and the larger Antarctic ice sheet has contributed an estimated -0.28 to $0.55\,\mathrm{mm\,a^{-1}}$ sea level equivalent between 1961 and 2003, and -0.14 to $0.55\,\mathrm{mm\,a^{-1}}$ between 1993 to 2003 (Lemke et al., 2007).

3. The sensitivity of glaciers provide a measurable response (*advance* or *retreat*) to a change in climate (Chinn, 1996). Individual glaciers respond differently to changes in the climate: (a) glaciers that are steep are more sensitive to climate change (Oerlemans, 1994), (b) maritime glaciers that are at low elevations and have high precipitation rates are more sensitive to climate change (Laumann and Reeh, 1993), and (c) glaciers in wet climates are more sensitive to mass balance changes than dry climate glaciers, such as Greenland and Antarctica (Kuhn, 1981; Oerlemans and Fortuin, 1992).

4. Glaciers may also provide additional information on local climatic conditions (i. e., temperature and precipitation) supplementing weather station data (see Chapter 2). Due to a glacier's response to air temperature and precipitation changes one can correlate glacier mass balance with meteorological variables measured at weather stations (see Chapter 4). In addition, meteorological data may be used to predict future changes to a glacier's mass balance based on the records of how a glacier reacted to past changes (see Chapter 7). When interpreting glacier fluctuations based on meteorological records one must keep in mind that a glacier integrates meteorological processes on a variety of time scales; the seasonal surface snow and equilibrium line altitude have a yearly cycle. The time for flow adjustment and size changes has a scale of 1-10 years (100 years for larger glaciers) and an average residency time for ice of 100-1000 years is in a temperate glacier (Kuhn, 1981).

5. Increases in anthropogenic aerosols in the atmosphere is of concern for maintaining a healthy living environment, especially with the additional concerns of overpopulation and increased demands on our natural resources (Hooke, 2005). Glaciological studies of ice cores and snow provide a baseline of pre-industrial levels of aerosols and a record of the changes in the aerosol concentration. In addition these glaciochemical studies can be utilised to provide proxy records of the annual snowfall and other paleotemperature records (see Chapter 6).

1.3. Physiography and glacerisation of Heard Island

The extensive glacier coverage of Heard Island has developed in response to a combination of factors. The island is positioned in a high latitude (53° S), maritime location resulting in a low seasonal range in temperature, frequent precipitation, increased and low lying cloud cover and strong winds (Thost and Allison, 2006). These climatic conditions are susceptible to both large scale synoptic events due to its location in a zone of strong westerly air flow and low temperatures (Taljaard and Van Loon, 1984) and small-scale regional variability due to the orthographic effects of the 2745 m Mawson Peak (Thost and Allison, 2006).

The large plateau area surrounding Mawson Peak, and the Big Ben Plateau (Figure 1.2), causes variability in the precipitation and winds and also creates orographic cloud types (Thost and Allison, 2006). The steep elevation of Big Ben results in a gradient in temperature, precipitation (and therefore snow accumulation), and wind speed. This explains why many of the larger tidewater glaciers are located on the western and southern coast of the island, which get the full force of the westerly winds and high precipitation rates.

The climatic conditions and glacier coverage of Heard Island are also a result of the island being located south of the Polar Front (PF). The PF marks the location where the cooler Antarctic surface waters sink below sub-Antarctic waters as the former moves northward (Deacon, 1933). The PF is an important climatic boundary in terms of the air-sea fluxes and the heat and salt budgets of the oceans (Moore et al., 1999) (see Section 3.2).

The widespread and diminishing glacial coverage (from approximately 80% in 1980 (Allison and Keage, 1986) to about 70% in 1988 (Ruddell, 2006)) of Heard Island and its location in a remote area of the southern Indian Ocean means that these glaciers and any changes in their shape and size are useful for monitoring climatic changes in this region.

Until very recently any understanding of the changes in the extent of the Heard Island glaciers have been derived from brief journal accounts, photographs and drawings made during the early sealing period and later as scientists began to explore this remote island from published reports, photographs, satellite images and eventually mass balance studies (see Appendix A.1 for a full history of visitations to Heard Island). The fluctuations of these glaciers have been discussed by Budd and Stephenson (1970); Allison and Keage (1986) and Budd (2000). But it was not until Ruddell (2006) that all of the glaciers were inventoried.

The glaciers of Heard Island can be separated into two main regions, Laurens Peninsula and Big Ben, and three sub-regions within Big Ben (Northern, Eastern and Southwestern coasts). Of the thirty-two glacier basins inventoried by Ruddell (2006) there were twenty-nine glaciers that were present in 1991 of which eight are located on the Laurens Peninsula and twenty-one

on Big Ben (Budd, 2000; Ruddell, 2006). A description and summary of the changes that have occurred on all of the documented glaciers on Heard Island is provided in Section 2.4.1.

Big Ben is a volcanic cone that has a diameter of 25 km, a height of 2745 m above sea level (asl) and a plateau with a shallow crater at approximately 2200 m asl, called the Big Ben Plateau (Figure 1.2). The Big Ben Plateau has an area of approximately 7 km^2 and its highest point is Mawson Peak at 2745 m asl. Glaciers extend down the slopes of Big Ben to the coast. The glaciated basins are separated by ridges and buttresses that extend from the plateau rim (e. g., North Barrier, Long Ridge, South Barrier and Holmes Ridge in the southeast and North West Cornice in the west) (Figure 1.2).

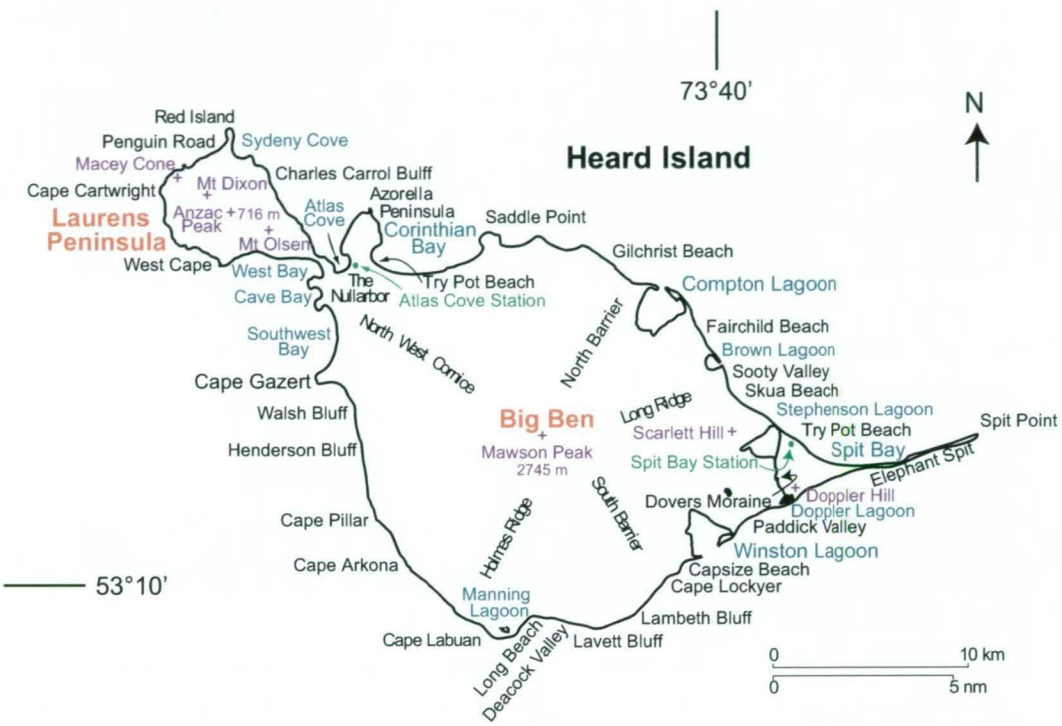

Figure 1.2.: A map of all of the common geographical features and place names on Heard Island that are referred to in this study (except the glaciers). Red lettering highlights the two dominant landforms, blue lettering indicates a coastal feature, black lettering a landform, purple lettering a volcanic cone or peak, green lettering the two main field stations. Adapted from the Australian Antarctic Division (AAD) map catalogue.

The northern coastline of Big Ben is dominated by tidewater glacier ice fronts and Corinthian Bay. There is one substantial ice-free area around Saddle Point where plant communities, bird and seal populations thrive (Scott, 1990). Continuing around to the east, the glacier fronts have retreated, beginning in the late 1950s, leaving the coast dotted with lagoons separated by beaches (e. g., Compton Lagoon, Fairchild Beach and Brown Lagoon) (Budd and Stephenson, 1970). Above Skua Beach is Scarlett Hill, a remnant volcanic cone, situated near Brown and Stephenson glaciers and often used as a landmark (Figure 1.2). One of the two frequently used science stations, Spit Bay Station, is located along the north eastern coast. Behind the station is Dovers Moraine, marking a former extent of the Stephenson Glacier. The principal feature on the eastern coast is a 10 km long narrow spit (Figure 1.2). Elephant Spit (typically referred to as 'the Spit') is continually changing and for periods resembles an assemblage of small shallow islands as opposed to a continuous spit.

Around the Spit and along the south eastern coast is Winston Lagoon. Beyond Winston Lagoon the southern coast is dominated by glacier fronts, beaches and capes (e. g., Cape Lockyer, Long Beach, and Cape Labuan) (Figure 1.2). The western coast of Big Ben is bounded by Cape Gazert in the south and Azorella Peninsula in the north. Between these two features is the Four Bay Region (Atlas Cove, West Bay, Southwest Bay, and Corinthian Bay) (Figure 1.2). It is here in the Four Bay Region that the oldest research station, Atlas Cove Station, is located. These bays are separated by The Nullabor, a flat periodically sea-water flooded plain, and a narrow ridge (less than 100 m wide), which separates Big Ben from the Laurens Peninsula.

The Laurens Peninsula is a 10 km diameter volcanic, mountainous headland that extends northwest of Big Ben (Figure 1.2). The highlands of the Laurens Peninsula have three major peaks, Mt Olsen, Mt Dixon and Anzac Peak, with a maximum height of 716 m at Anzac Peak. Similar to Big Ben, the Laurens Peninsula's southern and western coasts are dominated by capes (e. g., West Cape and Cape Cartwright). The glaciers of Laurens Peninsula have retreated to a small ice cap between Anzac Peak and Mt Olsen (Ruddell, 2006). On the northern coast is Red Island, a remnant volcanic cone. The island is frequently separated from the Laurens Peninsula by wave and storm action, which flood the beach separating these two features. As the hanging glaciers retreated from the steep bluffs (e. g., Charles Carol Bluff) along the north and eastern coastlines these regions have become the habitat of a variety of sea birds including many nesting albatrosses (Kirkwood and Mitchell, 1992).

1.4. Outline and aims of thesis

This study investigates the mass balance and meteorological records from Heard Island, with a focus on Brown Glacier.

The historical changes in Heard Island's glacier fronts was first summarised by G. Budd (1973) and later described in more detail by Ruddell (2006). Ruddell (2006) concentrated on the period between 1947 and 1988 (with some updates to 2000). This study has continued to update Ruddell's report to 2006 (Chapter 2). In order to put Heard Island into regional perspective an updated summary of the glacier fluctuations on the other sub-Antarctic islands is also presented. This is the first known summary made available since Hall (1990), and includes some initial attempts to summarise the more recent changes on the South Sandwich and Bouvetøya islands (Chapter 2).

Until the middle of the 20th Century there was a lack of meteorological information for the southern Indian Ocean. The end of WWII marked an increased interest in many countries of their Southern Ocean territories, resulting in several meteorological stations being established on sub-Antarctic islands (Chapter 3). These records have been used to provide a summary of the changes in the temperature and precipitation for other sub-Antarctic islands (Chapter 3). Jacka et al. (2004) summarised the changes in temperature for the southern hemisphere, however they did not include Heard Island, which is now included here. Precipitation records from the islands of the southern Indian Ocean are also summarised (Chapter 3).

Thost and Allison (2006) provided a summary of the local climate on Heard Island. This study updates the Thost and Allison (2006) report from 2000 to 2007, and uses earlier reports from the Australian Bureau of Meteorology (e. g., Shaw (1955)). A more detailed investigation into the orographic factors and their possible effects on the glaciers is also given (Chapter 4).

With the regional and local fluctuations in the glaciers and changes in the climate of the southern Indian Ocean discussed, an analysis of two summer surveys of Brown Glacier was completed (Chapter 5). The first survey was completed in 2000/01 by Martin Truffer, Doug Thost and Andrew Ruddell (Truffer et al., 2001), and the second in 2003/04 by Doug Thost, Martin Truffer and Shavawn Donoghue (Thost et al., 2004). These two surveys represent the most comprehensive study on any of Heard Island's glaciers (Chapter 5).

Thost and Truffer (2008) reported the initial calculation of changes in volume and area of Brown Glacier from these two surveys. Chapter 5 of this thesis uses the two surveys to establish a summer ablation rate, measured from a combination of net balance stake networks and downward looking sonar measurements of the glacier surface.

During the 2003/04 field season several ice cores and crevasses walls were sampled to estimate an annual net balance from oxygen isotope and glaciochemical analysis (Chapter 6). This was the first time a study of this magnitude had been attempted on Heard Island and also the first look at a low elevation glacier, as opposed to a short sample sequence from near the summit of Big Ben in 1983 (Spencer et al., 1985). A method is proposed for inferring the degree of smoothing on the glaciochemical seasonal signal by meltwater effects. This resulted in an estimate of the net balance of Brown Glacier, despite it being a low elevation, relatively warm site.

The summer and annual precipitation measurements and estimated summer ablation rate were then used to estimate the annual net balance of Brown Glacier for three difference periods: 1950, 2001 and 2090. A mass balance model was developed that integrated a degree day model for the annual ablation and an annual accumulation profile from annual precipitation records and estimates of net balance change with elevation (from ice core records) (Chapter 7). These two profiles were then used to estimate the net balance, which was compared to the glaciochemical net balance values, the estimated equilibrium line altitude and measured mass flux values.

The velocity and ice thickness of Brown Glacier were modelled using a flowline model developed by Ruddell (1995) (Chapter 7). The mass flux was used to calculate the ice thickness, basal shear stress, normal stress, sliding velocity and total velocity of the glacier. The modelled values were constrained by the measured surface velocity and ice thickness values from survey 1 and 2. These models were used to estimate past and future changes in the mass balance and dynamics of Brown Glacier. The model was used to estimate the 1950 mass balance and dynamics and to predict the change in the mass balance between 2000 and 2090 (Chapter 7).

Finally, a summary of all of the results from this thesis is presented in Chapter 8.

2. Recent changes in glacier extent on sub-Antarctic islands

2.1. Introduction

The temperate glaciers of the sub-Antarctic islands are located in cold, wet, maritime environments making them valuable climatic indicators for the Southern Ocean. Changes in glacier fronts have been widely used as an important indicator of climate change (Lemke et al., 2007). Glacier fluctuations are the result of regional and local climate variability. There have recently been studies (e. g.,Oerlemans, 2001) that have strengthened the link between field mass balance studies and modelling studies which have led to an improved link between glacier mass balance and the climate (Oerlemans, 2005).

Climatic changes are not reflected in glaciers immediately, instead glaciers have a delayed response to climate change that predominately depends on the geometry and the local climatic setting. Oerlemans (2005) suggests that this lag in glacier fluctuations can vary from 10 years for the steepest of glaciers to a few hundred years for larger glaciers with small slopes. However he found from a summary of the changes in 169 glaciers worldwide that the typical range in response is from 40 to 100 years. The majority of the glaciers on the sub-Antarctic islands are small, steep sloped glaciers suggesting that they are some of the quickest to respond to changes in the local climate setting.

Several studies (e. g., (Braithwaite, 2002; Cogley, 2005)) have shown that glacier length fluctuations are a result of many climatic parameters. However mass balance is primarily effected by air temperature, solar radiation and precipitation (Oerlemans, 2005). Solar radiation is the main source of melt energy whereas decreases in mass balance are mostly due to increases in temperature and decreases in precipitation (Braithwaite, 1981).

A review of the fluctuations of glaciers on the sub-Antarctic islands provides a more complete record of climatic changes that are occurring on these islands than the intermittent meteorological records and sporadic mass balance studies that are currently available.

This study catalogues the changes in the glacier fronts on Heard, Kerguelen, Crozet, Marion, Bouvetøya, South Georgia and South Sandwich islands to identify any regional trends. From the time of their discovery until the present, glaciers on these sub-Antarctic islands have been reacting to changes in the climate, from early periods of stability to more recent periods of dynamic change.

2.2. Islands of the sub-Antarctic

Sub-Antarctic islands for the purpose of this study, are defined as those islands that are located north of the Antarctic seasonal sea ice zone. They range across the Antarctic Circumpolar Current (ACC) (Section 3.2) and are often divided into regions based on the location of the Polar

Front (PF), which is the strongest front of the ACC. Included in this study are a few exceptions to this definition the South Sandwich Islands, which may be found within the seasonal sea ice zone, and Macquarie Island, which for the purpose of this study is excluded as there is no evidence of glaciers (past or present) on the island (Mercer, 1967).

The sub-Antarctic islands, by the above definition, can be divided into three oceanographic regions: the southern Indian Ocean, the southern Atlantic Ocean and the Scotia Sea. The sub-Antarctic islands of the southern Indian Ocean include Heard and McDonald, which are south of the Polar Front, Kerguelen Archipelago (situated on the Polar Front), and Crozet Group and Prince Edward Island Group, which are located to the north of the Polar Front (Figure 2.1).

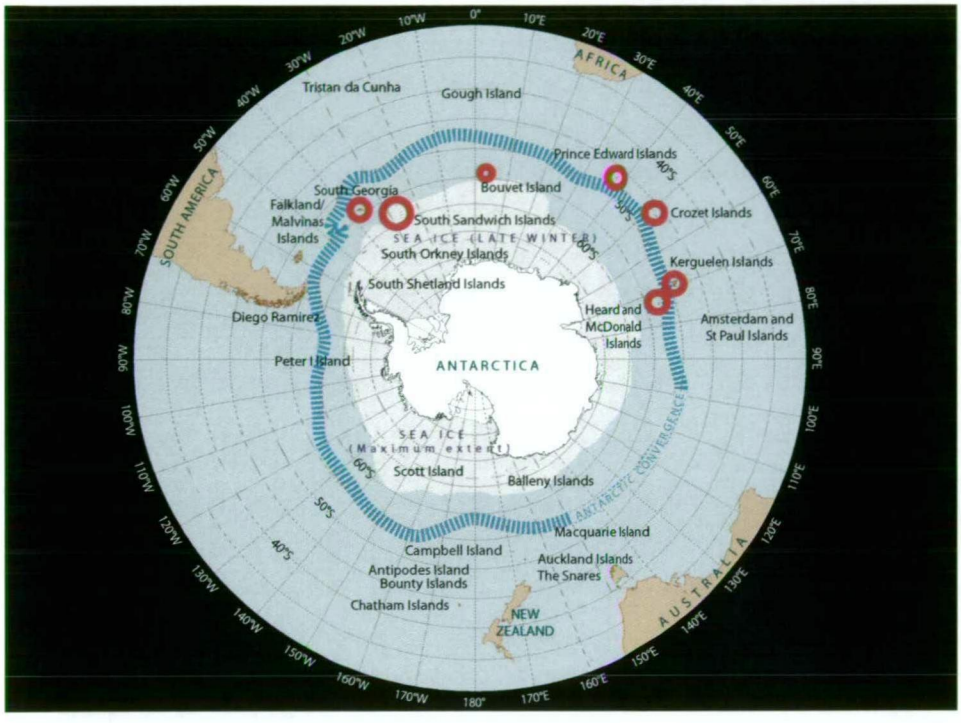

Figure 2.1.: Locations of the sub-Antarctic islands as defined in this study. This map has been modified from a figure supplied by Antarctic Tasmania (2006).

All the sub-Antarctic islands of the southern Indian Ocean are volcanic in origin, with Heard, McDonald, and Marion currently active. Heard, McDonald, and Kerguelen islands are some of the only aerial platforms of the Kerguelen Plateau, which is the largest volcanic plateau in the Southern Ocean extending 2200 km in a northwest - southeast direction and lying in waters from 1000 to 4000 m deep. Marion Island, the largest of the Prince Edward Island Group, is one peak of a large submarine shield volcano that rises 5000 m from the sea floor to the highest point on the island at 1242 m asl (Sumner et al., 2004). Crozet island is located on the Crozet Plateau, which is also volcanic in origin.

All of these islands are located in a region of strong westerly winds, high precipitation, high cloud cover and mean annual temperatures ranging from 1.7 to 5.6° C and total annual precipitation ranges of 500 to >3000 mm (Section 3.5).

Bouvetøya, the only sub-Antarctic island in the southern Atlantic Ocean, is located south of the Polar Front and is the most isolated island on earth. Its nearest landmass is the Antarctic coast line 1600 km away.

The islands of the Scotia Sea include South Georgia, South Sandwich, South Orkney, and South Shetlands although only South Georgia and South Sandwich fall within this study's defined sub-Antarctic region. The majority of the South Sandwich Islands are volcanically active. Many of these islands are also ice covered (some estimates are 80% coverage) (Kemp and Nelson, 1932). South Georgia is the only island in this study that is not volcanic in origin. This oceanic island is part of the Scotia Arc, an eastward salient in the Andean-west Antarctic structural belt. Both the South Sandwich and South Georgia islands are located to the south of the Polar Front in a region of high precipitation and winds, low temperatures and cloudy skies.

2.3. Data sources and methods

The glacial history of very few of these sub-Antarctic islands has been studied in detail, which is not surprising given their remote locations, inaccessibility and harsh weather conditions. As a result, much of the glacier records for these islands are from anecdotal evidence (Hall, 1990) and more recently from more detailed glaciological studies (e. g., Thost et al. (2004); Sumner et al. (2004)) or from analysis of satellite imagery (e. g., DigitalGlobe, Landsat, and MODIS).

Anecdotal evidence is the basis for most of the early, 1800s, glacier history of these islands. Explorers who "discovered" these islands all reported on the physical and geographical appearance of their finds. The majority of the glacial histories presented here use these reports as a starting point. Later, from the mid 1800s to early 1900s, historical narratives, drawings and photographs of the sub-Antarctic islands were more commonly used.

Between the early 1900s and the 1940s there were very few visits to the sub-Antarctic islands. It was only after WWII that many national programs began to look southward once again. Beginning in 1947 manned field stations were being established on Marion, Heard, Kerguelen, and Crozet islands (Section 3.3). These stations enabled more detailed studies of the island's natural environment, including the glaciers. It was also during this period that some of the first aerial surveys were made of the islands, Heard in 1947 and Kerguelen in 1963.

Following this initial influx of information on the glaciers it was again more difficult to find detailed studies. Some of the most detailed glacier histories have only just been published in the last few years e g., Gordon et al. (2008) on South Georgia from the early 1980s to 2005; Sumner et al. (2004) on Marion from 1990s to early 2000s; and Ruddell (2006) for Heard Island from 1947 to 1997. All of these summaries concentrate on single islands. In order to look at the regional changes that have been occurring, in the context of the wider changes in climate around the world, a summary of all of the glacier histories of these islands is necessary. The two most complete summaries for the sub-Antarctic islands have been by Mercer (1967), who published a Southern Hemisphere Glacier Atlas and Hall (1990), who looked at glaciation on Macquarie, Heard, Bouvetøya, Crozet, Kerguelen and Marion islands. In order to update these summaries additional sources were found from a combination of published studies, satellite imagery, amateur photographs, and photographic surveys.

2.4. Changes in the glaciers of the sub-Antarctic

A description is given of the changes to the glaciers on each of the sub-Antarctic islands, as defined in this study. The islands have been separated into three regions: the southern Indian Ocean, the southern Atlantic Ocean and the Scotia Sea.

2.4.1. Islands of the southern Indian Ocean

The islands of the southern Indian Ocean include Crozet, Marion, Kerguelen, McDonald and Heard. These islands, except McDonald Islands, have only been visited relatively frequently since the establishment of local meteorological stations.

Crozet The Crozet Group consists of five islands. The eastern islands include Île de la Possession (the largest island in the Crozet group) at 46°23' S 51°37' E and Île de l'Est. The western islands include the main island of Île aux Cochons and two islets (Îles des Pingouins and Îles des Apôtres). Crozet Islands are located north of the Polar Front and have a relatively low overall elevation, therefore it is not surprising that at present there are no glaciers or permanent snow or ice coverage found on the islands (Hall, 1990). This is different from when the island was first sighted, by Marion du Fresne aboard the *Mascarin,* in January 1772, who observed a snow covered island. Later, when the HMS *Challenger* visited in January 1874, the island was entirely snow free (Mercer, 1967). One of the few other observations of snow cover was in the 1980s when a small semi-permanent snow field on Île de l'Est was observed (Hollin and Schilling, 1981). Given the elevation of the islands (~900 m asl) it is unlikely that there has been permanent ice on these islands for some time as 900 m is well below the regional equilibrium line altitude (ELA), which is the elevation at which the amount of accumulation equals the amount of ablation on a glacier (Cogley, 2005) (see Section 5.5.1). If an ELA rises to a level that is higher than the local mountains, glaciers will cease to exist.

It is likely that the initial snow coverage observed in 1772 was just a summer snow fall. Information about paleoglacier features on the islands are scarce(Hall, 1990). There does not appear to be any recent (Pleistocene to present) evidence of glaciation on Île de la Possession, which being the highest is most likely to have been glaciated (Bellair, 1964).

Marion The two main islands of the Prince Edward Island group are Marion and Prince Edward islands. Prince Edward Island is located at 46°37' S 37°57' E and 19 km to the north of Marion Island. Prince Edward Island is 44 km^2 with steep escarpments on the northwest and southwest coasts. The highest peak on the island is 722 m asl located at the centre of the island. Observations on Prince Edward Island have indicated that there is no evidence of glaciation (Hall, 1983). This may be due to recent volcanic activity, strong wave action on the western side of the island and the small size and low elevation of the island (Hall, 1990).

Marion Island is located at 46°54' S 37°45' E. The island is 19 km long and 12 km wide. Marion has a total area of 290 km^2 with 72 km of cliff face dominated coastline. The highest peak on the island is State President Swart Peak at 1230 m asl. The ice and permanent snow cover on Marion Island has been slowly declining over the last 50 years (Sumner et al., 2004). In 1954, the ice and permanent snow cover was observed down to 600 m asl (Sumner et al., 2004). By 1965/1966, the average summer snow line, a term often used interchangeably as

a visible indication of the ELA, was estimated to be between 650 and 850 m asl (Verwoerd, 1971). In the late 1970s the summer snowline was at 950 m asl and the permanent snow and ice cover had decreased to an area of $< 3\,km^2$ (Hall, 1983, 1984). In 1965/66 the Ice Plateau, which was a small, thin, shallow sloping alpine glacier located to the north of State President Swart Peak, was first identified (Sumner et al., 2004). From the late 1960s, this small glacier (< 50 m thick) continued to retreat, until 1997 when it was reduced to small patches of permanent snow in wind protected south-facing slopes and in some areas of the basin floor (Sumner et al., 2004).

Kerguelen The Kerguelen Archipelago centred around 49°20' S 69°30' E consists of 300 islands most of which are of insignificant size (total area of 401 km^2) and therefore most studies concentrate on the largest island, Kerguelen Island (Figure 2.2). Kerguelen Island is approximately 100 km wide and long and contains all of the glaciers in the Kerguelen Archipelago (Mercer, 1967). The area of this island is 5,799 km^2, approximately 750 km^2 of which was ice covered in 1963 (Hollin and Schilling, 1981).

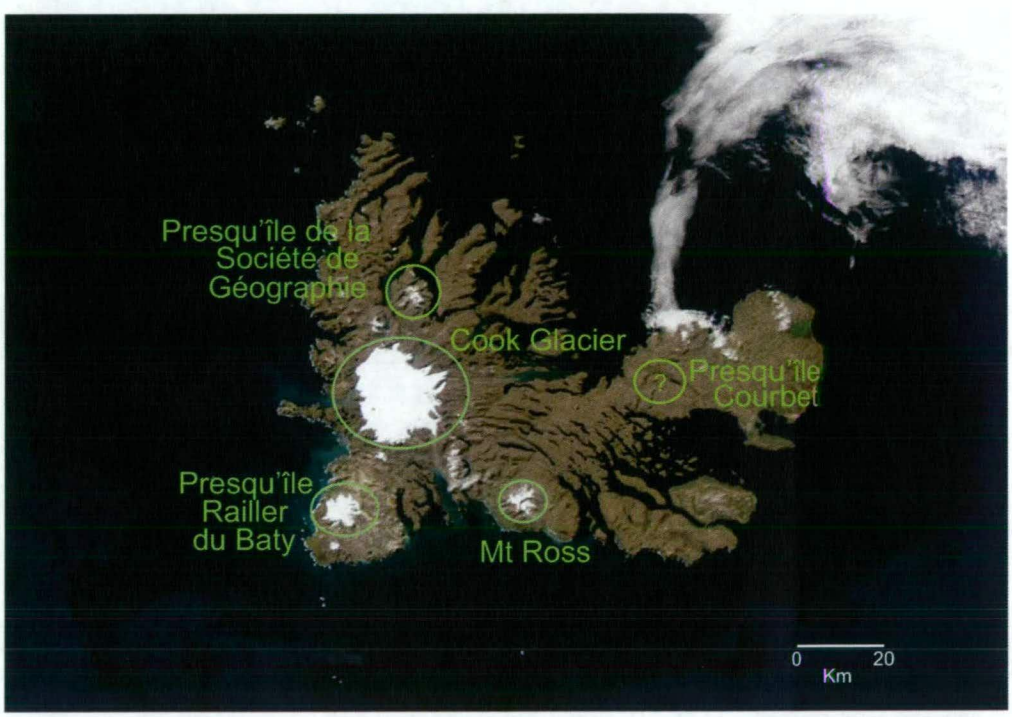

Figure 2.2.: A Moderate-resolution Imaging Spectroradiameter (MODIS) image from 8 June 2006 with the glaciated and paleoglaciated regions of the Kerguelen archipelago indicated (adapted from MODIS Rapid Response Project NASA/Goddard Space Flight Center).

The glaciers of Kerguelen Island can be separated into five regions the Presqu'île de la Société de Géographie, Cook Glacier and environs, Presqu'île Railler du Baty, Mont Ross, and Péninsule Courbet (Figure 2.2).

The Presqu'île de la Société de Géographie region is located in the north (Figure 2.2). In 1962 aerial photographs and land surveys showed that there were nine glaciers, which appeared to be have an equilibrium mass balance (Bauer, 1963). No mention of the present state of the glaciers in this region nor any recent images of this locale could be found for this study.

In the late 1960s, the Cook Glacier was an ice field of 500 km^2 (Figure 2.3A), reaching an elevation of 1100 m asl and had 40 outlet glaciers (Mercer, 1967). The 1960s firn limit varies

from 600 to 900 m asl (Bauer, 1963). Recession of the Dumont d'Urville Glacier (Figure 2.3A) was first noted by the ship *Gazelle*, which passed the island between 1874 and 1876 (Aubert de la Rue, 1932). Further retreat was noted in 1928 and 1932 on the eastern side of the ice field though no retreat was noted on the western end of the ice field (Aubert de la Rue, 1932). The 1961 to 1963 surveys indicated that the northern glaciers descend in ice falls (Bauer, 1963). The western glaciers showed little sign of retreat and were very active, especially the Curie and Pasteur glaciers (Figure 2.3A), which were the only Kerguelen glaciers to calve into the sea (Bauer, 1963). 1960s photographs of the eastern section of the ice field shows that the glaciers had shallow gradients and were very crevassed. Both the eastern and northern glaciers terminate in proglacial lakes (Mercer, 1967). A recent, November 2002, astronaut photograph (Figure 2.3A) shows that the glaciers in this region have continued to retreat in particular along the eastern margin.

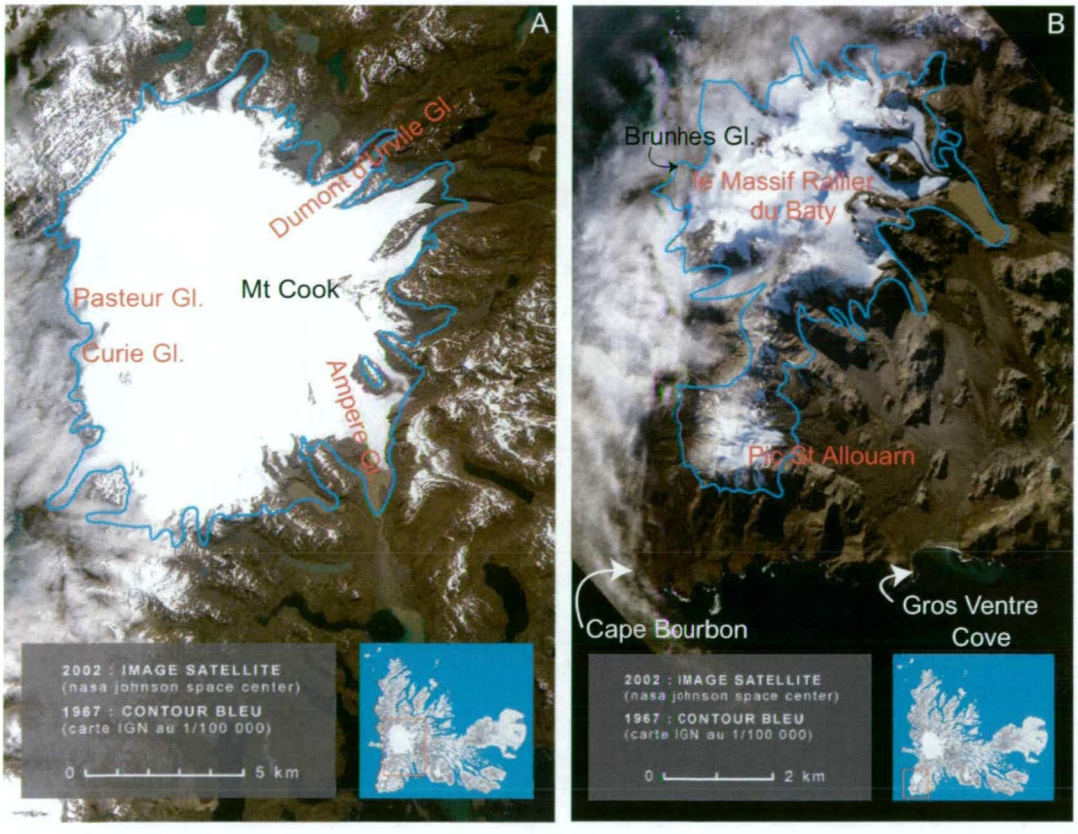

Figure 2.3.: A) 2002 astronaut photographs of the Cook ice field and **B**) the Presqu'île Railler du Baty. Each with the 1967 glacier outline from the French IGN (Institut Geographique National) map overlaid. (Astronaut images from the Earth Sciences and Image Analysis Laboratory, NASA Johnson Space Center. Mt Cook image: ISS005-E-21806 29 November 2002 06:08 UTC. Presqu'île Railler du Baty image: ISS011-E-5340 02 May 2002 09:16 UTC; satellite and overlay combined images from http://www.kerguelen-voyages.com, 12 June 2006).

Ampére Glacier is the largest glacier flowing from the Cook Ice Field and drains one-sixth of the total glaciated area (Vallon, 1977) (Figure 2.3A). The present day Ampére Glacier reached its maximum extent near the turn of the nineteenth century (Frenot et al., 1993). Since the early 1800s the glacier had two distinct periods of retreat. The first period was between 1799 to 1965, when Ampére Glacier was characterised by small fluctuations which resulted in 1 km of retreat

and seven identifiable terminal moraines (Frenot et al., 1993). The second period between 1966 to 1993 was of a relatively quick retreat resulting in a total retreat of 3 km and no re-advance or stabilisation periods (Frenot et al., 1993). This relatively quick retreat has continued with an estimated 5 km of retreat between 1967 and 2002 (http://www.kerguelen-voyages.com, 13 Aug 2006).

The glaciers of the Presqu'île Railler du Baty region consist of ice falls, which are debris covered and have extensive ice-cored moraines (Mercer, 1967) (Figure 2.3B). The glaciers can be separated into two regions le Massif Railler du Baty and the Pic Saint Allouarn. The Allouarn at 1000 m asl had three glaciers, which terminated at 500 m asl and had extensive moraines in the 1960s (Figure 2.3B). The Massif Railler du Baty is 1000 m high and was the accumulation area of 14 glaciers. The Brunhes Glacier on the west side of this region reaches the coast and was just short of being a tidewater glacier (Bauer, 1963). The glaciers in this region have retreated since 1967 (Figure 2.3B). In 2002, the Brunhes Glacier is further from the coast and most of the eastern glaciers have retracted back towards the peaks (Figure 2.3B).

Mont Ross is about 2000 m asl and is the highest point on the island. Mont Ross has many cirque, valley and hanging glaciers. On the eastern side of the mountain is the avalanche fed Buffon Glacier, which reaches the sea in debris covered ice cliffs but no calving was evident in the 1960s (Bauer, 1963). By May 2005 the Buffon Glacier appears to have retreated further inland as has many of the other smaller glaciers in this region according to an astronaut photograph from the Earth Sciences and Image Analysis Laboratory, NASA Johnson Space Center (Image: ISS011-E-5345 02 May 2005 09:16 UTC).

The small glaciers that were present on the Péninsule Courbet disappeared between 1931 and 1952 (Frenot et al., 1993). In 1902, small cirque glaciers were observed on Mt Crozier, Mt Werth and Mt. Wyville-Thompson on the Péninsule Courbet (Werth, 1921). In 1928 and 1931 on the south side of Mt Werth was the small glacier, Gazert Glacier (Aubert de la Rue, 1932). On the northwest and southwest slopes of Mt Crozier were several small glaciers (Aubert de la Rue, 1932). In 1953, Mt du Château had three small ice remnants which had disappeared by 1957 leaving only six glaciers on the Peninsula: two each on Mt Werth, Crozier and Amery (Mercer, 1967). By 1962, the glaciers on Mt Werth and Mt Crozier had disappeared (Bauer, 1963). No additional images or published reports were found on the changes of the glacier fronts in this region.

McDonald Islands The McDonald Islands are located at 53°02' S 72°36' E. There are several islands in the group - McDonald, Meyer Rock, Conning Tower Rock, other small unnamed rock islets and until 2000 Flat Island. The largest island in the group, McDonald Island, had an area of 2.45 km^2, in 2002. This island is currently volcanically active and has recently increased in size encompassing Flat Island (Manning, 2002; Stephenson et al., 2005). There are currently no glaciers on McDonald Island and the recent volcanic activity has probably erased any paleoglacier features that may have been present on the island.

Heard Island Heard Island is located in an isolated region of the southern Indian Ocean at 53°06' S 73°06' E. Glaciers covered 70% of this 367 km^2 island in 1988. Since there has been no single year when all of the Heard Island glaciers have been observed Ruddell (2006) used a compilation of satellite images and aerial photography from the period 1988 to 1991 to provide

a baseline of glacier extent. These satellite images were supplemented by aerial photographs taken during the 1986/87 summer field season.

From this complement of images the glacier boundaries and other landforms were outlined by screen digitisation and used to produce a Geographical Information System (GIS) derived map of the past glacier extents (Figure 2.4). In certain areas a more detailed look at the glacier boundaries were necessary especially due to debris-covered ice or seasonal snow cover that may have obscured the true glacier extent (Ruddell, 2006).

In conjunction with this GIS map, Ruddell (2006) provides an inventory of all thirty-two glacier basins on Heard Island, including three that no longer contain a glacier (non-glacierised basin), which are presented in Appendix A.4. Of the thirty-two glacier basins inventoried by Ruddell (2006) there were twenty-nine glaciers that were present in 1991 of which eight are located on the Laurens Peninsula and twenty-one on Big Ben (Budd, 2000; Ruddell, 2006). In this study the glaciers of Heard Island are separated into two main regions, Laurens Peninsula and Big Ben, and three sub-regions within Big Ben (Northern, Eastern and Southwestern coasts).

The Laurens Peninsula is a remnant volcanic peak located to the west of Big Ben. Atlas Cove, located between the Laurens Peninsula and Big Ben, is the safest harbour on the island, hence this cove was the landing point for many of the early expeditions. The eight glaciers on the Laurens Peninsula extend from Anzac Peak (716 m asl), Mt Dixon, and Mt Olsen. From 1902 to 1929, the majority of the glaciers in the Atlas Cove area had little change in their extent (Budd and Stephenson, 1970). By the 1940s the continuous Mt Dixon ice cap, which extended to 190 m asl (Ruddell, 2006) had retreated to 200 m asl by 1948 (Lambeth, 1950). Jacka Glacier, the largest glacier on Laurens Peninsula, advanced towards the coast until it begun to recede by the late 1940s (Ruddell, 2006) followed by widespread retreat by 1954 (Budd and Stephenson, 1970).

The majority of the other glaciers in the Laurens Peninsula region also showed little change in the early years of observations. By 1954 Jacka Glacier experienced widespread retreat which continued throughout the 1960s. The Laurens Peninsula experienced considerable thinning and retreat of its summit ice caps during the 1980s. The ice boundary had retreated on average 500 m in the north and only slightly less in the south (Allison and Keage, 1986). Jacka Glacier in 1980 had also retreated but to a lesser extent due to its greater catchment area than the surrounding ice cap (Allison and Keage, 1986). All of the Lauren Peninsula glacier fronts were above 400 m asl by 2000 (Kiernan and McConnell, 2002).

Further along the coast to the east of Atlas Cove are the Northern glaciers. These glaciers extended from either the top of Big Ben or from part way down its slopes. Many of these glaciers reached the sea and may have been tidewater glaciers in the 1800s and early 1900s. The larger glaciers in this region, including the Baudissin, Challenger, Downes and Ealey glaciers, showed some thinning and in some cases a slight recession in their extents between the early 1900s and 2000s (Ruddell, 2006). By comparison the smaller glaciers, such as the Mary Powell, Nares and AU1041, had all begun to show signs of retreat by the 1960s, which has continued to the 2000s (Ruddell, 2006). The Nares Glacier retreated 0.5 km from the beach to an elevation of 200 m asl between 1947 and 1997 (Ruddell, 2006).

The Eastern coast glaciers are a combination of larger glaciers that extend from the summit of Big Ben to the coast and smaller glaciers that extend from around 1000 m asl to the coast.

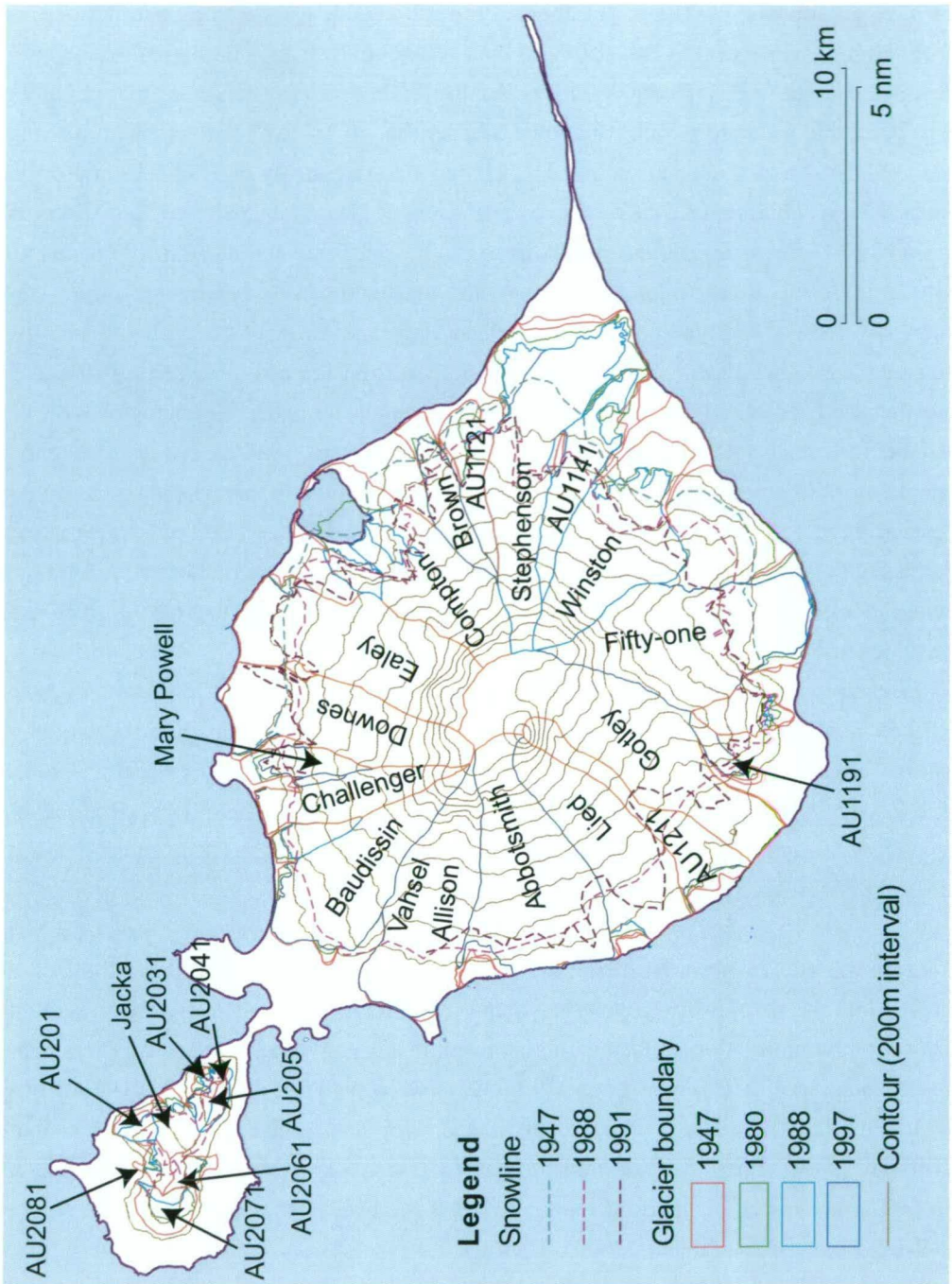

Figure 2.4.: A map of the major glacier locations on Heard Island. The Laurens Peninsula glaciers are labelled in black. The Big Ben glaciers are labelled according to coastal region; the Northern Coast is in blue, the Eastern Coast is in green and the Southwestern Coast is in pink. Note that both names for the Allison and Vahsel glacier basins are labelled. Map provided by the AAD Data Centre 2007.

The glaciers along the eastern coast of Heard Island show the most dramatic retreat compared to any other glaciers on the island. The first aerial flight over Heard Island in 1947 indicated that Winston Glacier, one of the larger glaciers, had already begun to retreat from an earlier position as indicated by the proglacial lagoon that had formed and which was open to the sea. Between 1947 and 1963 Winston retreated 1.6 km (Budd and Stephenson, 1970) and therefore appeared

to have the most rapid retreat, possibly resulting from tidewater calving and not necessarily from climate. However this was followed by a period of advance in the 1970s, which was later lost again in the 1980s (Ruddell, 2006). By the 1960s several of the other glaciers along the east coast had begun to retreat (Budd and Stephenson, 1970): AU1121 retreated to a stagnant ice field, Brown and Stephenson glaciers had begun to retreat. By the 1980s Compton Glacier had the most substantial retreat of any of the glaciers on Heard Island, it was then 1.6 km inland from its 1947 tidewater glacier front (Allison and Keage, 1986) and was 2.5 km inland by 1987 (Ruddell, 2006). By the mid 1980s Brown and Stephenson were beginning to show signs of increased retreat, both had developed proglacial lagoons. Brown Glacier, being smaller, had retreated to higher elevations and a total of 1.2 km from the coast between 1947 and 2000. Stephenson Glacier had the largest snout of any of the glacier in the eastern region with 30% of its ablation area below 400 m asl in 1980 (Allison and Keage, 1986). Between 1947 and 1987 Stephenson decreased in area by 18 % (Ruddell, 2006) although this was not a steady retreat, instead there was a dramatic acceleration in retreat from 1987 to 2000 of ~100 m a^{-1} of the northern margin (Kiernan and McConnell, 2002). This increased retreat has continued to 2006 with the opening of a water way between the two proglacial lagoons that have formed near the terminus of Stephenson Glacier.

There are very few observations or reports on the glaciers along the Southwestern coast due to their relative inaccessibility and the predominately harsher weather conditions along this coast. Fiftyone, Lied, Abbotsmith, Allison and Vahsel glaciers are fed by the Big Ben Plateau and extend to the coast in steep ice cliffs which were actively calving in 1947 (Ruddell, 2006). The Deacock and AU1191 glaciers terminated along a narrow coastal strip and at the start of a coastal plain, respectively (Ruddell, 2006).

There was little change to the larger glaciers along the Southeastern coast (Gotley, Lied, Abbotsmith and Allison) between 1947 and 2000 (Ruddell, 2006) and they all still actively calved into the sea. However there had been some thinning of their inland margins (Ruddell, 2006) implying that climate factors in may result in a negative mass balances. There appeared to be some continued retreat of the Fiftyone Glacier shown in 1997 RADARSAT imagery (Ruddell, 2006). By 2000, the Deacock Glacier only just reached the top of an inland rock cliff. This was a retreat of 1 km in distance and 350 m in elevation since 1947 (Ruddell, 2006). In 1997, the Vahsel Glacier still terminated near the beach but appeared to have stopped or slowed calving rates (Ruddell, 2006).

2.4.2. An island in the southern Atlantic Ocean - Bouvetøya

Located at 54°26' S 3°24' E, Bouvetøya (Bouvet Island) is the most isolated island on Earth given that the nearest substantial landmass is more than 1,600 km away. Bouvetøya's highest peak is Olavtoppen, at 935 m, which is on the rim of an ice filled crater of an inactive volcano, Wilhem II Plateau. The island is situated approximately 500 km south of the Polar Front.

Glaciers cover 93% of the 54 km^2 island (Ashworth et al., 2000). The eastern end of the island is entirely covered in ice that reaches the coast in a broad front (Mercer, 1967). The northern and western sides of the island are steeper and have less snow coverage. The steep cliffs along the north, west and southwest coasts inhibit landing sites, as do the sea level terminating glaciers along the south and east coast (Ashworth et al., 2000), making the island very difficult to land on by sea, hence there have been few visits.

There are few published glaciological studies on Bouvetøya. The Valdivia Expedition in 1891 made some sea-based observations of Horntvedtbreen, located on the north coast near Possadowsky Glacier, and the surrounding glaciers. This expedition was followed by the Norvegia Expedition from 1927 to 1930 during which aerial photographs were taken in 1929/30. These photographs were used to determine terminal changes in the Christensenbreen, on the south coast, between 1891 and 1929, during which there appears to be little or no change. But from 1929 to 1955 there was more rock exposed surrounding the glacier (Mercer, 1967). In 1929, during the Norvegia Expedition, the snowline was observed to be at 100 to 200 m asl (Holtedahl, 1929). Later in 1955 a South African expedition found less snow and ice coverage than in 1929 (Mercer, 1967). Photographs taken in the late 1970's by Norwegian Antarctic Research Expeditions (NARE) were compared to the 1929 aerial photographs (Orheim, 1981). NARE in 1976/77 and 1978/79 observed that these glaciers had retreated to 140 to 200 m asl (Orheim, 1981). Orheim (1981) observed that the ELA of the glaciers ranged from 200 to 350 m asl. The highest ELAs being on the glaciers located along the north and west facing slopes, similar to the ELA observations made in 1929. Orheim (1981) goes on to suggest that the glacier frontal positions are determined by the topography of the island and therefore are not very sensitive to climate change. Yet he finds a trend in the climatic conditions over the last 50 years which has been reflected in the retreat of glaciers in seven locales ($-0.12\,km^2$ total area loss) where only one glacier has advanced (by $0.12\,km^2$) over this period (Orheim, 1981), which implies a net area change of zero for the total glacier coverage over this period. Since the 1970s there have been no additional studies specifically on the glaciers of Bouvetøya despite an expedition in 1985 to map the island and later expeditions in 1996/97, 1998/99, 2000/01, 2001/02 and 2007/08.

2.4.3. Islands of the Scotia Sea

The Scotia Sea is part of the Southern Ocean between Tierra del Fuego, the Antarctic Peninsula and South Georgia. The aerial landforms along the Scotia Arc include Shag Rocks, South Georgia, the South Sandwich Islands, the South Orkney Islands and the South Shetland Islands.

The islands from this region have been visited more often than the southern Indian Ocean sub-Antarctic islands and Bouvetøya because these islands are located near South America and have been the location of extensive whaling from the late 1800s to the middle of the 1900s.

South Georgia South Georgia, located at 54°20' S 37°00' W, is the largest of the islands in the Scotia Arc. South Georgia is a long (170 km), narrow (2 to 40 km), mountainous island (Figure 2.5). Its highest peak is Mt Paget at 2934 m asl with 19 other peaks over 2000 m asl. The island is dominated by two ranges, the Allardyce and Salvesen, which extend over two-thirds of the length of the island along the southwestern shore. Northwest of the Allardyce Range the peaks are more scattered and lower (700 to 1000 m asl). Many of these high peaks support the glaciers that cover 56 to 58% of the island (in 1959 to 1989) (e.g., Smith, 1960; Hayward, 1983; Clapperton et al., 1989) making it the most glaciated island in the Scotia Arc with a total glacierised area of $1955.1\,km^2$ (in 1958) (Hayward, 1983).

The island can be divided into three areas of glaciation: northeast of the Allardyce and Salvesen Ranges, southwest of the Allardyce and Salvesen Ranges and northwest of the Allardyce Range (Hayward, 1983). The glaciers to the northeast of the Allardyce and Salvesen Ranges

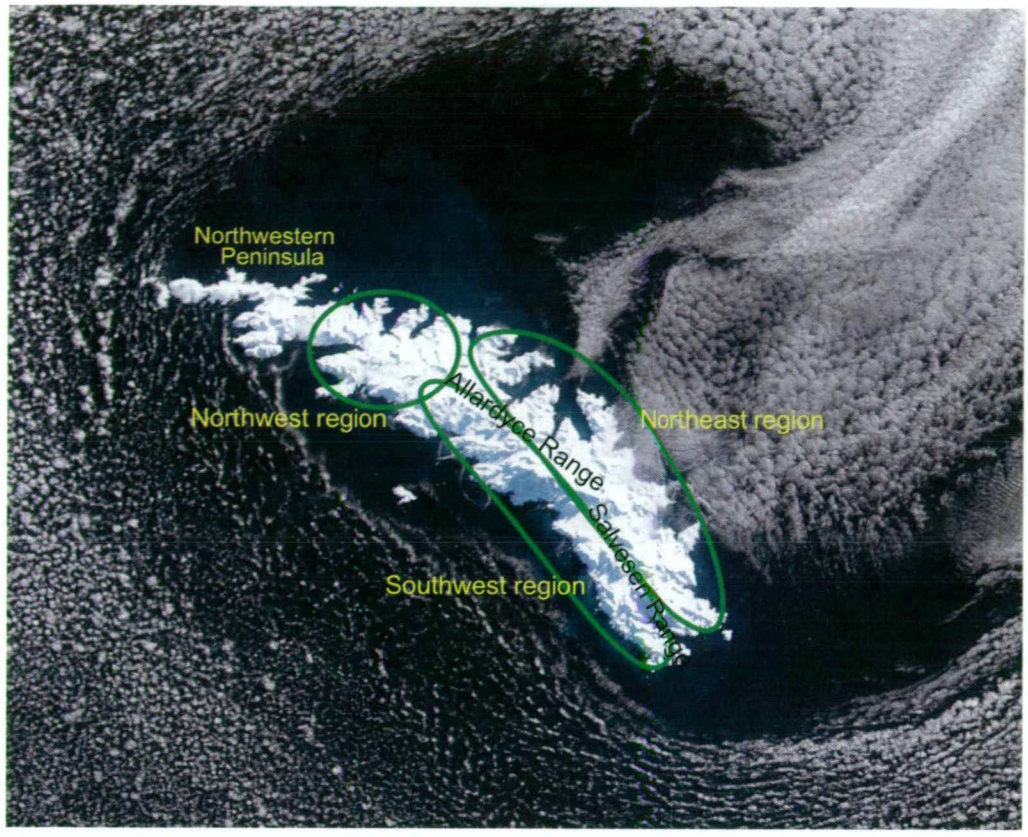

Figure 2.5.: A MODIS satellite image of South Georgia (available at http://earthobservatory.nasa.gov/Newsroom/).

are generally cirque glaciers. The glaciers to the southwest of the Allardyce and Salvesen Ranges are steeper, cirque glaciers that flow into the sea. The glaciers to the northwest of the Allardyce Range are in a region of low peaks with gentle sloping, wide glaciers that flow from large snowfields (Hayward, 1983). The area of the northwestern peninsula is the only part of South Georgia that has remained ice free since occupation due to its low topography (Hayward, 1983).

The island has been occupied continuously since 1904 – first by whalers, after 1965 by government officials, and currently by the British Antarctic Survey (BAS). Apart from some minor glaciology work by the German International Polar Year Expedition in 1882/83 there were no glaciological studies on South Georgia until 1957/58 when Smith (1960) of the Falkland Islands Dependencies Survey (now BAS) spent two years studying the Hodges Glacier and a few other glaciers. Then from 1971 to 1977 BAS maintained a glaciological program, concentrating on the mass and energy balance of Hodges Glacier (Hayward, 1983). Between 1955 and 1982 the Hodges Glacier had retreated along both its front and lateral margins (Figure 2.6A and B). The glacier continued to retreat through to 2002 (Figure 2.6C), by which time there had been significant retreat of the glacier over this 20 year period such that one could almost struggle to call it a glacier any more (A. Ruddell pers. com. 2002).

The changes in frontal extent of the South Georgia glaciers can be summarised by a slight advance around 1910 and followed by a short retreat of some glaciers (Hayward, 1983). This was soon followed by another advance, with a maximum in the late 1920s (Hayward, 1983). There was a small retreat through the 1940s and a small advance in the 1950s (Hayward, 1983).

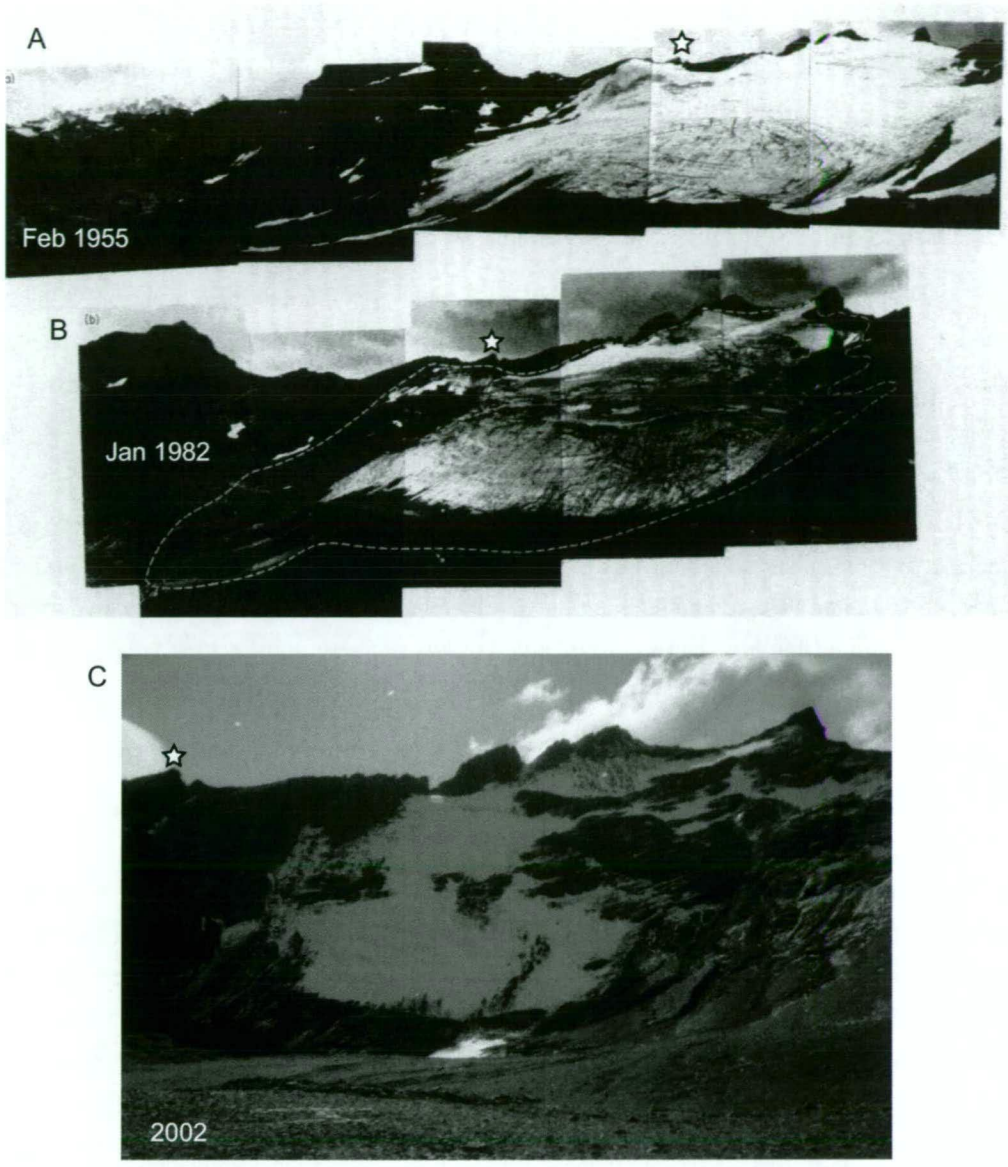

Figure 2.6.: A compilation of the glacier front changes on Hodges Glacier, South Georgia from: **A**) 1955, **B**) 1982 and **C**) 2002. Note the recession of the lower glacier tongue and thinning of the ice of the left and right headwalls between February 1955 (Photo: H. Pretty, British South Georgia Expedition) and 23 January 1982 (Photo: J. Gordon) (Gordon and Timmis, 1992). There are also several new rock outcrops exposed in 1982. Between 1982 and 2002 (Photo: S. Lurcock) there has been considerable retreat of the glacier. The white stars mark the same peak in all photographs. Note that the glacier has retreated further up valley by 2002.

Since the 1950s there has been a slow retreat for all except the larger glaciers (Hayward, 1983; Gordon and Timmis, 1992) followed by a continuing retreat through the early 1980s. Gordon et al. (2008) recently provided an update of South Georgian glaciers from the early 1980s to the mid 2000s. They observed the frontal changes on 36 of the 160 glaciers that are found on South Georgia. Of these glaciers, 28 are retreating, two are advancing and six are relatively stable (Gordon et al., 2008).

South Sandwich The South Sandwich Islands are a group of eleven islands centred around 57°45' S 26°30' W. The island group can be split into three regions: the Traversay Islands (Zavodoski, Leskov and Visokoi islands), the Candlemas Islands (Candlemas and Vindication islands), Southern Thule (Bellinghausen, Cook and Thule islands); and into three main islands: Montagu, Saunders and Bristol. The islands bend along a ~400 km arc making up the eastern edge of the Scotia Sea ranging from 58°18' S to 59°28' S and 26°14' W to 28°11' W.

The *Discovery* voyage encountered the South Sandwich Islands in February 1930 (Kemp and Nelson, 1932). Following the *Discovery* cruise very little information on the glaciers of these islands appears to be available except for their present extent. In fact many sources (e.g., Mercer, 1967; French, 1974) still refer to Kemp and Nelson (1932) for information on the glacial history of these islands.

Zavodovski Island has a glacierised area near the summit on all but the western side, as volcanic activity is concentrated on this steep western side of the island. Photographs compared between 1932 and 1962 indicated that there is little change in the islands features over this period (it is assumed that the glaciers are included in this statement not just the volcanic features) (Holdgate, 1963). It is unclear from recent photos if the glaciers have changed in size.

Visokoi Island was predominately glacier covered, in 1932, despite being volcanically active (Kemp and Nelson, 1932). No recent images of the island were found to compare with the 1932 photograph.

The southern region of Candlemas Island was almost completely covered in glaciers in 1932 (Kemp and Nelson, 1932) (Figure 2.7A). A recent satellite image of the island (2006 Google Earth-DigitalGlobe/NASA/Europa Technologies) shows that there may be some decrease in the glacier extents (Figure 2.7B). Many of the finer features in Figure 2.7B such as: (a) meltwater lakes forming at the terminus of what appears to be one of the larger glaciers, (b) a vegetation line, and (c) distinct meltwater streams above the cliff lined coast, are better identified from the original image (available from Google Earth), due to the limited image resolution reproduced here. Each of these small scaled features indicates that there has been some shrinkage of the northern glaciers on Candlemas Island.

In 1932, Vindication Island was volcanically inactive (Kemp and Nelson, 1932; Mercer, 1967; French, 1974; Holdgate, 1963) and had one thin glacier that flowed down the northeastern side of the peak (Kemp and Nelson, 1932) (Figure 2.7C). The glacier has contracted in size to occupy only the summit of the island (Figure 2.7B).

In 1932, glaciers on Sunders Island extended to the coast on the eastern and western sides of the island, where the northern side of the island was relatively snow free. No recent images of the island could be found.

Montagu Island is the largest of the South Sandwich Islands. Mt Belinda, at 1371 m asl, is heavily glaciated. In 1932, the glaciers radiated from the top of Mt Belinda to the coast terminating either in long steep ice cliffs, like the 8 km long one along the east coast, or in crevassed ice falls extending to sea level or as hanging glaciers above cliff faces (Kemp and Nelson, 1932) (Figure 2.8A and B). A satellite image from 2006 (Terre/ASTER image NASA) may show that some of the glaciers may no longer reach the sea along the eastern coast (Figure 2.8C).

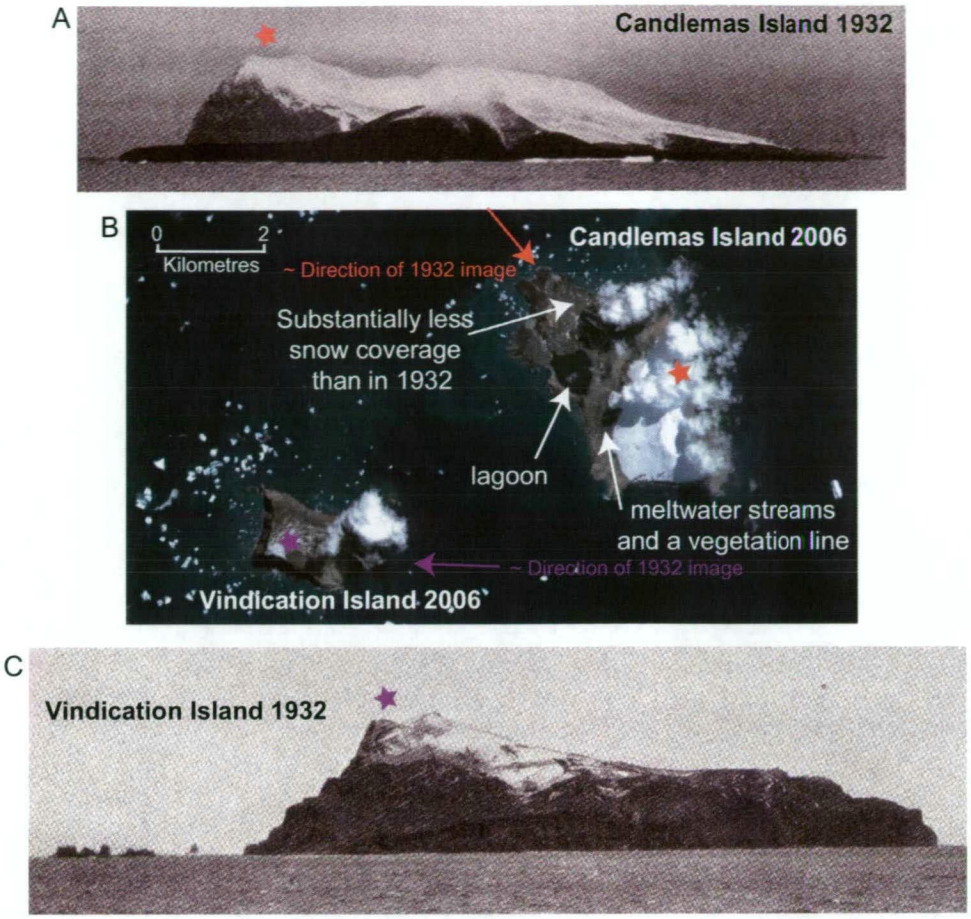

Figure 2.7.: Images from Candlemas and Vindication islands. **A**) Kemp and Nelson (1932) note that the Candlemas 1932 photograph shows the island seen from the NW. At the back of the image are the high glaciated summits of the south-eastern part of the island. In the foreground, the north-eastern basaltic plateau with its active volcanic cone. **B**) The middle image is of Candlemas and Vindication islands from a recent satellite image (2006 Google Earth-DigitalGlobe/NASA/Europa Technologies). **C**) Kemp and Nelson (1932) note that Vindication is seen from the east in this 1932 photograph . The smaller features to the left include Caster and Pollut rocks. The stars and arrows in the images are to help orientate of the peaks on the two islands.

In 1932, Bristol Island was almost entirely covered in glaciers. The majority of these glaciers extended to the coast, and the rest terminated as hanging glaciers (Kemp and Nelson, 1932). No recent images of the island could be found.

Cook is the largest and highest island in the Southern Thule Group, reaching an elevation of 1,077 m (French, 1974). In 1932, the island was entirely covered in glaciers. An ASTER satellite image from 2003 of the island is inconclusive as to whether there has been any change in the glacier size.

Thule Island is the southern-most island of the South Sandwich island chain. In 1932, the island was covered in glaciers, except in the southwest where there was a large rock outcrop that the glaciers flowed around, and a lava plateau in the southeast, which was snow free (Kemp and Nelson, 1932). An ASTER satellite image from 2003 of the island is inconclusive as to whether there has been any change in the glacier size (http://www.volcano.si.edu/world, 15 April 2006).

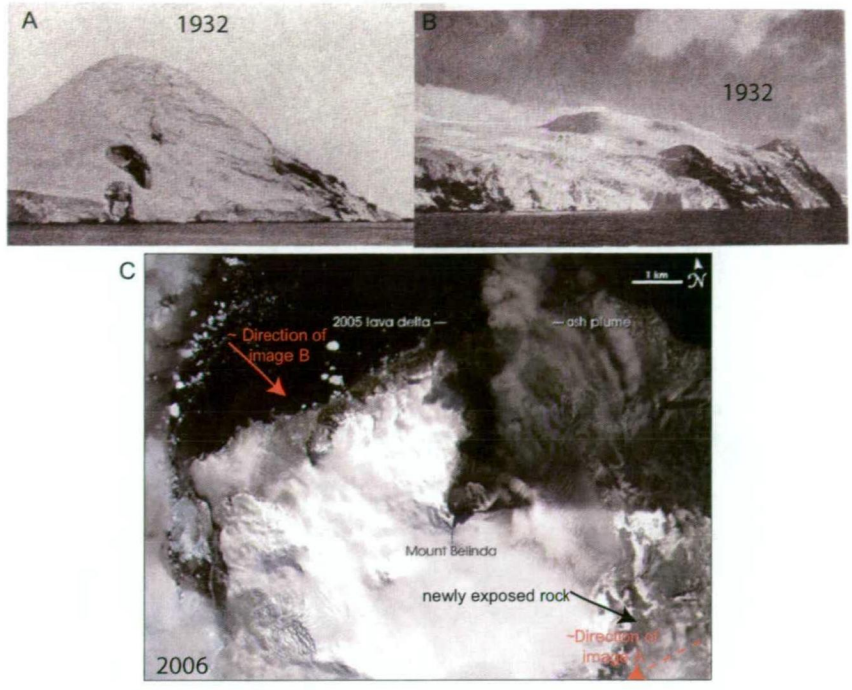

Figure 2.8.: Two photographs of Montagu Island taken in 1932. **A**) Kemp and Nelson (1932) note that this 1932 image is of a conical hill at the south-eastern corner of the island. There are indications that this promontory still retained some of its volcanic heat. **B**) This 1932 image is of the north-eastern end of the island as seen from the NNW. It shows rock outcrops and a tidewater glacier (Kemp and Nelson, 1932). **C**) The bottom image is an Advanced Spacebourne Thermal Emission and Reflection Radiometre (ASTER) satellite image of the island taken from NASA's Terra satellite on 28 October 2006. The approximate view point of the photographs are indicated on the satellite image of Montagu.

2.5. Regional implications

In the late 1700s and early 1800s all of the southern Indian Ocean sub-Antarctic island glaciers were relatively stable, with only small or minor fluctuations (Figure 2.9). This is true for all the islands except for the Crozet Group, where there is no evidence of recent glaciation. South Georgia, South Sandwich Islands and Bouvetøya were also relatively stable from their discovery to the early 1900s (Figure 2.9).

By the 1950s to 1960s the glacier frontal positions were observed to have begun to retreat on Marion, Kerguelen, Heard, South Georgia and Bouvetøya. Difficulties arise when attempting to narrow the timing of this event due to the sporadic visits to the islands before the end of WWII.

The retreat of the glacier fronts that began in the 1950s and 1960s has continued today. By 1997 all of the glaciers on Marion had retreated to a small, isolated snow pack in the lee of the summit crater. On Kerguelen the five glaciated regions had all decreased in size with the Presqu'île Courbet glaciers disappearing altogether. On Heard dramatic retreat was evident on the east coast, Laurens Peninsula and the lower elevation glaciers. The larger northern and southeastern coastal glaciers had experienced only slight thinning. On South Georgia all but the largest of the glaciers had begun to show signs of retreat. Bouvetøya remains the most ice covered of these islands, yet those glaciers too were beginning to show evidence of retreat and thinning. On the South Sandwich Islands it is assumed, supported by retreat observed in

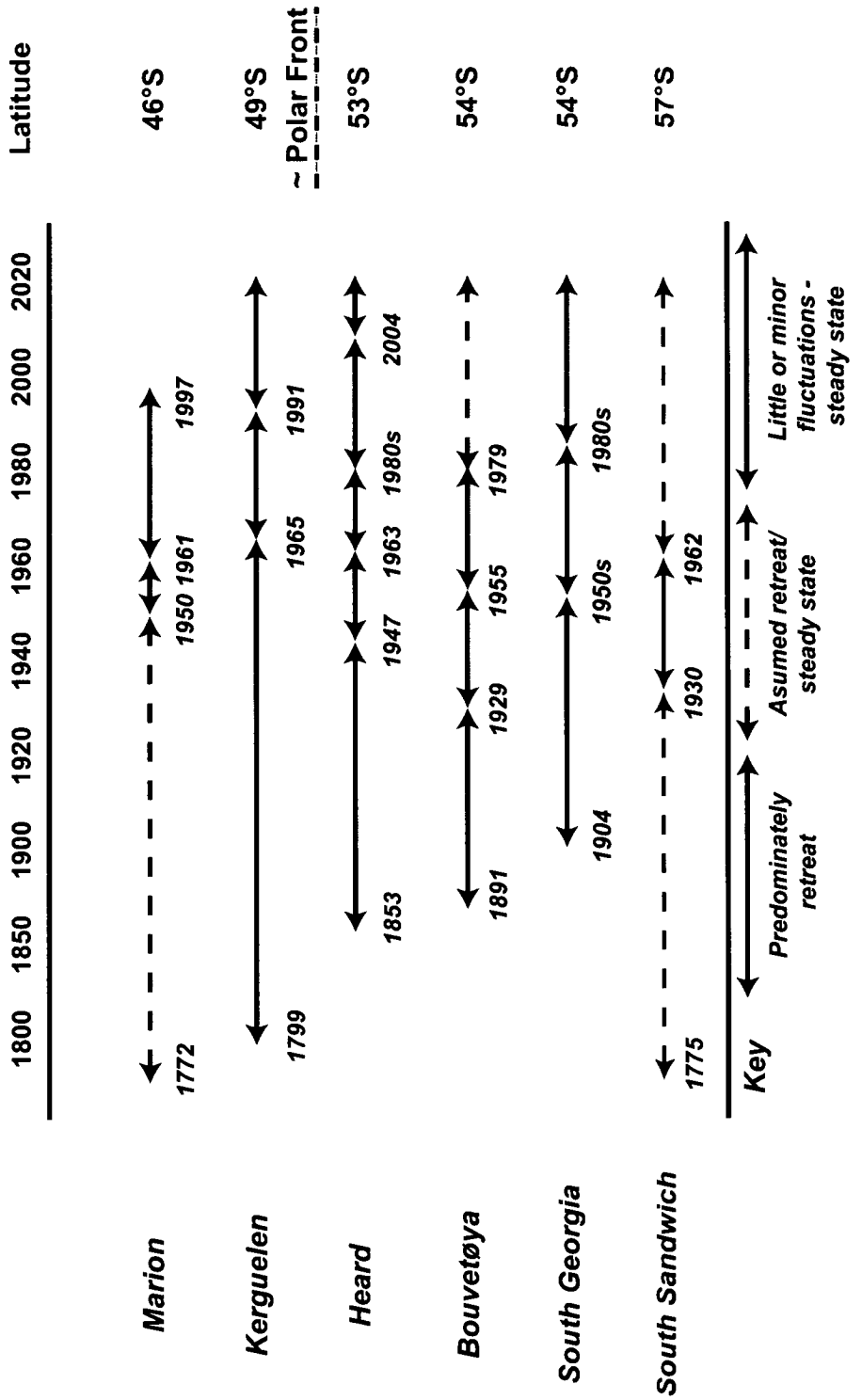

Figure 2.9.: Approximate time line of the recorded changes in the glacier fronts of the sub-Antarctic islands from north to south.

the Candlemas Group, that the retreat occurring on neighbouring South Georgia is likely to be mirrored on these islands.

The four southern most islands in this region, Heard, South Georgia and Bouvetøya (and possibly South Sandwich), have experienced a smaller change in glacier extent than the northern islands. This is because Marion, Crozet and Kerguelen, are located to the north of the

Polar Front, whereas Heard, Bouvetøya, South Georgia and South Sandwich islands are south of the Polar Front (see Section 3.2 for location of the Polar Front). The influence of the Polar Front can been seen best by comparing the climate on Kerguelen and Heard islands. These two islands are only 440 km apart yet they are separated by the Polar Front, which results in a significant difference in the temperatures on the two islands, with Kerguelen annual temperatures typically being between 2.1 and 3.7° C warmer then Heard (see Section 3.5). The greater change in temperature for latitudes above the Polar Front result in the more rapid decrease in glacier coverage than the lower temperatures found on islands located to the south of the Polar Front. Temperature records collected on the SIO sub-Antarctic islands (see Section 3.3) also show that there is a greater rate of warming occurring in the north (e. g., Marion) compared to the south (e. g., Kerguelen and Heard).

2.6. Conclusions

The changing climate especially the increasing temperature and decreasing precipitation (see Section 3.5) in the sub-Antarctic has resulted in the retreat of many of the glaciers on Marion, Kerguelen, Heard, Bouvetøya, South Georgia and South Sandwich islands. Further increases in temperature as predicted by the recent IPPC report (IPCC, 2007) will result in additional retreat and eventual disappearance of these glaciers over time. This review of the glacier changes that have occurred over the last 100 years emphasises the need for more detailed mass balance studies, which can be used to quantify the ongoing changes in these glaciers and the local climates in which they exist.

3. Regional climate variability of the southern Indian Ocean

3.1. Introduction

There are very few published studies that concentrate on the climate of the southern Indian Ocean alone, therefore one must derive the historical climatic conditions from broader scale reports. From the mid 1800's until 1920, when sailing ships criss-crossed the region, a clear indication of the historical weather patterns could be derived from their sailing routes. Few ships sailed south of 50° S at the beginning of the 1900s therefore little was known about Antarctic waters (Taljaard and Van Loon, 1984). It was not until motorised vessels ventured further south in search of whaling grounds that weather records for the region south of 50° S became available. Further, it was not until after WWII, that a better understanding of the climate of the southern Indian Ocean was developed, with the establishment of meteorological observation stations on several mid-latitude islands.

Temperature and precipitation records are both available from the majority of the land-based meteorological stations in the southern Indian Ocean. These stations are spread over a wide latitudinal range (37° S to 54° S) and are the best available data for comparison of the variation in temperature and precipitation across this region. Temperature and precipitation are closely linked to one another, and are essential climatic factors to examine to determine their relationship to glacier mass balance. The height of the equilibrium line altitude (ELA) is the determining factor as to whether a glacier continues to exist (Section 5.3.1). The amount of winter precipitation and variability in summer temperature are dominant factors that control the height of the ELA.

A review of the meteorological records from Heard, Kerguelen, Marion, Crozet, and New Amsterdam islands highlight the limited availability of data for the southern Indian Ocean. Despite the sparsity of data, this study estimates any changes in the last ~60 years of temperature and precipitation for each meteorological station and attempts to link these changes to variations in the local glaciers.

3.2. Background on the southern Indian Ocean

The Indian Ocean is bounded by Africa, Asia, Australia and the Southern Ocean (at 60° S) and separated from the Atlantic Ocean by the 20° E meridian (south of Cape Agulhas, South Africa) and from the Pacific Ocean by the 147° E meridian (south of Hobart, Tasmania). It is the third largest ocean behind the Pacific and Atlantic oceans but bigger than the Southern and Arctic oceans, with an approximate area of 68.6×10^6 km^2 (CIA factbook, 12 Jan. 2006).

The Indian Ocean can be separated into at least three different regions; northern, equatorial, and southern. It is in the southern Indian Ocean (hereafter referred to as SIO) that Heard, Ker-

guelen, Marion, Crozet and New Amsterdam islands are located. The SIO northern boundary varies between published reports (e.g., Taljaard and Van Loon, 1984; Xie et al., 2002) but an approximation would be at 30° S. While the eastern, western and southern boundaries are delineated by the neighbouring oceans at 20° E, 147° E and 60° S respectively (Figure 3.1).

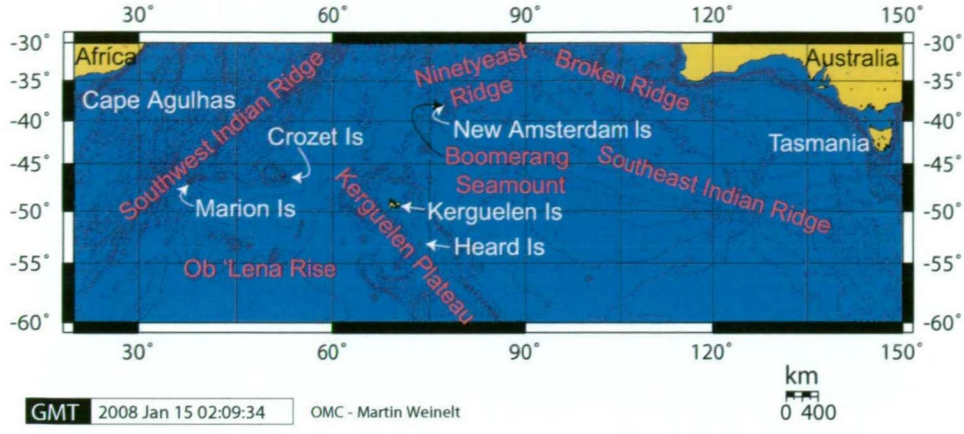

Figure 3.1.: A map of southern Indian Ocean region including some of the major subsurface features (ridges, rises and plateaus) and land masses. Not all of the features of the Indian Ocean are shown (e. g., Java Trench). This map was created using the Generic Mapping Tools (GMT) program and the Online Map Creation (OMC) website (http://www.aquarius.ifm-geomar.de/omc_intro.html, 15 January 2008).

The climate of the SIO is influenced by the synoptic scale eddies. The mean tropospheric winds are at a maximum in the westerlies direction around 45° S (Turner and Pendlebury, 2004). In general, to the north of this region there tends to be more anticyclone eddies where as to the south there tends to be more cyclonic eddies dominating (Turner and Pendlebury, 2004). The climate of the SIO is also dominated by the influence of the Antarctic Circumpolar Current (ACC). To the north of the ACC there is a ridge of high pressure at about 25° to 35° S and a trough at 65° S. In between are strong westerly winds and frequent storms. The essentially uninterrupted fetch of the winds around the Antarctic continent results in the largest average wave height of any of the oceans (Tomczak and Godfrey, 1994). This region of strong winds also has a broad band of precipitation, although in general there is little rain or snowfall data measured across the SIO (Tomczak and Godfrey, 1994), however temperature data has a much wider coverage, the temperature south of 40° S decreases more rapidly then between 40° S and the equator (Turner and Pendlebury, 2004).

The main oceanographic features of the SIO are frontal bands consisting of several circumpolar quasi-uniform belts divided by fronts and of narrow regions of sharp changes in the vertical temperature, salinity and nutrient structure (Belkin and Gordon, 1996). There are several different definitions of these fronts which seems to depend on the data set and the authors, examples are listed in Stramma (1992), Park et al. (1993), Orsi et al. (1995), Belkin and Gordon (1996), Sparrow et al. (1996), and Moore et al. (1999).

The Antarctic Circumpolar Current (ACC) is the dominant feature in terms of transport in the southern hemisphere (Rintoul et al., 2001) (Figure 3.2). This current is driven by the strong westerly winds that are found between 45° and 55° S (Orsi et al., 1995). The width of the ACC varies considerably with changing longitude and is strongly effected by local topography. The boundaries of the ACC have been defined by Orsi et al. (1995) as the region between

the southern extent of the Upper Circumpolar Deep Water (UCDW), which is characterised by low oxygen and high nutrient concentrations, and the northern extent of the Sub-Antarctic Surface Water (SASW), which is cooler and fresher than the nearby Subtropical Surface Water (STSW).

The ACC is associated with several frontal jets, which are responsible for the eastward mass transport. The dominant ACC fronts are identified, from north to south, as the Sub-Antarctic Front (SAF), the Polar Front (PF), and the Southern ACC Front (SACCF) (Figure 3.2). Some of the surrounding fronts that are also referred to in this thesis are the Sub-tropical Front (STF) and the Agulhas Return Front (ARF) (Figure 3.2), both of which are to the north of the ACC.

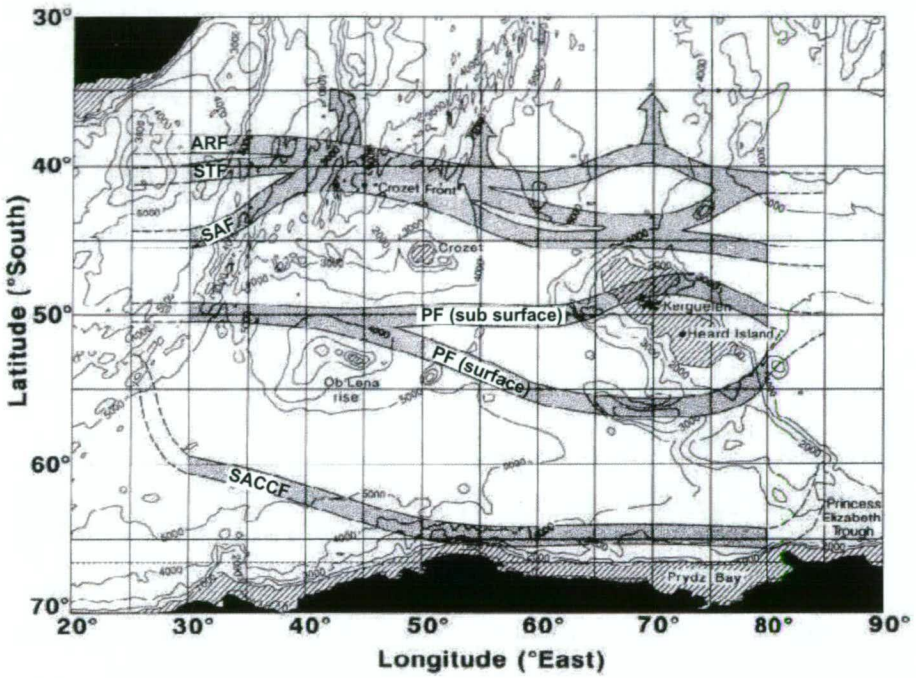

Figure 3.2.: Schematic summary of the positions of the ocean fronts determined from the analysis of the Hydrographic Atlas of the Southern Ocean by Sparrow et al. (1996). ARF: Agulhas Return Front; STF: Subtropical Front; SAF: Sub antarctic Front; PF: Polar Front; and SACCF: Southern Antarctic Circumpolar Current Front. Adapted from Sparrow et al. (1996).

A variety of factors are used to distinguish the fronts within the ACC, although most often it is the potential temperature and salinity (Orsi et al., 1995; Sparrow et al., 1996; Belkin and Gordon, 1996). These fronts are not always distinct features. In fact in the SIO these fronts can merge. For instance, both the SAF and PF and the STF and ARF are found to be in close proximity (Rintoul et al., 2001) (Figure 3.2). The merging of these systems produce some of the largest temperature and salinity gradients in the world's oceans (e.g., Orsi et al., 1995; Sparrow et al., 1996). In addition to the merging of fronts there are regions of the SIO (e. g., near the Kerguelen Plateau) where SAF and PF both split into two branches (Rintoul et al., 2001).

Oceanography near the Kerguelen Plateau There has been much debate as to whether the PF is north or south of Kerguelen Island (e.g., Belkin and Gordon, 1996; Sparrow et al., 1996; Moore et al., 1999; Rintoul et al., 2001), although most studies agree that the subsurface

and surface PF paths are persistently split through this region. Sparrow et al. (1996) noted that the subsurface PF path tends to pass north of Kerguelen Island and the surface path passing southward crossing the Kerguelen Plateau between ~ 56 to 57° S in a region of deeper bathymetry. But Moore et al. (1999) found that the PF varies over a wide range in this region from mapping satellite data from 1987 to 1993, spanning nearly 10° of latitude. Generally the PF is found close to Kerguelen Island, which is reflected in the island's warmer sub-Antarctic climate and biogeography, compared with Heard Island, which has a cooler sub-Antarctic climate and biogeography and is located well south of the PF (Belkin and Gordon, 1996).

3.3. Meteorological stations in the SIO

There are five sub-Antarctic meteorological stations that are examined in this study. The majority of these stations recorded temperature, pressure, wind speed and direction, precipitation, and relative humidity. In this study the temperature and precipitation data were concentrated on. Air temperature is one of the easiest variables to measure and most widely available meteorological variable for many locations in the SIO. Precipitation records in the SIO are available also from the majority of the stations. These two variables are important factors in the relationship between glacier mass balance and climate.

3.3.1. Marion Island

The first of the SIO stations was opened by South Africa on Marion Island (the largest of the Prince Edward Islands) at Transvaal Bay in 1947 (Figure 1.1) (http://marion.snap.org.au, 11 April 2007). This meteorological station was one of the prime reasons for the island's continued occupation. In fact, the Marion meteorological station has the longest, uninterrupted meteorological records of all the southern Indian Ocean stations. Today the station is predominantly automated although surface observations and twice daily radiosondes are still launched by hand (http://marion.snap.org.au, 11 April 2007). Observations include temperature, rainfall, sunshine, radiation, wind speed and direction, barometric pressure, humidity, sea surface temperature, cloud type and weather conditions. The upper air radiosondes record temperature, pressure, humidity, wind speed and wind direction up to 30,000 m elevation.

The Marion Island meteorological station (World Meteorological Organization (WMO) # 68994) measured air temperature at a site 24 m asl from April 1948 to present, with one gap in data between April 2004 and April 2005 due to a faulty computer on the island (pers. com. V. Smith, 15 May 2007). The maximum and minimum daily temperatures for September 1948 to February 2007 for Marion Island were provided by the South African Weather Service (pers. com. C. de Villiers, 2 May 2007). Monthly temperature records (April 1948 to July 2006) are also available on the Antarctic READER website at: www.antarctic.ac.uk/met/READER/temperature.html. The average values listed on the website are from a combination of sources but predominately from the monthly issues of South African Weather Service CLIMAT publication. The Antarctic READER website data were checked using the South African Weather Service hourly temperature data by V. Smith, resulting in the correction of some READER website data (pers. com. J. Jacka, 14 April 2007).

The monthly average temperatures used in this study for Marion Island were derived by combining the Antarctic READER website (April 1948 to December 1999), the corrected va-

lues of V. Smith (January 2000 to December 2003), the daily average maximum and minimum values from the South African Weather Service Service (January 2004 to March 2004) and the monthly issues of CLIMAT (May 2005 to July 2007) (Figure 3.3 and Appendix C.1).

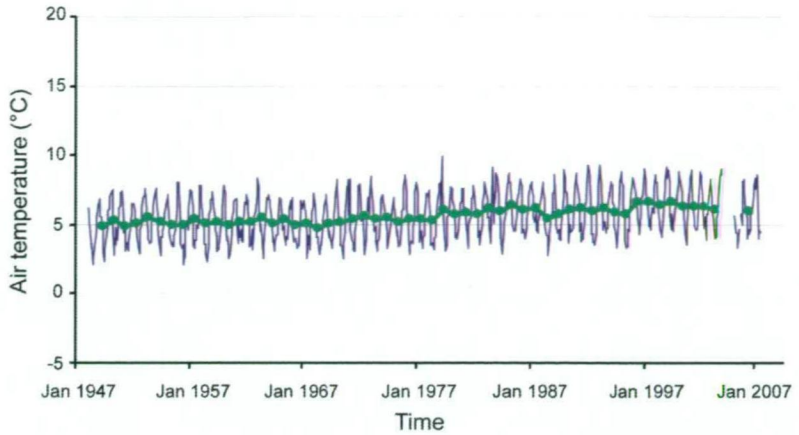

Figure 3.3.: Marion Island monthly temperature records from April 1948 to July 2007 and the annual average temperature (green line) for years with no more than one month of missing data

Precipitation records for Marion Island were provided by the South African Weather Service (pers. com. C. de Villiers, 2 May 2007). Measurements were made of daily rainfall in a rain gauge located at 24 m asl. The precipitation records in this analysis are from January 1949 to July 2007 (Figure 3.4 and Appendix C.1). These records are essentially continuous except for a few total monthly values missing and no data for April 2004 to April 2005. Additional monthly values were removed if the South African Weather Service indicated that the values were unreliable due to missing daily values.

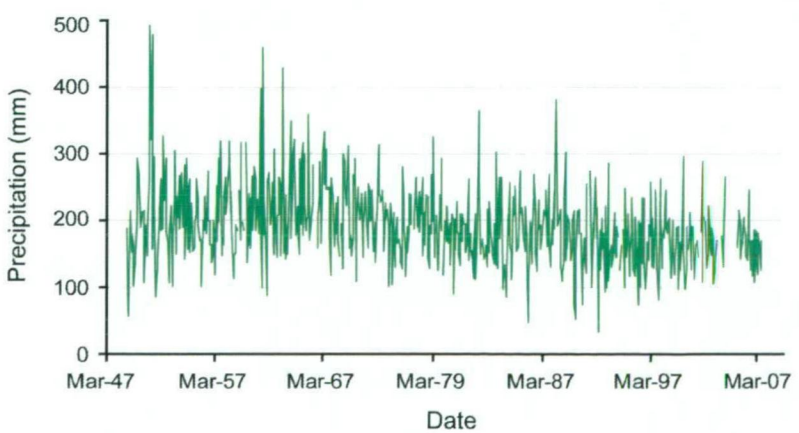

Figure 3.4.: Marion Island total monthly precipitation from 1948 to 2007.

3.3.2. Heard Island

The next station to be opened was on Heard Island, by Australia, on 1 February 1948 at Atlas Cove (Figure 1.1 and Table 3.1) and was located 3 m asl at 53°01'12" S 73°23'24" E. It remained open until December 1954 recording surface temperature, relative humidity, precipitation, wind speed and direction, barometric pressure, mean sunshine duration and included daily radiosonde launches. Subsequent to the closure of the Atlas Cove station, intermittent

observations were made during the 'summer' months. For example, in 1963, 1986, and 1987 at Atlas Cove (Table 3.1).

Table 3.1.: A list of the reported Atlas Cove and Spit Bay measured meteorological variables and dates of observation. Not all records mentioned in other studies could be found for analysis in this study. The available records can be obtained from Australian Government Bureau of Meteorology (BoM) and from the published Heard Island field reports as noted in the text.

Station	Meteorological observation	Dates of operation
Atlas Cove	Rainfall, Air temperature (wet and dry bulb), dew point, wind speed and direction, barometric pressure, mean sunshine duration	February 1948 to December 1954
Atlas Cove	Air temperature, relative humidity, wind speed and direction, air pressure	February 1963
Atlas Cove	**No records found**	January 1965
Atlas Cove	Air temperature, wind speed and direction, air pressure, cloud cover	April to October 1969
Atlas Cove	Air temperature, relative humidity, wind speed and direction, precipitation, radiation, cloud cover, air pressure	February to March 1971
Atlas Cove AWS	Air temperature	April 1980 to February 1983
Atlas Cove	**No records found**	January to February 1983 (Project Blizzard)
Atlas Cove AWS	*Faulty transmission*	September to November 1985
Spit Bay	Air temperature **No records found**	September to November 1985
Atlas Cove	Air temperature, relative humidity, wind speed and direction, barometric pressure, cloud cover	November 1986 to January 1987
Atlas Cove/Spit Bay	Air temperature. **No records found**	September 1987 to February 1988
Atlas Cove AWS	Temperature, wind speed and direction, radiation	March to September 1988
Spit Bay	Precipitation type, air temperature, wind speed and direction, barometric pressure, cloud cover and height, and dew point	May to June 1990
Spit Bay	Rainfall, air temperature, wind speed and direction, air pressure, cloud cover, sea surface temperature	March 1992 to February 1993
Spit Bay AWS	Air temperature, air pressure	July to November 1995
Atlas Cove AWS	Air temperature, air pressure	May 1997 to present
Spit Bay AWS	Air temperature, air pressure	April 1997 to present

Additional annual systematic synoptic observations were made at Spit Bay Station, on the eastern coast of Heard Island, from March 1992 to February 1993 (Table 3.1). The station was located at 53°06'25"S 73°43'16"E and at 12 m asl. Synoptic observations have also been made at Spit Bay during the shorter summer seasons (Table 3.1).

In addition to the manned meteorological stations on Heard Island, various AWS have been deployed near both the Atlas Cove and Spit Bay stations (Table 3.1). These AWS have had variable success since the beginning of the 1980s. The Atlas Cove AWS site is located at 5 m asl on a low lying volcanic sand covered isthmus (The Nullabor) and is generally exposed to the prevailing westerly winds and maritime conditions (Thost and Allison, 2006). Although there can be some screening of the wind from Laurens Peninsula for the most part the Atlas Cove station is well situated to record the prevailing conditions on the western end of the island (Gibbs et al., 1952). The Spit Bay AWS is located at 12 m asl where the prevailing weather

conditions are strongly influenced by the topography of Big Ben (Thost and Allison, 2006) and Dovers Moraine (Green, 1993b).

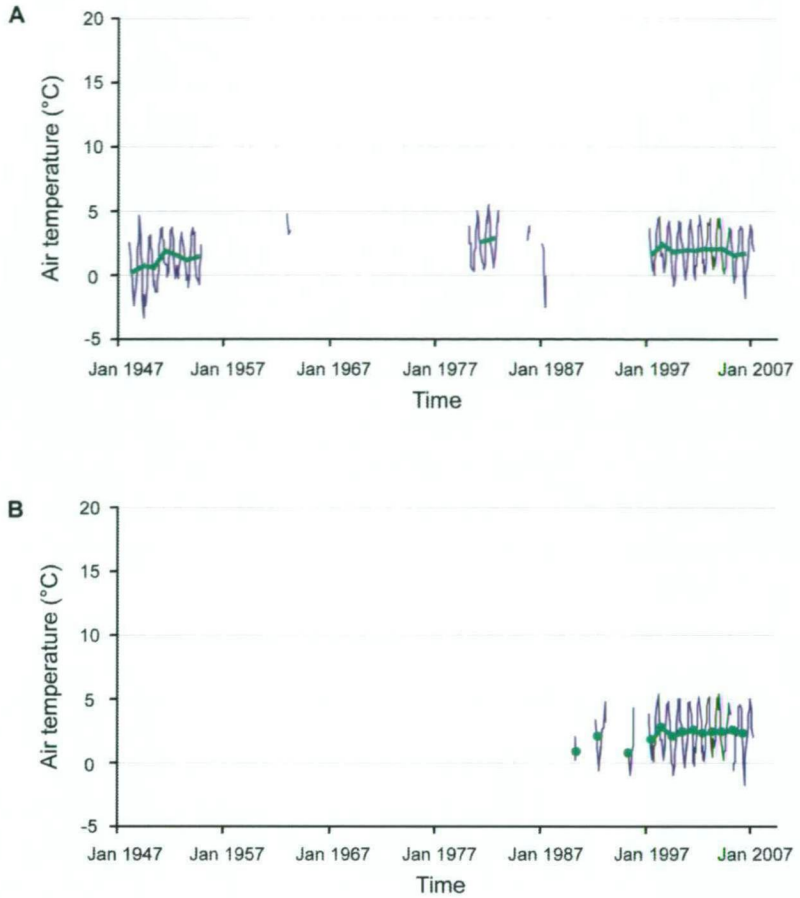

Figure 3.5.: Heard Island monthly and annual (green line) temperatures, **A**. Atlas Cove 1948 to 2007 and **B**. Spit Bay 1990 to 2007.

Temperature records at Atlas Cove (WMO #300005) consist of two long periods of measurements from 1948 to 1954 and 1997 to 2007 and several shorter periods of records, including, 1963, 1971, 1980 to 1983, 1986/87, and 1988 (Figure 3.5, and Appendix C.2). The Atlas Cove records are available in a variety of forms. The 1948 to 1954 data are published in ANARE Research Notes (Gibbs et al., 1950; The Central Office, Meteorological Branch, 1953a,b,c; The Bureau of Meteorology, 1955a,b, 1957) and made available in digital format by BoM. These manual measurements were made every ~3 hours from 1 February 1948 until 31 December 1954. The 1963 records were manually recorded every ~3 hours by ANARE expeditioners from 30 January to 7 March 1963 and made available in digital format by BoM. Between 3 April and 20 October 1969 measurements were made every two to four hours and are now available in electronic format from the Antarctic, Climate and Ecosystem Cooperative Research Centre (ACE CRC). From 27 January to 8 March 1971 six hourly observations were made of the air temperature and sent twice daily to BoM via Mawson Station (Allison, 1980). The 1980 to 1983 data were made available by BoM. These monthly average temperature records were calculated from AWS data that operated from April 1980 until February 1983. The 1986/87 summer temperature records (24 November 1986 to 20 January 1987) were measured manually by ANARE expeditioners at ~ 3 hour intervals. In 1988, an AWS was again installed

at Atlas Cove. It recorded 4, 2 and 1 m air temperature (AiT4, AiT2 and AiT1, respectively) and 10 cm subsurface temperature (SST.1) from 2 March 1988 until 30 May 1988 then intermittently until 3 September 1988 when the instrument failed. Finally in 1997 another simple AWS was deployed at Atlas Cove. This instrument continues operation to present. The AWS records air temperature at 1 to 6 hour intervals, these data are available from BoM.

Spit Bay (WMO #300085) temperatures have been recorded intermittently over the last 20 years (Figure 3.5 and Appendix C.2). The first few measurements were recorded during summer expeditions (1985 and 1987/88, although these records could not be found) with the first annual temperatures recorded from March 1992 to February 1993 (Table 3.1). Not until an AWS was installed at Spit Bay were more continuous records available from April 1997 onwards. Upon the recommendation of BoM the May and June 2005 records were removed from further analysis (high peak in temperature) (pers. com. D. Thost, 7 August 2007).

The daily precipitation records for Heard Island are shorter than those from the surrounding islands. On Heard Island the daily precipitation was measured at Atlas Cove between February 1948 and December 1954 and February 1971 (Figure 3.6). Daily precipitation was also measured from Spit Bay from March 1992 to February 1993 (Figure 3.6). The most recent precipitation measurements were collected at four fields camps (Capsize Beach, Jacka Valley, Spit Bay and Brown Hut) from the end of December 2003 to the middle of February 2004 (Figure 3.6). The total precipitation from these three stations over the 66 days of collection during 2003/04 was: 653 mm at Brown Hut, 257 mm at Spit Bay, 316 mm at Capsize Beach and 499 mm at Jacka Valley (only the January values are used in Figure 3.6).

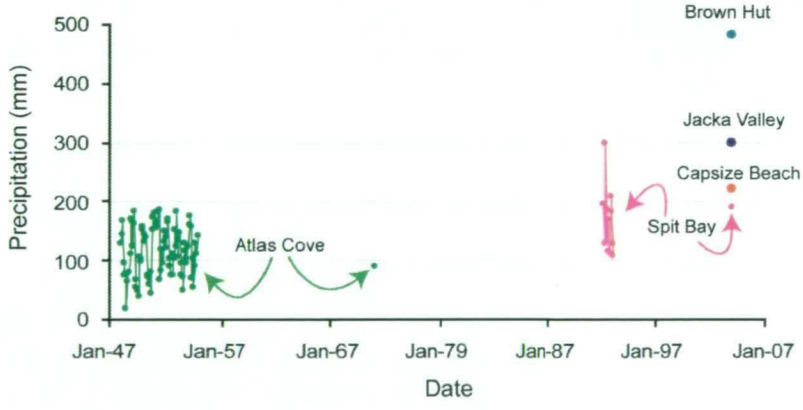

Figure 3.6.: Heard Island monthly precipitation records.

3.3.3. The French islands – New Amsterdam, Kerguelen and Crozet

In April 1949, the French parliament approved construction of a meteorological station on New Amsterdam Island (Figure 1.1). The Martin de Viviés Station, which began operation on 11 March 1950, was included in this study, even though it is a mid-latitude island, because it has some of the longest continuous meteorological records in the SIO. The station is located at 37°48' S 77°32' E and an elevation of 28 m (Auzeneau, 1994). The observations made at this station include temperature, precipitation, relative humidity, air pressure, wind speed and direction and daily radiosonde launches (beginning in March 1951) (http://www.ucm.es/info/cif/station/fr-marti.htm, 11 April 2007).

On 2 January 1950, the French began operating a meteorological station at Port-aux-Français, Kerguelen Island, at 49°21' S 70°13' E and 12 m asl (Auzeneau, 1994) (Figure 1.1). Observations made since 1950 include temperature, precipitation, relative humidity, air pressure, wind speed and direction and daily radiosonde launches (Auzeneau, 1994).

In 1961/62, the French also installed an AWS on Crozet Island at Alfred Faure station (Figure 1.1) (Auzeneau, 1994). A second AWS was erected in 1969 and remained in operation until 1980 (Auzeneau, 1994). Beginning in February 1973 a manned station began observations at 46°26' S 51°52' E and 142 m asl (Auzeneau, 1994). The manned station recorded surface measurements including temperature, precipitation, relative humidity, air pressure, wind speed and wind direction, and cloudiness (Auzeneau, 1994).

The three French island stations: Martin de Viviés Station (WMO # 61996) on New Amsterdam, Port-aux-Français (WMO # 61988) on Kerguelen and Alfred Faure (WMO # 61997) on Crozet, have measured air temperature both manually and with AWS (Appendix C.3, C.4, and C.5). The monthly and annual average air temperatures for these islands were compiled from several sources, including, (a) the Antarctic READER website, which has the oldest records up until 1985, (b) L. Testut at the Laboratoire d'Etudes en Géophysique et Océanographie Spatiales (LEGOS) provided daily average temperatures from 1980 to the mid 2000s (pers. com. L. Testut, 14 May 2007), (c) Y. Frenot at Université de Rennes has provided Kerguelen temperatures for 1989 to 2002 (pers. com. D. Thost, 18 June 2007), and (d) P. Pettre at Météo-France has provided the most recent data (last 3 to 6 years depending on the station) (pers. com. P. Pettre, 1 September 2007).

The New Amsterdam Island Station has been recording air temperature from April 1950 to present (August 2007) at a site that is 28 m asl. The average monthly and annual air temperature for New Amsterdam Island in this study were calculated from the Antarctic READER website (April 1950 to December 1985), the LEGOS data (January 1986 to June 2003) and the Météo-France data (January 2004 to August 2007) (Figure 3.7A).

The first air temperature measurements for Crozet Island that could be found began in January 1965 after which there are sporadic monthly records until January 1969. The Antarctic READER website has the majority of these early data and the last few months of 1996 (May to December), although there is a three year gap between January 1986 and December 1988. Météo-France provided the last of the temperature measurements (January 1990 to April 1996) (pers. com. P. Pettre, 1 September 2007). The last available annual record for Crozet was 1995. Paul Pettre (pers. com., 16 June 2007) has mentioned that the Crozet meteorological station was closed in the 1990s to be replaced by an AWS and that the AWS is not recording reliable measurements (Figure 3.7B).

The Kerguelen Island Station began measuring air temperature for three months in 1950 (January to March) then began more continuous records from January 1951. The Kerguelen average monthly and annual air temperature measurements were from the Antarctic READER website (January to March 1950 and January 1951 to December 1985), Y. Frenot data (January 1986 to December 1988 and January 2003 to December 2005), the LEGOS data (January 1989 to December 2002) and Météo-France data (January 2006 to August 2007) (Figure 3.7C).

The daily precipitation measurements for New Amsterdam, Crozet and Kerguelen were obtained from Météo-France (pers. com. P. Pettre, 24 August 2007) (Appendix C.3, C.4, and C.5).

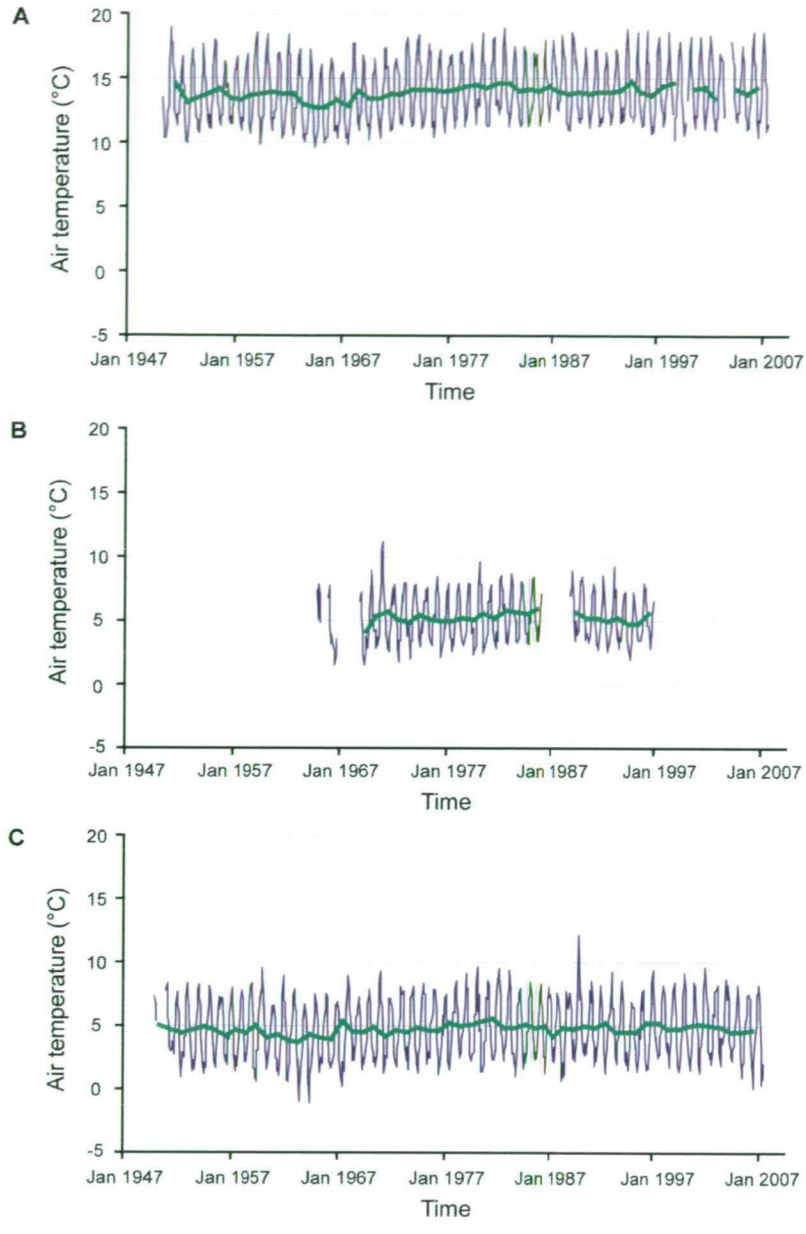

Figure 3.7.: The monthly and annual (green line) temperature records from the three French islands, **A**. New Amsterdam, **B**. Crozet and **C**. Kerguelen.

Precipitation on New Amsterdam was measured at 28 m asl from April 1950 until present (August 2007). There were no significant gaps in data (only 9 days in this period were missing) hence all of the monthly precipitation records were retained (Figure 3.8A).

The first available daily precipitation measurements for Crozet were measured at 142 m asl. The records range from January 1974 to present (August 2007) (Figure 3.8B). There are several gaps in the precipitation data, for example, eleven days in March 1974 where there are no data, all of the precipitation values are entirely or partially missing from Jan 1975, Feb to Dec 1987, Oct to Dec 1996, among other periods and finally records from December 1994 until December 1999 were removed due unreliability of the AWS over this period. All of these months that had more than six days of missing data were removed from the Crozet monthly precipitation calculations.

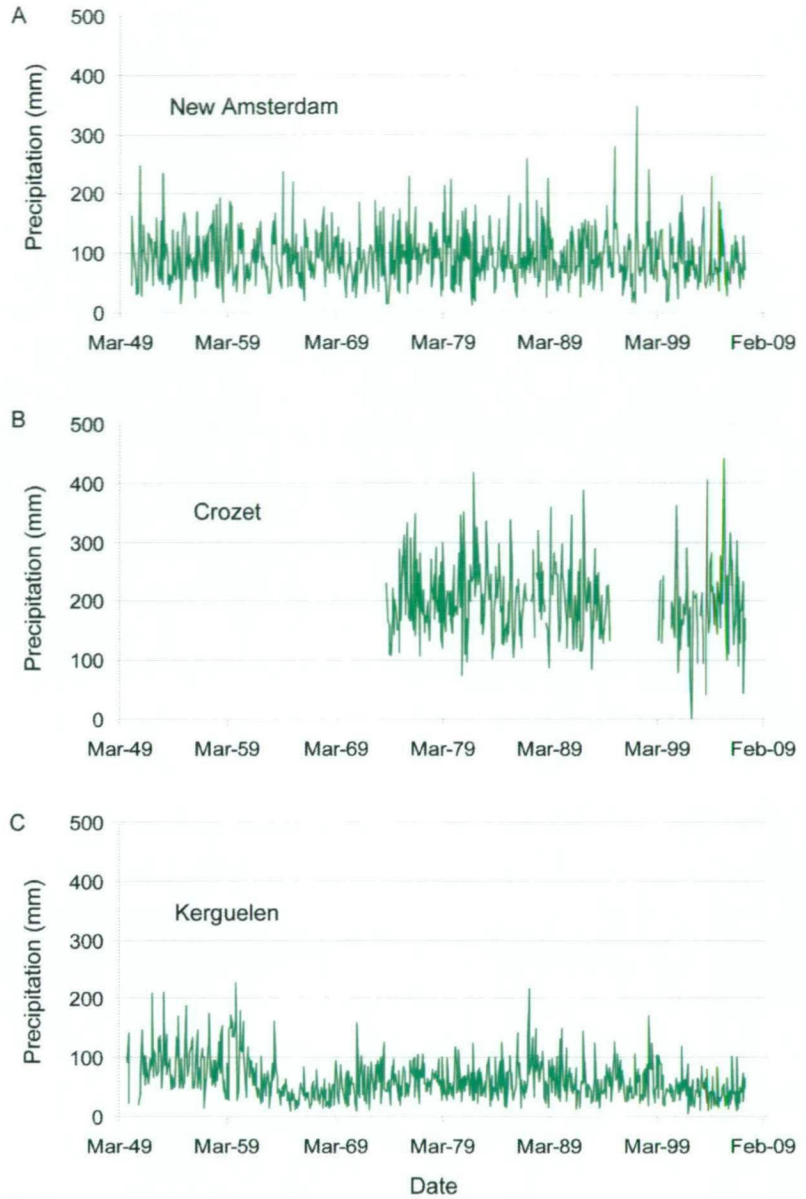

Figure 3.8.: Total monthly precipitation from the three French islands in the southern Indian Ocean, **A**. New Amsterdam, **B**. Crozet, and **C**. Kerguelen.

The daily precipitation was measured at Kerguelen beginning in January 1950 for three months. Then there was a nine month break in data until continuous daily measurements were made from January 1951 to present (August 2007) at 12 m asl (Figure 3.8C).

3.4. Analysis of meteorological records

The meteorological records from sub-Antarctic islands can be used to identify regional trends in temperature and precipitation and to estimate the long term annual temperature at Heard Island using a proxy model based on the annual temperatures at Kerguelen.

3.4.1. A proxy temperature record for Heard Island

The Atlas Cove, Heard Island, temperature record has significant periods when there are no monthly or annual values, making it difficult to examine the long term trends in temperature. In order to estimate the Atlas Cove annual temperatures between 1954 and 1997 a proxy temperature model was developed. Jacka and Ruddell (1998) used four stations (Kerguelen, Marion and New Amsterdam islands and Cape Leeuwin, Australia) to determine the best proxy temperature for Heard Island. They found that the best linear regression model was based on the 1950 to 1954 annual temperature data from Kerguelen (KI) and Atlas Cove (HI).

$$\mathrm{HI} = 1.519 \times \mathrm{KI} - 5.511 \tag{3.1}$$

The validity of the model was tested by comparing to the 1981 to 1982 (pers. com. J. Jacka, 16 May 2007) and the 1997 to 2005 temperature data from both islands. The Jacka and Ruddell (1998) (J&R) model gives a good approximation of the 1980s data but not the 1990s data. Therefore Thost and Allison (2006) (T&A) and Thost and Truffer (2008) (T&T) developed new linear regression models for Heard Island based on Kerguelen Island temperature records (Figure 3.9). The best fit model was the T&T ($R^2 = 0.78$):

$$HI_{proxy} = 1.1662 \times KI_{actual} - 3.6833 \tag{3.2}$$

The modelled data and the measured data are presented in Figure 3.9.

This proxy temperature for Heard Island can then be used in conjunction with the temperature records from the other sub-Antarctic meteorological station to examine the regional trends in temperature.

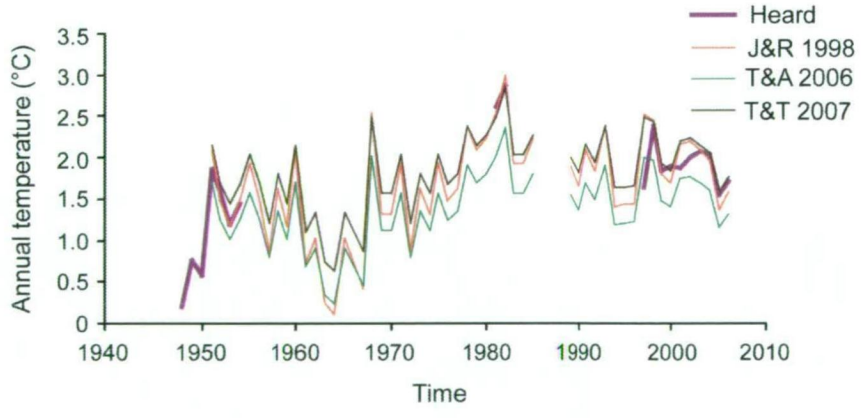

Figure 3.9.: The measured and modelled annual temperature data for Atlas Cove. The T&T 2007 proxy model (brown) is the best fit to the Heard temperature records (purple).

3.4.2. Temperature and precipitation on the sub-Antarctic islands

A trend in the temperature data sets from Marion, New Amsterdam, Crozet, Kerguelen, and Heard islands and the SIO sea surface temperature (SST) records were derived from the mean annual temperature using similar statistics to those used by Jacka et al. (2004). A trend in the precipitation from Marion, New Amsterdam, Crozet, Kerguelen and Heard islands were

derived from the total annual precipitation and using similar statistics as for the temperature data sets.

For each station the mean temperature (*total precipitation*) ($\bar{y}$) of the individual temperatures (*precipitation*) (y_i), the standard deviation, and the trend (the slope (b) of a linear regression fit through the annual mean (*total*) data), and the t statistic ($n-2$ degree of freedom), where n is the total number of years.

To test if the slope is significantly different to zero the following quantities are used:

$$S_{xx} = \sum(x_i - \bar{x})^2 \tag{3.3}$$

$$S_{yy} = \sum(y_i - \bar{y})^2 \tag{3.4}$$

$$S_{xy} = \sum(x_i - \bar{x})(y_i - \bar{y}) \tag{3.5}$$

where x_i is the individual year and $\bar{x}$ the average year.

The t statistic is then given by:

$$t = \frac{b}{\frac{\hat{\sigma}}{\sqrt{S_{xx}}}} \tag{3.6}$$

where,

$$\hat{\sigma} = \sqrt{\frac{SSE}{n-2}} \tag{3.7}$$

and the sum of the squared errors (*SEE*) can be expressed as:

$$SEE = S_{yy} - bS_{xy} \tag{3.8}$$

Only years with more than 11 months of temperature (*precipitation*) were used in this analysis. The temperature (*precipitation*) for the missing datum was calculated from the average long term temperature (*precipitation*) for that month.

This analysis is then used to determine the significance of the trend in the temperature and precipitation data from the SIO sub-Antarctic islands (Tables 3.2 and 3.3).

3.5. Discussion of the regional temperature and precipitation changes in the SIO

3.5.1. Temperature trends

The sub-Antarctic islands of the southern Indian Ocean are separated by 20° of latitude and 75° of longitude. Hence each of these stations has differing climatic regimes. New Amsterdam, the northern most island in the SIO, is located to the north of the STF defining it as a mid-latitude rather than sub-Antarctic island, yet temperature records for this island are included because it is one of the longest continuous records (Appendix C.3). Crozet, Marion and Kerguelen islands are located near or just to the north of the PF, the temperature records from these three islands

Table 3.2.: Statistical calculations for the southern Indian Ocean station annual surface temperature data. Adapted from Jacka et al. (2004) with new data (italics) added when possible. Trends that are significant to the 99% or 95% level are indicated.

Station	Mean temp (°C)	Stdv (°C)	Trend (°C 100a^{-1})	Data period	t statistic ($n-2$ d.o.f.)
Marion	5.6	0.5	+2.7	1949-2002, *2002-03, 2006*	11.5 (99)
Crozet	5.3	0.4	+0.4	1969-84, 1988-93, *1994-96*	1.2
Kerguelen	4.7	0.4	+1.0	1951-85, 1989-2000, *2000-06*	3.3 (99)
New Amsterdam	13.9	0.5	+1.4	1951-86, *1987-88*, 1989-97, *1998-99*, 2000-02, *2004-2006*	0.8
Heard (Atlas Cove)	1.7	0.7	+1.7	*1948-54, 1981-82, 1997-06*	3.2 (99)
Heard (proxy)	1.8	0.5	+1.4	*1951-2002*	3.6 (99)
SST SIO	11.1	0.2	+0.1	*1949-2006*	0.9

Table 3.3.: Statistical calculations for the SIO stations total mean annual precipitation records. Trends that are significant to the 99% or 95% level are indicated.

Station	Latitude	Total mean annual ppt (mm)	Stdv (mm)	Trend (mm 10a^{-1})	Data period	t statistic (n-2 d.o.f.)
New Amsterdam	37° S	1119	130	−8	1950-2007	−0.7
Crozet	46° S	2370	389	−65	1974-2007	−0.8
Marion	46° S	2315	321	−137	1949-2007	−6.4 (99%)
Kerguelen	49° S	753	237	−74	1951-2007	−4.3 (99%)
Heard	53°S	1438	282	-	1947-54, 1992	-

are similar (Appendix C.4, C.1, and C.5). Heard Island is located south of the PF and therefore has cooler temperatures than the other four islands (Appendix C.2).

The mean annual temperatures for Crozet, Marion, Kerguelen, New Amsterdam, and Heard islands are compared to the sea surface temperatures (SST) compiled from NCEP Reanalysis data (pers. com. J. Roberts, 7 December 2007) provided by the NOAA-CIRES Climate Diagnostic Centre (http://www.cdc.noaa.gov/, 7 December 2007) (Figure 3.10). The SIO SST values used are the mean annual skin temperature for the area between 20° E: 140° E and 30° S: 60° S.

The additional years of data (up to eight years) and the inclusion of Heard Island (Atlas Cove), and SST SIO data confirm an increasing temperature trend as Jacka et al. (2004) found. The t statistic has strengthened at Marion from 10.9 to 11.5 (significant at the 99% level), even with two years of missing data (Table 3.2). The trend in the Kerguelen data has remained essentially the same (significant at the 99% level). However both the Crozet and New Amsterdam trends have become less significant. This is especially evident at New Amsterdam, which with the inclusion of seven additional years, the t statistic has decreased from 3.9 to 1.2 (Table 3.2). Also the trend in temperature at Crozet with the addition of six years, was dramatically different from the Jacka et al. (2004) results. Jacka et al. (2004) calculated a 100 year trend of + 1.5° C whereas the new trend is + 0.4° C (Table 3.2).

The average trend for this region of the SIO is + 1.3° C 100 a^{-1}, although there is some variability in each of these long term temperature trends. Most of the island stations had a

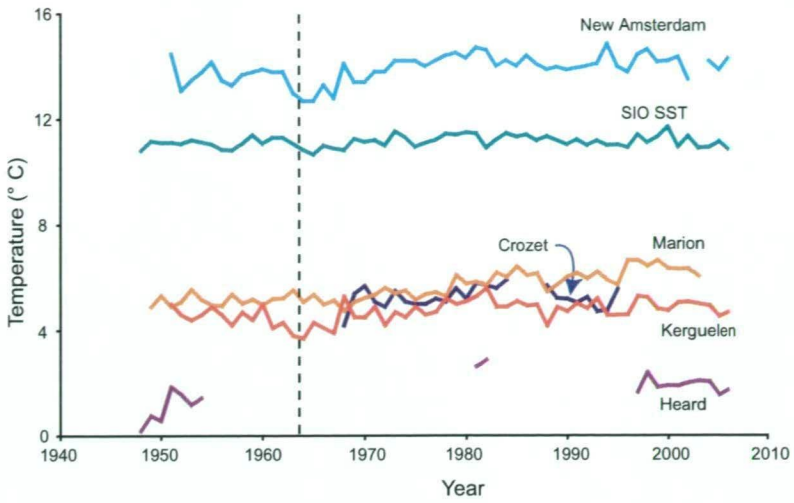

Figure 3.10.: Mean annual temperature trends of the relevant mid-latitude and sub-Antarctic islands of the southern Indian and Atlantic oceans and the SIO SST mean annual temperature between 20° E: 140° E and 30° S: 60° S. Dotted line marks a change in temperature trends in the early 1960s at the majority of the island stations.

period of cooling temperatures through the 1950s (Figure 3.10). Beginning in the 1960s all of the islands had an increase in temperature that continued until 2006. This increase is earlier than the 1976 'climate shift' identified by Trenberth (1990) marking when global temperatures began to make a discernible upward trend attributed to greenhouse gases (Trenberth et al., 2007).

At New Amsterdam, Kerguelen and Heard islands the shift in the annual temperature trend between the early 1960s and early 1980s (Figure 3.10) is coincident with the higher retreat rates of the glaciers on these islands (Figure 2.9). The Marion Island records did not have a decrease in temperature in the 1980s. It is possible that a combination of the continuing high temperatures and geothermal heating from ongoing volcanic activity has resulted in the small perennial snowfield that existed on Marion Island disappearing. The shifts in temperature in this region provides evidence that the retreat of the SIO sub-Antarctic glaciers is likely to be linked with increasing temperatures.

The Crozet records are not used in this comparison because they did not have a significant t test value and unlike New Amsterdam, which also does not have a significant t test value, the shorter temperature data set from the Crozet records make any comparisons between the other islands doubtful.

3.5.2. Precipitation trends

Global trends in precipitation are difficult to determine. A limited number of long term measurements, changes in collection instruments, high regional variability and limited technology in detecting precipitation over the oceans, are just some examples of the limitations in deriving a global trend in precipitation.

In the SIO precipitation records are available from the same occupied stations as the temperature records (Figure 3.11). Marion, New Amsterdam and Kerguelen have the longest, most complete records. Alfred Faure station, Crozet, has incomplete records from 1974 to present

(August 2007) (pers. com. P. Pettre, 15 June 2007) and Atlas Cove station, Heard, was closed after 1954.

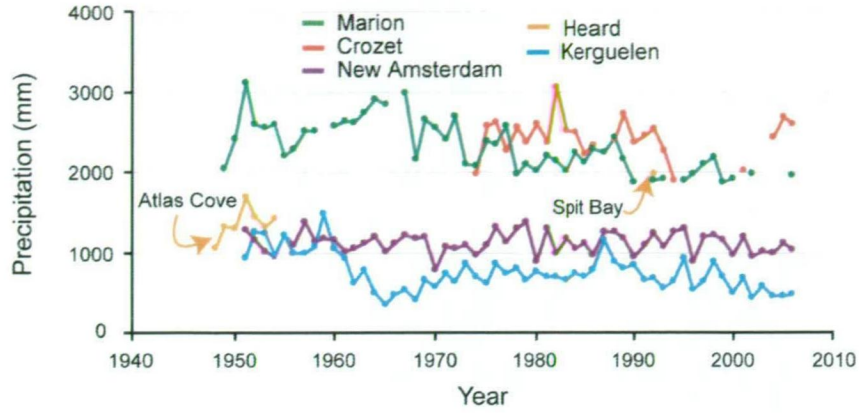

Figure 3.11.: The total annual precipitation for the sub-Antarctic islands

Although there are fewer precipitation records than temperature records, there is still a good latitudinal distribution of stations (Table 3.3). Marion, Crozet and Spit Bay have recorded almost double the precipitation measured at Atlas Cove, New Amsterdam and Kerguelen. This implies that the regions around 46° S in the SIO and on eastern Heard Island are wetter then regions to the north (New Amsterdam, 37° S) and south (Kerguelen, 49° S and Atlas Cove, 53° S) (Table 3.3).

In general there has been a decrease in precipitation in the SIO region (Table 3.3). The most dramatic decrease has been at Marion Island, which is decreasing 137 mm per decade. Both Crozet and Kerguelen islands also have a decreasing trend in precipitation of >50 mm per decade. New Amsterdam is also decreasing at a much lower rate than the other three islands. Heard Island has too few annual precipitation measurements to determine a statistically significant trend. However, given the regional trends it is likely that precipitation has been decreasing over the last century.

A decrease in precipitation on the SIO islands is likely to be effecting the glacier coverage on the individual islands albeit to a lesser degree than temperature. Less precipitation on these islands implies that there is less accumulation on the glacier. This would lead to a negative mass balance especially combined with higher temperatures, which would decrease the amount of precipitation that falls as snow.

3.6. Conclusions

The temperature and precipitation records from the meteorological stations in the SIO provide a good indication of the regional trends for the last 60 years. The increasing temperatures measured at all of the stations and in the SST data shows that, similar to the average global temperature (Trenberth et al., 2007), this region of the SIO is warming. The variability in this warming illustrates how important it is to increase the collection of meteorological variables across this region in more detail. In the last ~40 years there has been an increase in satellite coverage and technology, the ARGO buoy deployment program, and for paleo-climate variability an increased number of sediment cores from the ocean floor, which is beginning to provide a wider coverage of the region.

The sub-Antarctic meteorological stations provide some of the few measurements of precipitation in the SIO. Satellite technology still does not allow for good quality measurements of precipitation, therefore it is these few stations that provide the best information on possible trends across the region. All four of the stations (except Heard) indicate that there has been a decreasing precipitation over the last ~ 60 years by 137 mm to 8 mm.

The meteorological records from the sub-Antarctic stations have also been used to look at the trends in temperature. In the last ~ 60 years the temperature has been increasing at all of the stations. If the temperature continues to increase on these islands the length of the snow season will continue to shrink as temperatures will remain at $\geq 0°$ C for longer periods of the year (Trenberth et al., 2007). Globally this has resulted in a steady increase in the mean winter accumulation and summer melting over the last half century (Lemke et al., 2007).

The increase in temperature and decrease in precipitation are strong indicators of climate change. This changing climate has resulted in the retreat of the glaciers on all of the sub-Antarctic islands in the SIO with the northern-most islands being affected more dramatically then the southern islands.

4. Local climate variability on Heard Island and its relevance to glaciers

4.1. Introduction

There have been few published reports on the climate of Heard Island. The first meteorological observations on Heard Island were made by the sealers, whalers and initial scientific voyages in the 1800s and early 1900s. Many of these observations only cover a few days and are buried in journals of these first visitors to the island (e.g., Roberts, 1950; Crowther, 1970; Keage, 1981; McGowan, 2000). Gibbs et al. (1952) supply one of the few summaries of the meteorological conditions at Atlas Cove during the initial ANARE years. Allison and Keage (1986) provided a summary of the climatic changes on Heard Island between the initial ANARE years (1948 to 1954) and the 1980s, along with the changes in the island's glaciers. The most recent and thorough study on the available climate records was by Thost and Allison (2006). They published a complete summary of the measured climatic variables on Heard Island up until 2000.

This present study updates the climate records between March 2000 and May 2007 that were not included in the Thost and Allison (2006) paper. In addition, it begins to link the climate with changes in the glacier extent and uses the data to look at the variability of the climate around Heard Island in relation to the topography and other related factors. Big Ben has one of the strongest effects on the local Heard Island climate. The high elevation range of this small island results in strong orographically induced precipitation, violent wind gusts, variation in cloud cover and föhn winds (Thost and Allison, 2006). These orographic influences also effect the variability of accumulation on the glaciers and support strong gradients in temperature with elevation (Thost and Truffer, 2008).

The climate data used in this study includes, temperature, precipitation, relative humidity, wind direction and speed, and air pressure. Each of these variables are discussed highlighting the limited data and any instrument failures that may have occurred during the field season. These variables are then used to look at the orographic effects, local variability, lapse rates and frequency of föhn winds on Heard Island.

4.2. Heard Island meteorological stations and instrumentation

The two longest climate records on Heard Island are from Atlas Cove and Spit Bay (Figure 4.1). A detailed description of these two stations and their dates of operation was given in Section 3.3, a summary is also provided in Table 4.1. In addition to these two stations there are several short term records that are available for Heard Island (Table 4.1). The most recent data,

which is concentrated on in this chapter, was collected during two fields seasons in 2000/01 and 2003/04.

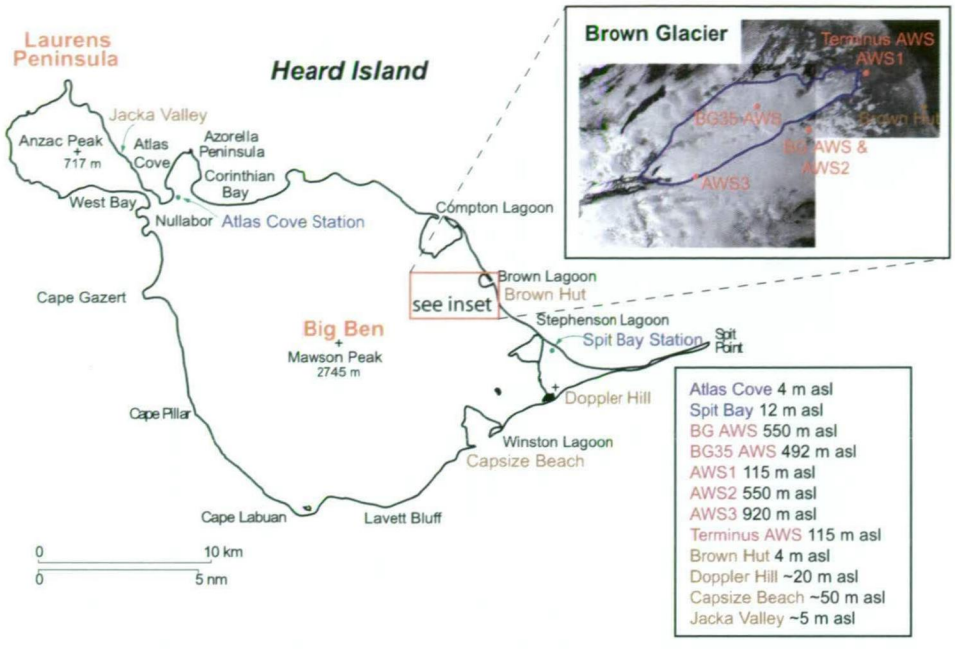

Figure 4.1.: Map of Heard Island showing sites of the major weather observations (listed in box). The two semi-permanent stations (Atlas Cove and Spit Bay) are labelled in blue. The pink labels are stations that are located more than 100 m above sea level. The brown labels indicate coastal stations that were in operation during the 2003/04 field season. Adapted from a map provided from the AAD Data Centre, inset image is the January 2003 Digital Globe image.

In 2000/01 an AWS (BG AWS) was deployed at 550 m asl on a rock outcrop near Brown Glacier (Figure 4.1 and Table 4.1). Also in 2000/01, a mobile AWS (BG35 AWS) was deployed on Brown Glacier at 492 m asl (Figure 4.1 and Table 4.1). During 2003/04, several AWS and manual meteorological records provided additional data. Three mobile AWS (AWS1, AWS2, and AWS3) were stationed near Brown Glacier, one of which was left to record over-winter (re-named Terminus AWS) (Figure 4.1 and Table 4.1). Additional manual temperature, relative humidity and precipitation measurements were made at the Jacka Valley, Capsize Beach, Doppler Hill, Spit Bay and Brown Hut coastal field camps during 2003/04 (Figure 4.1 and Table 4.1).

A description of each of the stations and AWS running times, the types of instruments deployed and the sensitivity of sensors are given in Tables 4.2, 4.3 and below.

Atlas Cove Atlas Cove meteorological station began operation in January 1947 and collected continuous records until December 1954 when the station was closed (Table 4.1). The meteorological records were made every 3 hours (Table 4.2). Additional measurements of air pressure and air temperature were measured during several summer expeditions including 1963 and 1971, and by a land-based buoy from 1997 to present (Table 4.1 and Appendix C.2).

Spit Bay The Spit Bay meteorological records include air temperature and air pressure records from 1997 to present (Table 4.2) using the same type of buoy as at Atlas Cove. The Spit

Table 4.1.: The position, variables measured, and operation dates of the stations used in this study. It is unknown if the Terminus AWS remains in operation after being left at the end of the 2003/04 field season to record measurements for as long as possible.

Station	Elevation (m asl)	Latitude	Longitude	Meteorological observation	Dates of operation
Atlas Cove	3	53°01'12" S	73°23'24" E	Air temperature, precipitation, wind speed and direction, air pressure, mean sunshine duration	January 1948 to December 1954
Atlas Cove	5	53°01'12" S	73°23'24" E	Air temperature, air pressure	April 1997 to present
Spit Bay	12	53°06'25" S	73°43'16" E	Air temperature, precipitation, wind speed and direction, air pressure, cloud cover, sea surface temperature	March 1992 to February 1993
Spit Bay	12	53°06'25" S	73°43'16" E	Air temperature, air pressure	April 1997 to present
BG35 AWS	492	53°04'55" S	73°37'59" E	Air temperature, relative humidity, wind speed, snow surface height	October 2000 to November 2000
BG AWS	550	53°05' S	73°38' E	Air temperature, wind speed and direction, short wave radiation, relative humidity	Intermittently from November 2000 to August 2002 (only the air temperature at 2 m and relative humidity were recorded for the entire period)
Spit Bay camp	10	53°06'25" S	73°43'16" E	Air temperature, precipitation	December 2003 to February 2004
Capsize Beach	~ 50	53°08'00" S	73°43'22" E	Air temperature, precipitation, relative humidity	December 2003 to February 2004
Brown Glacier Hut	4	53°04'50" S	73°40'28" E	Precipitation	December 2003 to February 2004
AWS1	115	53°04'40" S	73°39'20" E	Air temperature, precipitation, wind speed and direction, solar radiation and relative humidity	December 2003 to February 2004
AWS3	920	53°05'45 S	73°36'42" E	Air temperature, precipitation, wind speed and direction, solar radiation and relative humidity	December 2003 to February 2004
AWS2	550	53°05'23" S	73°35'52" E	Air temperature, wind speed, relative humidity	December 2003 to February 2004
Jacka Valley	~ 5	53°00' S	73°20' E	Air temperature, precipitation, relative humidity	December 2003 to February 2004
Doppler Hill	~ 20	53°09' S	73°38'2 E	Air temperature and relative humidity	December 2003 to February 2004
Terminus AWS	115	53°04'40" S	73°39'20" E	Air temperature, precipitation, wind speed and direction, solar radiation and relative humidity	February 2004 to ??

Table 4.2.: The record intervals and length for the AWS and coastal observation stations on Heard Island. (Variable = 10 min to 5 hours) (JV = Jacka Valley, CB = Capsize Beach, and DH = Doppler Hill)

AWS	Temper-ature	Air pressure	Relative humidity	Wind speed	Wind direction	Precipi-tation	Solar radiation	Month/ Year	Record length
AC	3 hr	3 hr	3 hr	3 hr	3 hr	3 hr	3 hr		1948-54
AC AWS	variable	variable	-	-	-	-	-		1997 - 2007
SB AWS	variable	variable	-	-	-	-	-		1997 - 2007
Brown Glacier									
AWS1	10 min	10 min	10 min	10 min	10 min	10 min	10 min	Jan-Feb 2004	58 days
BG35 AWS	30 min	30 min	-	30 min	-	-	-	Nov. 2000	28 days
BG AWS	variable	variable	variable	variable	-	-	variable		Nov 2000-Aug 2002
AWS2	10 min	10 min	-	10 min	-	-	10 min	Jan-Feb 2004	50 days
AWS3	10 min	10 min	10 min	10 min	10 min	10 min	10 min	Jan-Feb 2004	51 days
Coastal field camps									
JV	30 min					24 hr			
CB	30 min					24 hr			
DH	30 min					24 hr			

Bay Station and AWS also measured air pressure from May to June 1990, April 1992 to March 1993, July to November 1995. The available daily average values for Spit Bay are presented in Appendix C.2. Intermittent wind speed and direction records for Spit Bay from 1992 to 1993 were of instantaneous wind direction (typically measured daily every morning) and an estimate of wind force (speed) (Table 4.1). There were additional wind speed and direction measurements made between May to June 1990 (Appendix C.2). The 1990 Spit Bay wind records were of instantaneous wind speed and direction (measured at 9:00 and 15:00 Local Standard Time (LST)) and the maximum daily gust.

BG AWS The BG AWS was a more permanent AAD AWS consisting of a 4 m high aluminium tower with a number of sensors (Table 4.3). The tower was erected on 31 October 2000 on a rocky outcrop at 550 m asl (Table 4.1). Temperature was recorded every hour at 2 m and 4 m above the surface. Also at the 4 m level were hourly measurements of relative humidity, wind speed (hourly average) and direction and total solar radiation (Table 4.2). The results of these measurements were uploaded to a NOAA satellite on average every two hours. There were some problems with instruments: the 4 m temperature, wind speed and direction failed in February 2001 and the relative humidity and 2 m air temperature sensors failed in August 2002. In 2003/04 the mast and sensors were removed and returned to Australia.

BG35 AWS A mobile AWS (BG35 AWS) operated continuously between 29 October to 25 November 2000. The sensors were located approximately 1.5 m above the glacier surface.

Table 4.3.: Accuracy of sensors used on the AWSs and manual sites on Heard Island

Instrument	BG AWS	BG35 AWS & AWS2	AWS1 & AWS3 & Terminus AWS	Spit Camp & Brown Hut	Capsize Beach & Doppler Hill & Jacka Valley
Temperature		$< \pm 0.3°$ C	$< \pm 0.3°$ C		$\pm 0.3°$ C for -40 to 0° C and $\pm 0.2°$ C for 0 to 70° C
Precipitation			0.2 mm	±2mm	±2mm
Air pressure		$< \pm 0.3$ hPa	$< \pm 0.3$ hPa		
Relative Humidity		±2% for 0 to 90%, ±3% for 90 to 100%	±2% for 0 to 90%, ±3% for 90 to 100%		±2%
Wind speed		$\pm 0.3\,m\,s^{-1}$ for wind speeds $\leq 10\,m\,s^{-1}$ <2% for wind speeds $> 10\,m\,s^{-1}$	$\pm 0.3\,m\,s^{-1}$ for wind speeds $\leq 10\,m\,s^{-1}$ <2% for wind speeds $> 10\,m\,s^{-1}$		
Wind direction		$< \pm 3°$	$< \pm 3°$		
Solar radiation			$100\mu V/W/m^2$		

Measurements were made every half hour of temperature, relative humidity, wind speed (half hourly average and maximum gust) and wind direction (Table 4.2 and 4.3).

AWS1 and AWS3 AWS1 and AWS3 were *Vaisala* mobile automatic weather stations. AWS1 was located on bedrock near the terminus of Brown Glacier (Table 4.1). AWS3 was located on a small outcrop on the eastern margin of the glacier (Table 4.1). These two AWS recorded maximum, maximum and minimum temperature, relative humidity, wind speed and direction and solar radiation, at 10 minute intervals (Table 4.3). The AWS ran continuously from the end of December 2003 to the middle of February 2004, except AWS3 which had a power failure on 11 January 2004 resulting in a gap in data of 29.16 hours (Thost et al., 2004).

Both AWS1 and AWS3 were equipped with a tipping bucket rain gauge. Unfortunately neither rain gauges worked very well. AWS1 rain gauge filled with grit and high winds at AWS3 ripped the aluminium arm from the central pole.

AWS2 The mobile AWS used on the glacier (BG35 AWS) were redeployed near the BG AWS site and renamed AWS2 in 2003/04. The minimum, maximum and average temperature was recorded every ten minutes at AWS2 from the end of December 2003 to the middle of February 2004 (Table 4.2 and 4.3). AWS2 also measured relative humidity but the relative humidity measurements were suspect (Thost et al., 2004). Once the AWS2 measurements were found to be unreliable the BG35 AWS relative humidity measurements were re-examined and also found to be suspect, and were hence removed from further analysis.

Coastal sites In 2003/04 small weather observation stations were located at Jacka Valley, Capsize Beach, Doppler Hill, Spit Bay and Brown Hut (see Appendix C.6 for location and set up of coastal weather stations). The Jacka Valley and Capsize Beach camps had a T-Tec data logger that recorded temperature and relative humidity every 30 minutes and a rain gauge (Table 4.2 and 4.3). Doppler Hill station consisted of a T-Tec data logger attached to a star picket 1 m above a black sandy surface (Table 4.2 and 4.3). Brown Hut only had a rain gauge and Spit Bay, along with the AWS measurements, also had a rain gauge (Table 4.2). The rain gauges at each site were of 24 hour accumulated rainfall recorded at 8:00 Local Time each day (Table 4.2).

Terminus AWS On 18 February 2004 the AWS3 (with the precipitation sensor from AWS1) was relocated to near the terminus of Brown Glacier and began recording temperature, relative humidity, wind speed and direction and precipitation every three hours (Table 4.2). At present it is unknown if this AWS is still recording data until an additional trip is made to Heard Island to down load the data.

4.3. Climate measurements recorded on Heard Island

The temperature, precipitation, relative humidity, wind speed and direction, and air pressure data are examined from the various meteorology sites described in Section 4.2. The complete data sets for these AWS and coastal sites are available in Appendix C.6 and are described in more detail in the following sections.

4.3.1. Temperature

The Atlas Cove average monthly temperature varies seasonally from a maximum between December and March and a minimum between June and September. There does not appear to be a shift in the temperature seasonality between 1947 and 1954, 1980 and 1983 and 1997 and 2007 (Figure 4.2). February has typically been the warmest month on record and the coldest month tends to vary between June to September.

The coldest temperature recorded at Atlas Cove was $-9.7°$ C on 17 June 1988 (Appendix C.2). The warmest temperature recorded at Atlas Cove was 15.8° C on 4 February 2004 (Appendix C.2). The high temperatures recorded at Atlas Cove are probably due to warm synoptic systems (see Section 4.4.4 for discussion).

Between 1998 and 2007, the seasonal variability in air temperature at Spit Bay ranges from a maximum in January and April to a minimum between June and September. The average annual temperature at Spit Bay was 2.4° C between 1998 and 2006. The minimum temperature recorded at Spit Bay was $-1.0°$ C on 17 June 1990 and a maximum of 25.3° C on 10 June 1988 (Appendix C.2). Spit Bay has a much higher monthly extreme maximum temperature than those recorded at Atlas Cove. For every annual record available the annual extreme maximum temperature is $> 15°$ C and of the 125 months of available records 80 of these have an extreme maximum of $> 10°$ C. There does not appear to be any seasonal pattern to these extremes in temperature.

The annual temperature records at BG AWS had a maximum daily average temperature of 11.29° C on 12 January 2001 and a minimum daily average temperature of -10.82° C on 19 June

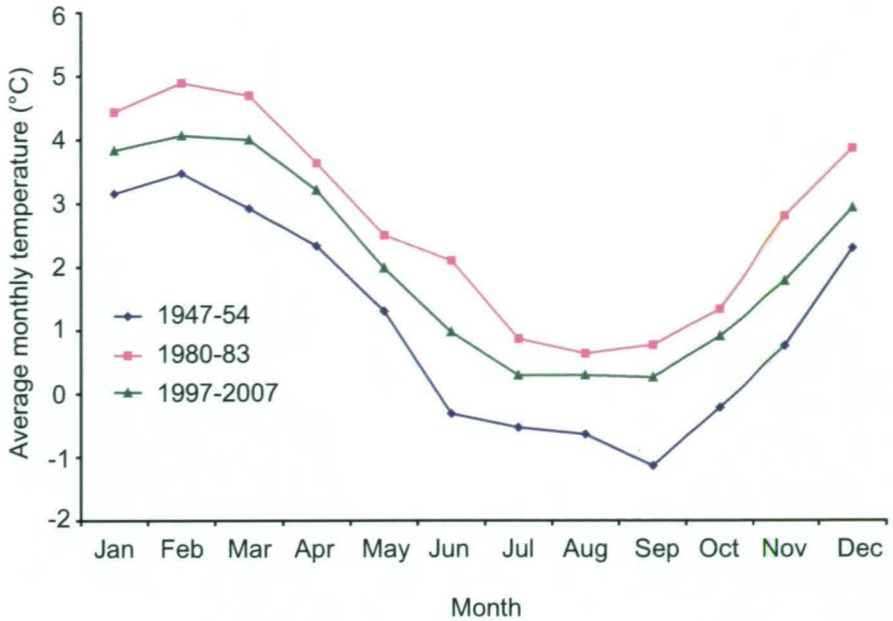

Figure 4.2.: Atlas Cove average monthly air temperature records from 1947 to 1954, 1980 to 1983 and 1997 to 2006.

2001 (Figure 4.3). The annual temperature at 550 m have a seasonal range from a maximum in January-February and a minimum in August-September.

The shorter summer temperature records on Brown Glacier indicate that there is a greater increase in temperature between 115 m and 550 m than between 550 m and 920 m (see Section 4.4.3). There are also periods when the high elevation AWS have measured higher temperatures than AWS1 located near the coast. This is discussed in more detail in Section 4.4.4.

The T-Tec temperature records at the three field camps show that there is little difference between Doppler Hill and Capsize Beach air temperature (Figure 4.3 and Table 4.6), which are only 6 km apart. It should be noted however that the Doppler Hill temperature sensor was unshielded whereas the Capsize Beach one was housed in a Stephenson screen. Given the similarity between the two site's average, maximum and minimum temperatures it may be that the radiative effects on the unshielded Doppler Hill sensor are small.

The Jacka Valley air temperature are lower and with less warming periods compared to Doppler Hill and Capsize Beach (Figure 4.3). The highest daily average temperature recorded at Jacka Valley was 7.15° C where as it was 11.04° C at Capsize Beach and 9.49° C at Doppler Hill.

4.3.2. Precipitation

Heard Island is a very wet environment. Observations from Atlas Cove between 1948 and 1954 recorded a mean annual precipitation of 1361 mm ($1\sigma = 196$) (Thost and Allison, 2006) with annual ranges from 1293 mm in 1950 to 1695 mm in 1951 (Table 4.4 and Appendix C.2). On average there was precipitation on 276 days (or 75%) of the year, over this seven year period, with the highest number of days with precipitation occurring in 1949 (300 days or 82%).

There is also a seasonal variation in precipitation. The mean monthly precipitation varies from 57 mm in August to 158 mm in April. Precipitation tends to be higher from March to May

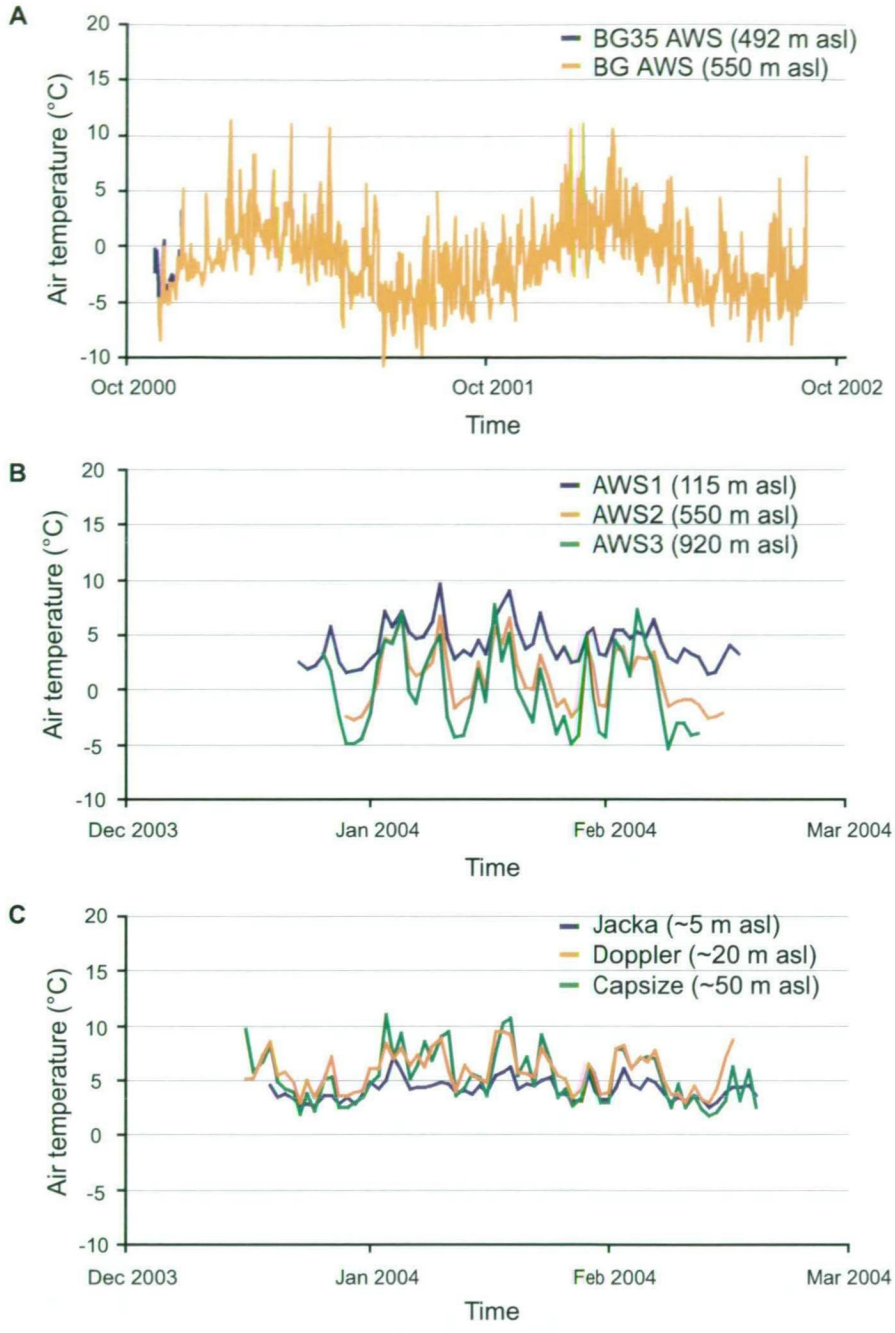

Figure 4.3.: Brown Glacier and the coastal daily air temperature records from both field seasons. **A**. BG35 and BG AWS, **B**. AWS1, AWS2 and AWS3, and **C**. Capsize Beach, Doppler Hill and Jacka Valley.

than in the cooler months (August-September). This increased precipitation during the warmer parts of the year is expected in regions where the cyclonic activity is unabated throughout the year (Taljaard and Van Loon, 1984).

The total Spit Bay precipitation recorded between March 1992 and February 1993 was 1971 mm (Table 4.4). The highest monthly total was recorded in May (300 mm) and the lowest in February (109 mm). The Spit Bay total precipitation is almost 300 mm higher than the maximum annual precipitation recorded at Atlas Cove. This higher precipitation total is also

Table 4.4.: Summary of the precipitation records (in mm) from Atlas Cove (AC), 1948 to 1954, and Spit Bay (SB), March 1992 to February 1993, from BoM data.

Month	1948	1949	1950	1951	1952	1953	1954	AC average	SB 1992/93
Jan		168.9	156.7	153.2	131.8	122.7	102.6	139.3	128
Feb	128.8	122.7	151.4	179.6	122.2	183.9	125.2	144.8	109.1
Mar	167.6	164.1	131.8	154.9	140.2	105.7	160.8	146.4	195.3
Apr	144.0	181.6	144.3	160.3	170.9	133.1	173.5	158.2	128.2
May	95.3	163.1	140.0	167.6	164.6	147.6	157.0	147.9	299.8
Jun	76.2	65.5	72.4	181.6	102.9	95.8	69.6	94.9	189.1
Jul	76.7	53.6	73.7	184.7	89.9	75.9	103.1	93.9	130.4
Aug	18.5	49.0	57.7	67.8	74.4	73.4	55.1	56.6	171.1
Sept	65.3	38.1	70.1	83.1	74.9	47.8	89.2	66.9	115.2
Oct	76.5	105.2	43.2	117.6	110.5	116.1	129.8	99.8	112.3
Nov	81.0	102.6	79.5	95.5	103.1	128.8	111.8	100.3	208
Dec	112.3	96.8	12.2	149.4	152.9	94.5	143.0	131.6	184.2
Total	**1042.2**	**1311.1**	**1292.9**	**1695.2**	**1438.4**	**1325.1**	**1420.6**	**1360.8**	**1970.7**

reflected in the greater number of days that precipitation has occurred at Spit Bay (329 days or 90%) than Atlas Cove (maximum was 300 days) (Green, 1993b).

4.3.3. Relative humidity

Relative humidity values at Atlas Cove are shown in Table 4.5. There was some problems with the reliability of relative humidity measurements at several sites. The more reliable measurements were made at Jacka Valley, Capsize Beach, Doppler Hill and AWS1 (Table 4.5).

Table 4.5.: Relative humidity (RH) measurements recorded at the BG35 and BG AWS in 2000/01, and in 2003/04 from Jacka Valley, Capsize Beach and Doppler Hill and at AWS1. (nr = not reliable)

	BG35 AWS		BG-AWS		Jacka Valley		Capsize Beach		Doppler Hill		AWS1	
	Temp	RH	Temp	RH	Temp	RH	Temp	RH	Temp	RH	Temp	RH
Average	−2.9	nr	−3.6	82.6	4.6	96	6.3	83	6.4	85	4.98	77
Std Dev	2.7	nr	2.5	13.1	1.4	6.6	3.7	12.0	3.1	15.7	2.61	13
Maximum	12.5	nr	13.5	100	10.5	100	20.3	100	18.9	100	15.02	100
Minimum	−9.4	nr	−9.8	28	0.9	65	0.6	20	0.9	44	0.28	22
Time frame	Nov 2000				end Dec 2003 to mid Feb 2004							

4.3.4. Wind speed and direction

Annual wind direction and speed have been measured at Atlas Cove and BG AWS. Summer wind speed and direction were recorded at BG35 AWS, AWS1 and AWS3. The winds at Atlas Cove between 1947 and 1954 were predominately from the west and southwest. This is in part due to the barriers of Big Ben to the east and Laurens Peninsula to the west. The short summer measurements seem to indicate that the winds have greater speeds and from a more NW direction at BG AWS and BG35 AWS. AWS3 is located close to the steep slopes of Big Ben Plateau resulting in more westerly winds occurring at this site.

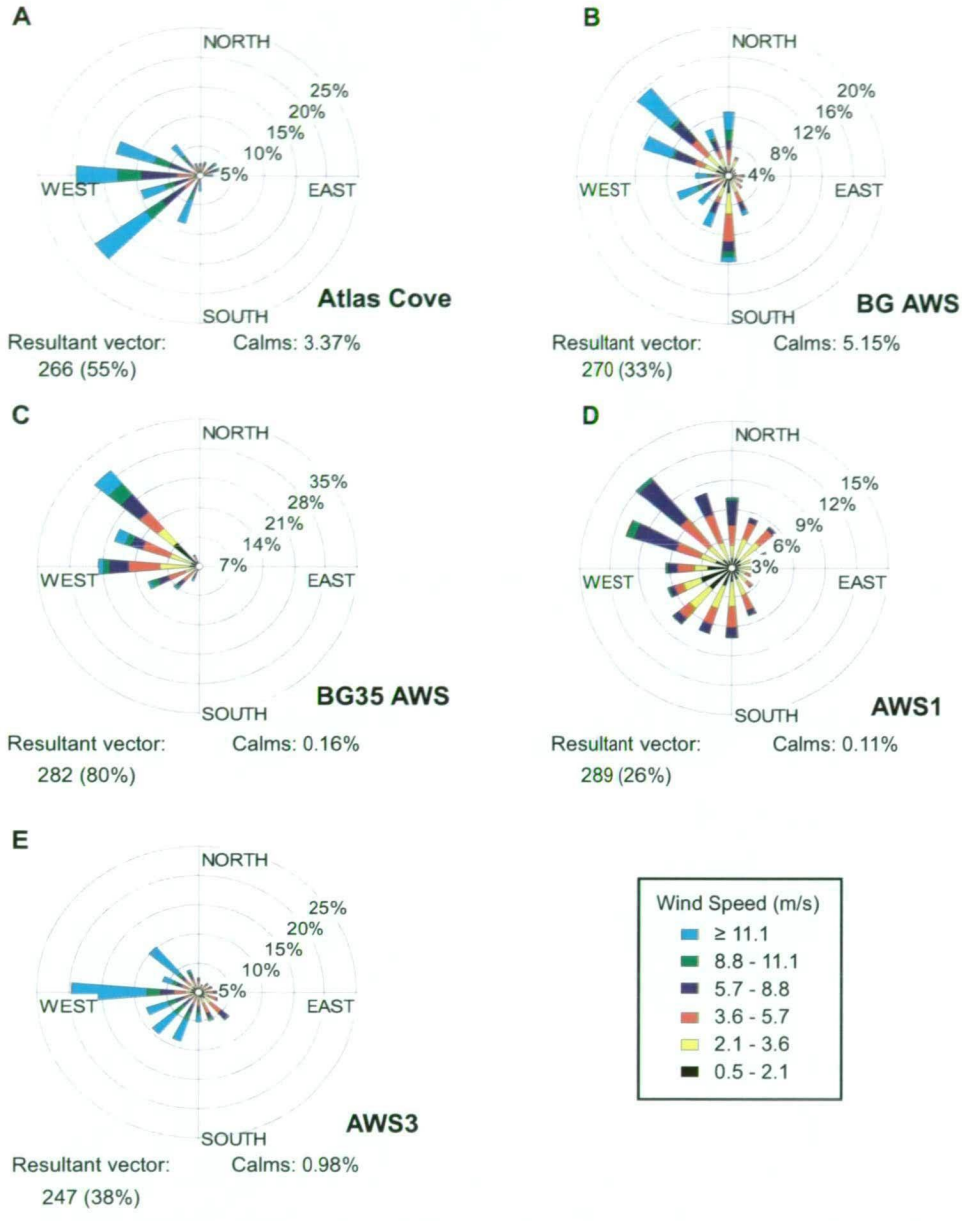

Figure 4.4.: Wind roses for: **A**. Atlas Cove 1948 to 1954, **B**. BG AWS, **C**. BG35 AWS, **D**. AWS1 and **E**. AWS3. The vectors are the mean direction of wind for each AWS and are computed from the vector sum of the unit vectors that represent the various wind directions in the data (due to program limitations there are a different scales for each site). The wind roses were created using the Lakes Environment WRPLOT View freeware program (http://www.weblakes.com/lakewrpl.html, 12 February 2008).

4.3.5. Air pressure

The available daily average air pressure values for Atlas Cove and Spit Bay are presented in Figure 4.5 and Appendix C.2. The air pressure values at Atlas Cove and Spit Bay show that there is a wide range of pressure systems that pass over Heard Island each year.

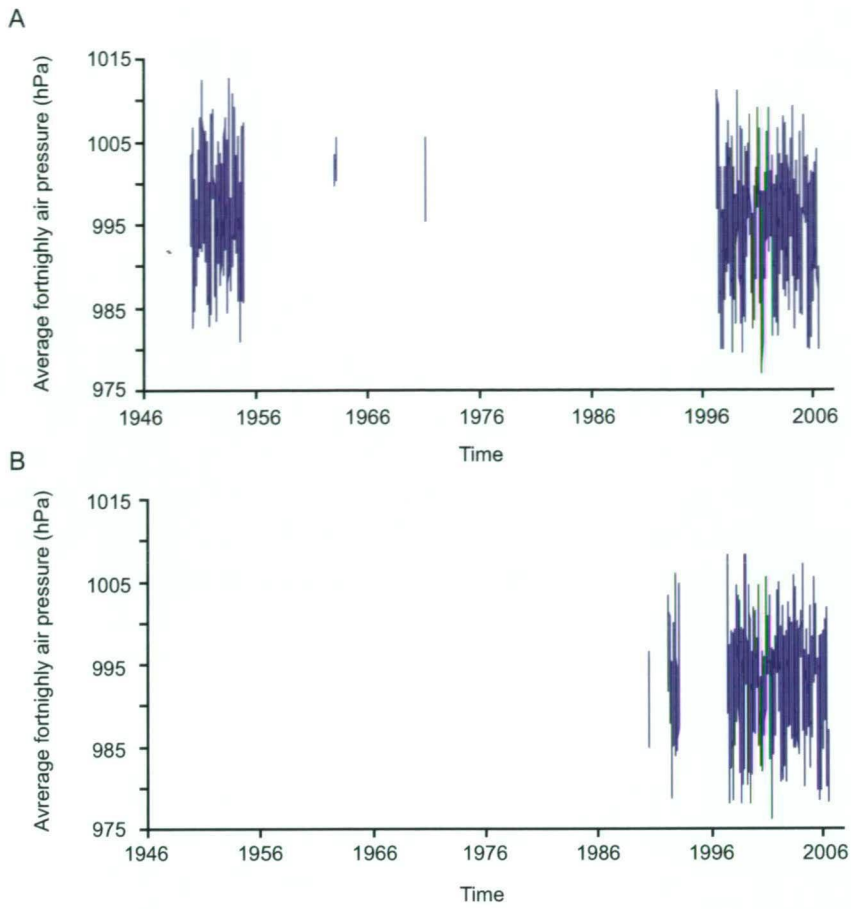

Figure 4.5.: The average fortnightly (14 point running mean) air pressure measurements at **A**. Atlas Cove and **B**. Spit Bay

4.4. Local variability and orographic effects on temperature and precipitation across the island

Annual temperature and precipitation data have been collected predominately from Atlas Cove and Spit Bay stations. These records are used to show any long term changes in temperature and precipitation on the island and to look at any small-scale regional or annual variations between the two sites. More recently there have been several summer temperature and precipitation records from field camps, these smaller, short term stations can be used to investigate coastal variations in temperature and precipitation around the island.

4.4.1. Coastal temperature and relative humidity variations on Heard Island (summer 2003/04)

During 2003/04 air temperature was recorded at six field camps (Figure 4.1). These six sites (including AWS1 at 115 m asl) provide an illustration of the variability of the temperature around the island (Table 4.6).

Spit Bay and AWS1 (Figure 4.1), located on the northeast coast, recorded cooler average temperatures than Capsize Beach and Doppler Hill (Table 4.6). This is expected from the

AWS1 site given that it is over 100 m asl, however the higher AWS1 and sea level Spit Bay records still have similar average, minimum and maximum temperatures.

Table 4.6.: Temperature records from the near coastal stations from the end of December 2003 until the middle of February 2004 from Thost et al. (2004) and AWS1 at 115 m asl.

Temperature (°C)	Capsize Beach (50 m asl)	Doppler Hill (20 m asl)	Spit Bay (12 m asl)	Atlas Cove (4 m asl)	Jacka Valley (5 m asl)	AWS1 (115 m asl)
Average	6.3	6.4	4.5	3.9	4.6	5.0
Maximum	20.3	18.9	13	7.8	10.5	15.0
Minimum	0.6	0.9	0.8	1	0.9	−0.5

Atlas Cove and Jacka Valley, the two northeastern stations, have similar average temperatures (Table 4.6). It is interesting to note that there is little difference between the Jacka Valley temperature records, which are sheltered from the predominate westerly winds, and Atlas Cove temperature records, which are located in a more open site.

Only complete annual records were used to calculate the annual temperature for Atlas Cove (Figure 4.6). The average annual temperature from the 1948 to 1954 period was 1.1° C which is more than one degree lower than the average annual temperature from 1982 to 1983 of 2.8° C and from 1998 to 2006 of 2.0° C. However, it should be noted that the 1980 to 1983 data were recorded from an unshielded instrument. As only the monthly data were available, no comparison could be made between the night and day temperatures to determine any possible radiation error.

Although the Atlas Cove data set is almost 30 years longer than the intermittent Spit Bay record some comparisons can be made. Over the last few years (1998-2006) the annual Spit Bay temperature has always been higher than at Atlas Cove by between 0.2 and 1.0° C (Figure 4.6). Spit Bay also tends to have much higher extreme maximum temperatures than Atlas Cove due to increased föhn wind frequency recorded on the eastern, leeward side of the island (see Section 4.4.4).

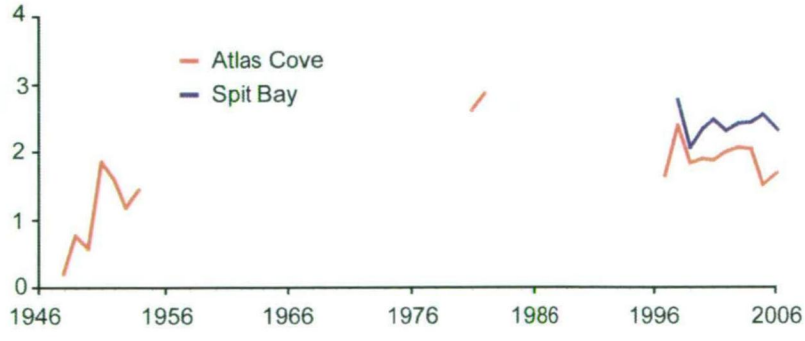

Figure 4.6.: Annual temperature records from Atlas Cove and Spit Bay.

Relative humidity was measured at four of the coastal sites: Capsize Beach, Doppler Hill, Jacka Valley and AWS1 (Table 4.5). The variability in the relative humidity measurements between the coastal sites suggest that there maybe variation in relative humidity due to aspect. The southern and western coasts are in the direct path of the prevailing winds and therefore moisture source, resulting in higher relative humidity values. In comparison, the northeastern

regions of the island are blocked from the prevailing winds by Big Ben creating a relatively lower relative humidity. These measurements suggest that there is drier air on the leeward side of Big Ben compared to the windward side.

4.4.2. Precipitation at elevation

The precipitation at higher elevations on Heard Island is strongly influenced by orographic effects (Allison and Keage, 1986). The two most important controls of orographic precipitation distribution are slope and elevation and to a lesser degree geometry, orientation of the mountain range and local climate regime (Roe et al., 2003). In a simple system precipitation would decrease with elevation as temperature and atmospheric moisture decrease but this does not factor in the relationship between precipitation and wind strength or storminess (Roe et al., 2003). In many mountainous regions the attitudinal increase of precipitation is due to a combination of higher intensities and greater duration of precipitating storms (Barry, 1992).

The 2000/01 sonic ranger located on Brown Glacier at an elevation of 500 m had a net accumulation of 258 mm w.e. for November (see Section 5.5.3). In addition to the sonic ranger results a net balance estimate of 6 to 7 m a^{-1} w.e. was made in 2000/01 based on three summer dust layers found in a crevasse wall located at 1050 m asl (Truffer et al., 2001). In 2003/04, three additional crevasses were investigated for 'summer dust layers' but only one layer was found at 920 m asl, at 6.67 m below the surface. This dust layer did not correlate with estimates of the total net balance at this crevasse site obtained from oxygen isotope and glaciochemical analysis (see Chapter 6 for more details).

Also in 2003/04 measurements of the total melt across the glacier based on the measurement of ablation and the meltwater stream flux indicate that the precipitation increases with elevation (see Section 5.5.4) This indicates that storms that pass over Brown Glacier are of a high enough intensity, or for long enough periods, to create a gradient of increasing precipitation with elevation.

4.4.3. Heard Island free-air lapse rates

A free-air lapse rate was calculated from Atlas Cove daily radiosonde temperature records (launched at 9:00 or 10:00 LST, UTC ~+5, depending on the year). These records of day time temperatures give an average lapse rate of $-0.007°$ C m^{-1}, with monthly means ranging from -0.006 to $-0.008°$ C m^{-1}, for elevations between 0 to 300 m asl (Table 4.7). Until 2000 this was the only lapse rate available for Heard Island.

Table 4.7.: Monthly lapse rates (° C m^{-1}) from the 1948 to 1954 Atlas Cove radiosonde temperature data

Elev. (m)	Jan	Feb	Mar	Apr	May	Jun	Jul	Aug	Sept	Oct	Nov	Dec	Mean
0-300	-0.0057	-0.0067	-0.0064	-0.0064	-0.0067	-0.0074	-0.0067	-0.0073	-0.0080	-0.0077	-0.0073	-0.0064	-0.0069
300-1000	-0.0046	-0.0052	-0.0047	-0.0049	-0.0052	-0.0057	-0.0056	-0.0057	-0.0063	-0.0060	-0.0054	-0.0048	-0.0053
1000-2000	-0.0039	-0.0037	-0.0039	-0.0040	-0.0047	-0.0052	-0.0054	-0.0049	-0.0054	-0.0053	-0.0045	-0.0037	-0.0046
2000-2750	-0.0039	-0.0032	-0.0039	-0.0041	-0.0048	-0.0051	-0.0052	-0.0048	-0.0048	-0.0052	-0.0051	-0.0044	-0.0045

The Atlas Cove mean annual lapse rate shows a seasonal signal, with steeper lapse rates in winter/early spring than summer (Figure 4.7). The steeper lapse rates in winter and early spring

at Atlas Cove may be a product of the longer nocturnal hours, cooler winds at night and snow cover over the majority of the island from autumn to spring. This seasonal signal is similar to the signal found in the Colorado Rockies (Pepin and Losleben, 2002), though different from lapse rates derived over larger altitudinal ranges (e. g., Italian Alps and northern Britain) (Cline et al., 1998; Pepin, 2001; Rolland, 2003).

Previous studies have shown wide variation in surface lapse rates. These variations are due to fundamental controls on lapse rates including; air mass movement (Fleagle, 1946; Yoshino, 1966; Harding, 1978), seasonality (Pepin and Losleben, 2002; Rolland, 2003), diurnal effects (Barry, 1992; Pepin et al., 1999; Rolland, 2003), topography (Pielke and Mehring, 1977; Rolland, 2003), cloudiness (Pepin et al., 1999; Pepin and Losleben, 2002), föhn winds (Barry, 1992), ground cover (Barry, 1992) and humidity (Sturman and Tapper, 1996).

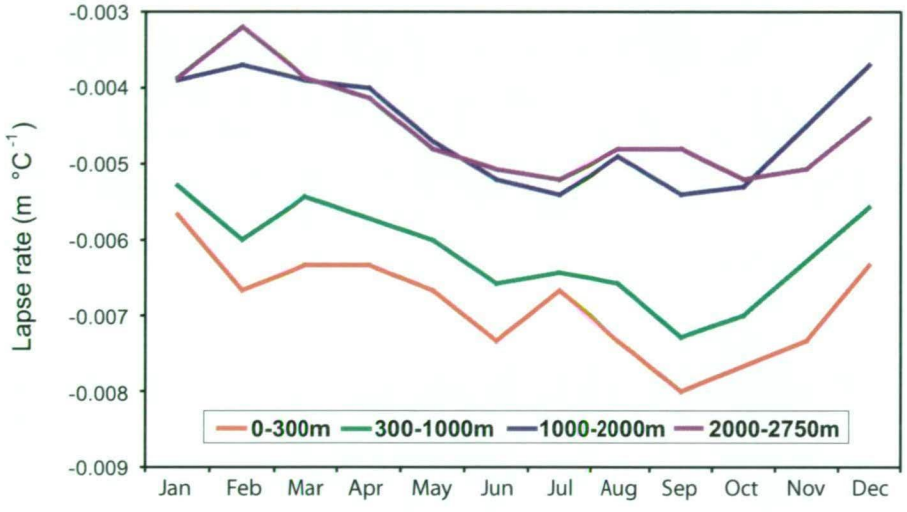

Figure 4.7.: Monthly lapse rates from the 1948 to 1954 radiosonde data at Atlas Cove

More recently surface lapse rates were calculated for Brown Glacier between AWS1 and AWS2 (lower) and between AWS2 and AWS3 (upper). The AWS1-AWS2 lapse rate has a maximum frequency at $-0.010^{\circ}\,\mathrm{C\,m^{-1}}$ and an average lapse rate of $-0.008^{\circ}\,\mathrm{C\,m^{-1}}$ (Figure 4.8). The average lapse rate for AWS2-AWS3 was $-0.003^{\circ}\,\mathrm{C\,m^{-1}}$ and it also had a distinctive bimodal distribution (Figure 4.8) with peaks near -0.003 and $0.013^{\circ}\,\mathrm{C\,m^{-1}}$. The lower lapse rate also had a bimodal distribution but was not as pronounced.

This bimodal distribution may be a result of föhn winds which could increase the number of temperature inversions recorded (see Section 4.4.4). Although temperature inversions typically occur at night under clear skies, when long wave radiant energy loss from the surface to the atmosphere is more efficient, temperature inversions can also occur due to cold air advection related to frontal activity, subsidence associated with an anticyclone and advection of a warm air mass over a colder surface (Barry, 1992; Matthias, 2004).

The diurnal lapse rate records from 3 hourly mean data suggests that AWS3 recorded shallower lapse rates during the day than AWS1 (Figure 4.9). The lower and upper diurnal lapse rates also appear to have a inverse relationship, when the upper lapse rate is at its shallowest the lower lapse rate is at its steepest.

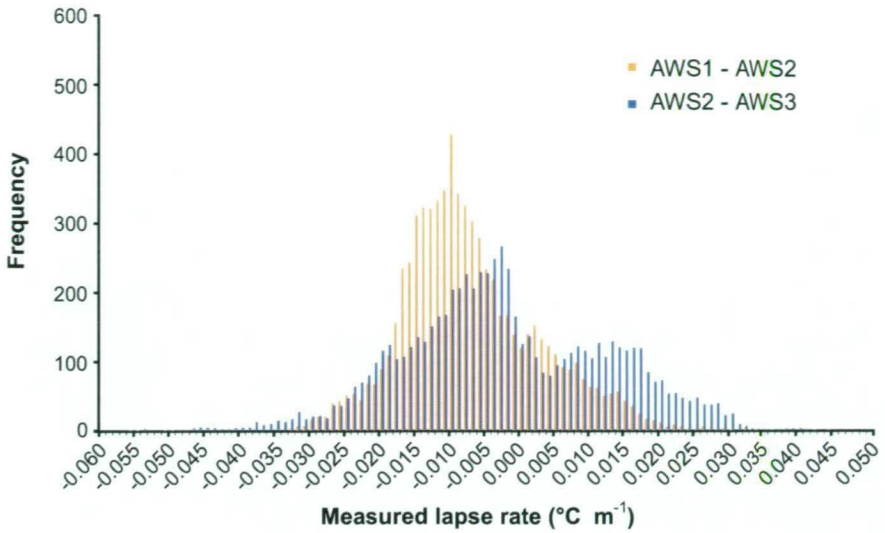

Figure 4.8.: Frequency distribution of ten minute lapse rates calculated from the temperature records between AWS1-AWS2 (115 to 550 m asl) and AWS2-AWS3 (550 to 920 m asl).

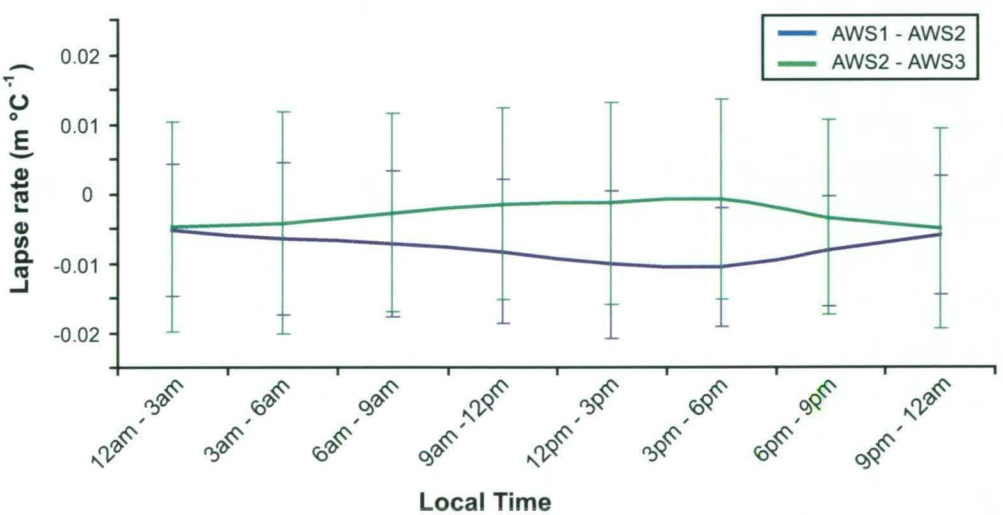

Figure 4.9.: The average and standard deviation of three hour (LST) lapse rates between AWS1 - AWS2 and AWS2 - AWS3.

4.4.4. Föhn wind activity in mountainous regions

A *foehn* or *föhn* wind is a warm, dry, down-slope wind descending the lee side of the European Alps as a result of synoptic-scale, cross barrier flow over the mountain range (AMS, 2000). A typical föhn wind is produced from moisture loss due to orographic lifting on the windward side and the compression of air as it descends on the lee side of the mountain range (Sturman and Tapper, 1996).

This process of föhn wind development is unlikely for Heard Island as winds of greater than 60 m s^{-1} would be necessary to create the kinetic energy to reach the top of the Big Ben caldera (Thost and Allison, 2006). Although winds of this magnitude have been recorded on Heard Island there are more instances of föhn wind events than high wind events. Thost and

Allison (2006) propose that föhn winds on Heard Island are more likely to be the result of standing wave motion forcing air from higher levels to descend (e.g. Barry and Chorley, 1976). The winds that pass over the top of Big Ben are at higher speed as they do not encounter the barrier of Big Ben to slow them down, creating standing waves on the downwind side of Big Ben. As wind velocity increases it becomes more likely that turbulent downwind flow will occur, causing the high level winds to descend to ground level and be transported in strong down draughts. As the air descends it warms at the dry adiabatic lapse rate, resulting in a higher temperature than the surrounding atmosphere.

Föhn winds are an important aspect of the climatic conditions on Heard Island. The high temperatures recorded at Spit Bay and Brown Glacier indicate that föhn winds would play an important, although unquantified part in the mass balance of Heard Island's glaciers (Truffer et al., 2001; Thost and Allison, 2006). These high temperatures also influence the mean temperature calculations for the eastern meteorological stations on the island.

Föhn winds are recognisable by a sharp increase in temperature and wind and a decrease in relative humidity (Brinkmann, 1971). This change in synoptic condition occurs over short time periods (Boon and Sharp, 2001; McGowan et al., 2002).

In this study, a föhn wind event on Heard Island was defined as an abrupt temperature rise, a coincident increase in wind speed, and decrease in relative humidity (where records were available). In addition, due to the orientation of Big Ben and its role in föhn wind development, the direction of the surface winds were also examined.

There have been several reports of warm temperatures on Heard Island at both Atlas Cove and Spit Bay but not all of these are related to föhn winds. The Atlas Cove, Spit Bay, Brown Glacier and coastal warm events are examined separately:

Atlas Cove The available meteorological records for Atlas Cove between 1948 and 1954 provide inconclusive information on the likelihood that föhn wind events occur at this windward site. There are nine measurements of high temperatures ($\geq 10°$ C) at Atlas Cove but only one had a corresponding low relative humidity ($< 50\%$) and all of these high temperature events occur during WNW, W or WSW winds (Figure 4.10). Example B in Figure 4.10 was the only period found that had both an increase in temperature and a decrease in relative humidity. On the 14 January 1954 at 14:00 LST the temperature was 6.1° C, the relative humidity was 70%, and the winds were from the SW at 25 kts. By 17:00 the temperature had increased to 10° C, the relative humidity had dropped to 20% and the winds had swung to the W at 19 kts. Three hours later the winds were still from the W but had decreased in strength to 12 kts and the temperature had dropped to 4.4° C and the relative humidity had risen to 91%. This six hour period was during the tail end of a high pressure system (peaking at 1011.5 hPa at 2:00 on 14 January) that had crossed the island from the SW. Further these westerly winds are not likely to have produced a föhn wind due to the low altitude of Laurens Peninsula (716 m asl), which is not high enough (nor were the winds strong enough) to generate a föhn wind.

The air temperature measurements for Atlas Cove from April 1997 to August 2006 have 13 instances, over 10 days, when the temperature was $> 10°$ C. These high temperatures correlate with high air pressure measurements, as indicated in more detailed examples in Figure 4.11.

Hence, it is concluded that the majority of high temperature events at Atlas Cove are due to warm synoptic events, which is supported by coincident high air pressure measurements.

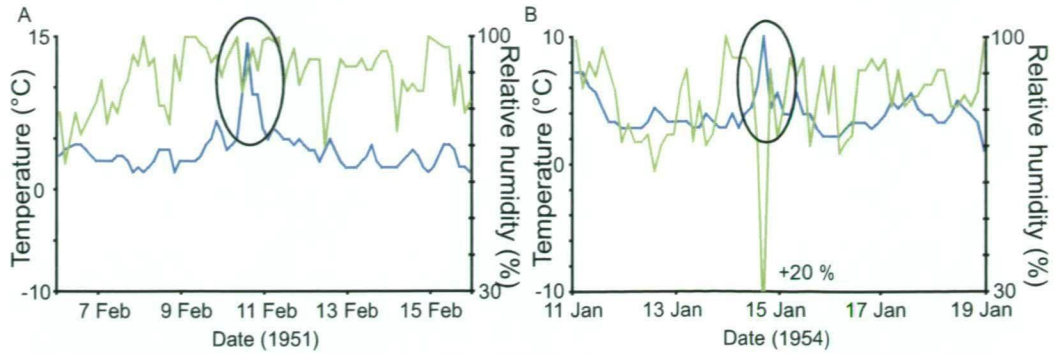

Figure 4.10.: Two detailed plots (A and B) show an increase in temperature but no corresponding decrease in relative humidity (**A**) and the only period found when there was both an increase in temperature (blue) and decrease in relative humidity (green) (**B**). Note the two different temperature scales.

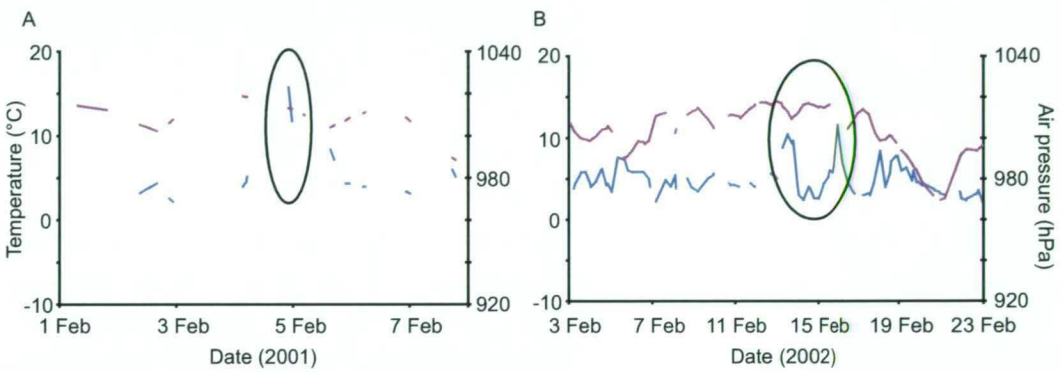

Figure 4.11.: Temperature (blue) and air pressure (purple) measurements at Atlas Cove. Two detailed plots (**A** and **B**) both show that higher temperatures (> 10° C) correlate with high air pressure measurements.

No matter the cause of these warm events they will be a significant contributor to the surface ablation on the northeastern side of the island.

Spit Bay There are no relative humidity nor recent (1997-2007) wind speed and direction measurements for Spit Bay making the classification of föhn wind events difficult. In addition, temperature and wind measurements from April 1992 to March 1993 at Spit Bay were only recorded once a day. Therefore the maximum temperature recorded for that period is unlikely to be coincident with the air pressure and wind direction measurements.

Despite these limitations it is possible to infer that föhn wind events occur at Spit Bay. This is based on over 300 measurements of temperature over 10° C, including 10 that are > 20° C from the two combined data sets. It is probable that many of these warm temperature records are of föhns despite the lack of supplementary relative humidity or wind data. Figure 4.12 shows two examples of high temperature records at Spit Bay that are from a warm synoptic system passing over the island or a föhn wind.

The possibility that there are frequent föhn winds at Spit Bay is also supported by the observation of standing waves and föhn walls above Spit Bay. A föhn wall cloud forms over a ridge or isolated peak when the air is forced to ascend raising the air to the saturation level, often the cloud appears as a wall with fibrous elements dissipating downward from the peak (Barry,

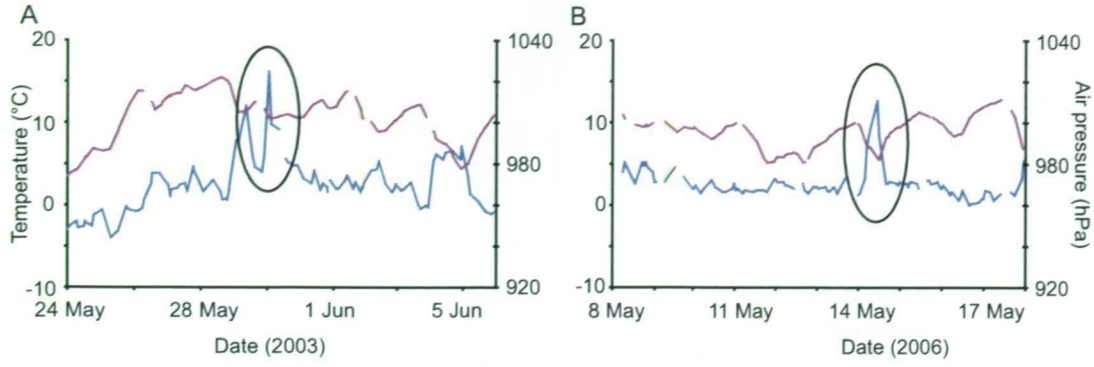

Figure 4.12.: Temperature (blue) and air pressure (purple) measurements at Spit Bay. The two plots (A and B) indicated that the higher temperatures > 10° C at Spit Bay are probably from a combination of (**A**) high pressure events and (**B**) föhn winds.

1992). These cloud features have been observed at on the eastern side of Heard Island most recently by Truffer et al. (2001) in November 2000.

Brown Glacier The BG AWS has the longest temperature and relative humidity records of the various AWSs in the Brown Glacier region. BG AWS also recorded wind speed and direction. These sensors only worked for a short time, followed by intermittent measurements before failing three months after the AWS was installed. Hence föhn winds were identified from the temperature and relative humidity measurements. There are 31 periods of föhn conditions when the temperature was > 10° C and relative humidity was < 60% and two additional periods when temperature was high, relative humidity was low and there was an increase in wind speeds. The duration of the föhn conditions measured at BG AWS ranged from a single measurement to 58 hours from the 11 to 13 February 2002. Föhn winds also occur at lower temperatures, these are more evident in winter when the average temperature is much lower to begin with.

The shorter temperature, relative humidity and/or wind data sets from the BG35, AWS1, AWS2 and AWS3 also recorded föhn winds. Truffer et al. (2001) reported that there were two föhn winds while BG35 AWS was in place. The first on 4 November and the second on 25 November when temperature was above 0° C for 10 hours and the wind direction measured at BG AWS at the same time indicated that the winds were directed preferentially down valley. There may be three additional föhn winds over the 28 day period the AWS was in operation, on the 29 October, 31 October and 6 to 7 November each of these periods had both an increase in temperature and wind speed.

During 2003/04 all three of the AWS recorded föhn winds. One example of a föhn wind and how it propagates down Brown Glacier is illustrated in Figure 4.13. This figure shows föhn winds that occurred over the 9 and 10 January 2004. At AWS3 the high temperature (> 5° C), high winds (> 20 m s^{-1}), and low relative humidity values were evident from 9 January at 9:10 LST until 10 January 8:50. The winds during this period were predominately from the SW. At AWS2, 400 m lower on the glacier, there was an increase in temperature (> 10° C) and an increase in wind speed from 9 January at 22:10 to 10 January at 13:50. At AWS1, near the terminus of the glacier, high temperature (> 10° C) and low relative humidity values were measured, however the wind speed was not high (< 10 m s^{-1}) and the wind direction was

variable from 9 January 23:00 to 10 January at 18:00. The differences in the timing of the event has an error of up to one hour based on where it was estimated that the change began and finished.

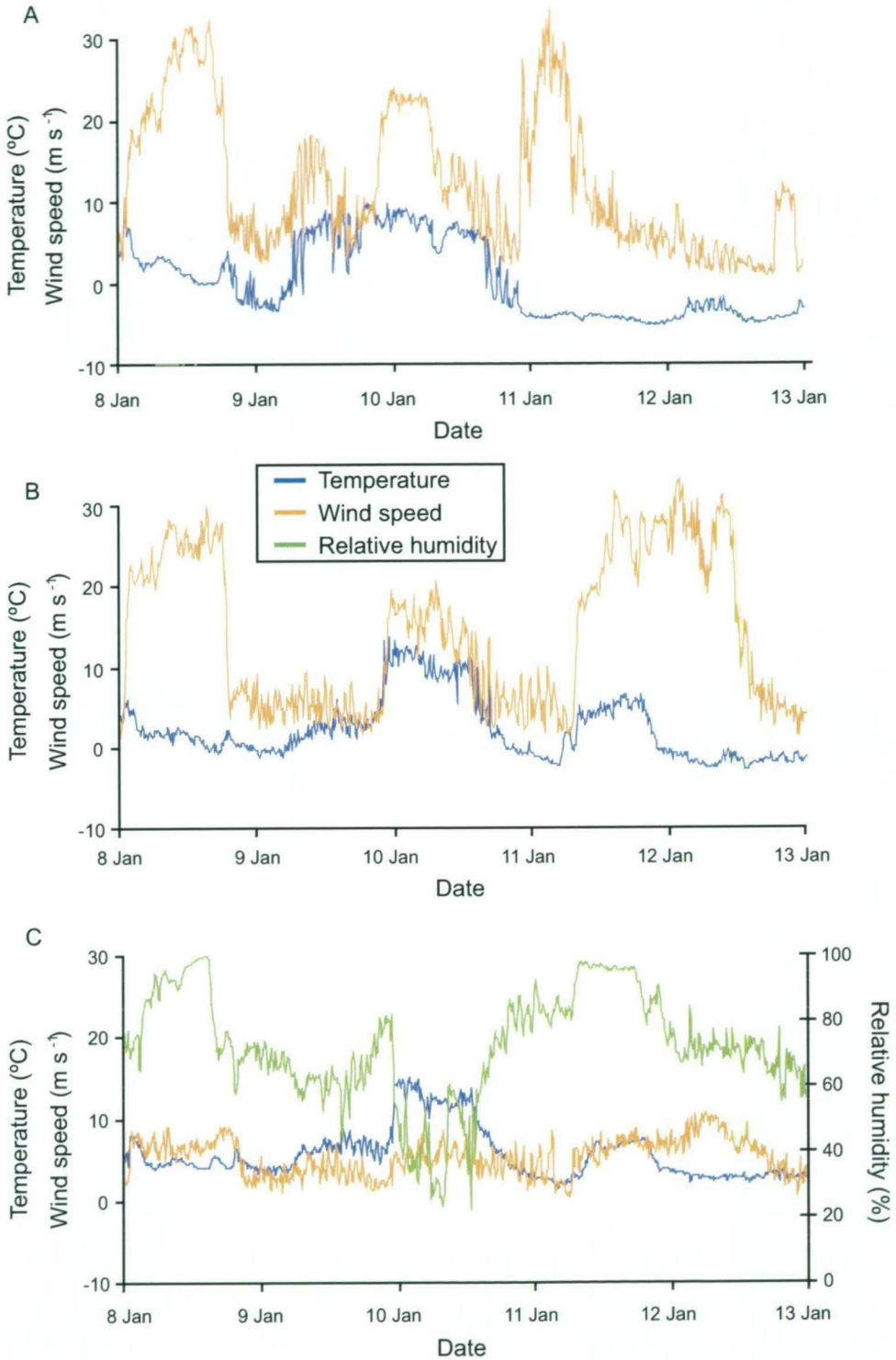

Figure 4.13.: A föhn wind recorded on Brown Glacier during the second field season at all three AWS on 9 to 10 January 2004: **A**. AWS3, **B**. AWS2, and **C**. AWS1.

There were several other föhn winds measured at both AWS2 and AWS3, e. g., 26 December, 4 January, 2 February and 5 February. Some föhn winds were only measured at AWS3, e. g.,

17 January. These differences show that föhns can be an isolated event and may not propagate down a single glacier valley.

Coastal sites At Capsize Beach, located on the southeast coast, there were seven days with föhn wind conditions, however two of these may not have been a föhn wind due to persistent high temperatures, followed by a drop in relative humidity, then an increase in relative humidity while temperature stayed elevated.

At Doppler Hill, also on the southeast coast, there were 21 days when the temperature was close to 10° C and relative humidity between 50 and 60%. Indicating that there could have been up to 21 instances when föhn wind conditions occurring at Doppler Hill. There were 6 periods where föhn wind conditions occurred over two successive days, however the relative humidity increased to ~ 100% at night and temperature dropped a few degrees, except from 19 to 20 December, therefore it is uncertain, with the available data, if these are two separate föhn winds or one continuous one. The longest period where föhn conditions persisted, at Doppler Hill, began on 19 December at 1:00 LST and continued until 20 December 2003 at 16:00. Over this 39 hour period the relative humidity remained between 50 and 60% and the temperature ranged from a high of 15.1° C at 10:00 to a low of 3.6° C at 4:00.

Capsize and Doppler are in close proximity (within 6 km) of each other, yet there does appear to be a difference in the frequency and length of föhn winds. There were four föhn winds that were measured at both sites during 2003/04 on the 19 December, 3 January, 18 January and 5 February. All of the föhns at Capsize were for shorter periods then at Doppler. This difference may be due to localised topography and the difference of wind direction at each station.

At Jacka Valley it is difficult to make any conclusive remarks about föhn activity without any wind direction data. However there are two periods from Jacka Valley that may represent a föhn wind. The temperature and precipitation records for the 3 February and 18 February were compared to the air pressure measurements from Atlas Cove over the same period, these conditions occurred as a high pressure system of 1005 hPa and 1007 hPa, respectively, crossed the island. Therefore it is assumed that Jacka Valley, like Atlas Cove, is not likely to have any föhn winds.

4.5. Conclusions

Meteorological records for Heard Island are infrequent and sporadic yet they do provide data from which a broader understanding of the island's climate can be inferred. The 1947 to 1954 Atlas Cove synoptic records have provided the most complete records of the climate on Heard Island. The additional records from short summer expeditions and a few, mostly isolated annual records from around the island provide snap shots of the climate. The combination of all available data sets provides a basic understanding of the changes that have occurred across the island.

The orographic variability caused by the Big Ben massif affects the distribution of temperature, precipitation, and winds across the island. Atlas Cove tends to have lower temperatures, lower measured precipitation, and no föhn wind events compared to Spit Bay.

The Atlas Cove records have shown that there has been a ~ 1° C increase in temperature since the 1950s and that between 1947 and 1954 precipitation occurred on average 276 days

per year. The shorter Spit Bay records have indicated that the leeward side of Big Ben has a higher incidence of high temperature events than at Atlas Cove between 1998 and 2006.

The lack of annual temperature records between 1954 and 1980 leaves some room for interpretation. However based on the proxy temperature model (see Section 3.4.1) the temperature on Heard Island probably began increasing in the 1960s. These higher temperatures may be partially responsible for the increased retreat of Heard Island glaciers from 1960s to 1980s (see Section 2.4.1).

Difficulties arise when trying to compare the precipitation records from Atlas Cove and Spit Bay due to the nearly 50 year separation between records. Measurements of precipitation during 2003/04 (see Section 3.3.2) indicated that precipitation totals measured at the field camps were higher than the corresponding Atlas Cove monthly totals. The total January precipitation at Atlas Cove (1948 to 1954) was 139 mm compared to the total January 2004 precipitation at Jacka Valley of 299 mm (closest site to Atlas Cove), 190 mm at Spit Bay, 222 mm at Capsize Beach (on the southeast coast) and an impressive 483 mm at Brown Hut (lucky us!) (Thost et al., 2004). These records could suggest that that along with the 1992/93 precipitation records, that the precipitation on Heard Island has increased. However, when compared to the precipitation on neighbouring sub-Antarctic islands, which have a decreasing precipitation over the last ~ 60 years (see Section 3.5.2), it is concluded that the 2003/04 field season may have just occurred during a very wet January.

The above changes in the temperature and precipitation on Heard Island are both important influences on the mass balance of the local glaciers. Föhn winds also play an important but as yet unquantified role in the mass balance of Heard Island glaciers. Föhn wind effects have been shown to occur more often at higher elevations on Brown Glacier than lower elevations. These winds also predominately occur on the eastern side of the island due to the orographic effects of Big Ben. This high frequency of föhn winds would create a higher average temperature for the eastern side of the island, which are likely to influence lapse rate calculations especially on the upper glacier.

The lapse rate for Heard Island was calculated from 1950 radiosonde data from Atlas Cove. A more detailed, lower elevation lapse rate was also calculated for Brown Glacier from the air temperature data at AWS1, AWS2 and AWS3. The resulting lapse rate for Brown Glacier was $-0.003°\,C\,m^{-1}$ from 920 m to 550 m and $-0.008°\,C\,m^{-1}$ from 115 m and 550 m.

5. Brown Glacier morphology, dynamics and mass balance

5.1. Introduction

Previous chapters have shown that the glaciers of Heard Island have been retreating and/or thinning for at least the last 50 years due to changes in the regional climate. To better understand the processes of glacier change on Heard Island, a 'benchmark' glacier was chosen based on its geometry and logistical characteristics (from parameters suggested by Kaser et al. (2003)).

Brown Glacier, located on the northeast coast of Heard Island (Figure 5.1), is 4.8 km long with an area of 3.77×10^6 m^2 (in 2004). Brown Glacier has a simple geometry of one relatively well defined accumulation area and one tongue. Its size is neither too small, where local climate effects could dominate and the relative surface area to volume change would be to big, nor too large, which would increase logistical difficulties. Brown Glacier's surface is relatively smooth and uniform though there are large crevassed areas below 250 m asl, which make access to the lower glacier difficult late in the ablation season. In contrast to the majority of the other glaciers on Heard Island there is easy access to the glacier, which is important when considering the number of equipment loads and visits to the survey sites. Weather conditions were also considered. Brown Glacier, located on the northeastern coast, is in a region that has more fine weather days, a fairly predictable wind direction, and easy and safe exit points from the glacier if visibility were to deteriorate rapidly. Brown Glacier is also relatively debris free therefore should have a less complicated interpretation of the glacier's sensitivity to climate change.

Brown Glacier flows in a northeast direction extending from an elevation of ~ 1100 m to 80 m asl terminating above Brown Lagoon, which had an area of 0.42 km^2 and an estimated volume of 1.3×10^7 m^3 (in 2004). The extent of the 2004 glacier and lagoon is dramatically different when compared to the first known photograph of Brown Glacier, taken in 1947, showing the glacier terminating in the sea and filling its basin to just below the top of the lateral moraines (Figure 5.2A). Since 1947 each subsequent observation of the glacier has shown a substantial retreat of the terminus and a general thinning of the glacier, which has continued to present (January 2006 is the last clear satellite image available of the glacier).

By 1963, the glacier had retreated more than 100 m from the coast, the ice cliffs had disappeared, and broad pebble beach had formed separating a small lagoon from the sea (Figure 5.2B). By 1971, the glacier had retreated an additional 350 m inland and was terminating into a proglacial lagoon. There was a land vegetation survey during the summer of 1986/87 around the moraines of Brown Glacier. Observations indicate that there was possibly a very small beach in front of the glacier but some sections may still have been floating in the lagoon. Field parties did not walk in front of the glacier but instead found alternate routes to traverse the shore (J. Scott pers. com., 26 October 2006). The next aerial survey, during the summer of 1987/88, was in conjunction with vegetation studies. These photographs showed that Brown

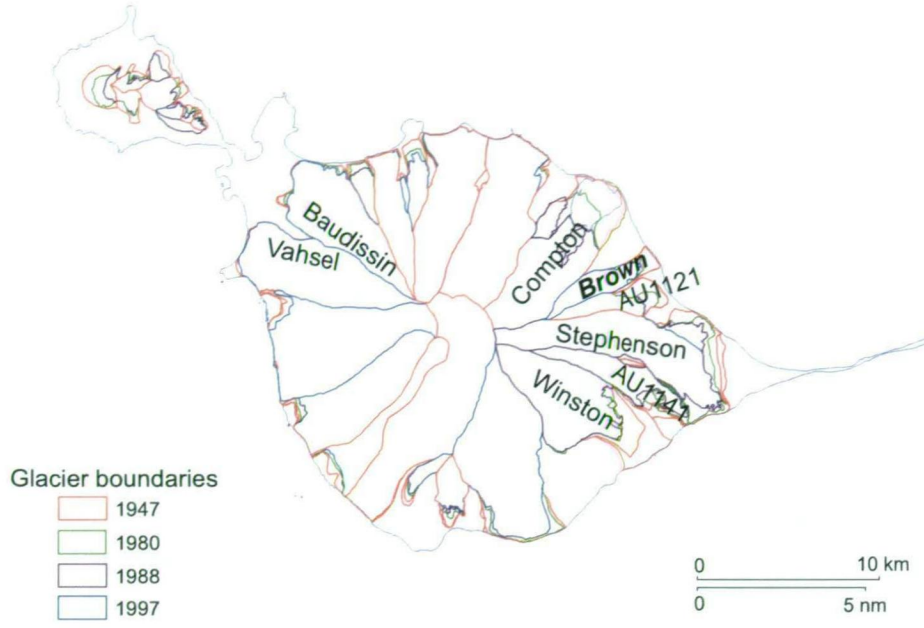

Figure 5.1.: The location of the Baudissin and Vahsel glacier both of which were part of earlier mass balance surveys on Heard Island, and the location of Brown Glacier and its neighbouring glaciers. Map adapted from AAD Data Centre, map catalogue #12817

Glacier had continued to retreat along its lateral margins and the lagoon had grown in size (Figure 5.2C). In 1990, another aerial survey shows that the Brown Glacier was narrowing along its lateral terminus but the tip of the snout was still abutting the lagoon terminating on a small beach (Figure 5.2D). By 2000, the glacier had retreated further from the lagoon (Figure 5.2E). This retreat continued to 2004 with more channelled bedrock being exposed (Figure 5.2F).

Most recently satellite images of eastern Heard Island have shown that there was a continued retreat of Brown Glacier terminus of 108 m^2 between the 17 January 2003 and 30 January 2006 Digital Globe Multi Spectral Images (see Appendix B.2).

This chapter examines the two field seasons that Brown Glacier was surveyed, the first was from November 2000 to January 2001 (2000/01) and the second was from the end of December 2003 to mid February 2004 (2003/04). These two surveys represent the most comprehensive measurements and observations of any glacier on Heard Island to date.

There are only two reported surveys of Heard Island glaciers preceding the Brown Glacier surveys. One was on the Baudissin Glacier in 1948 (Lambeth, 1950) and the other was on the Vahsel Glacier in 1971 Allison (1980). There are also unpublished velocity and ablation measurements on Vahsel Glacier during the summer of 1986/87 by P. Keage (A. Ruddell unpub data, 23 November 2001) and unpublished velocity and net balance measurements on Brown Glacier from 1992 to 1993 by Vrana and Ruddell (unpub).

The initial survey of Brown Glacier was developed by A. Ruddell and described in Truffer et al. (2001). The goal of the study was to characterise one of Heard Island's glaciers that had a relatively simple geometry and was easy to work on. The field plan included collecting data on the dynamic characteristics, mass balance, sub-glacial topography and recent fluctuations of Brown Glacier. Once the data was collected it was to be used to construct and validate a numerical model of the glacier (e. g., see Chapter 7).

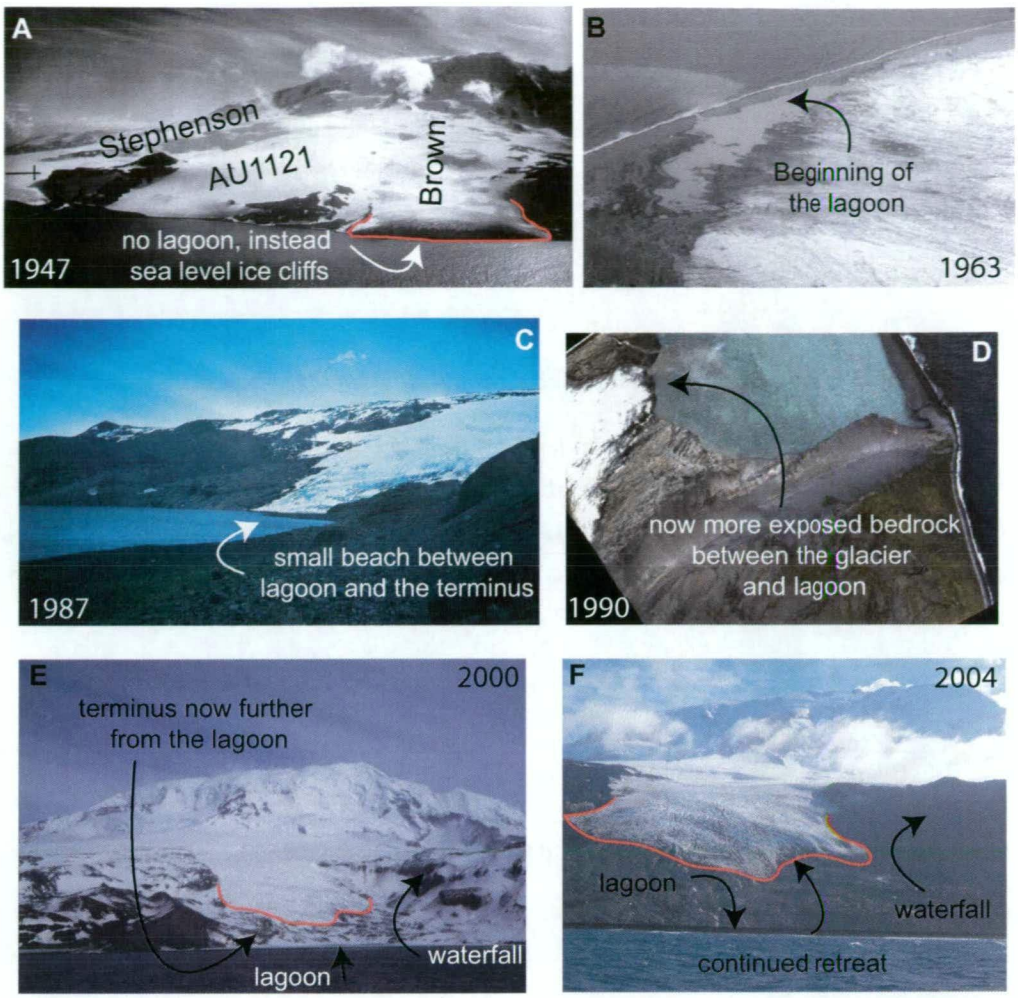

Figure 5.2.: A photographic compilation of the frontal changes to Brown Glacier between 1947 and 2004. Most of these photographs were taken on an opportunistic basis and therefore are not from the same orientation. Markers have been added to the photograph to help in distinguishing the changes in the glacier over time. Photo credits: **A**. RAAF, **B**. Budd and Stephenson (1970), Plate 5, **C**. J. Scott, **D**. AAD, **E**. D. Thost, and **F**. S. Donoghue.

This first survey of Brown Glacier was undertaken from the middle of October until late November 2000 by three glaciologist from AAD: Martin Truffer, Doug Thost and Andrew Ruddell, operating from a small field camp (Brown Hut) near the foot of the glacier. During 2000/01 the following field measurements were completed as listed in Truffer et al. (2001):

- A differential Global Positioning System (DGPS) survey of the surface elevation along the centreline of the glacier and across five transverse sections
- A DGPS survey of the location of the present terminus and the 1947 moraines
- Bathymetric measurements of Brown Lagoon
- Detailed ice thickness measurements across a transverse profile of the glacier at 500 m, and spot radar measurements of ice thickness across three other profiles
- Surface velocity measurements along the centreline of the glacier (10 locations) and along two transverse profiles at 500 m and 400 m asl. Most of these sites were measured

over two epochs, and time varying velocity measurements were made for nearly four weeks at one site

- Surface mass balance measurements during November at the location of all the velocity measurements (other members of the Heard Island 2000/01 field season made additional measurements in mid-January)
- Temperature and density measurements, and snow sampling from a snow pit and a crevasse
- Detailed meteorological measurements from a temporary AWS (see Chapter 4).

The second field season 2003/04 was undertaken from late December 2003 until mid February 2004 by Doug Thost (AAD), Martin Truffer (University of Alaska, Fairbanks) and Shavawn Donoghue (UTAS). This second season, coordinated by D. Thost, was planned as a continuation of the first survey. The measurements made during this second season included (as listed in Thost et al. (2004)):

- Resurvey the glacier surface and terminus using DGPS
- Establish and resurvey the centreline from 2000/01 survey with the addition of several transverse profiles on the upper glacier
- Determine ice thickness at 750 m and 680 m asl, to supplement the 500 m asl profile from the first season
- Deploy three AWS (see Chapter 4)
- Collect ice cores from the surface of the glacier and ice samples from crevasse walls for oxygen isotope and trace ion chemical analysis (see Chapter 6)
- Deploy two sonic rangers to measure the diurnal variations in surface net balance
- Resurvey the bathymetry of Brown Lagoon, and survey Stephenson, Compton and Winston lagoons
- Measure outflow from Brown Lagoon.

5.2. Field methods

The field plans listed above revolved around the location of a stake network that was deployed on Brown Glacier. The distribution of stakes was along the approximate central flowline from Brown Glacier site 05 (BG05), approximately 500 m from the head of the glacier, at ~ 500 m intervals to Brown Glacier site 50 (BG50) near the terminus. With additional stakes at transverse profiles which varied between the two surveys.

In the first field season, twenty 2.5 m bamboo canes were deployed on Brown Glacier from 23 October to 25 November 2000 (Figure 5.3). At the end of November all but the longitudinal stakes were removed (BG05 to BG50) to meet environmental guidelines.

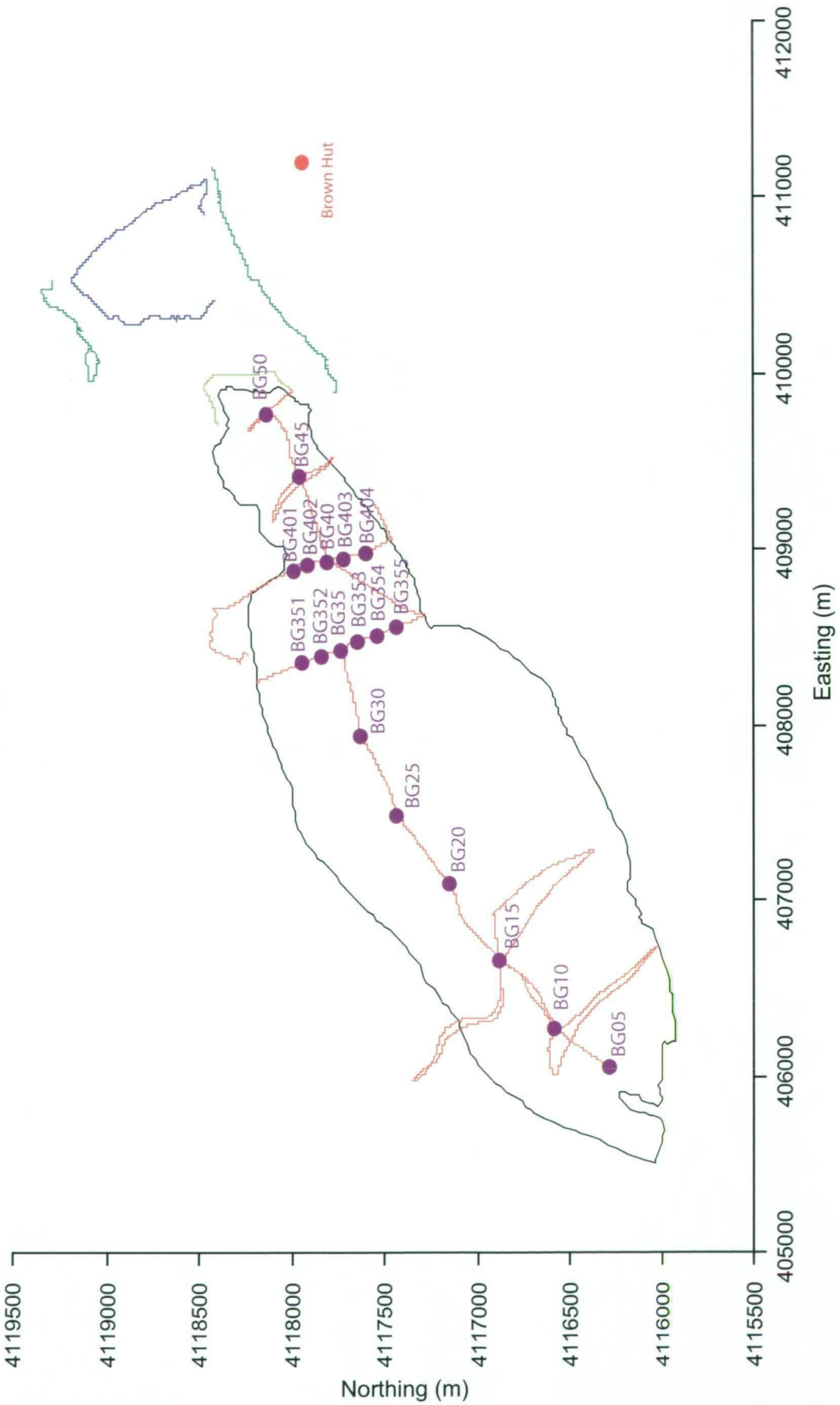

Figure 5.3.: The stake network and kinematic DGPS survey lines for the 2000/01 survey. The red lines indicate the survey lines on the glacier surface, the green lines are the moraine crests and terminus survey, the black line is the outline of the glacier as described in Section 5.3.1, the purple dots mark the location of the net balance stakes, and the blue line is the outline of the lagoon. The lagoon outline is not complete due to steep cliffs along the southern shore line.

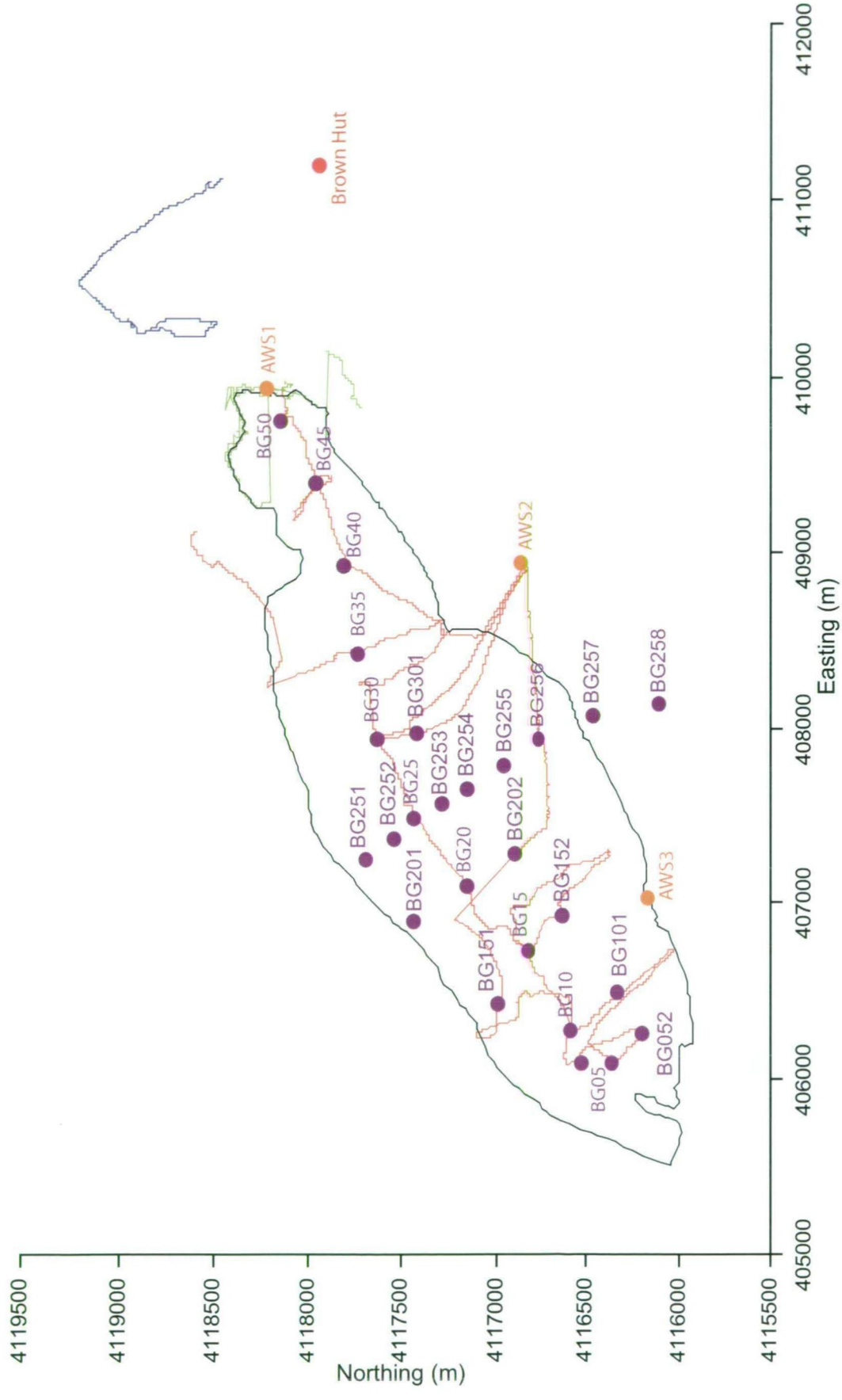

Figure 5.4.: The stake network and kinematic DGPS survey lines for the 2003/04 survey. The red lines indicate the major survey lines on the glacier surface, the green line is the terminus position (and a nearby rock outcrop), the purple dots mark the location of the net balance stakes, the blue line is the lagoon shore line, and the black line is the outline of the glacier as described in Section 5.3.1.

In the second field season, from 21 December 2003 to 17 February 2004, twenty-six 2.4 m fibreglass stakes were deployed (Figure 5.4). This was a period of high melt which necessitated frequent trips to the stakes to ensure that they had not melted out of the glacier. The stakes were placed along the same central flowline (BG05 to BG50) as in the first season, however the BG35 and BG40 transverse profiles were not repeated, instead five additional transverse profiles were deployed between BG25 and BG05 (Figure 5.4).

The stakes were then used as navigational points for the DGPS survey of the glacier surface, the ice radar data was collected along two of the net balance stake transverse profiles, the surface net balance was measured at each of the stakes, the stakes were used as reference points for the ice core and crevasse sampling. Additional survey of the glacier and surrounds included a measure of the lagoon bathymetry and the deployment of several AWS.

5.2.1. Differential GPS surveys

A Leica global positioning system (GPS) base station was set up on a rock outcrop near Brown Hut, at 53°04' 50.6748" S 73°40' 28.3220" E, during 2000/01 and reoccupied in 2003/04 (Figure 5.5). A roving automatic digital Garmin or Leica GPS was set to read at five second intervals was carried to record the glacier survey routes, the terminus position, surrounding rock outcrops and any other features of interest (Figure 5.3 and 5.4). The DGPS data was recorded at five second intervals and processed using the Leica Ski-Pro software (Thost et al., 2004). The GPS antenna was fixed to the surveyor's backpack. The estimated uncertainty in vertical position is ± 0.15 m (Thost and Truffer, 2008).

GPS measurements on Brown Glacier include a kinematic survey of the surface, which was undertaken in November 2000 and repeated in January 2004. The two surveys followed the same longitudinal profiles, however not all of the original survey lines were repeatable due to highly crevassed areas especially along the northern margin of the survey line. The terminus of Brown Glacier was also surveyed in November 2000, December 2003 and February 2004 in conjunction with surveys of the lagoon shoreline in November 2000 and December 2003.

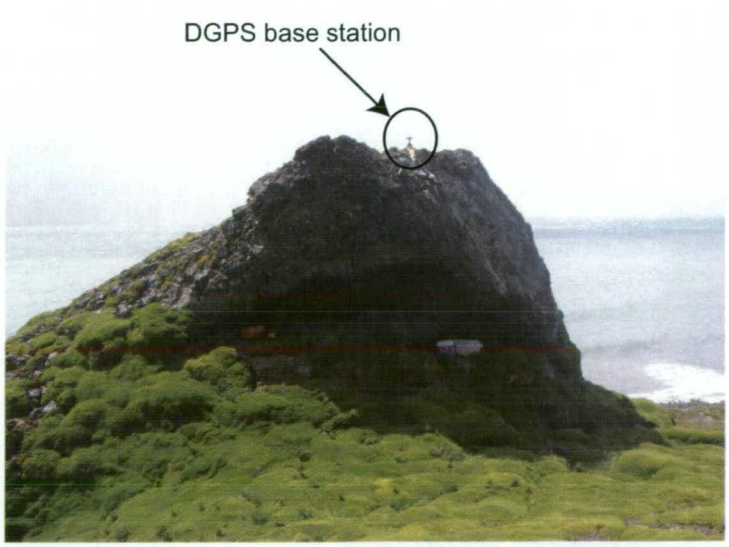

Figure 5.5.: The DGPS base station location near Brown Hut (photograph taken in 2004).

Static GPS measurement were made of the 20+ stakes during both field seasons to measure the surface velocity (errors of $\pm 0.003\,\mathrm{m\,d^{-1}}$ for the shortest epoch) (Table 5.1). Each epoch was intended to be approximately one to two weeks long. Repeated failure of the DGPS equipment at the beginning of the second season resulted in an extended January epoch. Happily these problems were remedied by the end of the field season.

Table 5.1.: Length of velocity measurements intervals for both field seasons.

	Dates	Average number of days between measurements
2000/01		
Early November interval	27-28 Oct. to 7-9 Nov.	8.9
Late November interval	7-9 Nov. to 21-22 Nov.	10.1
2003/04		
January interval	22-28 Dec 203 to 20-26 Jan 2004	30.5
February interval	20-26 Jan. to 9-12 Feb.	16.8

Additional static DGPS measurements were made in the second season near the BG50 stake, in the ablation zone, to measure the diurnal surface velocity variations. Six-hourly measurements began on 30 December 2003 and concluded on the 8 February 2004.

5.2.2. Lagoon bathymetry

The first bathymetric survey of Brown Glacier was conducted under difficult conditions from a small inflatable boat with no motor by M. Truffer and D. Thost in 2000/01 (Truffer et al., 2001). Depth measurements were made using a weighted line and the location recorded with a hand held Garmin GPS. The maximum depth recorded was 52 m and the outline of the lagoon was determined from a kinematic GPS survey (see Section 5.3.1).

A more detailed bathymetric survey was conducted in the second survey of Brown Lagoon (150+ depth measurements compared to 20 measurements in the first survey), and additional surveys were made of Compton, Winston and the northern Stephenson lagoons (Figure 5.6). Depth from the surface of Stephenson, Compton and Brown lagoons were measured using an acoustic depth sounder (Garmin "Fish Finder") mounted on an eighteen foot Zodiac Inflatable Rescue Boat (IRB). The location of each measurement was determined using a hand held Garmin GPS V. At various locations the depth recorded on the Fish Finder was checked with a 30 m tape measure, and the accuracy was found to be within 1 m and $\pm 5\%$ for depths > 30 m. The Surfer (Golden Software, Inc) mapping program was used to create bathymetric maps from these survey points.

Winston Lagoon was surveyed twice: the first time on 21 January 2004 and the second on 15 February. There were some modifications made to our set up of the Fish Finder for these surveys as a smaller inflatable boat was used. Otherwise our methods were the same.

5.2.3. Ice radar

The ice thickness of Brown Glacier was measured using a portable low frequency radio echo sounding (RES) system built by Icefield Instruments, Inc. On Brown Glacier both 5 and 10 m

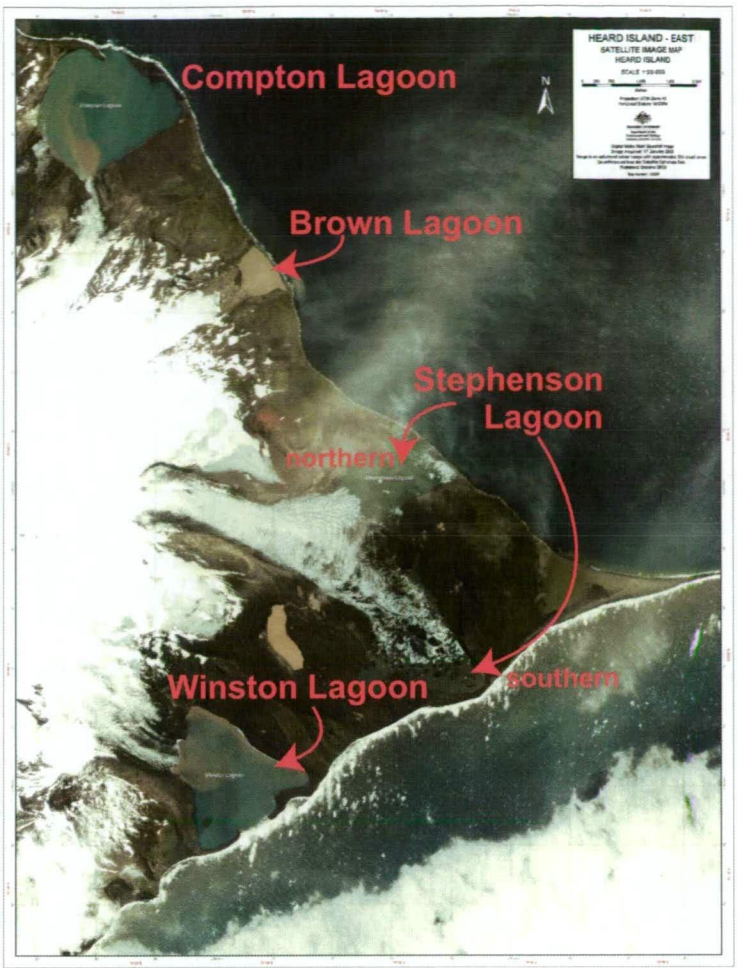

Figure 5.6.: Digital Globe Satellite image of the eastern lagoons in January 2003 (AAD Data Centre map number 13275).

dipole antennas were used, the length of which determines the frequency of the wave, 8.4 and 4.2 MHz respectively.

Numerous reflection points were acquired along lines tangential to the return ellipse which were used to define the glacier bed (Thost et al., 2004). The high frequency returns from the RES system were good despite problems sometimes encountered with small, steep walled glaciers (Welch et al., 1998), such as reflections in highly crevassed regions. To convert the travel time to ice thickness it is assumed that the radar travels through Brown Glacier ice at 170 m μs^{-1}, similar to other surveys (e.g., Copeland and Sharp, 2001). The reported thickness is within $\pm 10\%$. This difference is associated with density variation between ice and firn as well as reading the two-way travel time from the scope metre (Thost and Truffer, 2008).

Isolated ice thickness measurements were made at BG30, BG45 and BG50, and additional detailed ice thickness profiles were measured at BG35, BG25, and BG20 (Figure 5.3 and 5.4). The BG20, BG25, BG30 and BG35 profiles were in crevasse free areas providing a relative description of the bedrock topography, while the measurements at BG50 and BG45 were in crevassed areas resulting in very localised depth measurements.

5.2.4. Surface net balance

The surface net balance was measured from a combination of sonic rangers and surface net balance stakes.

Sonic rangers The surface height profiler used on Brown Glacier was a Campbell Scientific, Sonic Ranger SR50. The sonic rangers were erected on the glacier using aluminium bi-poles (Figure 5.7). The poles were revisited to ensure that the distance between the sensor and the snow surface was less than 10 m. The sonic rangers were set to measure the surface height every half hour with an accuracy of ±0.01 m. The measurements were corrected for the variance of the speed of sound in air using temperature data from AWS1.

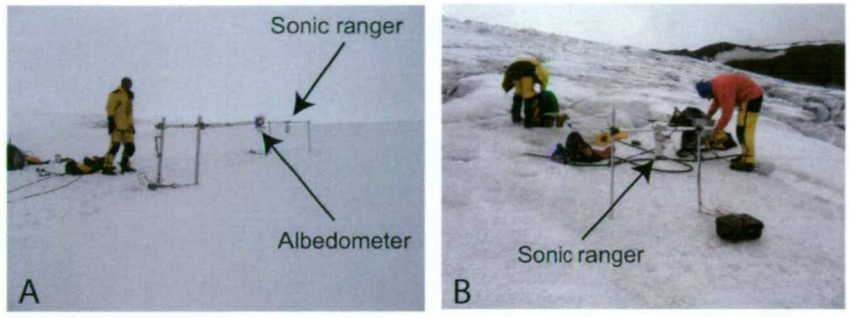

Figure 5.7.: Sonic ranger setup on Brown Glacier **A**. BG35-2004 sonic ranger is shown in the background with the albedometer in the foreground, and **B**. BG50-2004 (Photo D. Thost 2004) the sonic ranger is in the foreground with a GPS at the feet of the person to the left. The BG35-2000 set up is not shown.

Net balance from stake networks The most widely used method to measure the loss of solid ice to ablation is by a network of ablation stakes on a glacier. On Heard Island neither of the survey networks were left in place for a full season, instead the first survey began in early spring and finished in summer, and the second survey began in summer and finished in late summer.

In 2000/01, the height of the net balance stakes above the snow surface were measured to the nearest 0.005 m (estimated error ±0.01 m) on an opportunistic basis (e. g., in association with GPS surveys) every few days from 23 October to 25 November (Truffer et al., 2001) (Appendix D.1). Additional measurements of the longitudinal stakes were made on 12 January 2001, by P. Scott and A. Locke (Truffer et al., 2001).

In 2003/04, the height of the net balance stakes above the glacier surface was measured (to the nearest 0.005 m and an estimated error ±0.01 m) every few days during GPS surveys, ice radar surveys and en route to core and crevasse sampling sites (Appendix D.1). The stakes were measured between 23 December and 18 February.

5.2.5. Ice and snow sampling

In 2000/01, a 0.8 m snow pit was dug near the BG35 stake, ~ 100 m below the ELA (see Section 5.5.1), to measure snow density, temperature and collect oxygen isotope samples (Truffer et al.,

2001). Oxygen isotope samples were also collected from a crevasse wall at 1050 m asl on Brown Glacier (Truffer et al., 2001) (see Section 6.4 for crevasse location). Details on the results of the oxygen isotope analysis can be found in Section 6.7.7.

Additional oxygen isotope samples were collected in 2003/04 from two ice cores and three crevasses (see Section 6.4 for core and crevasse locations). These snow and ice samples were also analysed for trace ions and visible stratigraphy. Results can be found in Section 6.6.

5.2.6. Mobile automatic weather stations

Two AWS were deployed during the 2000/01 season, BG AWS and BG35 AWS. Three additional AWS were installed in the 2003/04 season. Details of operational period and instruments can be found in Section 4.2.

5.2.7. Meltwater survey

Measurements were made of water discharge from Brown Glacier melt streams and the lagoon outlet to investigate the total runoff for this glacier basin. The flux of the six meltwater streams and the lagoon outlet were measured on 31 December 2003 (Figure **??** and Table 5.2). The total flux from these six streams was $1.35\,m^3\,s^{-1}$ compared to the flux from the lagoon outlet stream of $1.48\,m^3\,s^{-1}$. There was a 9% difference between the lagoon outlet and the total flux from the six meltwater stream measurements, with more flux measured from the lagoon outlet then from the six streams.

Although this difference between the lagoon outlet and meltwater streams was 9 % it was assumed that the extra lagoon flux was from meltwater stored in the lagoon (lag effect). In order to make some comparison with total runoff for the summer from the lagoon outlet measurements only, it was assumed that the measured flux from the lagoon outlet and the six streams were similar enough to continue to only measure the lagoon outlet, five additional times throughout the summer. The lagoon outlet flux measurements provided an average flux over the summer of $3.33 \pm 2.14\,m^3\,s^{-1}$, resulting in a total runoff flowing through the lagoon outlet of $12.95 \times 10^6\,m^3$, over a 45 day measurement period.

5.3. Morphology of Brown Glacier

The 2000/01 kinematic surveys were the first detailed surface elevation survey of any Heard Island glacier. This survey followed the longitudinal stake profile with additional traverse profiles at BG50, BG45, BG45, BG15 and BG10. This survey measured the glacier surface of the northern margins of the glacier which were inaccessible in 2003/04. There were a total of 684 coincident points between the two surveys (Figure 5.3 and 5.4) (Thost and Truffer, 2008). Additional coverage of the southern margins of the glacier were also surveyed in 2003/04.

The kinematic surveys from two season were used to develop a digital elevation model of Brown Glacier. With a digital elevation model, and hence the surface topography, established any change in the surface height between the two seasons could be calculated and the lagoon outline and terminus locations could be determined with more accuracy.

Table 5.2.: Cross-sectional flow rates for the Brown Glacier outlet streams on 31 December 2003 and the measured flux for the lagoon outlet stream on five additional days.

Date	Site	Cross-section area (m^2)	Width (m)	Av. flow (ms^{-1})	Max. flow (ms^{-1})	Flux (m^2s^{-1})
31/12/03	Stream 1	0.298	0.56	0.16±0.02	0.37±0.05	0.05
31/12/03	Stream 2	0.015	0.6	0.81±0.04	1.39±0.09	0.01
31/12/03	Stream 3	0.447	4.2	1.11±0.03	1.63±0.07	0.49
31/12/03	Stream 4	0.103	0.66	0.56±0.02	1.03±0.09	0.06
31/12/03	Stream 5	0.706	2.9	1.00±0.08	1.59±0.07	0.71
31/12/03	Stream 6	0.08	0.9	0.44±0.08	1.44±0.34	0.04
	Total Stream					**1.35±0.30**
31/12/03	Outlet	2.487	11.85	0.59±0.05	1.01±0.02	1.48
15/01/04	Outlet	4.019	13.7	1.37±0.11	3.63±0.11	5.52
23/01/04	Outlet	3.375	12.2	0.80±0.07	2.60±0.11	2.70
29/01/04	Outlet	2.586	12.8	0.58±0.02	1.83±0.05	1.49
7/02/04	Outlet	5.906	14.4	1.10±0.03	3.42±0.09	6.48
11/02/04	Outlet	3.818	13.7	0.61±0.01	2.01±0.06	2.33
	Av. lagoon flux					**3.33±2.14**

5.3.1. Mapping the glacier

An important part of the Brown Glacier survey was determining the present and estimating the 1947 boundaries of the glacier. The outline of Brown Glacier is difficult to distinguish at elevations above 550 m where the rock outcrops disappear and are replaced by a small ice field. On this ice field the boundaries between Compton and AU1121 glaciers from Brown Glacier are obscure, instead ice velocities and contour shape were used to define the ice divide between these three glaciers (Thost et al., 2004).

Contour maps were produced from RADARSAT images of the island and GPS surveys. The most recent map for Heard Island was published in 2004 by AAD (Ryan, 2004).

The first contour map and outline of Brown Glacier was defined using a DEM with a 50 m grid derived from RADARSAT data. A new 40 m grid DEM was developed in 2004 using the additional GPS points measured during the second survey (Figure 5.8A) (Thost et al., 2004). Thost et al. (2004) found that this new DEM improved the delineation of the ice divides and accompanying estimates of the glacier area and hypsometry. However they warn that at elevations above 400 m there are still some uncertainties in the glacier boundaries and therefore glacier area.

To reconstruct the 1947 Brown Glacier the lower contours were derived from the elevation of the lateral moraine crests and mapped in convex down glacier lines as is typical of ablation areas (Figure 5.8B). The upper glacier in 1947 was assumed to be very similar to the present (< 10 m in elevation difference). This is illustrated by comparing the 1947 aerial photographs and the RADARSAT image, which shows that the rock outcrop that AWS3 was located on in 2003/04 was of a similar size in 1947 (Thost and Truffer, 2008). The terminus was assumed to be a 20 m ice cliff located along the current seaward side of the lagoon spit as observed in the 1947 aerial photographs and surveyed in 2003/04. The 1947 Brown Glacier DEM was assumed to represent the glacier surface topography for the period between 1947 and 1954 during which observations indicated that the glacier remained relatively unchanged (see Section 2.4.1).

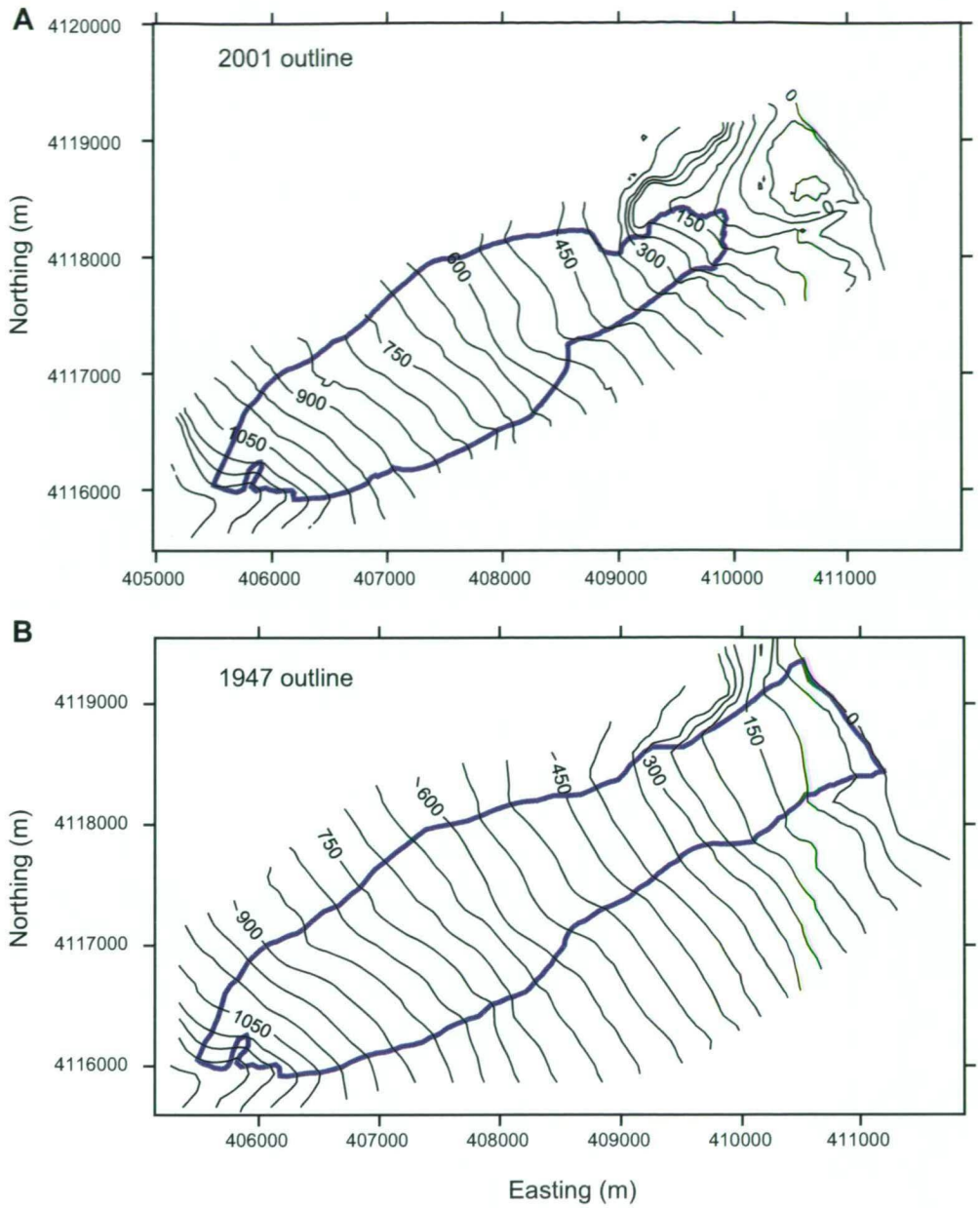

Figure 5.8.: The 1947 and 2001 outlines and contour maps for Brown Glacier.

5.3.2. Changes in the surface height and terminus

The elevation change between December 2000 and December 2003 was used to estimate the change in the surface height and calculate the total volume change on Brown Glacier by Thost and Truffer (2008). They divided the glacier into a grid and surface height changes were calculated at each point as a distance weighted average of all points within a 1000 m radius.

The surveys show that there has been a surface elevation change of the glacier by up to -11.7 m on the lower glacier with an average of -9.9 m below the BG40 survey stake, and -8.5 m on the upper glacier with an average of -5.9 m above the BG30 survey stake (Thost and Truffer, 2008). This is equivalent to an estimated loss of ice of $8.0 \pm 1.3\ 10^6\ m^3\ a^{-1}$. The error results from an estimated 0.4 m uncertainty in elevation from the correction between the January 2004 survey back to late December 2003, and an estimated error of 1.0 m from the

interpolation between the coincident points in each survey (Thost and Truffer, 2008). The DGPS errors are estimated at ±0.15 m range and are therefore negligible.

Thost and Truffer (2008) showed that over the long term (1947 to 2003) Brown Glacier has lost an average ice volume of ~ 3.1×10^6 a^{-1} and an estimated 29% of its original area. The total ice loss was calculated from both subtracting the 1947 DEM from the 2003 DEM and using the results from the bathymetric survey. They found that the lagoon area accounted for approximately 5% of the total ice loss. The ice volume over this period has decreased by ~ 1.743×10^8 m^3 ($3.06 \times m^3$ a^{-1}), which is equal to an average surface lowering of 28.2 m or 0.50 m a^{-1}. This is a minimum estimate as the ice volume loss was assumed to be zero at higher elevation on the glacier (>650 m). Thost and Truffer (2008) estimate this ice loss value could be underestimated by up to ~25%.

Additionally over the short term (2000 to 2003), a GPS survey was used to map the changes in the terminus position. Figure 5.9 shows the Brown Glacier terminus position on 23 November 2000, 31 December 2003 and 17 February 2004. Between 1947 and 2003 Brown Glacier has retreated a total of 1.2 km with an average retreat of the terminus of 20.3 m a^{-1} (Thost and Truffer, 2008). This retreat of the terminus is equivalent to the retreat rate from 1947 to 2003 of 20.9 m a^{-1} and from 1980 to 2003 of 20.6 m a^{-1}. This retreat rate across the lagoon would have been faster than on land, and likely to be disconnected from the climate signal.

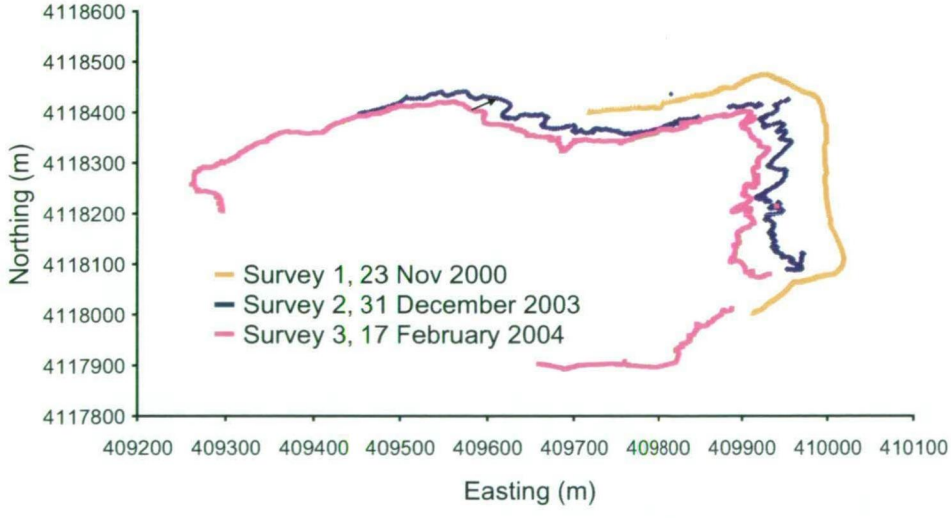

Figure 5.9.: Location of the 23 November 2000, 31 December 2003 and 17 February 2004 terminus positions of Brown Glacier. The 1947 terminus position (not pictured) was located further east along the seaward size of the present lagoon spit. (Adapted from Thost et al. (2004)).

5.3.3. Bathymetric maps

As the glaciers retreat inland proglacial coastal lagoons have been developing on the coastline of eastern Heard Island. Winston Lagoon was first observed during the 1947 aerial survey, with the other lagoons (Compton, Brown, and Stephenson) beginning to form in the 1960s and 1980s (Figure 5.6). These smallest and simplest of lagoons develop at the mouth of meltwater

streams (Bird, 1994) where moraines and sand bars along the coast act as barriers, which force the flooding of glacier carved valleys, abandoned by retreating glaciers. These simple moraine barriers tend to be breached from time to time by storm waves and glacial meltwater outflow only to be rebuilt by wave action. Most importantly, these lagoons are glacial features that preserve former glacier depth and help to estimate previous ice thickness.

The four main eastern lagoons were surveyed and a bathymetric map produced for each (Appendix D.2). These bathymetric maps are useful tools in interpreting the past ice thickness of the glacier. The maximum recorded depth from each lagoon provides a measure of ice thickness, assuming that there has been some sedimentation and/or erosion since the lagoon formed.

On 17 January 2004, the northern section of Stephenson Lagoon was surveyed. The maximum depth recorded was 113 m (Appendix D.2.1). There was some error in the acoustic depth sounder readings near the terminus due to reflections from submerged iceberg keels. These values were omitted from the bathymetric data.

On 3 February 2004 both the Brown and Compton lagoons were surveyed. The resulting bathymetric map of Brown Lagoon shows that the northern side of the lagoon was shallower than the southern side (Appendix D.2.2). Brown Lagoon was also the smallest and shallowest of all of the lagoons measured. Its maximum measured depth was 56 m, compared to ≥ 100 m recorded in the other three lagoons.

Compton Lagoon has a roughly symmetric bathymetry (Appendix D.2.3). The deepest measurements were made near the centre of the lagoon. Compton was the second shallowest of the lagoons with a greatest measured depth of 100 m. Compton Lagoon is open to the sea allowing more wave action to effect the glacier and resulting in increased retreat of the ice front. In addition the high sea water content and wave action in the lagoon has resulted in the lagoon staying ice free during the 1992/93 season compared to Stephenson Lagoon which was covered in ice (Green, 1993b).

Winston Lagoon has a more complicated bathymetry (Appendix D.2.4). A comparison with the bathymetric map produced by Kirkwood and Burton (1988) indicates that there has been no significant change in the lagoon over the last ~ 15 years. However there has been some change in the geometry of the lagoon due to the breach of the lagoon between March 2000 and December 2003, which resulted in the deepening at the breach channel by ~ 20 m.

These lagoon surveys indicate that the Compton, Brown and Stephenson glaciers were probably > 100 m thick in some parts of their ablation areas in the ~ 1950s based on moraine heights, aerial photographs and depth of the lagoon. The Winston Lagoon could have been as much as 200 m thick based on the 90 to 100 m lateral moraine heights, but it is more difficult to determine when the glacier reached the coast as the first aerial photographs show the lagoon fully formed, and breached, in 1947.

5.3.4. Ice thickness measurements

The lagoons provide an indication of the past ice thickness, while the present ice thickness was measured by RES. The majority of the RES traces depict bedrock that is less than 100 m below the ice surface. The maximum recorded ice thickness of 112 m was along the BG35 profile (Figure 5.10). This detailed profile also revealed a bedrock composed of two small parallel valleys separated by a subglacial ridge (Thost and Truffer, 2008) (Figure 5.10). This

subglacial ridge separates the lower glacier into a northern valley that terminates in a zone of slower moving ice above BG40 leaving only the southern valley to contribute to the glacier terminus. The cross sectional area of the BG35 profile is 6.02 ($\pm$0.24) 10^4 m^2.

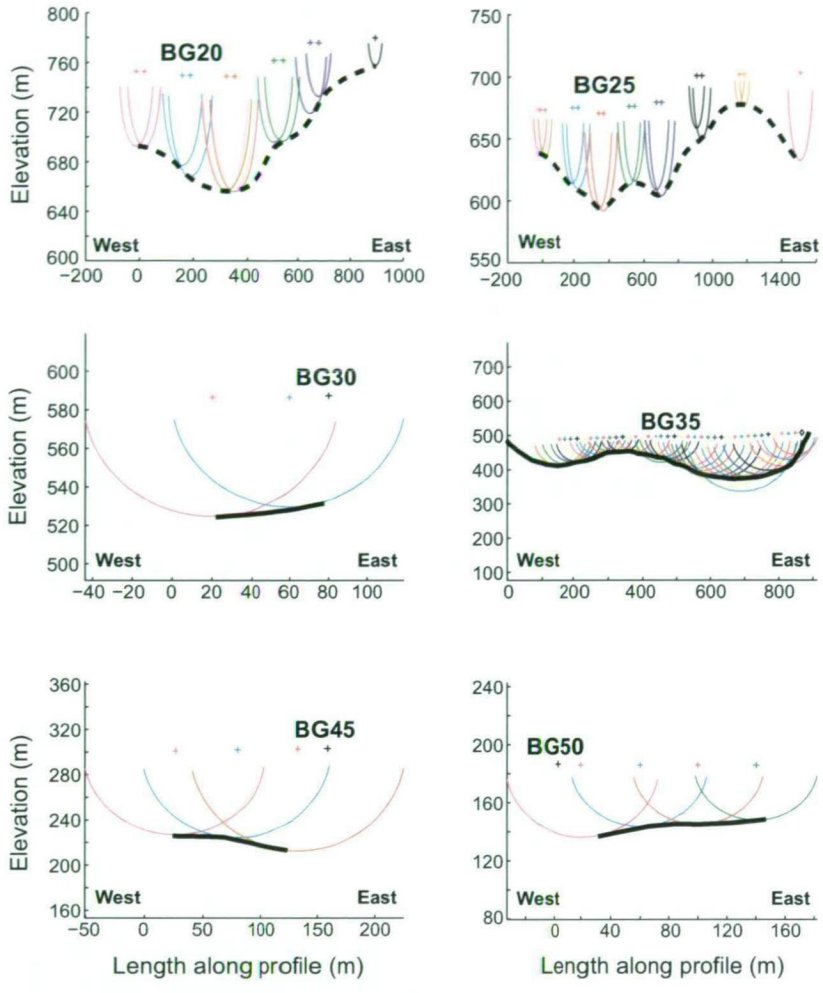

Figure 5.10.: Cross section RES profiles looking down glacier for all of the profiles. The 2003/04 bedrock outline are estimates only and shown as dashed lines.

Although the localised RES traces at BG30, BG45 and BG50 do not show as much detail as the BG35 profile they are useful for estimating average ice thickness along each profile of 58.8 m, 80.7 m and 41.8 m, respectively (Figure 5.10).

Comparatively, the more detailed BG20 and BG25 profiles, on the upper glacier, reveal more bedrock features (Figure 5.10). The southeastern margins of the RES traces show an ice divide between Brown and AU1121 glaciers. This is more evident in the BG25 profile than the BG20 profile. The BG25 trace also provides the first glimpse of the AU1121 glacier basin (Figure 5.10).

5.4. Surface velocity and mass flux

The ice thickness profiles at BG35, BG20 and BG25 can be used in conjunction with the surface velocity measurements that were measured during the two season to estimate the mass

flux through each cross section. The surface velocities can also be used to determine any seasonal changes and to look for diurnal variations in surface ice flow.

5.4.1. Surface velocity

The average surface velocity of Brown Glacier was calculated from DGPS measurements (Table 5.3 and 5.4). The surface velocities in 2003/04 averaged 0.101 m d^{-1} in the January interval and 0.069 m d^{-1} in the February interval, which is a change of 22.5% (Figure 5.11). Individual sites changed as much as 36% (0.101 to 0.071 m d^{-1} at BG25 and 0.042 to 0.027 m d^{-1} at BG256) (Thost unpub. data). In 2000/01, the surface velocities were closer in value with an average of 0.112 m d^{-1} in the early November interval and 0.103 m d^{-1} in the late November interval, which is an average difference of only 3.4% (Thost unpub. data).

Table 5.3.: Surface velocity measurements from the first field season. The sites are separated into the longitudinal profile followed by the two traverse profiles.

Survey site	Elevation (m)	Days in early November interval	Average velocity (m/d)	Days in late November interval	Average velocity (m/d)
2000					
BG05	1061	12.90	0.061	11.99	0.053
BG10	958	12.97	0.047	11.99	0.050
BG15	865	13.04	0.076	11.99	0.065
BG20	755	13.12	0.080	11.98	0.082
BG25	678	12.98	0.082	11.98	0.084
BG30	586	12.95	0.095	11.98	0.094
BG35	498	10.87	0.125	13.80	0.120
BG40	414	11.00	0.158	14.14	0.155
BG45	304	10.95	0.175	14.99	0.179
BG50	187	9.95	0.155	15.00	0.155
BG351	494			12.89	0.025
BG352	499			12.89	0.058
BG35	498	10.87	0.125	13.80	0.120
BG353	496			12.89	0.122
BG354	494			12.90	0.112
BG355	492			12.91	0.112
BG401	414	11.01	0.062	14.95	0.049
BG402	415	10.94	0.126	14.95	0.128
BG40	414	11.00	0.158	14.14	0.155
BG403	414	10.85	0.168	14.98	0.161
BG404	418	10.76	0.162	14.98	0.158

The greatest surface velocities measured for both seasons tended to be in the lower, steeper sections of the glacier (BG30-50). The highest velocity measured in either season was 0.179 m d^{-1} at BG45 in the first field season (Table 5.4). The measurements at BG151 and BG152 in 2003/04 of 0.187 and 0.342 m d^{-1} respectively, were suspect and therefore not considered further (Table 5.4).

The lowest surface velocities were measured in the upper sections and along the margins of the glacier. These regions include the BG05 and BG10 survey lines, the western sections of

Table 5.4.: Surface velocity measurements from 2003/04. The sites are separated into the longitudinal profile followed by the six traverse profiles. Each profile is organised in order from north to south across the glacier.

Survey site	Elevation (m)	Days in January interval	Average velocity (m/d)	Days in February interval	Average velocity (m/d)
2003/04					
BG05	1030	32.79	0.036	16.98	0.032
BG10	955	32.89	0.045	16.98	0.040
BG15	866	32.99	0.091	16.96	0.085
BG20	752	34.94	0.094	16.98	0.065
BG25	673	29.82	0.110	14.10	0.071
BG30	582	27.98	0.123	20.06	0.088
BG35	492	24.96	0.136	21.06	0.097
BG40	407	24.89	0.156	21.13	0.120
BG45	296	29.97	0.168	21.22	0.146
BG50	179	24.78	0.150	17.90	0.136
BG05	1030	32.79	0.036	16.98	0.032
BG052	1034	30.91	0.082	16.99	0.068
BG10	955	32.89	0.045	16.98	0.040
BG101	972	30.86	0.087	17.00	0.075
BG15	866	32.99	0.091	16.96	0.085
BG201	756	34.89	0.086	17.02	0.058
BG20	752	34.94	0.094	16.98	0.065
BG202	776	34.96	0.072	16.96	0.053
BG251	682			14.03	0.046
BG252	684			14.07	0.059
BG25	673	29.82	0.110	14.10	0.071
BG253	678	29.78	0.097	14.14	0.069
BG254	682	29.86	0.074	14.18	0.058
BG255	703	29.80	0.065	14.23	0.052
BG256	705	29.84	0.042	14.27	0.027
BG257	715			15.19	0.027
BG258	715			15.24	0.037
BG301	580	27.97	0.123	20.06	0.088
BG30	582	27.98	0.123	20.06	0.088

the BG35 and BG40 transverse profiles, and the eastern sections of the BG25 transverse profile (BG256-8), near the ice divide between Brown and AU1121 glacier.

The surface velocity vectors from the two field seasons indicate that the centre flowline of Brown Glacier is close to the longitudinal stake locations (Figure 5.11). This is especially evident on the lower glacier, except at BG35 and BG40 where the highest velocities along these profiles were measured at BG353 and BG403 both located to the north of the longitudinal profile.

When only the longitudinal profile is examined, from 2000/01, all of the surface velocities were equal between the two intervals within the estimated error, except BG20 and BG25 (Truffer et al., 2001) (Figure 5.12). The differences in the flow direction between the two surveys at BG20 and BG25 are not likely to be due to GPS error, instead seems to be due to error in recording (Truffer et al., 2001) (Figure 5.11). There is also an additional error in the velocity

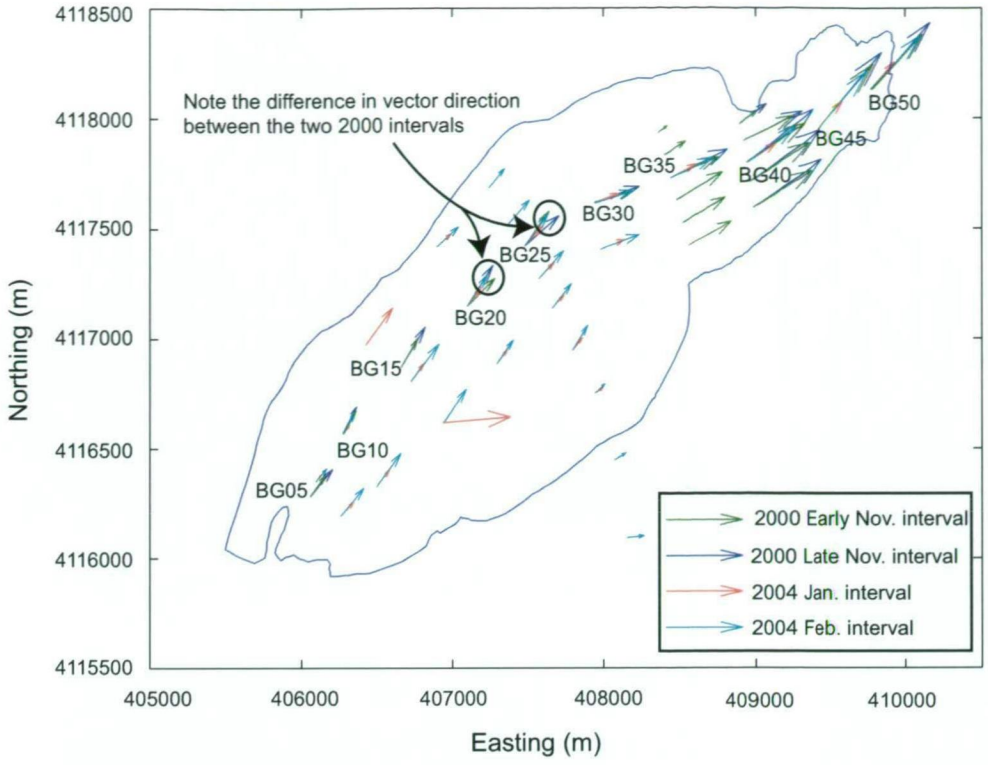

Figure 5.11.: The surface velocity vectors from the two field seasons DGPS surveys. The Brown Glacier outline and the locations of the longitudinal stakes are indicated. Note that the site of the BG15 and BG05 stakes were different for the two seasons.

measured at BG05 (by as much as 0.03 m d^{-1}) due to substantial pole tilt (Truffer et al., 2001). Given that the first survey velocities have not changed significantly between these two intervals there are no indications that there is an increase in velocity this early in spring. It is possible that these surveys were completed before spring conditions began as no widespread melt was observed during the surveys (Truffer et al., 2001).

In 2003/04, the surface velocity profile is near coincident with the first survey except at the BG05 and BG15 stakes (Figure 5.12). The velocities measured at BG05 in the second survey should have been higher given they were measured later in the melt season. Instead these lower values may be due to the 2003/04, BG05 stake being located 80 m north northeast and down slope of the 2000/01, BG05 stake, where the surface slope had a lower surface gradient (Thost and Truffer, 2008). The high velocity measured during the February interval could also be a result of the placement of the stake. In the second survey, the BG15 stake was located closer to the central flowline, which may explain the higher velocities at this stake than in the first survey.

Comparison with earlier velocity data In addition to the two field season's velocities, measurements from Brown Glacier were also measured over one period from 17 September 1992 to 25 February 1993 by A. Vrana. The measurements were along a transverse profile across the glacier at elevations of 600 to 720 m, near the BG20 and BG25 stake profiles (670 to 703 m asl) (Figure 5.13). A comparison between the average velocity over these three field

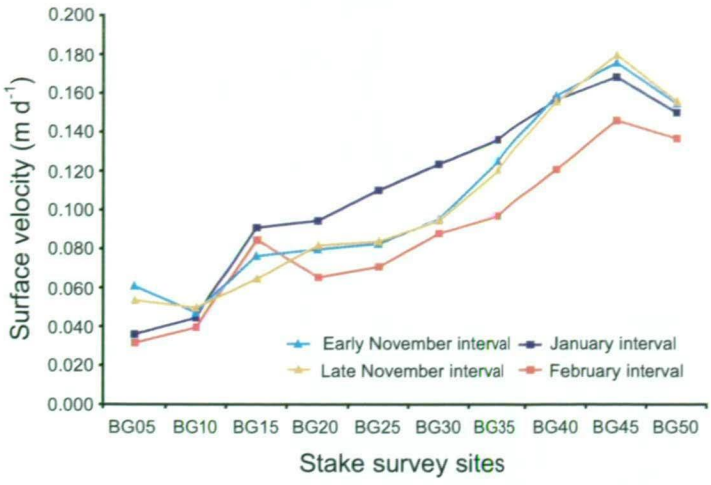

Figure 5.12.: Longitudinal profile surface velocity measurements from both DGPS surveys.

seasons (Table 5.5) shows that the highest velocities were measured between 27 October and 21 November 2000 and 27 December 2003 and 26 January 2004.

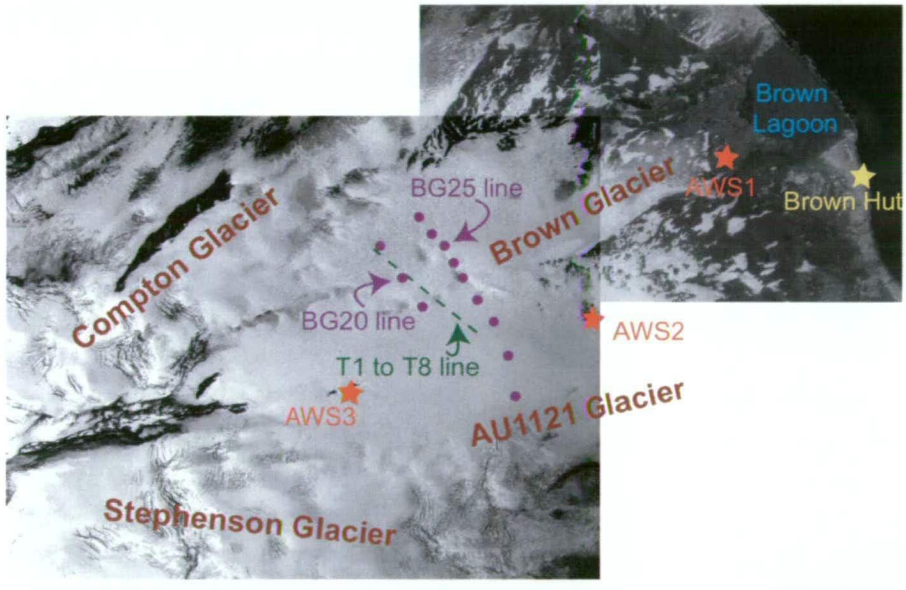

Figure 5.13.: Approximate location of the 1992/1993 survey line (T1 to T8) on Brown Glacier based on pers. com. with A. Vrana (21 January 2008). Background image: 2001 Digital Globe satellite image.

These records provide yet more evidence of the seasonal variability in Brown Glacier velocity. A measure of the annual velocity changes on Brown Glacier would provide greater insight into the changes that occur on the glacier throughout a balance year, but are unavailable.

5.4.2. Seasonal variability of velocity

While the velocity data from the two surveys does not allow a detailed analysis of the seasonal variation in velocity of Brown Glacier, there is an indication of a seasonal change in velocity. By averaging the velocities along the central flow line (longitudinal profile BG05 to BG50) for each interval, for both survey years, a seasonal variation becomes evident (Figure 5.14).

Table 5.5.: Comparison between the 1992 to 1993 and the velocity values from the two recent surveys.

Survey	Site	Start date	End date	Average velocity ($m a^{-1}$)
1992-93	600 to 720 m elev.	16 September 1992	25 February 1993	25.7
2000/01	BG25	27 October 2000	21 November 2000	29.2
2003/04	BG25 to BG256	27 December 2003	26 January 2004	29.2
2003/04	BG251 to BG258	27 December 2003	9 February 2004	21.9

This seasonal change profile suggests that the peak flow rates occur in mid-summer (January), following a period of near constant velocities in spring (Oct-Nov) (Table 5.4).

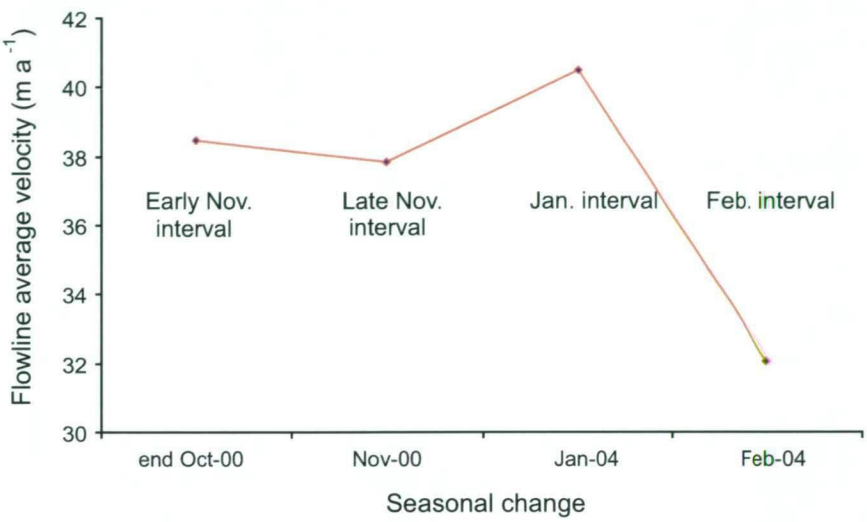

Figure 5.14.: Seasonal change in velocity measurements on Brown Glacier from the two field seasons.

Peak velocities are closely correlated to periods of high temperature and precipitation, which implies a correlation between large water input into the glacier and high water pressure events (Hooke et al., 1983, 1989; Jansson, 1996). There were several days in January when there was significant water running along the surface and many subsurface streams could be heard during surveying activities. Temperatures recorded at the AWS1 and the total precipitation recorded at Brown Hut are both higher in January than February (Table 5.6). Although it should be noted that the January survey period is almost twice as long at some sites as the February interval and may account for some of the differences when comparing the January and February temperature, precipitation and velocity records.

Table 5.6.: The change in average centre line velocity for both of the second survey intervals, the average of the 10 minute average temperatures from AWS1 (115 m) for both periods, and the total precipitation that occurred at Brown Hut during each interval.

	January interval	February interval
Average temperature (° C)	4.7	4.2
Precipitation ($mm d^{-1}$)	17	4
Velocity ($m d^{-1}$)	0.11	0.09

Seasonal changes in the velocity are a result of the variability in the supraglacier and englacial drainage systems. Supraglacial drainage systems, such as the dendritic drainage network in the surface snow, do not contribute significantly to the seasonal velocity variability (Benn and Evans, 1998). However when melting is high enough surface channels will form hastening the flow of water along the surface dropping into moulins or radiating towards the margins.

The supraglacier channels and the englacial moulins drainage networks are strongly dependent on the amount of water available during the melt season. However other studies show that not all high water events result in high velocity events, nor do high precipitation events late in the season produce high velocity events comparable to those that occur in the warmer months (e.g., Hooke et al., 1983; Iken and Bindschadler, 1986; Hooke et al., 1989; Jansson, 1996). Brown Glacier had a lower velocity in February then in January, this is despite the warm temperatures that were still present in February at sea level, Spit Bay average temperature for February 2004 was 4.2° C.

5.4.3. Diurnal variability in glacier speed

Diurnal velocity variability was measured near the BG50 stake from 30 December 2003 to 8 February 2004. Two periods of measurements are used to illustrate diurnal variability; the first was between 2 and 7 January 2004 (three measurements per day 6 to 12 hours apart) and the second was between 1 and 8 February 2004 (four measurements per day 6 hours apart). These two periods were selected because they are the longest period of continuous measurements available.

The 2 to 7 January epoch has no discernible time related variability (Figure 5.15A). This was also a period when the crevasses surrounding BG50 stake and GPS were still covered in snow bridges. Higher melt rates and therefore higher velocity occurred later in the season. Beginning around 10 January the surface snow and snow bridges began to melt exposing more crevasses and hence providing more conduits for surface meltwater and precipitation to more quickly reach the bedrock.

In contrast, the 1 to 8 February epoch did show a diurnal variability from 1 to 6 February. There were higher velocity rates measured at midnight than at midday (LST) (Figure 5.15B). This implies that more melt was reaching the bedrock later in the day and effecting the basal sliding and hence surface velocity.

This cyclical period ends after midnight on 6 February 2004. The 6:00 LST measurement on 6 February was very high (5.70 m d^{-1}), compared to the velocities measured over this period at the BG50 stake of 0.136 m d^{-1} from 22 January to 9 February. The event that has occurred over this period resulted in the velocities dropping to similar values as the January epoch, with less evidence of a diurnal cycle. Although no precipitation was recorded at Brown Hut on the 6 February, the peak in velocity could be attributed to a föhn wind that began at 4:20 LST on 5 February resulting in high temperatures until 21:30 (5 February) at AWS2 and until 3:20 (6 February) at AWS3. These high temperatures ($\approx$ 10° C) resulted in melting of the snow surface, which percolated into the underlying ice reaching the bedrock and causing an increase in basal sliding, which caused the short term increase in surface velocity. This is further supported by a high meltwater discharge of 6.475 m^2 s^{-1} measured at the lagoon outlet (on the 7 February), which is twice the average lagoon outlet discharge of 3.33 m^2 s^{-1}.

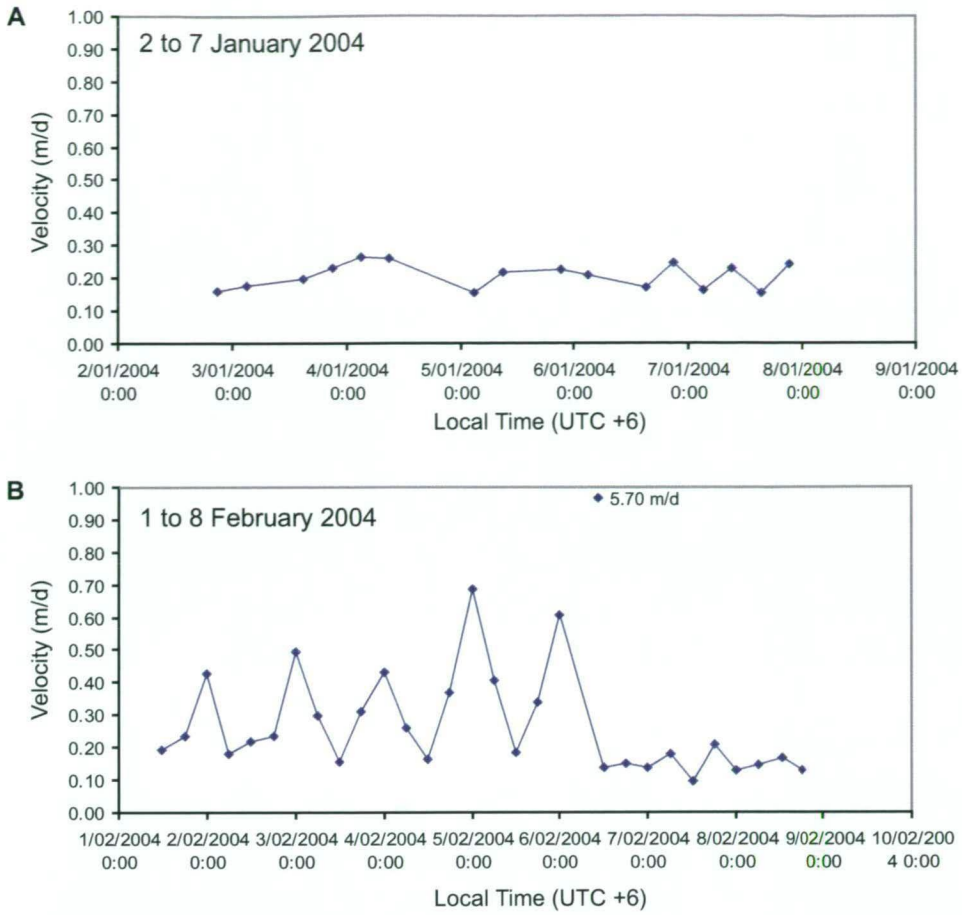

Figure 5.15.: Velocity measured by the DGPS unit near the BG50 stake. **A.** 2 to 7 January 2004 and **B.** 1 to 8 February 2004

5.4.4. Effects of geothermal heating on velocity

The volcanic activity on Heard Island may also influence the velocity of Brown Glacier. A volcano can effect the underlying and surrounding glaciers in a variety of ways: from increasing the geothermal heat, to melting the surface of the ice by lava flows, or dramatic changes in the subsurface topography.

Regions with high localised geothermal heat can result in faster ice flow (e. g., Iceland (Bourgeois et al., 2000)) due to the influence of increased meltwater at the base of the glacier. Although the mechanism and subglacial dynamics of the effects of geothermal heat are not well understood many attempts have been made to model the effects of geothermal heat on glaciers in volcanically active locales.

Williams (1998) modelled changes in the dynamics of the Mary Powell and Vahsel glaciers, located on the northern and western coasts of Heard Island. He found that a tenfold increase in geothermal heat flux had a negligible effect on the mass balance of these two glaciers. He calculated the geothermal contribution to the melt rate as being 2 to 5% at the ELA, whereas an increase of 1° C resulted in a 38% increase in melt rates at the ELA. In this current study, the seasonal changes found in the velocity of Brown Glacier between October and February also decreases the possibility that geothermal heat from the active Big Ben volcano are contributing significantly to basal melt. Sturm (1995), who was studying glaciers in Alaska on Mt. Wran-

gell, found that a glacier with little or no seasonal velocity change is likely to be influenced by volcanically derived geothermal heat, as volcanically derived water would be produced year round unlike surface melt and runoff.

It has already been mentioned that there was a change in the surface melt on Brown Glacier during 2003/04 (see Section 5.4.2). Also, during both surveys observations of the meltwater stream flow volume and the flow of the waterfall, that descends from a cliff below where the northern margin of the glacier terminates into an area of slow velocity. At the beginning of the first survey there was little surface melt and the waterfall did not start flowing until the end of the season. In 2003/04 there were high surface melt rates especially in January 2004 and the waterfall was flowing throughout the season. The waterfall was observed to have high flow periods in particular on 14 January 2004. At the same time the small sand delta near Brown Lagoon was flooded by meltwater.

The observations in this study have further contributed evidence that volcanically derived geothermal heat flux is not the driving force behind the retreat of Heard Island's glaciers as has already been reported by Allison and Keage (1986), Williams (1998), Thost and Truffer (2008), among others.

5.4.5. Mass flux

Nye (1965) showed how mean velocity, ($\overline{U}$), of a cross section of a glacier can be determined from the mean of the surface velocity (see Section 7.5.1 for more details). The ratio between the mean velocity over the surface (U_s) and the mean velocity over the section as described by Nye (1965) is presented in Table 5.7, for a channel of parabolic cross sectional shape. This Table shows that for $W > 2$, U_s is very close to $\overline{U}$, where W is the half-width/depth of the channel and f a stress shape factor dependent on the shape and dimensions of the cross section, which Nye (1965) defines as differential motion only (DMO). These calculations are based on $n = 3$, which is the power law in Glen's (1955) flow law. $n = 3$ was derived from experiments on the steady creep of ice in the laboratory under uniaxial compressive stresses between 1 and 10 bars.

Table 5.7.: The velocity ratios in parabolic channels from Nye (1965).

W	1	2	3	4	5	∞
DMO	0.429	0.837	0.980	0.997	1.005	1.091

The surface velocity was measured over three transverse profiles (Table 5.3 and 5.4) and was used in combination with the RES data (Figure 5.10) to calculate the mass flux of Brown Glacier. The mass flux (Q_m) is calculated from $\overline{U}$ over the transverse profile and the cross sectional area of the glacier (Ω_g) calculated from the RES and DEM data (Table 5.8), and can be given by:

$$Q_m = \overline{U} \times \Omega_g \tag{5.1}$$

The ice flux through the BG35 profile was calculated from the average velocity measurements from both the early and late November epochs, and the detailed RES profile measured during 2000/01. The RES profile does not extend the entire width of the glacier (Figure 5.16).

The ice thickness for the northern margin of the BG35 profile was estimated based on the RES measurements. This resulted in an ice flux of 3.0×10^6 m^3 a^{-1} for the early November interval and 1.6×10^6 m^3 a^{-1} for the late November interval (Table 5.8).

Table 5.8.: Mass flux through three transverse profiles on Brown Glacier. The velocity is averaged over the length of the corresponding field season, (13 to 52 days). The relevant intervals are included for the two ice flux measurements.

Profile	Average velocity (m a^{-1})	Total cross sectional area (m^2)	Ice flux (m^3 a^{-1}), early Nov.	Ice flux (m^3 a^{-1}), late Nov.	Average ice flux (m^3 a^{-1})
BG20	26.0	73164	1.6×10^6 (Feb)	2.2×10^6 (Jan)	$1.9 \times 10^6 \pm 1.54 \times 10^5$
BG25	23.4	86599	1.7×10^6 (Feb)	2.5×10^6 (Jan)	$2.1 \times 10^6 \pm 1.10 \times 10^5$
BG35	35.1	64741	1.6×10^6 (late Nov.)	3.0×10^6 (early Nov.)	$2.3 \times 10^6 \pm 1.78 \times 10^5$

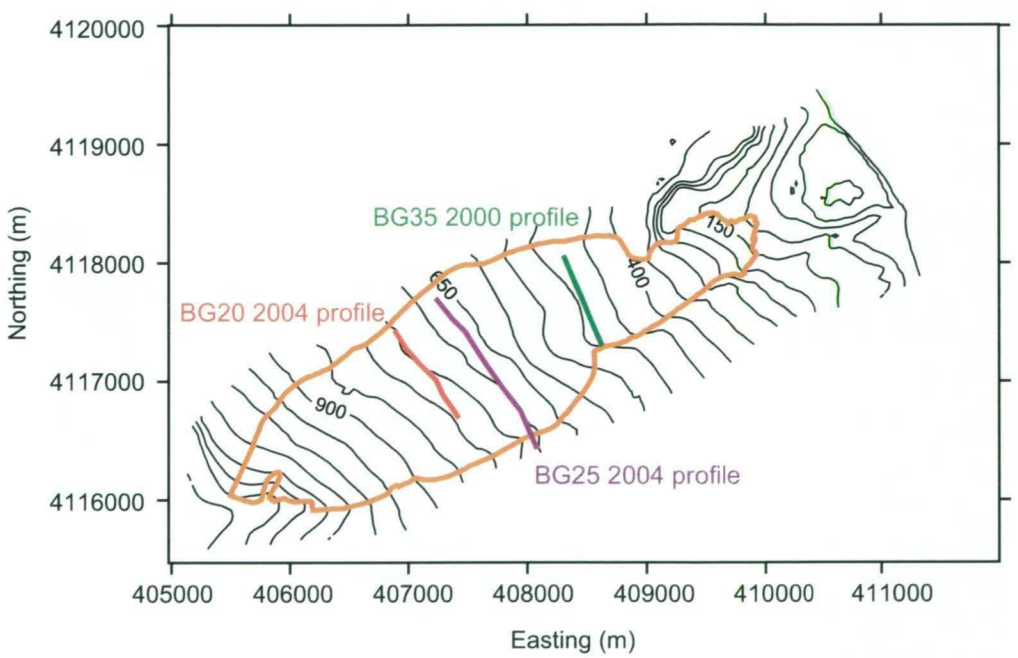

Figure 5.16.: The location of the BG20, BG25 and BG35 mass flux profiles.

The upper two profiles, BG20 and BG25 from 2003/04, also do not extend to the full width of the glacier, both survey profiles were restricted due to crevassed areas (Figure 5.16). Despite this limitation the ice flux through these less detailed profiles were estimated by projecting the trend in the bedrock of each profile to the estimated width of the glacier.

The BG25 RES profile extended 120 m beyond the southern margin of the glacier and was short 110 m of the northern margin of the glacier (Figure 5.16). The trend in the northern bedrock was used to project the ice thickness. The ice flux across the entire profile was estimated as 2.5×10^6 m^3 a^{-1} for the January interval and 1.7×10^6 m^3 a^{-1} for the February interval (Table 5.8).

The BG20 profile was 420 m short of the southern margin and 70 m of the northern margin (Figure 5.16). Again the trends in the bedrock was used to project the ice thickness. The ice

flux was then estimated as 2.2×10^6 m^3 a^{-1} for the January interval and 1.6×10^6 m^3 a^{-1} for the February interval.

5.5. Surface mass balance of Brown Glacier

The mass balance of Brown Glacier can be estimated based on the ELA, and surface net balance measurements.

5.5.1. Equilibrium line altitude

The upper part of a glacier is a region of more accumulation than ablation. This region is called the accumulation zone. Continuing down glacier, is the snow line. The snow line at the end of the melt season is often misinterpreted as being the same as the equilibrium line, which is where the amount of accumulation equals the amount of ablation on the glacier. Further down-glacier from the equilibrium line is the ablation zone.

There are several methods that can be used to estimate the ELA in remote locations. These include the snowline height at the end of summer, accumulation area ration (AAR), and surface contours. Each of these are investigated in order to estimate the 1947 and 2003 ELA. The shifts in the ELA between these two periods indicate changes in the climate conditions on Heard Island.

The ELA for Heard Island was first estimated from snowline elevation at the end of summer, assuming that in this maritime location that the ELA and snow line were coincident, by Lambeth (1950) in 1948 and 1949. He reported that the snowline of the Atlas Cove glaciers was at 300 m asl from December to April and at sea level from July to September. The next published observation of snowline height was in March 1971 by Allison (1980) on the Vahsel Glacier of 250 m asl.

These initial observations were supplemented by an aerial photographic survey in 1948, which was repeated in 1980. Later, in the 1990s, geo-referenced satellite imaging significantly improved the accuracy of Heard Island's glacier topography. Ruddell (2006) estimated the snowline elevation using both of these aerial surveys, but predominately used SPOT satellite images from 9 January 1988 and 31 March 1991. On both of these occasions the average snowline elevation was 315 m asl yet individual glacier's snowline ranged from 100 to 700 m asl (Figure 2.4). The highest snowline heights were observed on Compton, AU1141, Winston, AU1191, Gotley and AU1121 glaciers (Ruddell, 2006) indicating that there is a precipitation shadow to the east of the island, however precipitation records (Section 4.3.2) show that in some locations on the east get higher precipitation rates than the west. The lowest snowline heights were for glaciers along the northern part of the island from the Allison Glacier, in the west, to Stephenson Glacier, in the east (except Compton and AU1121 glaciers) (Ruddell, 2006).

The 1948, 1988, and 1991 observations are very similar, which is unusual given the typically variable climate of maritime glaciers (Ruddell, 2006). The low variability in snowline height on the island over the last ~ 50 years could be due to the satellite images only provide a 'snapshot' often at wrong time of year of the snowline. The SPOT satellite image for 9 January 1988 shows a predominately seasonal snow cover on the lee side of Big Ben, where despite a northerly

aspect there is a lower snowline height (Ruddell, 2006). This image suggests a high probability of the seasonal snow cover affecting the observed location of the snowline on Heard Island.

The snowline on Brown Glacier in February 2004 was observed to be between BG40 and BG45 at approximately 375 m asl. To determine any shift in the ELA between 1947 and 2004 two less accurate ways of estimating the ELA were used, accumulation area ration (AAR) and surface contours. The AAR, which is the ratio of the accumulation to ablation area, was used to estimate an ELA of 350 m in 1947 and ~500 m in 2004. An ELA of 350 m in 1947 and 600 m in 2004 were estimated based on where the surface contours change from concave to convex down valley.

5.5.2. Density of snow

The 0.8 m snow pit dug in 2000/01 near the BG35 stake is the only measured density value on Brown Glacier (Truffer et al., 2001). Truffer et al. (2001) found an average density of 790 kg m^{-3} (Figure 5.17), which is in the range of 'very wet snow and firn'. The density of snow and ice typically ranges from 50 to 70 kg m^{-3} for new dry snow, 400 to 800 kg m^{-3} for firn and 830 to 917 kg m^{-3} for glacier ice (Paterson, 1994).

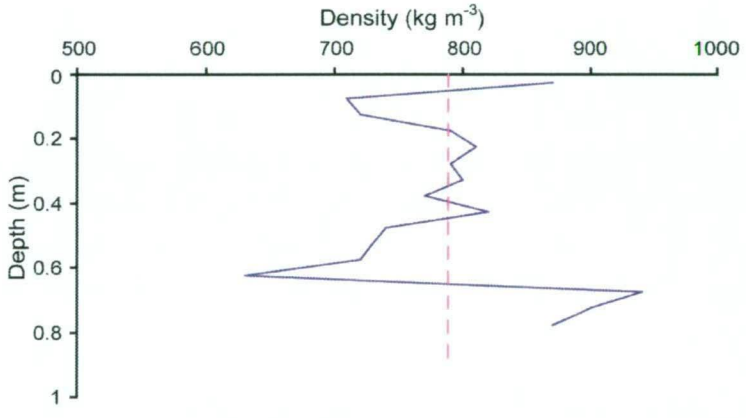

Figure 5.17.: Density profile from the 2000 snow pit at BG35. Red line is the average. Note there was one measured value of 940 kg m^3 which is greater than ice. The accuracy of these measurements are $\pm$ 5%.

The 2000/01 snow pit average density was used to estimate the surface density at other elevations on Brown Glacier in conjunction with surface and crevasse observations (Table 5.9). It was assumed that there would be a decreasing density of the surface snow with elevation, i. e., the accumulation area would be snow covered compared to the bare ice surrounding BG45 and coincidental BG50 stakes in the ablation zone. It is acknowledged that these estimated densities could be in error.

The average density of the ice cores and crevasse samples were assumed to be the same as the snow pit average of 790 kg m^{-3}. This is a best estimate given the limited measurements of density on Brown Glacier.

These density estimates were used to determine the snow water equivalent (SWE or w.e.), which is the amount of water equivalent of the snow pack. SWE is the essential snow pack measurement. SWE is defined as:

Table 5.9.: Estimated density of surface snow on Brown Glacier.

Site	Elevation (m asl)	Density (kg m^{-3})
BG05	1030	500
BG10	955	500
BG15	866	500
BG20	752	500
BG25	673	500
BG30	582	500
BG35	492	600
BG40	407	700
BG45	296	850
BG50	179	850

$$\text{SWE} = \frac{\rho \times \text{snow depth}}{\rho_w} \tag{5.2}$$

where ρ is the estimated density at that elevation and ρ_w is the density of water, and is typically given as m w.e. The SWE is used as a measure of the quantities of runoff and an estimate of the amount of liquid precipitation falling as snow (Singh and Singh, 2001).

5.5.3. Surface net balance measurements

The remote location, infrequent visits, variable surface conditions of Heard Island glaciers mean that there is only poor knowledge of Heard Island's surface mass balance. In both surveys stake networks and downward looking sonars were deployed to measure the distance to the glacier surface at a number of sites along Brown Glacier. These provided point measurements of the net balance which could be projected over larger areas of the glacier in order to determine the net balance of the glacier as a whole.

Downward looking sonars The results from the sonic ranger erected near the BG35 survey stake indicate that in 2000 there was net accumulation from the end of October until the end of November (average rate of 6 mm d^{-1} w.e.). The BG35 sonic ranger also recorded a possible föhn wind induced melting on the 25 November (Truffer et al., 2001) (see Section 4.4.4).

Two sonic rangers were erected in 2003/04, one at BG35 (492 m asl) and the other near the BG50 survey stake (179 m asl). There was a change in the BG35-2004 ablation from an average rate of -43 mm d^{-1} w.e. at the beginning of January to an average rate of -11 mm d^{-1} w.e. from the end of January to mid February. The net ablation at BG50-2004 remained relatively constant over the recorded period of 51 days with an average rate of -46 mm d^{-1} w.e.

Stake networks Stake height measurements in 2000/01 (Table 5.10) recorded net accumulation at and above BG20 from 23 October to 12 January. The BG25 stake recorded net ablation between 23 October and 22 November and between 23 November and 12 January. On the lower glacier (BG30 to BG50) net accumulation was recorded at all stakes except BG40 from 23 October to 22 November. There were two solid accumulation events recorded during November 2000, one between the 1 and 4 November and the other on 13 November (Truffer et al., 2001). After 25 November there were no measurements of the stake height until 12 January when two

Spit Bay expeditioners resurveyed the longitudinal stake line. Between 26 November and 12 January there was net ablation at and below BG40 (the BG50 cane was lost).

Table 5.10.: Net balance values for the stake network from 23 October 2000 to 12 January 2001. The densities used for water equivalent conversions are listed in Table 5.9.

Site	Elevation (m)	Total net balance (mm w.e.)	Average net balance (mm d^{-1} w.e.)
BG05	1061	453	9
BG10	958	580	11
BG15	865	843	18
BG20	755	105	2
BG25	678	−82	−2
BG30	586	720	14
BG35	498	1717	34
BG40	414	−309	−6
BG45	304	113	2
BG50	187	38	1

The 2003/04 stake network recorded an overall net ablation at all canes (Table 5.11). The highest ablation periods were between 2 and 10 January and 13 and 20 January. During both of these periods almost 1 m of snow loss was recorded for the canes between BG30 and BG50. Three solid accumulation events were recorded during the field season, one between 20 and 22 January, another between 26 January and 2 February, and the last between 12 and 13 February. The sporadic distribution of these solid accumulation events indicates storms in the area. It should be noted that these solid accumulation events do not show any indication of how much liquid precipitation may have fallen on the glacier over this period. Rainfall was only measured at Brown Hut and an estimate was made of average precipitation over the catchment (see Section 5.5.4).

Table 5.11.: Net balance for the 2003/04 stake network. Measurements were made between 30 December and 18 February. The densities used for water equivalent conversions are listed in Table 5.9.

Site	Elevation (m)	Total ablation (mm w.e.)	Average ablation (mm d^{-1} w.e.)
BG05	1030	−745	−147
BG10	955	−1133	−222
BG15	866	−1243	−244
BG20	752	−1253	−237
BG25	673	−1209	−230
BG30	582	−1258	−237
BG35	492	−1662	−302
BG40	407	−2342	−426
BG45	296	−2100	−403
BG50	179	−3094	−523

Net balance from surface measurements Stake networks provide a greater area of specific net balance measurements then the sonic rangers. Yet sonic rangers were useful in providing a more continuous record of the snow surface height. Comparisons made between the sonic ranger and the stakes indicate some differences between measurements (Figure 5.18).

In 2000/01, the BG35 sonic ranger and stake measurements correlated well over the entire 26 day period (Figure 5.18A). Due to intermittent readings of the BG35-2004 sonic ranger a comparison with the stakes is only possible for the beginning of the season (Figure 5.18B). The stakes alone provide a better estimation of the ablation for the rest of the season. The BG50-2004 stake and sonic ranger records differ slightly as the season progressed (Figure 5.18C). This divergence of measured heights could be due to the cane and the sonic ranger being ~ 50 m apart and therefore local variability of the glacier surface coming into effect (Thost et al., 2004).

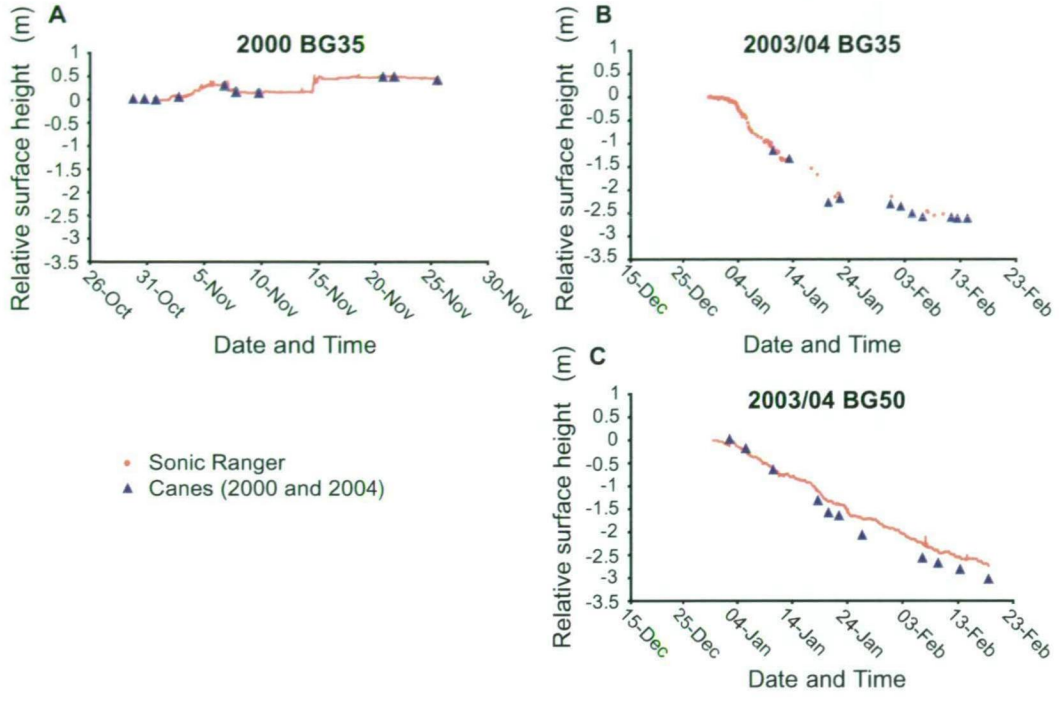

Figure 5.18.: Change in surface height recorded with the sonic ranger and compared to the cane measurements at: **A**. BG35 in 2000/01, **B**. BG35 in 2003/04 and **C**. BG50 in 2003/04.

The net balance measured along the longitudinal stake line between 25 October and 25 November 2000 was predominately of accumulation (Figure 5.19A). The next measurements of the longitudinal stake line net balance was between 26 November 2000 and 12 January 2001. During this period there was accumulation still occurring on the upper glacier and ablation had begun to dominate on the lower glacier (Figure 5.19A). The highest ablation period was recorded between 23 December 2003 and 22 January 2004. The net balance was more negative near the terminus then near the top of the glacier (Figure 5.19B). January was the peak ablation period in 2003/04 as records from 23 January to 18 February indicate that the over all ablation had once again decreased (Figure 5.19B). Although, as on every glacier, there was still more net ablation near the terminus than any where else on the glacier.

The seasonal and spatial variability of the net balance on Brown Glacier is assumed to be high, based on the high winds and localised accumulation observed on Brown Glacier in 2003/04. The variability in the net balance is noticeable in Figure 5.19.

Comparison with earlier data The net balance of Brown Glacier was also measured between 17 September 1992 and 25 February 1993 (1992/93) along a transverse profile located near the BG25 and BG30 profile (pers. com. A. Vrana, 21 January 2008). The profile ranged

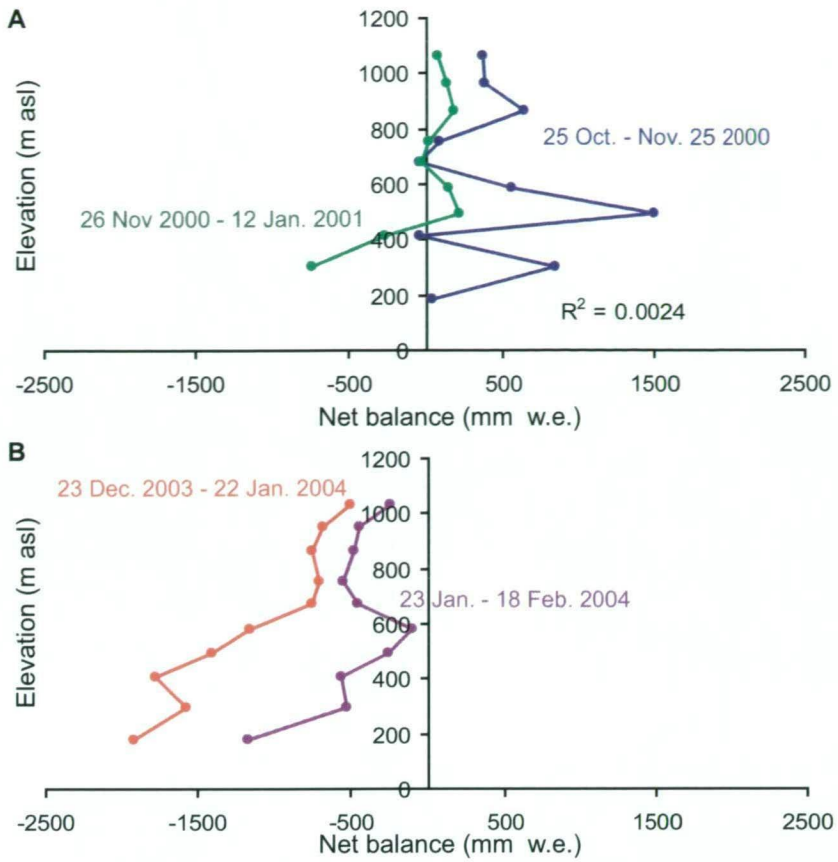

Figure 5.19.: Surface net balance for Brown Glacier longitudinal cane line in both seasons. The ice density used to convert to w.e. are listed in Table 5.9.

in elevation from 600 to 720 m. The total net balance over this 164 day period ranged from 7 mm d^{-1} w.e. to -15 mm d^{-1} w.e. (based on an estimated snow density of 300 kg m^{-3}). Three of the stakes from the 1992/93 profile (T2, T3 and T4) have the longest net balance records. These three stakes indicate that there are accumulation periods of up to 2.5 m (between 16 September and 29 October 1992) of snow in spring and in summer there was almost 3 m of ablation between the middle of January and February periods (Figure 5.20). In 1992/93 the highest ablation period was from the end of January until end of February, this correlates with the higher temperature recorded during this period.

These three records illustrate the variable nature of the net balance on Brown Glacier, each year is different, however a seasonal trend from late winter to late summer has become apparent. In general, there may be accumulation events through spring and summer, highest in spring, but by the end of December to early January ablation begins to dominate the net balance. It is difficult to determine when the ablation season ends as all three field seasons were terminated during the ablation season, hence it is assumed that accumulation must begin to dominate once again in March or later. This is supported by the precipitation and temperature records from Atlas Cove. March to May is when the highest annual precipitation was recorded at Atlas Cove between 1948 and 1954 (see Section 4.3.2) and March also marks the beginning of autumn.

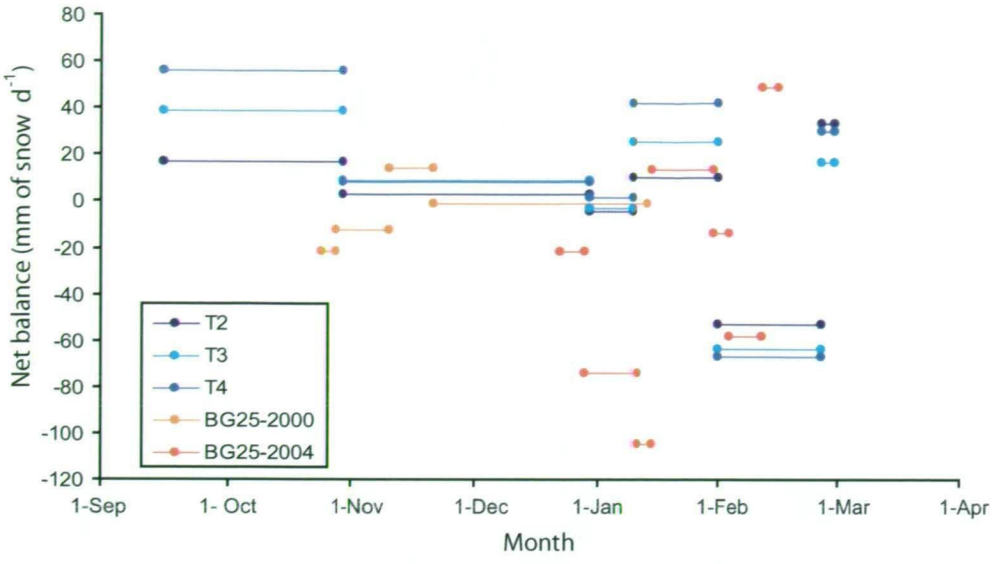

Figure 5.20.: The 1992/93 surface net balance (blues) compared to 2000/01 (orange) and 2003/04 (red) surface net balance measurement at the BG25 stake.

5.5.4. Average precipitation over the catchment

The total catchment area was determined from the 2001 Brown Glacier DEM (Figure 5.21). The catchment area is larger than the glacier outline described in Section 5.3.1, as the catchment area of Brown Basin includes some of the rock outcrops surrounding the glacier. The total catchment area (Ω_c) is 7.2 x10^6 m^2.

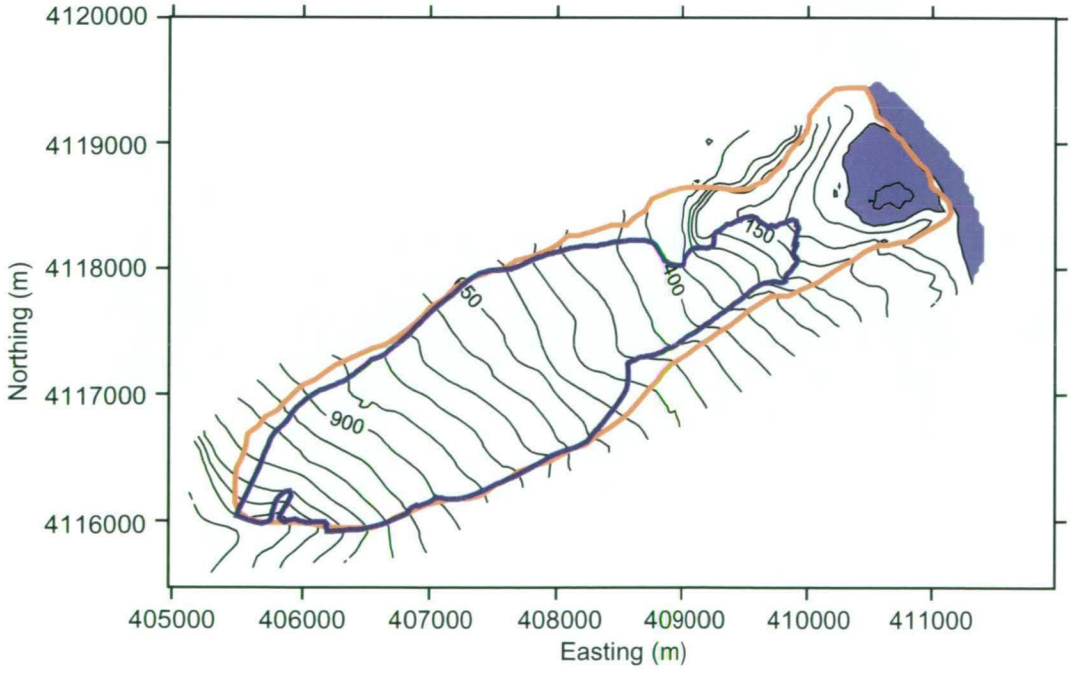

Figure 5.21.: The outline of the catchment area of Brown Basin (orange) and the 2001 glacier outline (blue).

Measurements were made of water discharge from Brown Glacier melt streams and the lagoon outlet to investigate the total runoff for this glacier basin. The meltwater runoff of a

glacier (R_t) is the total precipitation in the catchment area (P_c) plus the total melt from a glacier (m_t) less the amount of water stored in a glacier (S_w). The total runoff can be given by:

$$R_t = m_t + P_c - S_w \tag{5.3}$$

where,

$$m_t = \sum a\Omega_s \tag{5.4}$$

and

$$P_c = A_p\Omega_c \tag{5.5}$$

where a is the ablation over a surface area (Ω_s) and A_p is the average precipitation over the catchment.

The total runoff and catchment area measurements were then used to calculate the average precipitation over the catchment. The average catchment precipitation, A_p is given by:

$$A_p = \frac{R_t - \sum a\Omega_s + S_w}{\Omega_c} \tag{5.6}$$

and it is assumed that S_w equals zero.

Resulting in an average catchment precipitation of 1900 mm a^{-1}. The average precipitation over the catchment area is greater than to the precipitation measured at Brown Hut (555 mm) over the same period confirming that there is an increase of precipitation with elevation on Brown Glacier.

5.6. Conclusions

The surveys investigated here have provided more detail on the morphology, dynamics and mass balance of Brown Glacier than of any glacier on Heard Island. The benefit of having two field seasons means that we are able to asses inter-seasonal variability and the longer term changes on Brown Glacier.

For the first time we are able to estimate surface net balance for an eastern Heard Island glacier; these are the glaciers that are showing the most dramatic retreat compared to the rest of the island. The increased availability of satellite imagery over the island, in conjunction with land based GPS measurements have been used to produce the most accurate contour map of Brown Glacier.

The first bathymetric maps of Brown, Stephenson, and Compton lagoons with the additional kinematic surveys of the nearby moraines, the DEM and the 1947 aerial photographs have given a first indication of the past ice thickness for each of these glaciers.

The kinematic GPS surveys have also increased our knowledge of the dynamics of Brown Glacier in more detail. The 2003/04 survey of Brown Glacier has indicated that there is a seasonal variation in velocity. This reduces the possibility of geothermal heating from the continuing volcanic activity of Big Ben having a major influence on the glacier movement.

Measurements at BG50 indicates that for short periods of time (several days) there is a diurnal variation in velocity near the terminus of Brown Glacier. But additional longer term records are desirable to make further links to the meltwater outflow.

The meltwater flux through Brown Lagoon can be linked to some large velocity shifts near the terminus as recorded on 6 February 2004. The meltwater flux was also used to verify that the precipitation on Brown Glacier increases with elevation, which until now was only based on climbing party observations.

Several ice thickness profiles indicate that the bedrock topography of Brown Glacier has a small ridge line which channels some of the ice flow away from the terminus, which may also contribute to a more rapid retreating terminus.

The changes in the ELA observed between 1947 and 2003 may represent a shift in the climatic conditions on Brown Glacier. Changes in the altitude of the ELA gives an indication of climate change (Ohmura et al., 1992). The ELA fluctuates as climate conditions and mass balance change; it rises in warm, dry years and lowers in cold, wet years (Andrews, 1975). Due to the possibility of errors in the quality of topographic maps (and the DEM) and the effects of strong winds on the seasonal snow cover it is difficult to distinguish whether temperature or precipitation are the cause of the shift in Brown Glacier ELA without a better understanding of the size and shape of the glacier, long-term meteorological records and multi-year mass balance surveys.

Since 1947 the terminus of Brown Glacier has retreated a total of 1.7 km with an average retreat rate of 20 m a^{-1}. The kinematic GPS survey has indicated a significant surface lowering between the two field seasons. Brown Glacier has thinned by up to 11.7 m on the lower glacier with an average of 9.9 m thinning below the BG40 survey stake and 8.5 m on the upper glacier above the BG30 survey stake.

The ice thickness profiles were also used to estimate the mass flux over three profiles at BG20, BG25 and BG35. These mass flux values ranged from 1.6×10^6 to 2.2×10^6 m^3 a^{-1} for BG20, 1.7×10^6 to 2.5×10^6 m^3 a^{-1} for BG25 and 1.6×10^6 to 3.0×10^6 m^3 a^{-1} for BG35, which are useful in constraining mass balance models.

As we continue to increase our knowledge of Heard Island's glaciers we will be able to predict future changes on the island with more confidence. Mass balance and dynamic models have been developed to forecast these future changes and also to estimate the past characteristics of the glacier (see Chapter 7).

6. An estimation of net balance from ice and snow samples

6.1. Introduction

An understanding of the natural climate variability over the last 100 years on Heard Island has been hampered by the lack of continuous long term records. The collection and analysis of ice cores, and samples from crevasse walls and snow pits on Brown Glacier has provided some of the first insights into the annual snow accumulation on Heard Island, and its variation with elevation, as precipitation records on Heard Island have been basically non existent for sites above sea level (see Section 4.2).

Here an attempt is made to evaluate the highly variable seasonal and inter annual distribution of the net balance of isolated sites on Brown and Stephenson glaciers from stratigraphic markers. Stratigraphic markers are essential in the interpretation of annual and seasonal deposition events on a glacier. The stratigraphic markers used to measure the net balance on Heard Island are visible stratigraphy, oxygen isotopes, and impurities (e. g., trace ions) in the snow.

The first recorded study of snow properties and stratigraphy on Heard Island was in 1983 by Spencer et al. (1985), who analysed trace ion samples collected from a bergschrund wall at an elevation of 2450 m on the flank of Big Ben. Also in 1983, seven snow surface samples were collected between 300 and 2720 m asl along the eastern slope of Big Ben. In 2000, Truffer et al. (2001) collected density and temperature measurements and oxygen isotopes samples from a snow pit at 498 m asl near the BG35 survey stake and oxygen isotope samples from a 12 m crevasse at 1050 m asl on Brown Glacier. This current study investigates two cores, three crevasses, and 21 surface sites, sampled in 2004, on Brown and Stephenson glaciers. These were analysed for stratigraphic markers to determine if a seasonal signal is retained in the snow and ice at elevations below 1000 m asl.

6.2. Types of stratigraphic markers

On most glaciers snow accumulates each year to form recognisable annual layers marked by seasonal variations in physical, chemical, electrical, metamorphic and isotopic properties. There are several measurements that can be used to detect stratigraphic markers that indicate seasonality or reference horizons in ice cores. Examples of these include, remote sensing (Shuman et al., 1997), intensity of light through snow/firn/ice, electrical conductivity, (Kaczmarska et al., 2006), volcanic horizons (Palmer et al., 2001), pollen analysis (Short and Holdsworth, 1985) and nuclear testing (Schotterer et al., 2002). The three stratigraphic markers used to analyse the Heard Island ice core and crevasse samples are visible stratigraphy, oxygen isotopes and trace ions.

6.2.1. Visible Stratigraphy

The measurement of visible structures in snow and ice (Bradley, 1999) can be a very useful tool in making an initial net balance estimate while in the field. Visible structures found in glaciers include snow and firn layers, ice lenses, and debris bands. All of which highlight processes that occur during snowfall or subsequent metamorphism.

The terms 'snow' and 'firn', though often used interchangeably are distinguishable by age. Snow layers are the surface layer of newly fallen snow whereas firn layers are older snow that has been recrystallised into a more dense layer (Paterson, 1994). Snow layers on temperate glaciers are of the current balance year. Firn layers increase in metamorphism and density with each year and metamorphoses into ice after many years.

Ice lenses are often found in firn layers when it rains or periods of higher temperatures melt the surface snow. This water percolates through the porous surface layers eventually refreezing as an ice lens when temperatures are again lower (Paterson, 1994). Ice lenses can also be formed on a cooled wind scoured surface, which are later buried by freshly fallen snow.

Debris (dust and dirt) accumulates on a glacier from wind blown sediment from nearby rock outcrops, volcanic ash, or movement of sediment by melting and refreezing of the summer snow surface. As a result debris bands are not only an indication of annual accumulation they can also be widespread markers of volcanic events or periods of increased wind-deposited debris.

6.2.2. Oxygen isotopes

In polar snow and ice cores, the seasonal signal in oxygen isotopes provide a temperature proxy (Helsen et al., 2005). In general, there is a strong relationship between the average local temperature and the isotopic composition of local precipitation at high and mid latitudes (Helsen et al., 2005). This relationship between temperature, the amount of precipitation and the isotopes gives a signal in ice cores (Van Ommen and Morgan, 1997). This signal in the short term can be used to estimate a seasonal signal and in the long term a climatic signal. The short term signal (less than one decade) on Heard Island, is used to estimate the seasonal change in temperature as reflected in the δ of the ice and snow samples; higher (less negative) δ values tend to occur in summer and lower (more negative) δ values occur in winter.

The most commonly used annual marker in ice cores and crevasses is the seasonal variation of stable isotopes (Pohjola et al., 2002a). Stable oxygen isotopes occur in nature in three forms. ^{16}O is the most common oxygen isotope, it constitutes 99.76% of all of the oxygen atoms in water on earth, compared to ^{18}O (0.20%) and ^{17}O (0.04%) (Bradley, 1999). It follows that the most common water molecule is $H_2^{16}O$ with smaller amounts of $H_2^{18}O$.

The isotopic ratios of the various compounds in water are determined by small variations in the ratios reflecting the precipitation's origin. These changes in isotopic composition of water provide a recognisable signature, related to phase changes of the water cycle (Gat, 1996). Because it is more difficult to measure the rare isotopes precisely, the relative composition of the isotopic components as opposed to the absolute composition (Paterson, 1994) is used to determine the ratio of the concentrations of heavy and light isotopes (Bradley, 1999). The most common oxygen ratio used for determining annual markers is $\delta^{18}O$. $\delta^{18}O$ values are

expressed in terms of the relative deviations of $\delta^{18}O$ from Vienna Standard Mean Ocean Water (VSMOW) (Moser and Stichler, 1975), and defined as:

$$\delta = \left(\frac{[^{18}O] / [^{16}O]_{sample}}{[^{18}O] / [^{16}O]_{standard}} - 1 \right) x1000 \quad (6.1)$$

and expressed as δ in parts per thousand or permil (‰).

This relationship with the ocean water is possible because ocean water is relatively stable. When evaporation occurs from the ocean the water vapour is depleted of the heavier isotopic forms, $H_2^{18}O$, relative to the liquid (Paterson, 1994; Bradley, 1999) (Figure 6.1). When precipitation occurs from this air mass (under equilibrium conditions) the rainout becomes enriched in the heavier isotopes compared to the water vapour left behind (Figure 6.1). Lower $\delta^{18}O$ values are found at high latitudes due to the loss of heavy isotopes en route to those regions. This is called an isobaric cooling, which implies that the change in $\delta^{18}O$ is due to a systematic change brought about by an overall cooling at a particular level in the atmosphere rather than a cooling due to a change in elevation (Bradley, 1999).

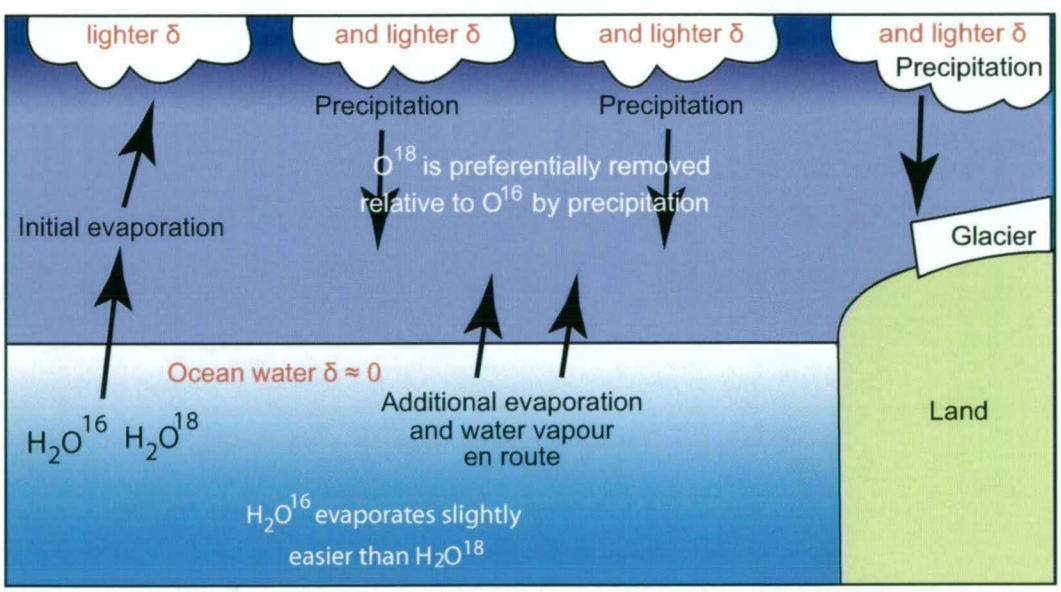

Figure 6.1.: A schematic of the evaporation and precipitation of oxygen isotopes under equilibrium conditions.

There is a large variability in the isotopic ratio and the composition of water vapour of an air parcel, which is dependent on its trajectory (i e., how many phase changes it has experienced and its temperature history) (Ridal, 2001). When rainout occurs inland the 'distance-from-source' effect results in decreasing $\delta^{18}O$ concentrations as the distance from the ocean source area increases (Koerner, 1979). Heavier isotopes are less pronounced when the air is transported inland since there is no further supply of isotopic rich vapour from the oceans. This effect can be seen in Tasmania where the isotopic values measured at Cape Grim on the west coast are higher than those measured in Hobart to the east (see Section 6.7.3).

The depletion of heavy oxygen isotopes in precipitation and vapour due to rainout can also be caused by orographic features (e. g., forced convection over mountains) and has been recognised in almost all major mountain belts in the world (Poage and Chamberlain, 2001). The Big Ben massif, on Heard Island, may effect the distribution of the atmospheric moisture carried

by the westerly winds, evident by the differences in precipitation rates between Atlas Cove, Spit Bay and Brown Hut (see Section 3.3.2). In regions, such as Heard Island, where there is a single dominate moisture source, the Indian Ocean, precipitation at high elevations or on the lee sides of mountain ranges are often strongly depleted in isotopic concentration compared to precipitation on the wind ward side (Poage and Chamberlain, 2001).

6.2.3. Trace ions in snow and ice

Impurities are either produced within the atmosphere during oxidation of trace gases involved in the sulphur, nitrogen, halogen and carbon cycles or introduced directly into the atmosphere like sea salt, volcanic material and dust emitted by wind from marine and continental surfaces (Legrand and Mayewski, 1997). Glaciochemical studies are not simply a measurement of aerosols and gaseous species, they can provide data concerning paleovolcanism events, response of high latitude atmosphere to anthropogenic effects (e. g., acid precipitation and ozone depletion), and the response of the atmosphere to other natural phenomena such as major and rapid changes in climate (Legrand and Mayewski, 1997).

Ice cores are unique because they provide records of aerosols and gas constituents in great temporal detail (Legrand and Mayewski, 1997). The time series of major anion and cation concentrations found in the snow and ice provides an estimate of the chemical composition of the snow, which is directly related to the changes in the atmospheric concentrations of trace ions throughout the year and over longer periods. The major source areas of trace ions are terrestrial dust, volcanoes and ocean surface salts (Legrand and Mayewski, 1997) (Figure 6.2). Other sources include extra-terrestrial (meteorites and interplanetary dust) and industrial pollution (Palmer, 2002) (Figure 6.2).

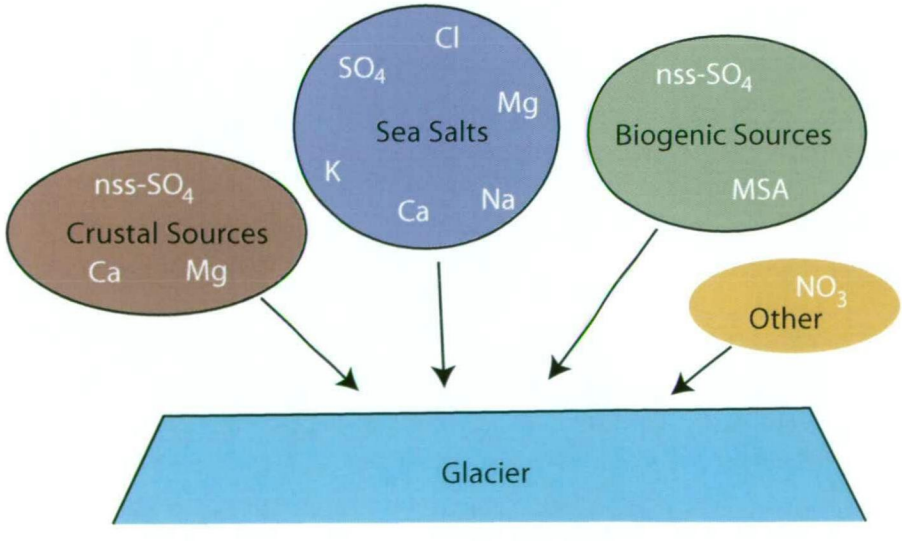

Figure 6.2.: Summary of the source areas for common atmospheric trace ions. Crustal sources include nss-sulphate (nss-SO_4), calcium (Ca), and magnesium (Mg). Sea salt sources include sulphate, chloride (Cl), magnesium, sodium (Na), calcium and potassium (K). Biogenic sources include sulphate and MSA. Nitrate (NO_3) is from other sources.

Seasonal signals observed in atmospheric aerosols deposited as accumulation of snow are very site specific. In order to determine the links between the measured concentrations in

the crevasse and ice core records from Heard Island the local seasonal signals must be identified. The chemical composition of aerosols deposited on Heard Island reflect its geographical location in the southern Indian Ocean. Heard Island is characterised by its mountainous topography resulting in a variety of climatic conditions over scales of tens of metres to several kilometres. Based on the conditions surrounding Heard Island it is assumed that the source areas of chemical species on Heard Island are likely to be a combination of local maritime, crustal and volcanic inputs, long range transport and a small input from anthropogenic effects. These assumptions are supported by reports on the chemical composition recorded at Amsterdam Island (Galloway et al., 1982), Crozet and Kerguelen islands (Baboukas et al., 2004) and near the summit of Heard Island (Spencer et al., 1985).

Naturally with Heard Island isolated from surrounding continental sources, a maritime source is likely to dominate the trace ion record. Trace ions with marine origins are dominated by sea salts. Sea salts are a major contributor to particulate matter in Southern Ocean atmosphere and precipitation. The dominant ions of dissolved inorganic salt matter of sea water are chloride (55.3%), sodium (30.8%), sulphate (7.8%), magnesium (3.7%), calcium (1.2%) and potassium (1.1%) (Wilson, 1975). Sea salts are incorporated into the marine atmosphere from sea spray, wave breaking and bubble bursting, and then transported by winds (Wagenbach et al., 1998). The dependence of sea salt transport on wind reveals a signal in ice records based on the frequency and intensive of storm events in the surrounding area. Generally, Heard Island is stormier in winter, however large storm events can occur at any time in the year (Thost and Allison, 2006) masking a seasonal signal.

Sulphur trace ion can also have a maritime source. The marine biogenic sulphur compound MSA (methane sulphonate or methane sulphonic acid) is produced by the atmospheric oxidation of DMS (dimethyl sulphide), which is emitted by marine biota (Saltzman et al., 1986). MSA concentrations in ice are effected by various factors including, the source location influencing primary productivity, phytoplankton species and the air-sea exchange of DMS, the atmospheric conditions influencing the oxidation pathways of DMS or altering the source location, and more locally, the condition at the glacier (O'Dwyer et al., 2000). Studies at Kerguelen Island 440 km to the north of Heard Island indicate that there is a seasonal signal (higher in summer) in the MSA concentration (Baboukas et al., 2004), corresponding to the proximity of the biogenic-rich oceanic Polar Front (Scaire et al., 1999). Heard Island is also close to the Polar Front (see Section 3.2) hence it is assumed that there would be be a seasonal variability in the MSA record.

Sulphate is the most prevalent aerosol oxidation product of DMS but unlike MSA, DMS is not the only source of sulphate. Sulphate is also produced by oceans due to the bursting of sea water bubbles (Nguyen et al., 1974), industrial pollution (e.g., Thompson et al., 2000) and volcanics (e.g., Legrand and Mayewski, 1997; Palmer, 2002). Generally, the high biological input during summer influences sulphate concentrations (Berresheim, 1987; Staubes and Georgii, 1993) creating a seasonal signal in ice cores.

There are two main sources of sulphate which can affect the seasonality, anthropogenic and volcanic. These two types of sulphate are often reported as non-sea-salt (nss)-sulphate. Although anthropogenic sulphur emission dominate in the northern hemisphere, in the southern hemisphere the natural sources of sulphur emissions (58% of total emissions) exceed those from anthropogenic emissions (Bates et al., 1992). Studies on Crozet, Amsterdam and Kergue-

len have shown that there is a higher influx of anthropogenic emissions at Crozet compared to Amsterdam and Kerguelen (Baboukas et al., 2004) due to Crozet's location closer to southern Africa. These stronger anthropogenic emissions have obscured any seasonality of the biogenic sources at Crozet, whereas a seasonality in the biogenic input is still evident at Amsterdam and Kerguelen due to the predominate wind direction at these islands. Heard Island is even further from anthropogenic sources and has predominately westerly winds that do not originate from South Africa (Young, 1999). Hence anthropogenic emissions would have little influence on the biogenic seasonality. Instead the majority of nss-sulphate input on Heard Island is probably from the volcanic emissions of Mawson Peak.

Crustal source of atmospheric aerosols include crustal weathering and weathering of organic material in soil (Millot et al., 2003). Crustal weathering emits calcium and magnesium into the atmosphere (Caulkett and Ellis-Evans, 1997). Heard Island glaciers are bounded by high altitude ridge lines and surrounded by an exposed rock coastline. Both of these features could produce any nss-calcium and nss-magnesium reflected in the trace ion record.

Another trace ion that is common in ice records is nitrate. Nitrates have several natural source areas including soil exhalation, biomass burning, lightning, galactic cosmic rays, stratospheric oxidation of nitrous oxide and ionospheric dissociation of nitrogen (Legrand and Kirchner, 1990). Despite numerous records of nitrates in ice cores a major source of nitrate has not been identified for high latitude regions (Legrand and Mayewski, 1997).

6.3. Environmental effects on the stratigraphic record

Ice cores from Greenland and Antarctic have provided the majority of the information concerning climate variability over both inter annual and ice age time scales. The initial concentration of ice core studies on ice sheets was due to these regions characteristically having positive mass balance and no melting (Koerner, 1997). Consequently continuous records of climate change are preserved (examples include ice cores from Byrd (Gow, 1970), Law Dome (Van Ommen and Morgan, 1997) and GISP2 (Gow et al., 1997)). Ice cores from glaciers, not a part of these main ice fields, have also been studied, but are harder to interpret, partly due to surface melting that occurs in summer or long periods of negative balance that could alter the original ice core record (Koerner, 1997; Isaksson et al., 2003). Yet a seasonal and long term climate record can also be determined from temperate glaciers (e.g., Aristarain and Delmas, 1981; Aristarain et al., 1982; Galloway et al., 1982; Thompson et al., 1998; Thompson, 2000; Aristarain, 2002; Godoi et al., 2002).

6.3.1. Post-depositional processes within the snowpack

Post-depositional processes such as meltwater percolation, migration, diffusion, wind drifting and erosion, ablation, sublimation, and evaporation can alter the ice and snow isotope and trace ion record (e.g., Schotterer et al., 2004). There have been many studies from temperate glaciers that indicate that meltwater percolation and migration of isotope and chemical species have influenced their measured values in the accumulated snow and ice (e.g., Thompson, 1979; Raben and Theakstone, 1994; Motoyama et al., 2000; Yuanqing et al., 2000), particularly evident in glaciers of lower elevations (less than 1500 m).

In temperate glaciers post-depositional processes can cause isotopic fractionation and migration, which may alter the original $\delta^{18}O$ profile, as meltwater has depleted isotopes ratios compared to the remaining snow cover (Schotterer et al., 2004). Post-depositional processes effect the distribution of oxygen isotopes and the isotopic lapse rate (see Section 6.7.4) can break down on temperate glaciers at elevations below 1000 m (Ruddell and Budd, 1990). The most important changes occur during the surface snow to firn transition (Arnason, 1969; Moser and Stichler, 1975; Thompson, 2000). Despite the effects of melt on the $\delta^{18}O$ record, a seasonal signal is still detectable in some ice core records where post depositional effects occur (Oerter et al., 1985; Yuanqing and Theakstone, 1994; Matsuoka and Naruse, 1999; Yuanqing et al., 2000; Taylor et al., 2001; Schotterer et al., 2004), enabling net balance to be estimated.

Trace ion records may also be obscured by post-depositional melting because as snow melts on the surface of glaciers the meltwater is at first held in capillaries and on pore walls where it will fill 5 to 10% of the pore space before it becomes more mobile (Colebeck, 1978 as cited in Tsiouris et al., 1985). As further melt develops the water mobilises solutes which it acquires from the pore walls by diffusion or convection. The order of elution is predominately due to the position of the solutes within, or attached to the outside of snow crystals, and also depends on the atmospheric history of the snow (Tsiouris et al., 1985). There have been several suggestions for the exact order of elution (e.g., Tsiouris et al., 1985; Goto-Azuma et al., 1993; Raben and Theakstone, 1994; Ilzuka et al., 2002). It appears that to some extent the elution order is site dependent, although most sources agree that sodium and chloride are the last to be removed (Tsiouris et al., 1985).

In some regions (i. e., at Baishui Glacier Mt Yulong, China) even with meltwater influence on the snow pack chemical records were found, but with a smaller amplitude then in pre-melt records (Yuanqing et al., 2000). Goto-Azuma et al. (1993) discovered layers of significantly high ionic concentrations found at snow/ice boundaries, which they attributed to superimposed ice formation during winter months. Motoyama et al. (2000) inferred that meltwater percolates through the snow cover transporting the impurities then refreezes them elsewhere providing a re-constructed signal but not the initial environmental signal in the snow.

Due to the high summer temperatures and influence of föhn winds on the glacier surface (see Sections 4.4.4) meltwater percolation is likely to be one of the dominate sources of post-depositional alteration of the Brown and Stephenson glaciers, trace ion and oxygen isotope records.

6.3.2. Seasonal signals in temperate glaciers

Oxygen isotopes This method was first developed for polar regions and more recently used to investigate the paleoclimate on high altitude temperate and tropical glaciers (e.g., Thompson, 2001; Schotterer et al., 2004). The stable isotopes in non-polar glaciers are often affected by meltwater percolation, which produces homogenisation and $\delta^{18}O$ enrichment (Thompson, 1979), as warmer temperatures produce both melt and rain.

It might be reasonable to assume that Heard Island would have a homogenised oxygen isotope record given its warm, maritime environment. Truffer et al. (2001) collected samples from a 0.8 m snow pit (BP1) near the BG35 net balance stake (at 498 m) and from a 12 m crevasse (C1) located at 53°05' S 73°35' E and an elevation of 1050 m on Brown Glacier. Isotope analysis revealed a nearly homogenised record with isotope values ranging from -9 to -11 ‰ in

the crevasse and −8 to −15 ‰ in the snow pit (Figure 6.3). In order to interpret the seasonal signals in these smoothed isotopes records a comparison is often made to additional parameters, for instance, Schotterer et al. (1997) used nearby temperature records, and Short and Holdsworth (1985) uses pollen deposition. Truffer et al. (2001) used the visible debris layers in the crevasse walls to estimate a net balance from C1; the debris layers identified at 2.6 m and 8.8 m were on the leading edge of the higher, summer isotope values (Figure 6.3A).

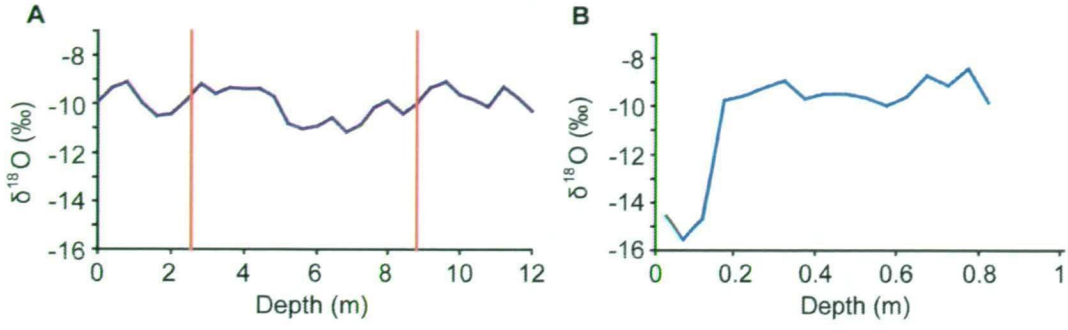

Figure 6.3.: The oxygen isotope results from the 2000 crevasse and snow pit. **A.** Crevasse $\delta^{18}O$ record. Red lines indicate debris layers. **B.** Snow pit $\delta^{18}O$ record. Figures based on data in Truffer et al. (2001).

Trace ions The concentrations of trace ions are much higher in temperate glaciers than in Antarctica (Thompson et al., 2003). The seasonal signals and long term climate changes found in ice records are very site specific. There have been no published studies found which have conclusively determined the source areas and seasonality of the precipitation on Heard Island. It is assumed that the maritime setting and the effect of dust and ash deposits on the glacier are the sources of the majority of the impurities deposited on Heard Island. As there are few anthropogenic sources of atmospheric aerosols in the vicinity of the isolated island. Nor is sea ice likely to effect the recent transport of aerosols as sea ice (in the form of pancakes and grease ice) was observed only 18 times in Atlas Cove between 30 July and 14 October 1948 (Lambeth, 1950) (there were no other records found of sea ice forming around Heard Island).

Spencer et al. (1985) analysed ice samples collected in March 1983 from a bergschrund on Big Ben at 2450 m asl, hereafter referred to as site SP83, as an initial investigation into whether glaciochemical studies on Heard Island were feasible. They analysed for fluoride (1 to 3.3 μ Eq L^{-1}), chloride (1 to 110 μ Eq L^{-1}), sodium (3 to 50 μ Eq L^{-1}), sulphate (1 to 9 μ Eq L^{-1}), bromide (0.5 to 0.2 μ Eq L^{-1}), nitrate (0.5 to 3.5 μ Eq L^{-1}) and iron (0.01 to 0.2 μ Eq L^{-1}) to a depth of 3 m (Spencer et al., 1985) (Figure 6.4). The trace ion analysis allowed them to make a first estimate of the winter accumulation of 1.0 m w.e. and summer accumulation of at least 1.2 m w.e. (as their snow pit did not necessarily represent a balance year) at an elevation of 2450 m on Big Ben.

The results of the Spencer study indicated that at higher elevations on Heard Island there is no seasonal signal in the fluoride, and that chloride, sodium and sulfate all have a similar ion profile (Spencer et al., 1985). Bromide concentrations had several maxima and nitrate has a maximum concentration between 0.2 to 0.4 m depths (Spencer et al., 1985). Spencer et al. (1985) suggest that marine-source ion species such as chloride, sodium and sulfate are useful

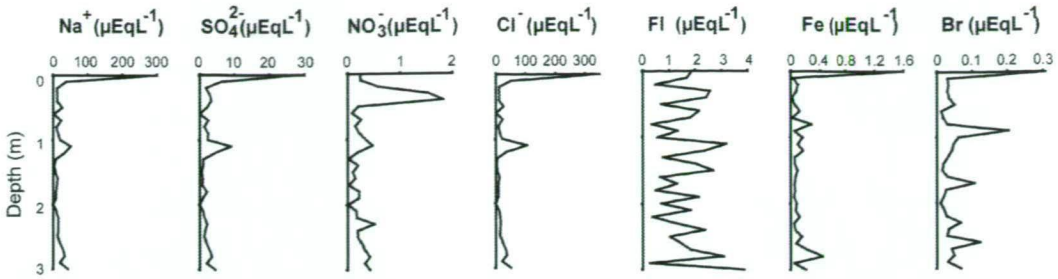

Figure 6.4.: The trace ion results from samples analysed by Spencer et al. (1985) in March 1983 (data supplied by P. Mayewski, pers. com. 8 July 2005).

in identifying seasons in snow pits on Heard Island and that nitrate may be a useful seasonal signal even though its source cannot be uniquely specified.

6.4. Sampling sites

Ice cores, crevasse and surface samples were collected from several sites on Brown, AU1121 and Stephenson glaciers. The two ice cores and three crevasses sites were located in the accumulation area, of either Brown or Stephenson glaciers (Figure 6.5 and Table 6.1). The surface samples were collected from 19 locations across Brown Glacier and two locations on AU1121 Glacier in both the accumulation and ablation areas. All of the samples were collected in January and February of 2004 in conjunction with the 2003/04 mass balance survey (as described in Chapter 5).

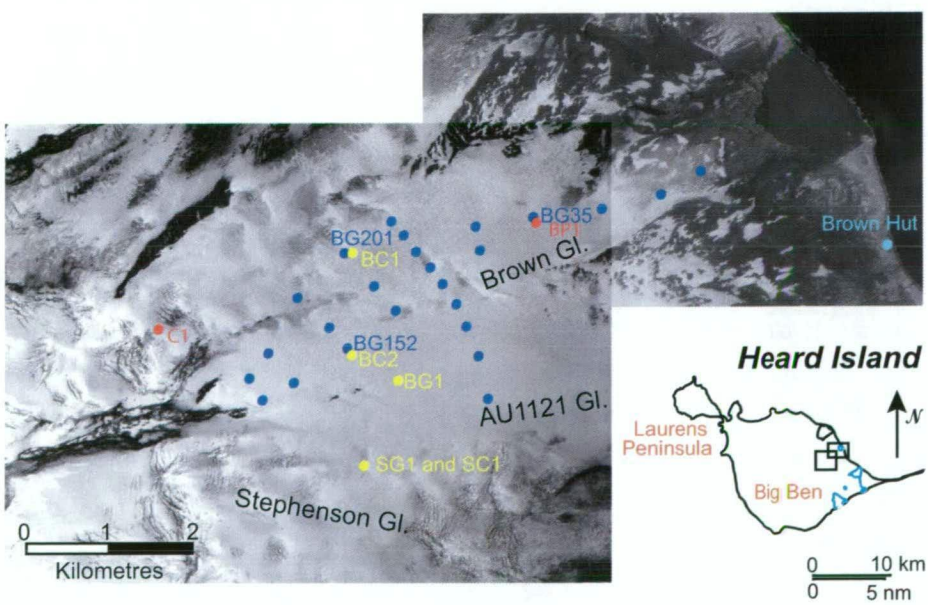

Figure 6.5.: The January 2003 Digital Globe satellite image of Brown, AU1121 and Stephenson glaciers showing the season 2 survey cane sites (blue), the 2004 Brown Glacier ice core (BG1), the Brown crevasses (BC1 and BC2) and Stephenson ice core and crevasse (SG1 and SC1) locations (yellow). In addition, the 2000 crevasse and snow pit sites (red) and Brown Hut (light blue) are shown. Inset map shows the location of the satellite image.

BG1 ice core The first ice core was drilled on 4 January 2004 on Brown Glacier. The coring site was located at 53°05'36" S 73°05'11" E and 799 m asl near the ice divide between Brown and AU1121 glaciers (Figure 6.5 and Table 6.1). The total core length was 3.34 m.

SC1 crevasse The SC1 crevasse was sampled on the 6 and 7 January 2004. This crevasse was located in Stephenson Glacier at 53°05'56" S 73°36'46" E and at 922 m asl (Figure 6.5 and Table 6.1). The SC1 crevasse ran 15 m northeast-southwest along the surface and was 2 m at its greatest width. The floor of the crevasse was 11 m from the surface. An additional 3 m of snow was removed from the floor to sample a further 2.4 m. The bottom of the crevasse was 1.5 m wide and narrowed toward the southwest to a few centimetres. To the northeast the crevasse narrowed and a snow ramp extended to the surface.

BC1 crevasse BC1 was located near the BG201 survey stake on Brown Glacier and was sampled on 14 January 2004. The position of BC1 was at 756 m asl and 53°05'3" S 73°36'35" E (Figure 6.5 and Table 6.1). The crevasse was sampled after a snowfall therefore the walls had a light coating of snow. The crevasse ran northwest-southeast, was 8 m long and 1.5 m wide, with a depth of 10.2 m.

Table 6.1.: A list of all ice core, snow pit and crevasse sampling sites on Heard Island.

Site	Glacier	Type of site	Date sampled	Latitude	Longitude	Elevation	Depth
BG1	Brown	Core	4/01/04	53°05'36"S	73°05'11"E	799m	3.34m
SC1	Stephenson	Crevasse	6 to 7/01/04	53°05'56"S	73°36'46"E	922m	13.4m
BC1	Brown	Crevasse	14/01/04	53°05'3"S	73°36'35"E	756m	10.2m
SG1	Stephenson	Core	16/01/04	53°05'56"S	73°36'46"E	922m	1.9m
BC2	Brown	Crevasse	9 and 11/02/04	53°05'31"S	73°36'39"E	869m	8.5m
BP1	Brown	Snow pit	31/10/00	53°04'55"S	73°37'58"E	498m	0.8m
C1	Brown	Crevasse	12/11/00	53°05'S	73°35'E	1050m	12m
SP83	Big Ben Plateau	Bergschrund	03/83	~53°06'S	~73°33'E	2450m	3.0m

This was the only crevasse that we sampled that had water dripping down the walls. Also, whereas in SC1 we were able to start at the bottom of the crevasse and work our way up the wall in a continuous sampling line, in BC1 due to ice columns, collapsed snow bridges and refrozen meltwater structures the sampling line was altered twice. The first was a shift following an ice layer from the 'cave' to a more open area (10.2 to 5.4 m), thereby preserving the layer sequence. The second change in the sampling line was to the opposite wall. In an attempt to represent a continuous sequence the opposite wall was sampled from 5.6 to 0.0 m. The over lap between these two sequences is short due to time constraints in the field.

SG1 ice core The SG1 ice core was drilled on 16 January 2004 at 53°05'56" S 73°36'46" E and 922 m asl on the Stephenson Glacier 1m from the SC1 crevasse site (Figure 6.5 and Table 6.1). The ice core was 1.9 m long.

BC2 crevasse The BC2 crevasse was located at 53°05'31" S 73°36'39" E and 869 m asl on Brown Glacier (Figure 6.5 and Table 6.1). BC2 was located 10 m to the southeast of the

BG152 stake. The crevasse was 1 m wide and 15 m long at the surface and 8.5 m deep. There were snow ramps to either side of the sampling wall extending to within 2 m of the surface.

On 9 February, BC2 was sampled from 8.5 to 2.9 m. A snow storm suspended sampling on the 10 and 11 February, and filled the crevasse with snow. On 12 February BC2 was sampled from 3.4 to 0.0 m, giving, 0.5 m overlap with the 9 February samples.

The collection of samples in the BC2 crevasse was complicated by the local weather. On the 9 February there were snow flurries. The snow would fall or be blown into the crevasse coating the walls and collection instruments. Precautions were taken to ensure that none of the falling and blowing snow entered the sampling bag.

On the 12 February we were unsuccessful in relocating the exact sampling site by GPS. Instead we removed ~ 3 m^3 of snow to a depth of 3.4 m in the same crevasse within 5 m of the original site (the accuracy of the GPS position) and collected samples from 3.4 m to the surface. There was a 0.5 m overlap in depth between these two sampling lines because due to failing light we only had time to expose 3.4 m of the crevasse wall.

Snow surface and rain water samples Snow surface samples were collected from 19 sites on Brown Glacier and two sites on AU1121 Glacier. There were four rainwater samples collected in a rain gauge near Brown Hut (Figure 6.5). There were four days of snow surface sampling. The first was 25 January 2004, where only two samples were collected at 715 m asl (BG258 and BG257) of the previous night's snowfall. The second day of sampling was on 26 January 2004 when samples were collected from all upper glacier canes ranging from 673 m to 1030 m asl (except for the two that were sampled the previous day). There are four samples that represent a fresh snowfall (at BG20, BG202, BG151 and BG15) that occurred during sampling. The third sampling date was 11 February 2004. One sample was collected from a snow bank on the lower part of the glacier at ~ 350 m asl. The final collection date was 12 February after a snowfall in the previous 12 hours. The canes on the upper Brown Glacier (756 m to 1030 m asl) were re-sampled with the addition of one new site at 407 m asl (BG40) on the lower glacier.

The rainwater samples were collected on 12, 14-15, 19 and 20 February 2004. The rainwater samples were collected from a rain gauge that was located at 4 m asl.

6.5. Stratigraphic sampling techniques and analysis methods

The ice cores, crevasse, surface and rainwater samples were intended to complement each other i. e., an ice core would be drilled then a nearby crevasse sampled to a greater depth, which could in turn be compared to the oxygen isotope values measured in the surface and rainwater samples. After some complications with the ice corer we realised that the crevasses would provide easier access to a much deeper record of stratigraphic markers and therefore likely to include a multitude of seasonal cycles rather than a partial cycle that was available from an ice core depth.

6.5.1. Field sampling techniques and storage

Crevasse sampling The crevasses were sampled from the bottom to the surface at 0.20 m intervals. At each 0.20 m interval an ice axe was used to chip away the surface melt layer. Then an auger or ice screw was used to extract ice from the wall (Figure 6.6). Both of the tools were 'cleaned' by drilling in the opposite wall and discarding the sample. Additionally, at each site the ice screw was drilled flush with the wall to ensure that the ice from the previous site was cleared from the barrel before sampling commenced at the new site.

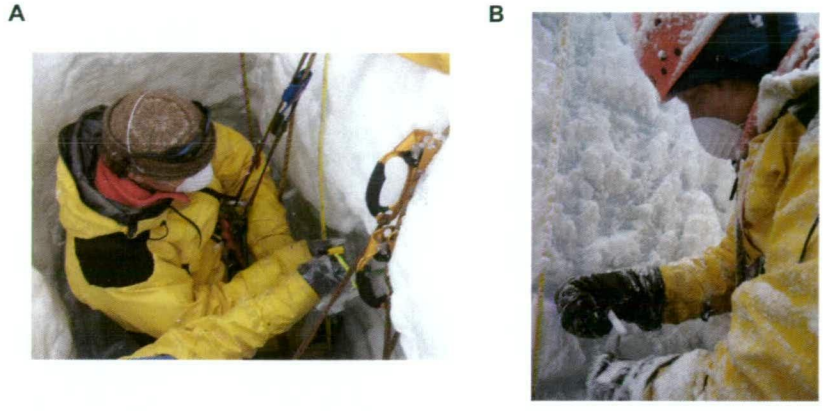

Figure 6.6.: Sampling for trace ions and oxygen isotopes in the BC2 crevasse. **A**. gloves and a dust mask were worn at all times, and **B**. samples were collected directly from the ice screw into the Whirl-Pak bag.

The first two crevasses sampled (SC1 and BC1) were collected with the intention of analysing for oxygen isotopes only. A pre-cleaned plastic dustpan was placed below the auger or ice screw to collect the ice samples, which were then stored in Whirl-Pak plastic bags for transport to sea level. The dustpan was wiped or knocked clean of snow and ice after each sample.

The last crevasse (BC2) was sampled for impurities and isotopes therefore a dustpan was not used. Instead the ice was collected directly from the ice screw barrel into a Whirl-Pak bag. Only gloved hands touched sampling equipment and dust masks were worn as an additional precaution against contamination.

Core sampling At each of the coring sites a tent shell was set up to create an isolated environment. A 72.5 mm diameter Kovacs corer was used to drill both of the cores (Figure 6.7A). To clean the Kovacs corer for trace ion sampling a 1 m core was drilled and discarded. Once coring began each section of the core removed was placed directly on a plastic covered V channel in the tent (Figure 6.7B). First all the visible features in the core were recorded. Then the core was cut into 0.10 m sections with a stainless steel pruning saw or paint scraper. All metal instruments where cleaned by abrasive action in a fresh snow surface before use. The paint scraper was then used to remove the outer centimetre of the core before storing the ice in Whirl-Pak bags (Figure 6.7C). When sectioning the core, plastic gloves and a dust mask were worn at all times to minimise contamination of the ice samples.

The Kovacs core barrel and extensions were each 1 metre long yet the corer tended to stick at shorter intervals. A typically core section length was 0.5 m to 0.2 m depending on the drilling site.

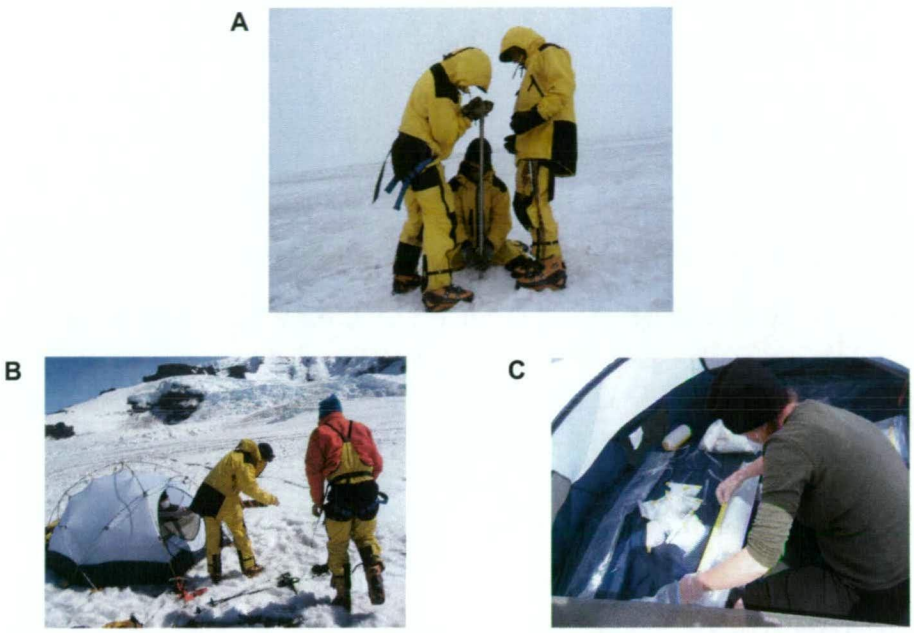

Figure 6.7.: Examples of coring at BG1 and SG1 **A**. the Kovacs corer, **B**. transferring the core into the tent and **C**. measurement of the core section.

Snow surface and rainwater sampling Surface snow samples were collected by scraping the top centimetre of fresh snow away from a 0.02 m^2 area of the surface. The fresh snow was then placed in a Whirl-Pak plastic bag for transport to sea level. The rainwater samples were collected from a rain gauge near Brown Hut. The rain was collected in a standard Bureau of Meteorology rain gauge. The gauge was checked each morning at 8:00 LST, which provided a 24-hour collection period (except between the 14 to 15 February where it was left for 48 hours).

Sample storage All samples were stored in high-density polyethylene 60 ml Nalgene bottles. The Nalgene bottles were cleaned prior to departure from Hobart. Each Nalgene bottle was rinsed three times with deionised milli-Q water, filled with deionised milli-Q water to rest for more than 24 hours (repeated three times) and then emptied for transport to Heard Island.

All crevasse, core and surface snow samples collected were transported to sea level. Here they were left to melt (+24 hours for the 30 ml w.e. crevasse and snow surface samples and +36 hours for the 0.10 m core sections) and bottled in Brown Hut. Extra care was taken in reducing possible contamination of impurities. When decanting the melted snow and ice from the Whirl-Pak bags into the Nalgene bottles plastic gloves and dust masks were worn and bottles were overfilled. All the sample bottles were then stored in a polyethylene plastic storage container, away from sunlight, near the coast until returned to Australia for analysis.

6.5.2. Stratigraphy logging

Snow and firn layers are typically described based on visible changes. Light coloured layers, which can appear opaque, white or clear, are produced when accumulation is greater than melt (winter). Darker layers (i. e., debris bands) are formed where there is increased melt, which consolidates sediment (summer) (Paterson, 1994). The thickness of snow and ice between two light layers may be equivalent to one year of net balance. If a debris layer or ice lens was present in the cores or crevasses the depth and the thickness of the layer was measured and recorded.

6.5.3. Analysis techniques for oxygen isotope

The snow/firn/ice samples were all melted in the field before being returned to Australia for analysis. Oxygen isotopes were measured using a VG Isogas SIRA mass spectrometer, with a VG isoprep 18 equilibration bench. The mass spectrometer was used to separate gas molecules according to their mass by laboratory technicians at the ACE CRC.

6.5.4. Analysis techniques for trace ions

All ice samples from Heard Island were melted in the field and returned to the AAD Ion Chromatography (IC) Laboratory at the University of Tasmania for analysis. The ice and snow from Heard Island were analysed for chloride, nitrate, sulphate, sodium, magnesium, calcium and MSA using suppressed ion chromatography, with assistance from laboratory technicians at the AAD IC Laboratory.

IC analysis techniques used to detect low level trace ion concentrations in Antarctic cores by Curran and Palmer (2001) were used for the Heard Island samples. All standards and samples were loaded by pipetting 5 ml into autosampler vials. In some cases there were large particles in the sample bottles. These were allowed to settle to the bottom of the bottles before supernatant water was drawn for analysis. A Dionex DX500 microbore (2 mm) ion chromatograph with a CD20 conductivity detector and a GP40 gradient pump were used to simultaneously separate and detect the anions and cations in the samples (see Curran and Palmer, 2001).

6.6. Results from stratigraphic analysis

The results of the stratigraphic analysis of the visible stratigraphy, isotopes and trace ions are presented.

6.6.1. Visible stratigraphy results

Freshly fallen snow and refrozen ice features on the walls of the BC1 crevasse obscured most of the structures in the ice. The best visible structures were in the 'cave', which had 0.01 to 0.02 m thick alternating white and opaque layers. Other structures included a debris band (0.03 m thick) at 2.90 m, the ice/compacted snow (firn) boundary at 0.80 m, and alternating opaque and white snow layers with an average thickness of 0.10 m at ~ 2.0 to 5.0 m depth (Figure 6.8A).

The falling and blowing snow in BC2 during sampling made observing the stratigraphy difficult. The crevasse appeared to have alternating white (0.10 m thick) and opaque (0.01 to

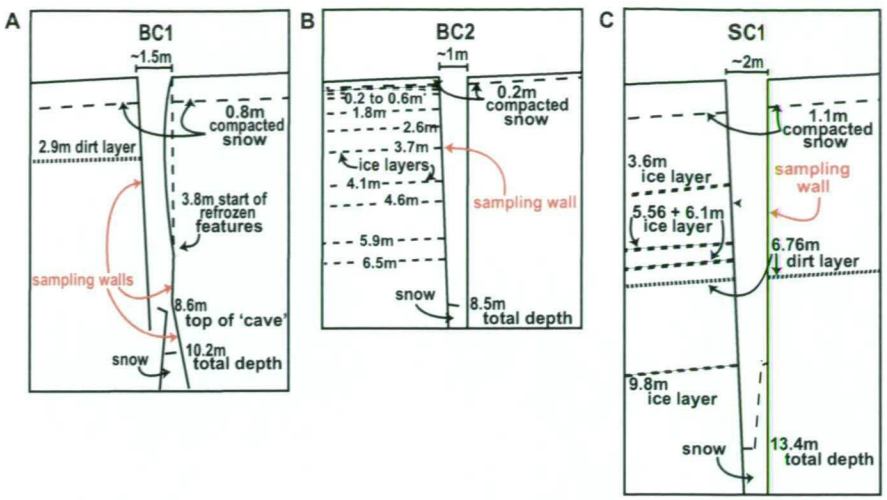

Figure 6.8.: Crevasse profiles for **A**. Brown Glacier crevasse 1 (BC1) , **B**. Brown Glacier crevasse 2 (BC2), and **C**. Stephenson Glacier crevasse (SC1). Not to scale.

0.02 m thick) layers. The majority of these observed structures were seen in the small section of the crevasse wall that was cleared for sampling. There were no debris bands observed and the BC2 ice/compacted snow (firn) boundary was at 0.20 m (Figure 6.8B).

The SC1 crevasse had snow free walls. Layers were evident along the entire depth of the walls ranging from a centimetre to 10's of centimetres thick (Figure 6.8C). Layers alternated between opaque and white in appearance. The opaque layers were thinner (approx. 0.01 m) than the white layers (approx. 0.05 m). The walls were composed of ice except for a 1.10 m thick compacted snow layer (firn) at the surface. There were ice layers at 9.80 m (0.01 m thick), 6.10 m (0.03 m thick), 5.56 m (<0.01 m thick) and 3.60 m (0.03 m thick) from the surface. At 6.76 m from the surface there was a 0.01 m thick debris band. There were smaller debris lenses, but these did not extend for any great distance and did not have a corresponding layer on the opposite wall.

In the BG1 core the majority of the samples were composed of 1 mm diameter snow grains and had < 1 mm grains of debris littered through the core length. Other structures included a dirt layer at 0.37 m and ice layers (Figure 6.9A). The ice layers ranged in thickness from 0.01 m to 0.04 m. The total core length was 3.34 m yet some of this was removed due to possible contamination of swarth in the core sections, resulting in a depth of 3.10 m.

The SG1 core tended to have alternating layers of compacted snow and ice of various thicknesses (Figure 6.9B). There was only one snow layer that had a high debris content at 0.17 m.

6.6.2. Results from the oxygen isotope analysis

The snow surface $\delta^{18}O$ results are shown in Figure 6.10. These can be separated into two groups. The larger group has $\delta^{18}O$ values ranging from -13 to -7 ‰ and the smaller group has samples ranging from -21 to -18 ‰ (Figure 6.10).

The mean isotope value for the Brown Glacier ice core and crevasses was -8.4 ‰ and for the Stephenson Glacier ice core and crevasse it was -9.4 ‰ (Figure 6.11). The range for all five sites was -10.5 to -7.6 ‰. There is little variation in the range of $\delta^{18}O$ values between

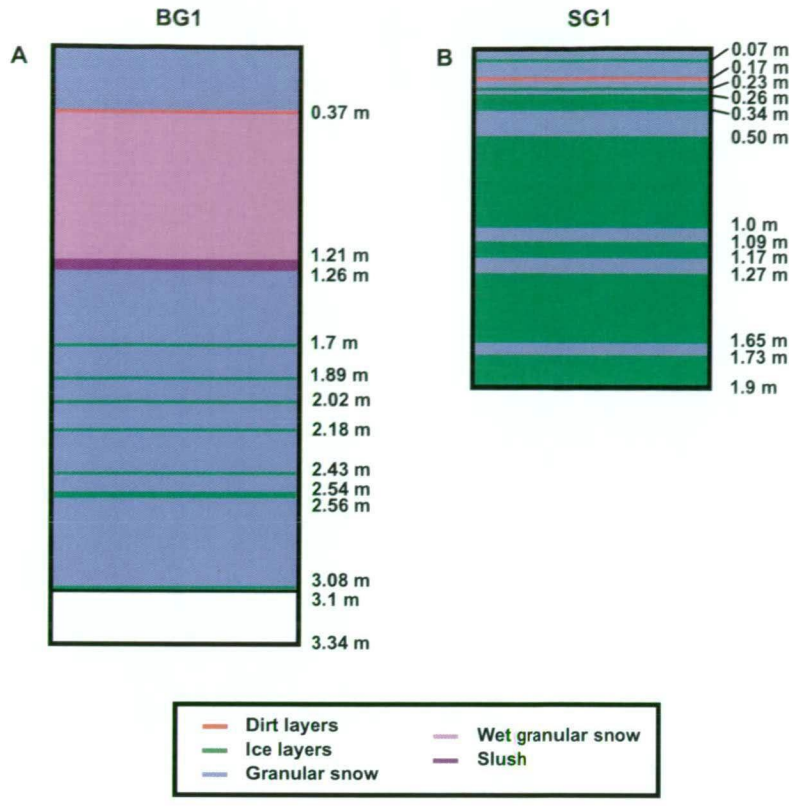

Figure 6.9.: Core profiles **A**. Brown Glacier core (BG1) and **B**. Stephenson Glacier core (SG1).

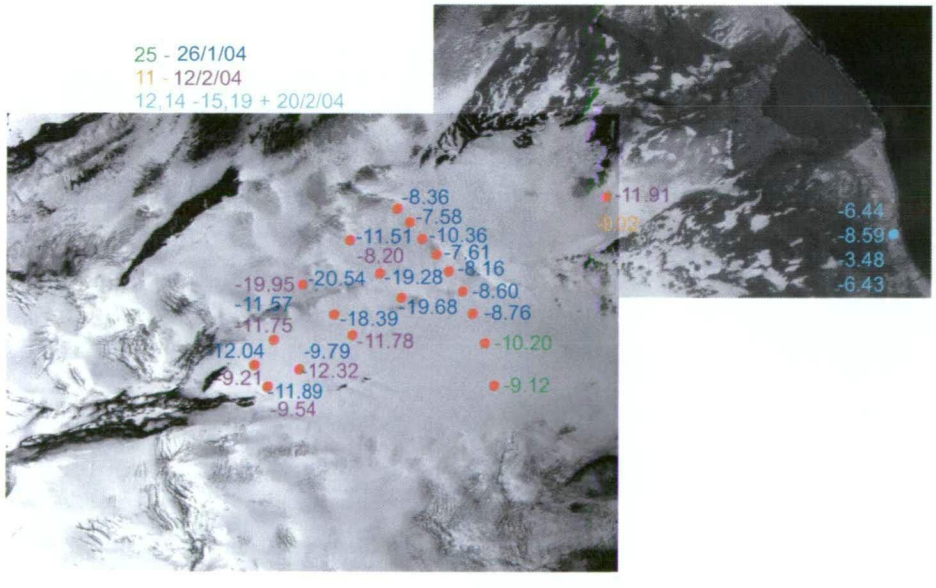

Figure 6.10.: Relative locations of the snow surface samples and oxygen isotopes values for each site shown on the 2003 Digital Globe satellite image. Colour coded according to date of collection. Rainwater samples are in light blue.

BG1, SG1, BC1, and BC2 (Figure 6.11). The BC1 and BC2 crevasse sites have an isotope record with more variability near the top of the crevasse then at depth. The two shallow cores,

BG1 and SG1, show a variability in the record for the top 1 or 2 m at each of these sites. The SC1 profile is different from all of the other sites (Figure 6.11). SC1 has a cyclical signal until 9 m. Below 9 m any cycles appear subdued.

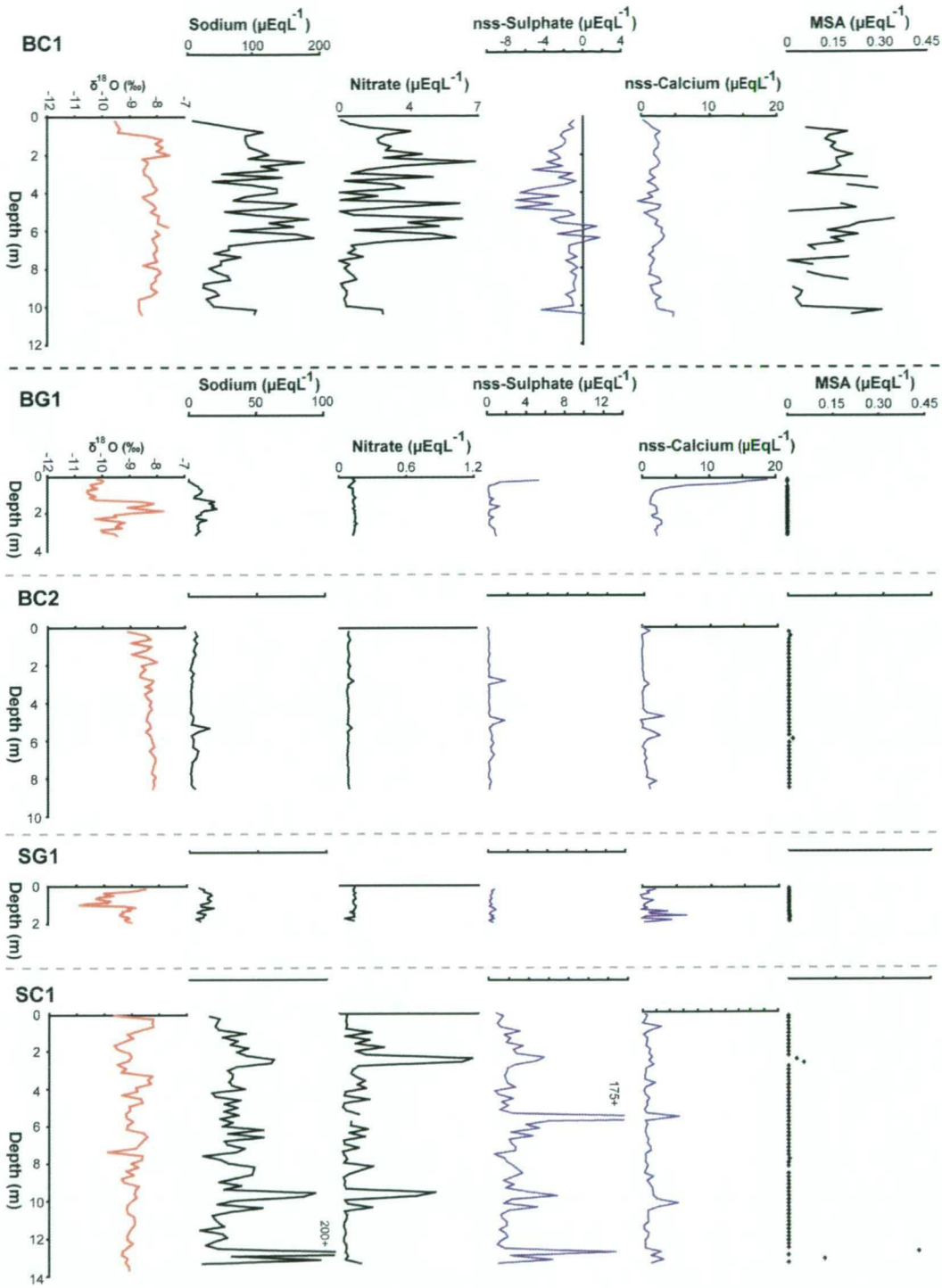

Figure 6.11.: Oxygen isotope and trace ion analysis results. **A**) BC1 crevasse, **B**) BG1 ice core, **C**) BC2 crevasse, **D**) SG1 ice core, and **E**) SC1 crevasse. The oxygen isotopes are displayed in red (left), the three measured trace ion values (sodium, nitrate and MSA) are displayed in black and the nss values (nss-sulphate and nss-calcium) are presented in blue. The vertical axis is unchanged to allow for a direct comparison with depth for each individual site. BC1 due to its high variability has a different concentration scale compared to the other four sites.

The rainwater samples ranged between −8.6 to −3.5 ‰ (Table 6.2). The highest value, −3.5 ‰, was recorded on 19 February and the lowest value, −8.6 ‰, was recorded over the 48 hour period between 14 and 15 February. The other two records from 12 and 21 February are both −6.4 ‰.

Table 6.2.: Results of the oxygen isotope analysis of rainwater samples from a rain gauge near Brown Hut

Sample name	$\delta^{18}O$ (‰)	Date Sampled	Precipitation recorded
RW-1	−6.4	12/02/04	1.5 mm
RW-2	−8.6	14 - 15/02/04	3.0 mm
RW-3	−3.5	19/02/04	4.6 mm
RW-4	−6.4	21/02/04	4.3 mm

6.6.3. Results from trace ion analysis

Representative trace ions species for each source area were plotted with depth (Figure 6.11). Sodium is a good representative of all the sea salt species (chloride, sulphate, magnesium and calcium) and nss-sulphate and nss-calcium provide an indication of the volcanic and crustal sources in the samples. Nitrate and MSA are also included because they have a different source area then the other trace ions analysed.

In the BC1 crevasse trace ion profile all seven of the measurable ions have a very similar signal (Figure 6.11A), although only representative species are shown here. The BC1 trace ion profile has a highly variable signal throughout its length compared to the other four sites. There are several maxima and minima, which are often close together creating a noisy signal. This crevasse site had the most complete MSA record. BC1 also has low nss-sulphate and nss-calcium concentrations.

The BG1 core has trace ion profiles that have distinct peaks. The ion concentrations for this core have a relatively similar profile (Figure 6.11B) except at the top of the core where there was an increase in nss-sulphate and especially nss-calcium. The other significant feature in this profile is a peak concentration for all measured values, except nitrate, at a depth of 1.7 m.

The BC2 crevasse has peaks at 3 and 5.5 m in most of the ion profiles (Figure 6.11C). The concentration of these two peaks varies between the ion species with higher concentrations of sulphate, sodium, and calcium.

The SG1 core though only 1.9 m in length is different from the other four sites. There is a variation between the different ions with depth. For example, in the top ~ 1 m of the core there are higher concentrations of sodium and nss-calcium compared to nss-sulphate yet at the bottom of the core all ions, except nss-calcium, appear to have lower concentration values (Figure 6.11D). The large variability between the ion profiles and short length of the core make it difficult to interpret the ion signals in this core or compare it to other sites.

Overall the SC1 crevasse has higher mean trace ion concentrations than BG1, BC2 and SG1. The SC1 profile has four high concentration anomalies (Figure 6.11E). The first is at 2.4 m where there is an increase in sodium, nitrate and nss-sulphate. The second is at 5.6 m where there is an increase in the nss-sulphate and nss-calcium measured values of 178.9 and 5.3 μ Eq L^{-1} respectively, but there does not appear to be a corresponding increases in the other

ions. The other two anomalies are distinguished by increases in all ion concentrations at 9.6 and 12.8 m depth (including MSA yet not in nitrate at 12.8 m) (Figure 6.11E).

6.7. Interpretation of stratigraphic analysis

Each of the stratigraphic markers are examined in more detail to investigate: local and regional precipitation, net balance estimates and identification of melt affected sites.

6.7.1. The visible stratigraphy record

There are several structures identified from the visible stratigraphy of Brown and Stephenson glaciers. However only a few of these structures could be used to estimate a net balance.

Debris bands observed in BG1, SG1 and SC1 provided a possible estimate of net balance. In BG1 and SG1 the debris bands were within 0.4 m of the surface, whereas in SC1 there was a 0.01 m thick debris band at 6.76 m (Figure 6.12). Only one debris band was observed at each of these sites therefore the estimation of the accumulation from debris bands alone would be $>0.17\,\mathrm{m\,a^{-1}}$ at SG1, $>0.37\,\mathrm{m\,a^{-1}}$ at BG1 and $>6.76\,\mathrm{m\,a^{-1}}$ at SC1.

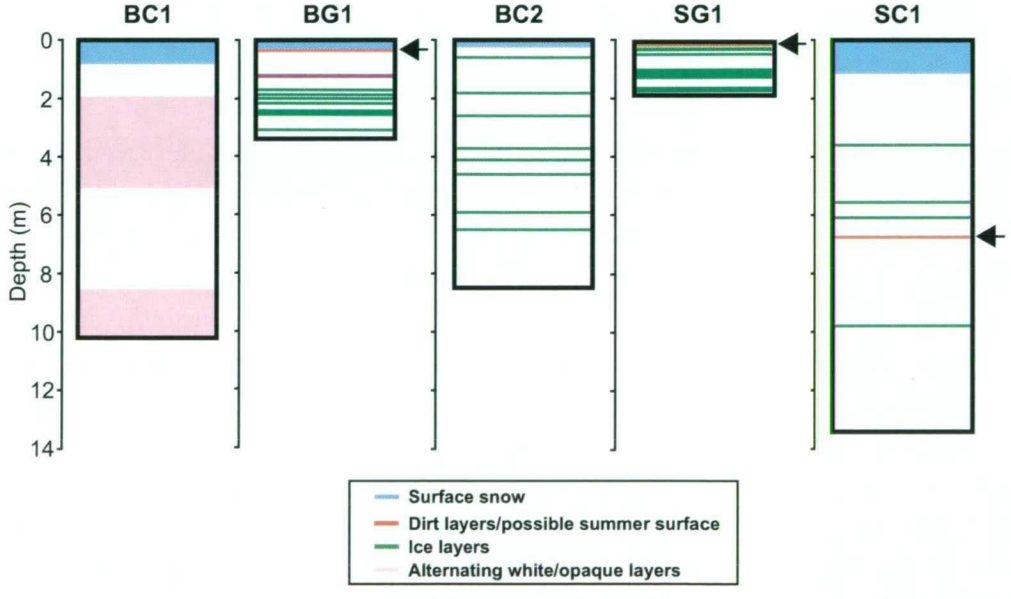

Figure 6.12.: A scaled illustration of the visible features observed in the ice cores and crevasses. Possible summer surface layers were identified (arrows) in order to determine a possible net balance estimate from visible stratigraphy alone.

Estimates based only on dirt layers as summer surface indicators may not be reliable for locations such as Heard Island. This is because at the centre of Heard Island is Mawson Peak, an active volcano, that erupts intermittently distributing wind blown debris on the island. Observations of the January summer surface of Brown and Stephenson glaciers was of a darken snow surface (Figure 6.13). This volcanic activity could hamper the determination of the net balance from dirt layers alone. As the distribution of ash lenses in the glacier record could obscure annual layering and could vary over a glacier depending on wind direction. Hence on Heard Island debris layers may provide an indication of volcanic activity rather than a marker

of the summer surface. As a result the visible stratigraphy of these ice cores and crevasses were not used to estimate the net balance.

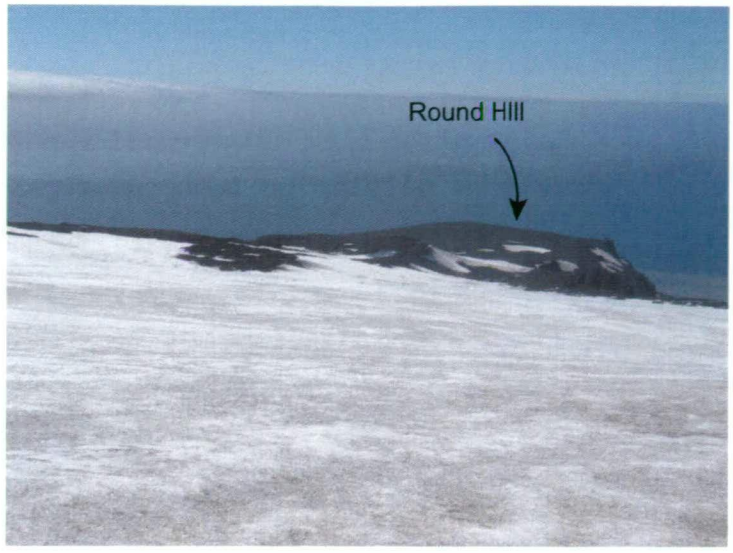

Figure 6.13.: The Brown Glacier January 2004 snow surface.

6.7.2. Nss sources in the trace ion record

Nss-sulphate The nss-sulphate record for Heard Island like other nss-sulphate records indicates that there is some fractionation in the snow pack (Palmer et al., 2001). In addition, high nss-sulphate peaks may be due to enrichment of sulfate deposition from volcanic emissions of Mawson Peak. The highest measured nss-sulphate peak, in SC1, is possibly due to an eruption that occurred in the last few years (Figure 6.11). The lower values in the other sites may be due to smaller volcanic events or blowing debris from an older volcanic event, fractionation or tropospheric emissions (Figure 6.11 and Table 6.3). Unfortunately none of these possible volcanic events corresponds with a debris layer in the crevasses and cores, which would have provided a visible indication of an eruption. The lack of a volcanic debris layer in the Heard Island ice core records may be a result of wind transport or as a result of meltwater locally super-cleaning the ions, by flushing away debris deposited in the upper surface layers of the glacier.

Table 6.3.: Mean nss-calcium and maximum nss-sulphate values (μEq L^{-1}) from the Brown and Stephenson Glacier sites.

Site	BC1	BG1	BC2	SG1	SC1
nss-sulfate	1.68	5.26	1.80	0.80	178.86
nss-calcium	0.07	0.38	0.20	0.19	0.08

Nss-calcium High nss-calcium average values at each of the sites, particularly at BG1, could originate from local rock outcrops (Figure 6.11 and Table 6.3). A high dust signal at these sites were expected given the close proximity of Long Ridge and other rock outcrops in the Brown

and Stephenson glacier basins and the near constant winds, which cross the upper glacier predominately from the south and southwest (see Section 4.3.4).

6.7.3. Regional seasonal signals in the Heard Island oxygen isotope values

The summer $\delta^{18}O$ values measured from rainwater on Heard Island provide an indication of the degree of oxygen isotope depletion in the water vapour deposited at sea level (-8.6 ‰, -6.2 ‰ and -3.5 ‰). These rainwater $\delta^{18}O$ values are within the same range as the longer, annual sea level data sets from Cape Grim (40°41' S 144°41 E), Margate (43°01' S 147°09' E), and Macquarie Island (54°30' S 158°57' E) (Figure 6.14). These three Tasmanian sites have a seasonal signal in the $\delta^{18}O$ record alternating between mean monthly values of -6.3 ‰ and -2.3 ‰ with a minimum value of -21 ‰ at Macquarie Island and a maximum value of 2.3 ‰ at Cape Grim (Figure 6.14) (V.I. Morgan and W.F. Budd pers. com. 2005). The variation in the Heard Island annual $\delta^{18}O$ rainwater values is unknown but because they fall within a similar range as the three Tasmanian sites it is assumed that Heard Island could have a similar 4 to 5 ‰ range in $\delta^{18}O$ values over the year at sea level.

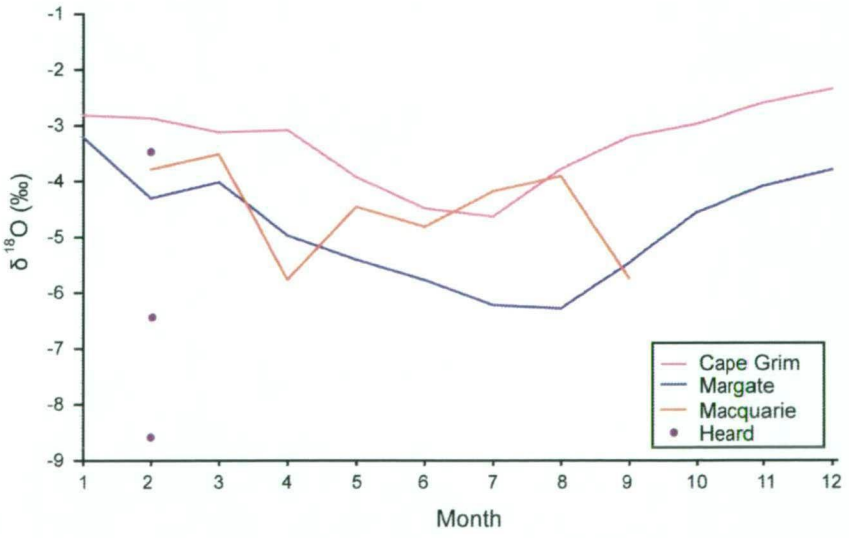

Figure 6.14.: Seasonal cycle of rainwater oxygen isotope samples from three Tasmanian sites (Cape Grim, Margate and Macquarie Island from the unpublished data of V.I. Morgan and W.F. Budd) and four days sampled on Heard Island.

The Brown Glacier samples are likely to have a lower isotopic value compared to isotopes deposited on the western side of the island. This continental effect is demonstrated by comparing the mean monthly isotopic values from Margate and Cape Grim (Figure 6.14). The Cape Grim average monthly values are higher then the Margate values because Cape Grim is located on the west coast of Tasmania and therefore is closer to the ocean source, which has a $\delta^{18}O \approx 0$. Margate on the other hand is located in the south of Tasmania. The westerly winds that bring precipitation to Margate must pass over the western half of the state before depositing heavier isotopes en route resulting in Margate having lower average monthly isotopic values.

6.7.4. Spatial distribution of oxygen isotopes on Brown Glacier

The variability of $\delta^{18}O$ accumulated on a glacier surface can be attributed to the combined effects of atmospheric circulation and glacier topography (Munro, 2005). As the sensitivities of temperature and precipitation anomalies on the glacier surface are characteristics that change from year to year in spatially diverse patterns. A compilation of this surface data can enable a better understanding of the variation in the depletion of $\delta^{18}O$ in precipitation in terms of the temperature and elevation at a particular location (Morgan, 1982).

A change in isotopic value with elevation is often expressed as an isotopic lapse rate, defined as the change in the $\delta^{18}O$ per 100 m increase in altitude. Isotopic lapse rates are fairly consistent worldwide though are better constrained at elevations of less than 5000 m (Poage and Chamberlain, 2001).

The first snow samples collected to investigate the surface spatial distribution of $\delta^{18}O$ on Heard Island where collected by M. Hendy and party, a group of climbers, who descended the northeastern slopes of Big Ben near Long Ridge, which is just above Brown Glacier, in 1983. These seven samples collected from elevations ranging between 2720 and 300 m asl were kept in storage for two years before analysis. It is assumed that all of the samples were stored in the same manner and therefore can assume that although the values measured may not be a true isotopic value, the relative difference between the samples should be approximately the same as if the samples had been analysed sooner. The Long Ridge-Big Ben surface samples have an average lapse rate of -0.25 ‰ per 100 m (Figure 6.15).

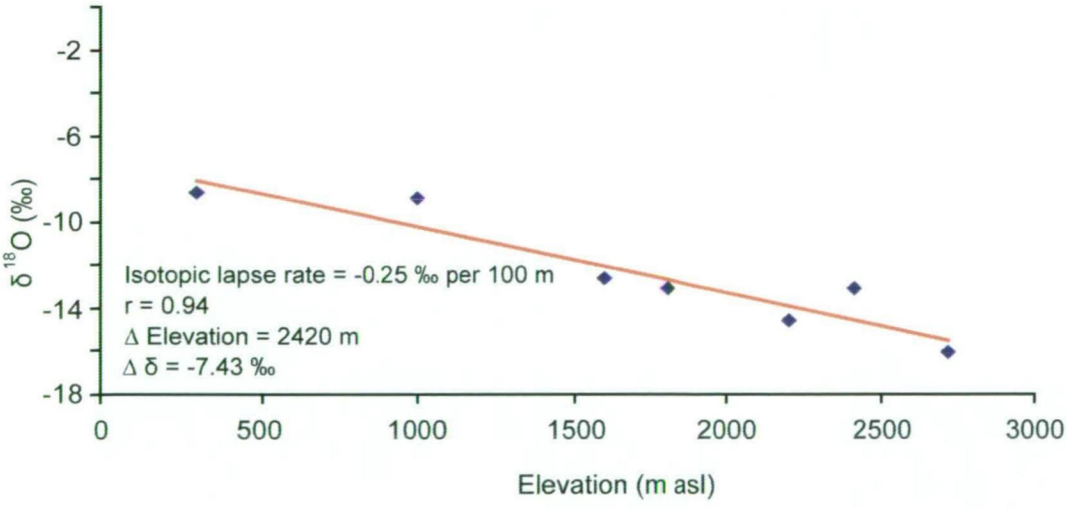

Figure 6.15.: The oxygen isotope values for surface snow samples collected by a climbing party in 1983.

The Brown Glacier isotopic snow surface samples, collected between 250 and 1034 m asl, provide an isotopic lapse rate (slope) of -0.58 ‰ per 100 m (Figure 6.16). The Brown Glacier rate is higher than other published isotopic lapse rates, whereas the Long Ridge-Big Ben rate is lower (e. g., -0.45 ‰ per 100 m at Mt Blanc, -0.35 ‰ per 100 m Cordillera Blanca, Peru (Poage and Chamberlain, 2001) and -0.30 ‰ per 100 m near Mt Blanc (Moser and Stichler, 1975)). The wide range in isotopic lapse rates seen globally are often the result of inconstant isotopic deposition due to the variability in storms making it difficult to make any definitive conclusions about the relationship between isotopic value and elevation change.

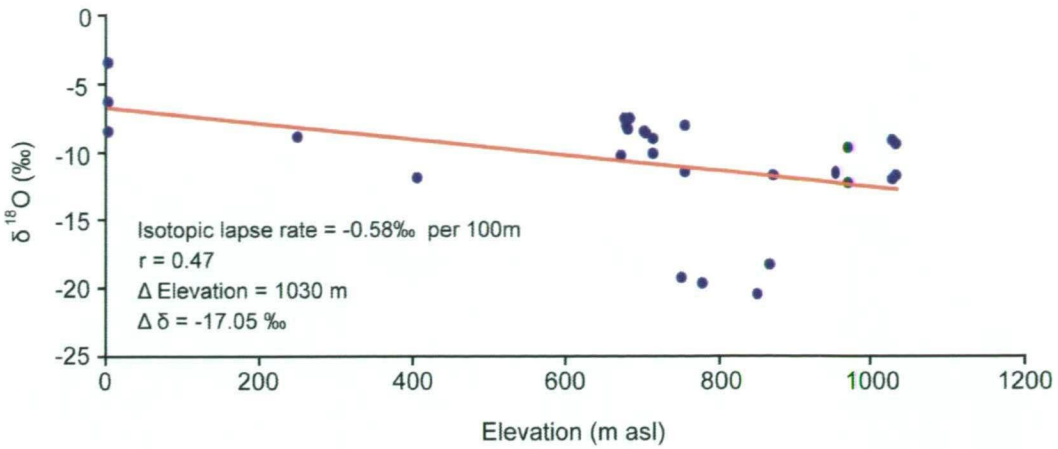

Figure 6.16.: The season 2 snow surface and rainwater results with respect to elevation.

6.7.5. Storm events in the isotopic record

The snow surface isotope samples also provided an opportunity to observe a change in the local atmospheric composition during a storm event. Storms or fronts that cross Heard Island build and progress toward the Island from the surrounding southern Indian Ocean waters. Once precipitation begins in a frontal system the oxygen isotope composition of the water vapour within the storm clouds begins to be depleted in heavy isotopes. The majority of fronts and storm systems that progress over Heard Island move relatively quickly depositing only relatively heavy isotopes (-11 to -7 ‰). On occasion storm systems will stall as the air flows over Big Ben. In these instances if precipitation continues the heavier isotopes in the water vapour becomes depleted leaving the lighter isotopes (-25 to -18 ‰) to be deposited.

On 26 January 2004 a stalling storm system passed over Heard Island. Early in the morning of the 26 January we experienced no precipitation during the traverse from sites BG256 to BG253. Then light snowfall began and the AWS3 located at 920 m asl recorded a drop in wind to below 5 kt from 12:30 to 18:50 LST that evening on Brown Glacier. Along the BG201 to BG202 traverse line and at BG15 and BG151 there was enough snow fall for a totally fresh snow sample to be collected. The δ^{18}O values from these samples range from -20.5 to -18.4 ‰. These lower values are similar to those measured at Law Dome (-24 to -18 ‰) (Van Ommen and Morgan, 1997), other coastal Antarctic sites (-28 to -15.2 ‰) (Morgan, 1982) and the B09B and C08 icebergs (-23 to -14 ‰) (Long, 2004). In order to illustrate the changes in δ^{18}O with time all of the samples collected on 26 January 2004 are plotted against time of collection (Figure 6.17).

These stalling storm systems may be a frequent event during a Heard Island summer as the snow surface samples collected on 12 February 2004 indicate a similar stalling storm system crossed Brown Glacier as evident by one surface sample (-19.95 ‰) collected at BG10. The stalled storm systems and their effects on isotopes described here have also been investigated by Holdsworth and Krouse (2002) at Mt Logan, Canada.

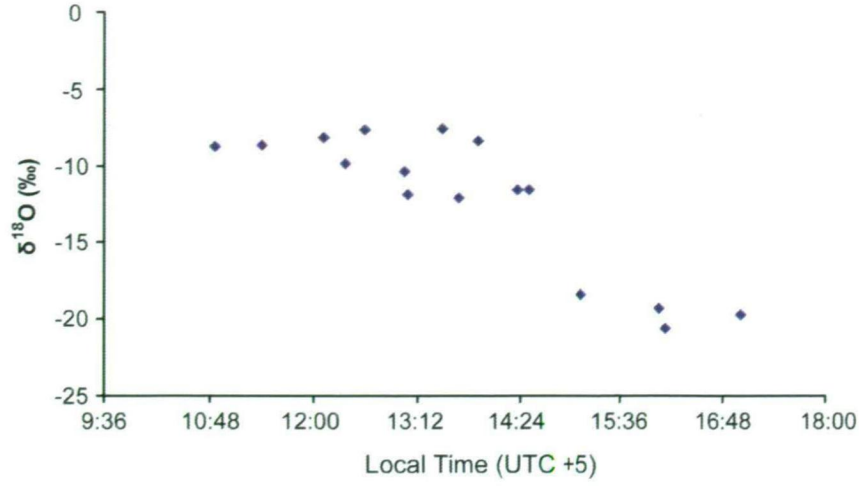

Figure 6.17.: Snow surface sample record with respect to time of collection on 26 January 2004. Precipitation began at around 14:00 Local time (UTC ~ +5) illustrating the difference in the previous day's snow fall (collected before 14:00), which have the higher $\delta^{18}O$ values, compared to the lower $\delta^{18}O$ values associated with the storm event. This shows that there can be changes in the isotopic composition of the water vapour when storms pass over Brown Glacier

6.7.6. Homogenisation of the isotope record

The Brown and Stephenson glaciers ice core and crevasse isotopic records reveal a homogenised isotope time series that has seasonal fluctuations around a mean isotopic value of -8.4 to -9.4 ‰. A comparison between the Heard Island isotope values and isotope records from other Southern Hemisphere locales (compiled by the International Atomic Energy Agency and the World Meteorological Organisation (WMO) in the Global Network of Isotopes from Precipitation (GNIP) (Appendix E.1)) indicate that the ice core and crevasse isotope values measured on Heard Island are similar to the isotopic values measured from other sub-Antarctic islands and some Antarctic Peninsula sites. This provides evidence that meltwater may only be depleting deposited isotopes (evidenced by the subdued record) rather than completely removing the isotopic seasonal signal.

The three longer crevasse records all have very smoothed $\delta^{18}O$ values especially with depth. Both BC1 and SC1 have smoothed $\delta^{18}O$ values that become more negative with depth, which is unusual as $\delta^{18}O$ typically is more positive with depth, like observed in BC2 (Figure 6.11) (Thompson, 1979). This decrease in $\delta^{18}O$ values is most likely to be due to post depositional processes, either meltwater percolation into the surface snow which then refreezes in winter, winter precipitation percolating into the snow surface during a winter föhn wind, or mixing of water vapour from evaporation of snow in the firn.

6.7.7. Seasonal signals in oxygen isotope records as annual markers

Brown Glacier is a relatively fast (average surface velocity from 2000/01 and 2003/04 field seasons was is $35.4\,m\,a^{-1}$) moving small temperate glacier with a mass turn over of <150 years. The isotopic samples in ice cores from slower moving glaciers with low accumulation rates (e. g., Antarctica) may be skewed by the ice flow of the glacier, affecting the interpretation of the seasonal signal due to the source locations of the deeper isotopes being from a cooler

surface further up glacier. The high accumulation rates measured at sea level and the high mass turn over from Brown Glacier implies that the variation in isotopes with depth is more likely to be a record of a seasonal signal rather than a climate signal.

To measure the thickness of the net balance layers the summer signals (less negative values) were identified. If these are true summer markers, then the distance between them represents an annual net balance. The measured thickness of the net balance from summer signals does depend on the interpretation of what is a summer peak, what is a storm signal and what variability may be due to sampling interval.

In an attempt to reduce the error in net balance from these five sites the thickness between summer signals were smoothed to highlight the seasonal trends (Figure 6.18). For all but BC2 the summer peaks were identified as a relatively sharp increases in oxygen isotope values throughout each of the core and crevasse isotope profiles. The summer peaks in BC2 could be interpreted in several ways, therefore the maximum and minimum layer thickness for this site is reported (Table 6.4). The average net balance derived this way from the ice cores and crevasses ranges from 2.3 m w.e. to 0.7 m w.e. (Table 6.4) (see Section 5.5.2 for densities used to calculate w.e.).

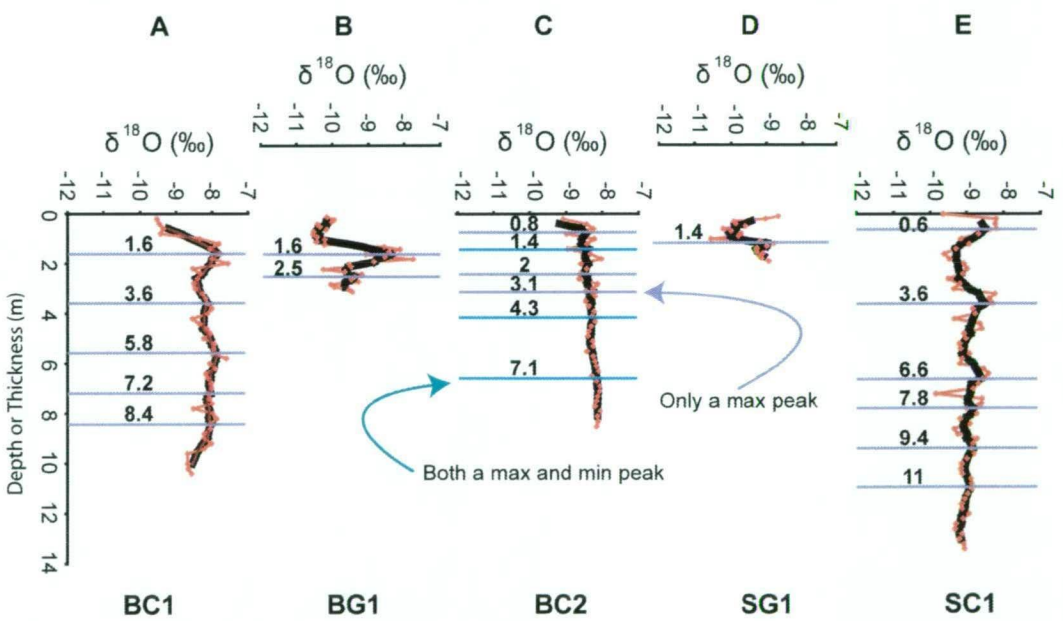

Figure 6.18.: Seasonal signals in the oxygen isotope records and the five point running mean. The summer signals have been identified in each of the ice core and crevasse profiles based on the mean values by defining a maximum and minimum range. The blue lines in BC2 represent a peak that was used to calculate both a maximum and minimum net balance, where as the grey peaks were only used for the maximum net balance value.

These 2003/04 net balance estimates differ from the estimates made from C1 (6 to 7 m a^{-1}) and the BP1 snow pit (>0.8 m a^{-1}) samples (Truffer et al., 2001). Truffer et al. (2001) based their estimation of the net balance on the $\delta^{18}O$ profile and debris layers. Their report did not consider the effects of volcanic events on the ice surface. If their results are analysed for summer isotope signals, without input from debris layer locations, there are up to five possible seasonal cycles evident (Figure 6.19 and Table 6.4). Providing an average net balance of 1.6 m a^{-1} w.e. This rate, for a higher elevation site, is similar to the average value obtained from the five $\delta^{18}O$ profiles from 2003/04 of 1.3 to 1.6 m a^{-1} w.e. (Table 6.4).

Table 6.4.: The average and range in the net balance of all Brown and Stephenson's sites estimated from the $\delta^{18}O$ seasonal signals by measuring the difference in thickness between the peaks in mean $\delta^{18}O$ in the Brown and Stephenson glacier profiles.

Site	BC1				BG1	BC2 (max)				BC2 (min)		SG1	SC1				C1			
Elevation (m asl)	756				799	869				869		922	922				1050			
Peak in $\delta^{18}O$ (m)	1.6	3.6	5.8	7.2	1.6	0.8	1.4	2	3.1	4.3	1.4	4.3	0.8	0.6	3.6	6.6	7.8	9.4	0.8	2.8	6.4	8	9.6
Next peak in $\delta^{18}O$ (m)	3.6	5.8	7.2	8.4	2.5	1.4	2	3.1	4.3	7.1	4.3	7.1	>1.9	3.6	6.6	7.8	9.4	11	2.8	6.4	8	9.6	11.2
Total thickness of period (m)	2	2.2	1.4	1.2	0.9	0.6	0.6	1.1	1.2	2.8	2.7	3	>1.1	3	3	1.2	1.6	1.6	2	3.6	1.6	1.6	1.6
Number of seasonal signals	4				1	4+				2		0	5						5				
Average net balance (ma^{-1})	1.7				0.9	1.3				2.9		>0.11	2.1						2.1				
Average net balance (ma^{-1} w.e.)	1.3				0.7	1.0				2.3		>0.9	1.6						1.6				

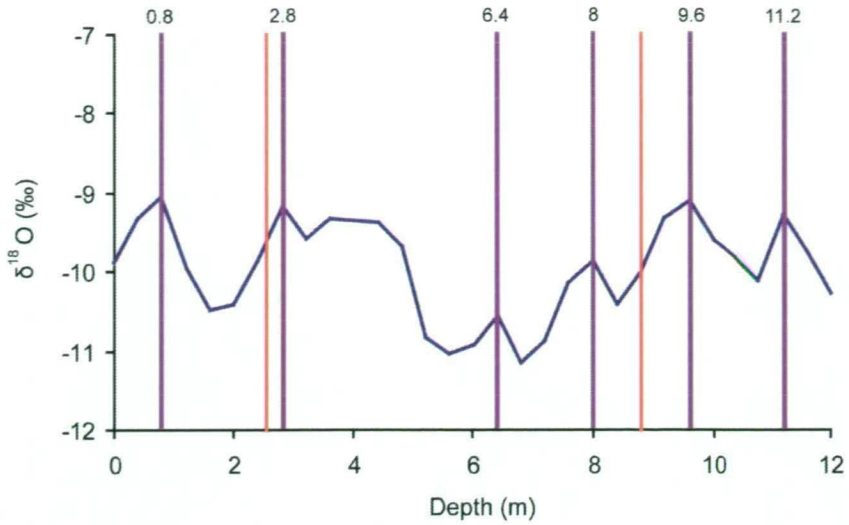

Figure 6.19.: 2000 C1 isotope record. Red lines are dirt layers observed by Truffer et al. (2001) and purple lines are a re-interpretation of the isotope peaks in the crevasse record.

This similarity implies that the location of C1 does not have a significant influence on the net balance at that site compared to the 2003/04 sites. Additionally these net balance values suggest that although there is interannual variability (0.6 to 3.6 m) the average net balance at elevations between 756 and 1050 m are similar.

6.7.8. Determining if the trace ion record was melt effected

Initially, due to concerns about meltwater effects on the trace ion concentration, there was some uncertainty about whether there would be a seasonal signal, especially given the wide range in concentrations measured. To determine if melt was a factor in the interpretation of the seasonal signals a comparison was made of the mean, maximum and minimum sodium, chloride, sulphate and nitrate concentrations at the 2004 sites and the higher elevation SP83 site (Table 6.5). This revealed a grouping of mean values between the sites. BC2, BG1 and SG1 each had lower mean concentrations compared to the higher mean concentration at BC1, SC1 and SP83. A better understanding of the ranges in concentration was found by using a simple statistical model (Figure 6.20).

A box and whisper plot was used to help interpret the distribution of data. Quartiles separate the original data into four equal parts each of these parts contains a quarter of the data. The box represents the median of the third quartile (top of box) and the median of the first quartile (bottom of box). The centre of the box is the median of all of the data. The range in the data is represented by the 'whiskers', the top is the highest value and the bottom is the lowest value. The cross hairs, when present, represent a value that falls well outside the range of the rest of the data, an outlier.

The range of trace ions in BC2, BG1 and SG1 are much smaller than the three other Heard Island sites (Figure 6.20) and the maximum and minimum concentrations in trace ions for other maritime locations (Aristarain and Delmas, 1981; Galloway et al., 1982; Palmer et al., 2001; Isaksson et al., 2003). This indicates that these three sites (BC2, BG1 and SG1) are regions of chemically homogeneous, low concentration snow pack, which is a feature of a snow pack that has been effected by post-depositional factors. A comparison between the SG1 and SC1 sites

Table 6.5.: Mean and range in trace ion concentrations from the 2004 and 1983 sites

	Cl^- (μEqL^{-1})	NO_3^- (μEqL^{-1})	SO_4^{2-} (μEqL^{-1})	Na^+ (μEqL^{-1})
BC1				
mean	87.95	1.93	9.06	92.0
max	180.04	6.81	24.47	189.75
min	15.86	0.01	0.79	14.23
n	51	51	51	51
BG1				
mean	10.60	0.14	0.67	8.99
max	24.08	0.16	5.98	20.77
min	4.90	0.09	0.16	0.01
n	29	29	29	29
BC2				
mean	4.36	0.09	0.30	4.06
max	8.44	0.13	2.04	15.53
min	2.59	0.07	0.07	1.79
n	43	43	43	43
SG1				
mean	11.40	0.13	0.44	11.04
max	18.51	0.14	0.90	17.65
min	0.59	0.05	0.10	5.33
n	20	20	20	20
SC1				
mean	35.12	0.16	5.78	35.46
max	207.12	1.15	203.27	204.70
min	9.62	0.03	0.57	8.33
n	67	66	67	67
SP83				
mean	30.69	0.33	3.05	25.65
max	341.30	1.82	26.96	287.52
min	0.28	0.01	0	0.15
n	30	30	30	30

provides an example of the variability of melt effected snow pack on Heard Island given that these two sites are less than 2 m apart.

The BC1 crevasse consistently has the highest mean, largest range and fewest outliers in concentration compared to the other sites (Figure 6.20). The range in concentration is similar to typical trace ion ranges in coastal Antarctic sites indicating that this site may be a good representative of the trace ion deposition on Brown Glacier (e.g., Herron, 1982; Savoie et al., 1993; Curran et al., 1998). Further this crevasse site was the only site to provide a complete MSA profile. Investigations have shown that MSA is one of the first ions to be removed from the snow pack by melt (e.g., Pohjola et al., 2002b; Pasteur and Mulvaney, 1999). Consequently the likelihood that melt has effected this record is low despite the presence of visible meltwater when sampling this crevasse.

A comparison between the SC1 crevasse and the SP83 sites reveals a similarity in the concentration range (Figure 6.20). This implies that melt influences at SC1 are low, given that SP83 is at a higher elevation (2450 m asl) and therefore assumed to have little or no melt. It is possible

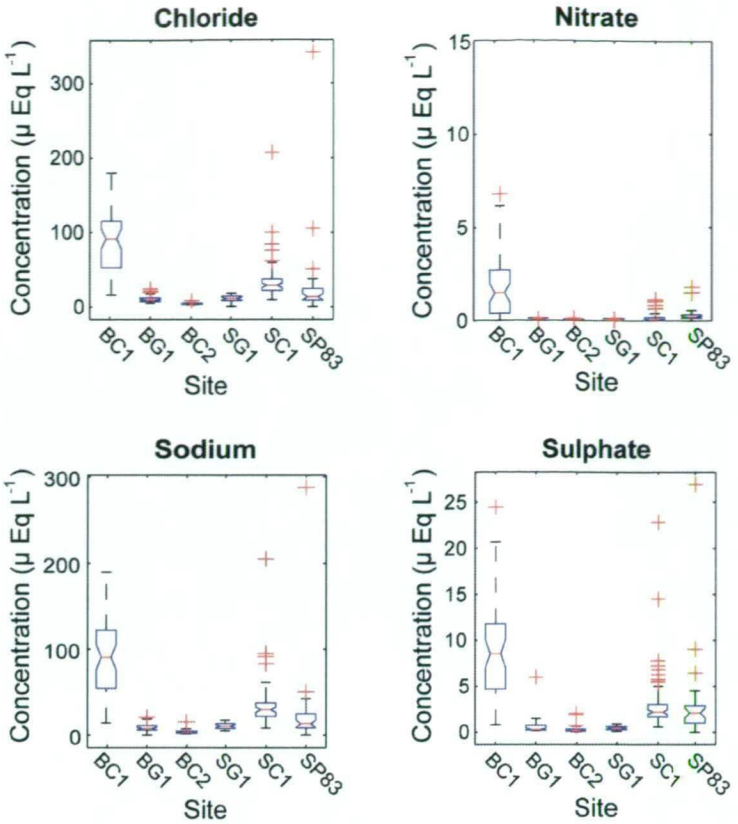

Figure 6.20.: A comparison of box and whisker plots for the four trace ions that were measured at both SP83 and the 2004 sites.

therefore to regard SC1 as a good representation of the seasonality on the Stephenson Glacier given its length, and low melt influences.

This interpretation of the Heard Island trace ion concentrations reveals that the BC1 and SC1 crevasses are likely to supply the best records for estimating the net balance and are the only sites used for further analysis in this study.

6.7.9. Seasonal signals in the trace ion record

The BC1 and SC1 trace ion signals (Figure 6.11) are unusual given that each ion has a very similar trend. This appears to be typical of Heard Island as the SP83 site had a similar synchronise signal.

The trace ions for BC1 and SC1 both have a high variability, which maybe due in part to sample intervals. To detect the summer signals the signal ratios between nitrate/sodium, sulphate/sodium and MSA/sodium were smoothed, as this signal will reduce any effects of concentration yet still highlight a summer signal. This summer signal is likely to be preserved even if bulk transport of the ions occur through the snow pack.

The nitrate and MSA in BC1 and SC1 are investigated because these two ions have less variability in their signals and both have higher concentration in summer compared to winter. If these peaks are true summer signals, then the distance between peaks is a measure of net balance. The measure of net balance for these summer signals depends on determining at what magnitude is a peak summer signal. To incorporate this possible error in the net balance a range

of maximum and minimum net balance values for BC1 and SC1 were calculated (Figure 6.21 and 6.22).

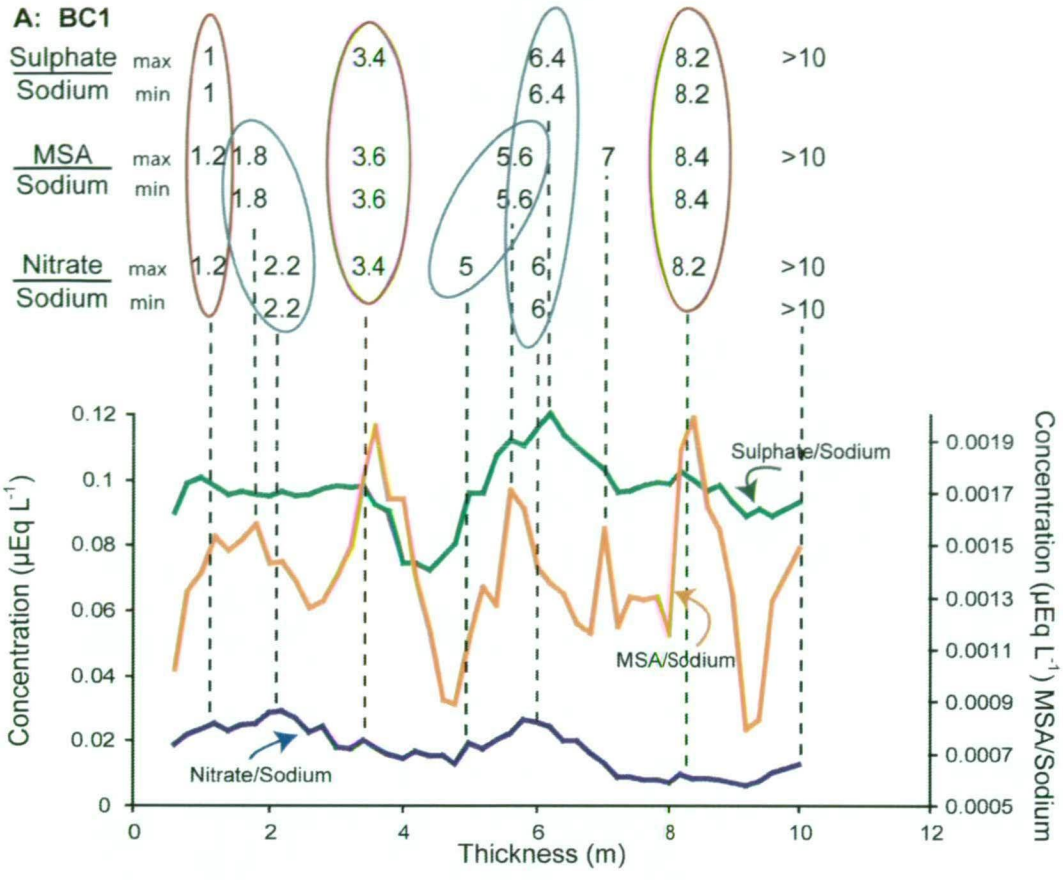

Figure 6.21.: The BC1 net balance values, based on the possible number of summer signals, for the ratios between the nitrate/sodium, sulphate/sodium, and MSA/sodium ratios; the maximum and minimum number of signals are listed for reach ratio. The red circles represent a summer peak that is identifiable in more than one ratio. The grey circles are possible summer peaks that are within 0.6 m between ratios.

The BC1 site has higher concentrations of most ions than the SC1 site and is also the only site that has more than four MSA values. The summer signal from the MSA/sodium ratio resulted in a range of average net balance values of 1.7 m or 1.3 m w. e. to 2.2 m or 1.7 m w. e. (Figure 6.21). The other two ratios nitrate/sodium and sulphate/sodium have a slightly larger range in values (Figure 6.21). The sporadic nature of the volcanic activity on Heard Island is very likely to mask the seasonal signal interpretation based solely on the sulphate/sodium ratio. To remove this possible error in interpretation the sulphate/sodium ratio was removed when comparing the ratios for overlapping seasonal signals. When the summer signals for the other three ratios are compared there are 5+ concurrent peaks (Figure 6.21). This analysis, assuming that this site is not melt effected, has resulted in a range in net balance for BC1 of ~ 2.4 m w. e. to ~ 0.5 m w. e. (see Section 5.5.2 for density of snow values used to calculate the water equivalent values).

Before the summer signals in SC1 are identified the volcanic signal at 5.6 m depth, indicated by an increase in sulphate and calcium measurements, was ignored (Figure 6.11). It should be noted that this volcanic signal may be masking a summer or winter signal. The two ratios used for SC1 are nitrate/sodium and sulphate/sodium (Figure 6.22). These two ratios resulted in a range of average net balance values of 1.6 m or 1.3 m w. e. to 2.6 m or 2.6 m w. e. for

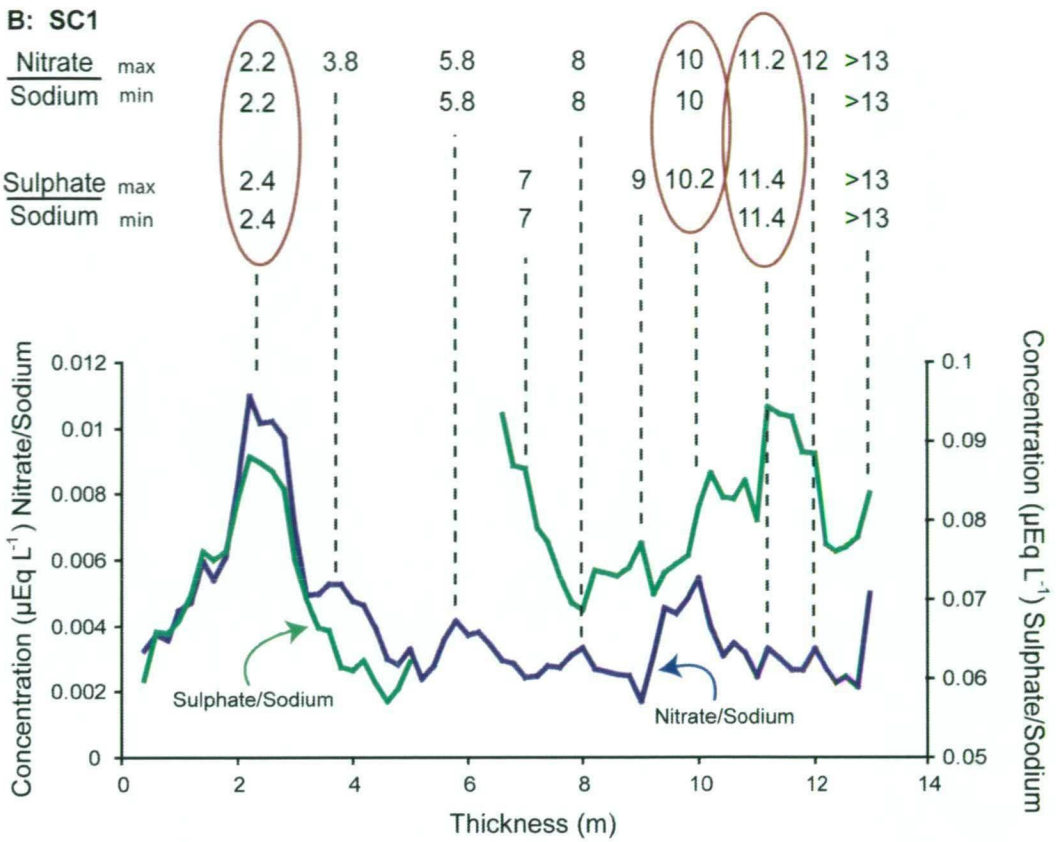

Figure 6.22.: The SC1 net balance values, based on the possible number of summer signals, for the ratios between the nitrate/sodium, sulphate/sodium, and MSA/sodium ratios; the maximum and minimum number of signals are listed for reach ratio. The red circles represent a summer peak that is identifiable in more than one ratio.

nitrate/sodium and 2.5 m or 1.8 m w. e. to 4.5 m or 3.6 m w. e. for sulphate/sodium. If the summer signals for these two ratios are compared for any overlap in signals there are few concurrent summer peaks (Figure 6.22). Again it was assumed that volcanic activity may be skewing the summer signal interpretation and therefore the net balance thickness was calculated from the summer peaks in nitrate/sodium only. Assuming that this site is not melt effected, the range in net balance values for this site could be from 2.1 m w. e. to 1.3 m w. e. (see Section 5.5.2 for density of snow values).

6.7.10. An estimation of annual net balance on Brown Glacier

Meltwater processes have not had such a detrimental effect on the SC1 and BC1 crevasse trace ion samples hence the average net balances thickness will be estimated from these two sites. The summer surface identified from the mean trace ion ratio signals in BC1 and SC1 are compared to the mean $\delta^{18}O$ values (Figure 6.23 and 6.24). This results in a thickness measurement of net balance and not an indication of the depth of the true net balance summer signals. This interpretation is used because it was assumed that the mean values of oxygen isotope ratio and the mean ratio values of the trace ion provide a signal that amplifies the seasonal signal at each site.

First the mean oxygen isotope ratio and mean nitrate/sodium ratios are compared; there are four possible corresponding peaks (*1* to *4*) (Figure 6.23 and Table 6.6). Two of these correspon-

ding peaks (*1* and *3*) have the nitrate/sodium summer peaks leading the oxygen isotope summer peak (Figure 6.23), which has been observed at other sites (e.g., McMorrow et al., 2004), therefore increasing the confidence that these peaks indicate a summer signal. The other two peaks (*2* and *4*) do not have this same relationship but are marked as being possible summer signals (Figure 6.23). These two peaks will also be compared to the location of the MSA/sodium mean values.

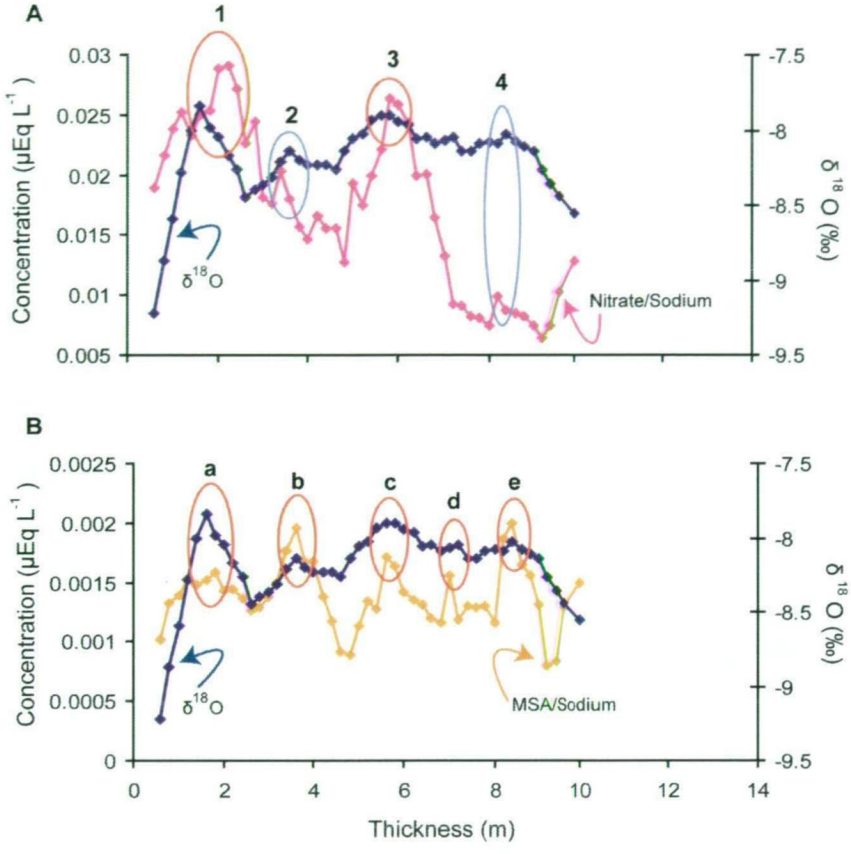

Figure 6.23.: BC1crevasse sites isotope and trace ion records with the summer signals indicated. **A**. Shows the relationship between the oxygen isotopes and nitrate/sodium ratio and **B**. shows the oxygen isotopes and MSA/sodium ratio.

A comparison between the mean oxygen isotopes and mean MSA/sodium ratio indicate that there are up to five possible corresponding peaks (*a* to *e*) (Figure 6.23). All but peak *d* have a nitrate/sodium summer signal that occurs at relatively the same thickness. As a result peak *d* is removed when calculating the net balance from the MSA/sodium mean ratio values (Table 6.6).

This net balance analysis of BC1 assumed that this 756 m asl site is not strongly effected by post depositional processes and that the mean oxygen isotope ratio and trace ion concentration represent a relative thickness of net balance. Using these assumptions, the net balance for BC1 is between 1.8 m w.e. and 1.6 m w.e. (Table 6.6).

The higher elevation (922 m) SC1 site did not have many detectable MSA values, therefore the mean oxygen isotope ratio are compared with the mean nitrate/sodium ratio to estimate a net balance (Figure 6.24). Seven possible corresponding peaks were identified, although peak *vii* was eliminated from the net balance calculation because of the uncertainty over which of the two isotopes peaks might correlate to the one nitrate/sodium peak. The remaining six summer

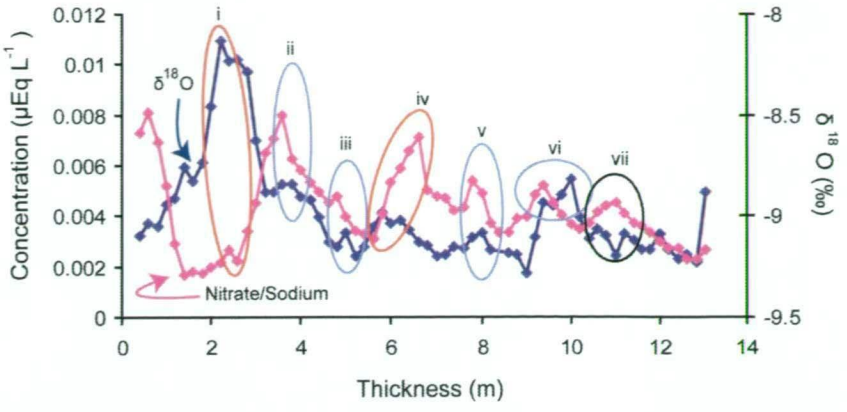

Figure 6.24.: SC1 crevasse site isotope and trace ion records including the summer signals.

Table 6.6.: The range in net balance estimates for Brown and Stephenson glacier sites.

Site	BC1			SC1	
Glaciochemical variable	$\delta^{18}O$	Nitrate/Sodium	MSA/Sodium	$\delta^{18}O$	Nitrate/Sodium
Number of cycles	3	3	3 or 4	5	5
Average net balance (m)	2.3	2	2.2	1.6	1.4
Average net balance (m w.e.)	**1.8**	**1.6**	**1.7**	**1.3**	**1.1**
Average net balance of site (m w.e)	1.7			1.2	

peaks can also be separated, peak *i* and *iv* were the only pairs that has the nitrate/sodium peak leading the isotope peak, the other four (*ii*, *iii*, *v*, and *vi*) do not. These other four peaks were still included in the calculation of a minimum net balance estimate for this site because both the oxygen isotopes and nitrate/sodium ratio peaks occurred at similar thicknesses when compared to the BC1 nitrate/sodium profile (Table 6.6).

Assuming the SC1, like BC1, is a site that has no significant post-depositional effects altering the glaciochemistry and that this comparison of mean oxygen isotopes and mean nitrate/sodium is the best possible representation of the summer signal in SC1, a net balance estimate is proposed. The net balance at SC1, 922 m asl, ranges between 1.3 m w.e. and 1.1 m w.e. (Table 6.6).

In order to investigate further the validity of this estimate of the net balance a comparison is made with the rainfall record at Brown Hut at 4 m asl. The 203/04 sea level precipitation measurements at Brown Hut (64 day period of season 2) of 653 mm is assumed to be indicative of a typical January to February period for this location, allowing further assumptions to be made about the annual precipitation at Brown Hut, which can then be interpolated further up the glacier. The Atlas Cove 1947 to 1954 precipitation records, which are the most complete records available, are also examined. These annual precipitation records indicate that typically the wettest months are January to May and the driest from July to September (see Section 4.2). Implying that it is probable that precipitation will be as high if not higher at Brown Hut from March to May until decreasing again in winter. Therefore the annual precipitation at sea level near Brown Hut could reach as much as 2800 mm (see Sections 3.3.2 and 4.2).

These two estimated net balance values from SC1 and BC1 are also compared to the net balance values determined by previous studies. The net balance estimate from this study is lower then the debris layer-based net balance estimate made by Truffer et al. (2001) of 6 to

7 m a^{-1} however they are closer to the net balance values estimated by Spencer et al. (1985). Spencer et al. (1985) estimated a winter net balance from the SP83 of 1.0 m and summer net balance of > 1.5 m, or a total of > 2.5 m. This seasonal difference in net balance is also reflected in the Atlas Cove precipitation records where the summer precipitation is approximately 50% greater than the winter precipitation. Additionally, given the height (2450 m asl) and aspect (westward facing) of SP83 it is expected that the net balance at this site would be higher than the SC1 and BC1 sites.

6.8. Summary

Ice core and crevasse samples collected from Brown and Stephenson glaciers have provided three different types of stratigraphic markers –visible stratigraphy, oxygen isotopes and trace ions. Initially it was assumed that the best estimate of the net balance of Brown and Stephenson glaciers would be from a combinations of these three components. Instead the visible stratigraphy records were found to be inadequate in establish an average net balance. Distinct summer layers could not be identified and volcanic debris from Big Ben interfered with the summer layer interpretation. Further, the oxygen isotope seasonal signals measured were reduced in amplitude and the trace ion signals were very noisy, although the seasonal cycles may have been retained in some of the records. By comparing the mean oxygen isotope values and ion summer signals, represented by the mean ratios between MSA/sodium and nitrate/sodium, a reliable indication of summer signal may be identified. Out of the five sites sampled only the BC1 and SC1 sites were used to determine the net balance as statistical analysis indicated that the trace ion records at the other three sites had been affected by post-depositional alteration of the chemical signal.

The net balance estimates from BC1 and SC1 are a best possible estimates for Brown Glacier given:

- the stratigraphic markers used in this analysis highlight unique horizons at specific sites and depths which are indicators of annual and seasonal deposition events,
- the few sites that were sampled which were found to be relatively free of significant post-depositional alteration of the glaciochemical signal,
- the typical seasonal variations in trace ion concentrations and oxygen isotope ratios are evident in the ice cores and crevasse records on Heard Island,
- the sporadic volcanic activity that alters the seasonal signals in the nitrate and to some extent calcium signals, reduces any confidence in using debris layers as summer surface markers,
- the possibility that distance between samples maybe responsible for some of the noise in the isotope and trace ion profile,
- the assumed densities of snow in Section 5.5.2 are the best possible approximation for calculating the snow water equivalent.

Based on these assessments, the interpretation of a net balance for Brown Glacier has a range in values from 1.3 to 1.1 m w.e. at 922 m and 1.8 to 1.6 m w.e. at 756 m providing a first estimate

at these elevations. The high variability on Brown Glacier would explain why the 920 m site was found to have a lower net balance then then 756 m site.

7. Modelling the past, present and future changes in Brown Glacier

7.1. Introduction

The mass balance of glaciers has been studied for various reasons including contribution to sea level change (e.g., Meier, 1984), future water policy and water management (e,g., Kaser et al., 2003) and as indicators of the changes in the local climate (e.g., Xie et al., 1999). Though there are many factors that alter the mass balance of a glacier, the change in glacier extent that has been observed globally is predominately due to either an increase of summer temperature, which effects melting, or winter (or annual) changes in snow accumulation.

Determining whether a change in mass balance is due to temperature or precipitation is difficult in remote areas where meteorological and mass balance records are limited. For instance, on Heard Island, sea level meteorological records must be integrated with historical observations and recent glacier surveys to interpret discontinuities in the mass balance data created by the frequently short, sporadic field seasons (see Chapters 2, 4 and 5).

Temperature and precipitation also effect the movement of glaciers. Dynamic variables, including ice flow, velocity, ice thickness and ice flux, are all influenced by the morphology of the glacier and to some extent the local climate.

There are no mass balance measurements on Brown Glacier before 1992, hence models are one of the few methods available to estimate the mass balance. In this present study, it was decided that the best ablation model for Brown Glacier was based on a degree day model. A degree day model is reliant on temperature which is one of the few variables that has an annual record near Brown Glacier. To model the accumulation, the summer precipitation at Brown Hut and the annual precipitation at Spit Bay were used to establish an annual precipitation near Brown Glacier. The sea level precipitation was increased at a constant rate and then compared to the net balance measurements from the crevasses, the estimated ELA and the measured mass flux. Once the net balance was estimated the dynamics of the glacier could be determined using a steady state model described by Ruddell (1995) to model the ice thickness and velocity.

Three different intervals were examined to compare the mass balance changes in the glacier; 1950, 2001 and 2095, and two intervals for the ice dynamics: 1950 and 2001. The 1950 interval was chosen as a representative year for the initial ANARE occupation from 1947 to 1954. This period has substantial meteorological records (1948 to 1954) and radiosonde measurements (1950 to 1953) available for Atlas Cove. It was also during this period (December 1947) that the first aerial photographs were taken of the terminus of Brown Glacier. These photographs along with the remnant lateral moraines surrounding Brown Glacier were used to construct the DEM for 1950 (see Section 5.3.1). 1950 also represents a time when the glaciers on Heard Island were assumed to be in equilibrium (see Section 2.4.1), most reached the shoreline and

some may have been tidewater glaciers. It is known from observations and photographs that by 1963 several glaciers had begun to retreat from the coast.

The year 2001 was chosen to represent this change from an equilibrium mass balance to the currently negative mass balance. 2001 was selected because it was during the 2000/01 mass balance survey of Brown Glacier (see Chapter 5). In addition, climate measurements (accumulation and temperature) were made and the BG AWS was installed at ~ 550 m asl along the southern lateral moraine of the glacier supplying the only annual high elevation temperature records on the island (November 2000 to August 2002) (Truffer et al., 2001) (see Section 4.3.1).

To predict a future mass balance of Brown Glacier the year 2095 was selected. 2095 is the average date for the climate projections for different emission scenarios in the Fourth Assessment Report of the Intergovernmental Panel on Climate Change (IPCC) (Meehl et al., 2007). The IPCC model scenarios were used to estimate the change in temperature from 1980 to 1999 and 2090 to 2099. For this study both the B1 and A2 model projections were used (Meehl et al., 2007).

7.2. Previous studies on Heard Island

There have been few mass balance models developed for Heard Island. Ruddell (1995) developed a mass balance and ice dynamics model for the New Zealand Alps. He began to investigate reinterpreting this model for use on Heard Island and made some initial estimates (pers. com. A. Ruddell, 26 August 2001).

Williams (1998) also used Ruddell's model to investigate the mass balance and dynamics of the Vahsel and Mary Powell glaciers and the effects of geothermal heat on these glaciers (see Section 5.4.4). More recently, Thost and Truffer (2008) investigated using an energy balance model for Brown Glacier. The limited meteorological records available for Heard Island (see Section 4.2) were insufficient to describe all of the processes that regulate the exchange of energy between the glacier surface and atmosphere which are necessary in an energy balance model. The uncertainties in the spatial variability of some of the data on the glacier surface conditions (e. g., due to surface shading, snow redeposition, wind and föhn wind, albedo and surface roughness) meant that a full energy balance model was not the most practical way to estimate the melt rates on Brown Glacier.

7.3. Modelling the mass balance gradient of Brown Glacier in 2001

The available mass balance measurements on Brown Glacier from the 2000/01 and 2003/04 seasons were used to model the annual net balance, these include, the summer ablation measurements from the BG50 sonic ranger and the net balance stakes, and the annual precipitation at sea level derived from the Spit Bay annual records and the summer precipitation at Brown Hut.

The summer ablation measurements combined with the BG AWS air temperature measurements were used to calculate the mean positive degree day sum in a degree day model, which is used to estimate the annual ablation. The annual accumulation was estimated from annual and summer sea level precipitation and air temperature measurements.

The resulting annual ablation, accumulation and net balance were then compared to the stratigraphy based net balance values from the BC1 and SC1 crevasse records (see Section 6.7.10), the mass flux measurements (see Section 5.4.5), and the estimated ELA (see Section 5.5.1).

7.3.1. Brown Glacier Degree Day Model (ablation)

Annual measurements of snow melt and glacier meltwater outflow are not easy to obtain. The difficulties are due to the high level of maintenance required by instrument networks (e. g., stake networks and sonic rangers) and the logistics of maintaining these sites (see Section 5.5.3). Solutions include the use of models to estimate the ablation on a glacier. There are two main types of melt models: energy balance and temperature index. In this study a temperature index model is used.

Temperature index models assume that there is is an empirical relationship between air temperature and ablation. They often match the performance of energy balance models on a catchment size scale (Hock, 2003). This is attributed to the high correlation of temperature with several energy balance components (Braithwaite and Olesen, 1990; Lang and Braun, 1990). Air temperature models tend to have good modelled results despite their simplicity (Hock, 2003). Hence they are useful for mass balance estimates in ice dynamic models (Oerlemans, 2001) and for predicting the response of glaciers to climate change (Braithwaite and Zhang, 1999).

Degree day models (DDM) have been applied to predict melt for flood monitoring and hydrological modelling, mass balance forcing in ice dynamic models and to predict the response of glacier mass balance to climate change (Hock, 2003). DDM assume an empirical relationship between air temperature and melt rates, usually expressed as positive (above the melting point) temperature sums (Hock, 2003) and assume that there is a constant relative contribution of each of the heat balance components, as long as the average heat balance conditions do not change significantly over a day or more (Lang and Braun, 1990). This relationship was first used for an Alpine glacier by Finsterwalder and Schunk (1887), since then the relation has been applied and further refined globally for the estimation of snow and melt runoff (e.g., Lang, 1968; Braithwaite, 1995; Singh et al., 2000; Szafraniec, 2002).

DDM are the most commonly used melt model due to:

- Wide availability of air temperature data,
- Relatively easy interpolation and forecasting possibilities of air temperature,
- Generally good model performance despite their simplicity,
- and computational simplicity (Hock, 2003).

The most basic DDM relates the amount of ice or snow melt, A, over a period, n, to the sum of the positive air temperatures, PDD, for a time interval Δt(d), during the same period. The factor of proportionality is the degree-day factor, DDF, expressed in mm d$^{\circ}$C^{-1} (Hock, 2003):

$$\sum_{i=1}^{n} A = \mathrm{DDF} \sum_{i=1}^{n} \mathrm{PDD}\Delta t \tag{7.1}$$

Commonly a daily time interval is used but hourly or monthly time intervals can also be used to determine the DDF.

The DDM used to predict the annual ablation of Brown Glacier is based on a model developed by Braithwaite and Olesen (1989). This DDM assumes that the ablation rate at any place on the glacier is proportional to the air temperature at the same place (1 to 2 m above the surface) as long as the temperature is at or above the melting point (Braithwaite and Olesen, 1989) and is given by:

$$a_r = \gamma + \omega T_t \qquad T_t \geq 0°\text{C} \tag{7.2}$$

where a_r and T_t are the ablation rate and temperature respectively at some time t, and γ and ω are constants. Physically γ represents the melting with air temperature of 0° C while ω describes the increase of ablation with temperature. This equation implies that part of the ablation energy is independent and part is controlled by air temperature (Braithwaite, 1995). A logical variable H_t is defined such that:

$$\begin{aligned} H_t &= 1.0 \qquad T_t \geq 0°\text{C} \\ &= 0.0 \qquad T_t \leq 0°\text{C} \end{aligned} \tag{7.3}$$

The total ablation A over a period of a time is given by:

$$A = \sum_{t=1}^{t=N} H_t a_r \tag{7.4}$$

where N is the period of time. Typically, a time interval of one day is used.

Combining Equation (7.2) and (7.4) gives:

$$A = \gamma \sum_{t=1}^{t=N} H_t + \omega \sum_{t=1}^{t=N} H_t T_t \tag{7.5}$$

where $\sum H_t$ equals the number of days (N^*) with temperatures at or above the melting point and $\sum H_t T_t$ equals the positive degree day sum (PDD) for the N day period. The mean daily ablation rate for the N day periods is A/N and given by:

$$A/N = \gamma(N^*/N) + \omega(\text{PDD}/N) \tag{7.6}$$

where N^*/N is the frequency of melting temperatures during the period and PDD/N is the mean of positive temperatures in the period.

A DDF is used to distinguish between the amount of melt that would occur under the same temperature on different snow or ice surfaces. DDF for ice (DDF_i) are typically higher than a DDF for snow (DDF_s) under otherwise identical conditions because of higher energy fluxes (Braithwaite, 1995) (Appendix F.1). DDF for snow and ice are typically determined from direct measurements (e. g., snow and ice block melting field experiments) (Singh et al., 2000), from energy balance calculations (Hock, 2003) or from the PDD of temperatures for a span of

ablation observations (Podlech et al., 2004)). By definition a positive degree day factor (DDF) is:

$$\mathrm{DDF} = A/\mathrm{PDD} \tag{7.7}$$

Combining Equation 7.6 and 7.7 gives the DDF as a function of γ and ω:

$$\mathrm{DDF} = \gamma(N*/PDD) + \omega \tag{7.8}$$

The two variables ω and γ are derived according to Braithwaite and Olesen (1989) by examining the relationship between the mean daily ablation and the average daily PDD. For Brown Glacier, the 30 December 2003 to 18 February 2004 temperature and ablation data provides the most detailed measurements of these two variables. Hence, this relationship was calculated from the daily average temperature records from the AWS1, at 115 m asl (see Section 4.1 for AWS location) and from the BG50-2004 sonic ranger daily ablation at 179 m asl (see Section 5.5.3) (Figure 7.1).

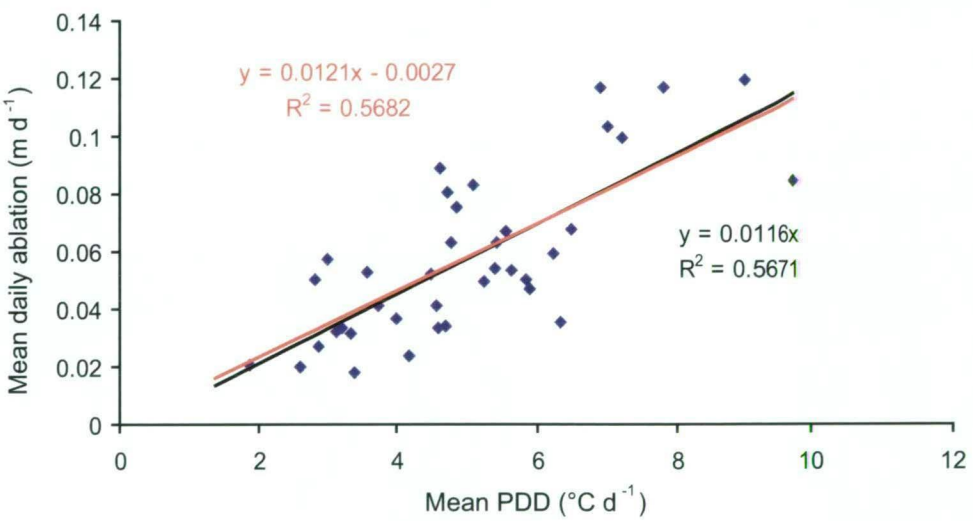

Figure 7.1.: The summer relationship between the mean daily ablation and the mean daily PDD at 179 m asl on Brown Glacier. The red line represents a linear trend through these values. The black line is a trend fit through zero.

Braithwaite and Olesen (1989) note that ω is equal to the slope and $\gamma(N^*/N)$ is equal to the intercept, resulting in an ω value of 12.1 and a γ value of 2.7 ($N^*/N = 1$ over this period) for the summer ice surface of Brown Glacier at BG50. The DDF is not generally the same as ω, and Braithwaite (1995) found that the variation in N^*/PDD decreases with increasing temperature resulting in the effect of γ on the DDF being progressively reduced. Hence ω tends to the DDF only in the limit of high temperatures. This present study has found that when the DDF for Brown Glacier is derived based on the PDD of transferred temperature for a span of ablation observations as suggested by Podlech et al. (2004) $\gamma(N^*/N)$ tends to zero (Figure 7.1) . Given the small $\gamma(N^*/N)$ value from this analysis, this study assumes that $\gamma(N^*/N)$ is equal to zero on Brown Glacier, hence the mean daily ablation for this glacier can be calculated by:

$$A/N = \omega(\mathrm{PDD}/N) \tag{7.9}$$

and assuming that ω is equal to the DDF:

$$A/N = \text{DDF}(\text{PDD}/N) \tag{7.10}$$

A DDF for Brown Glacier The above relationship between PDD and ablation suggests that for Brown Glacier the DDF at BG50 (a predominately ice surface) is 11.6 mm w.e. $d^{-1}\,°C^{-1}$. This DDF_i estimate is higher than most other published DDF_i (Appendix F.1) but similar to DDF_i for Spitsbergen of 13.8 mm w.e. $d^{-1}\,°C^{-1}$ (Schytt, 1964), for glaciers in the Greenland Ice Margin Project of 9.2 mm w.e. $d^{-1}\,°C^{-1}$ (Van de Wal, 1992) and for Aletschgletscher, Switzerland of 11.7 mm w.e. $d^{-1}\,°C^{-1}$ (Lang, 1986).

A high DDF_i was also derived using the ablation data for the Vahsel Glacier, Heard Island. The Vahsel Glacier DDF_i was based on the ablation measurements (converted to w.e. based on a density of 850 kg m^{-3}) every few days between 4 February to 5 March 1971 (Allison, 1980) from eleven stakes ranging in elevation between 132 and 210 m (see Section 5.4.1), temperature from the 1971 Atlas Cove meteorological records (Appendix C.2), and lapse rates derived from the 1950 radiosonde data (see Section 4.4.3). These variables provided a DDF_i of 9.4 mm w.e. $d^{-1}\,°C^{-1}$ for the Vahsel Glacier, assuming that ω is equal to the DDF despite the high $\gamma(N^*/N)$ value. This difference from Brown Glacier may be in part due to the Vahsel ablation records being for longer periods (e. g., three to eight days) rather then the short-termed pinger daily records used for Brown Glacier. However this ablation-PDD analysis of the Vahsel Glacier still gives a relatively high DDF for another Heard Island glacier.

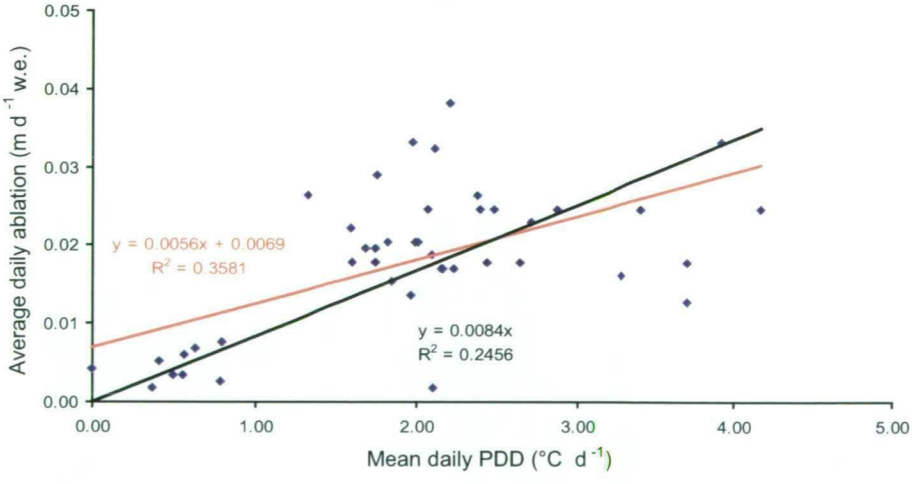

Figure 7.2.: The 4 February to 5 March 1971 relationship between the mean daily temperature and the mean daily PDD at elevations between 132 and 210 m for the Vahsel Glacier, Heard Island.

Instrument failure of the BG35-2004 sonic ranger did not allow for a DDF to be derived for snow (DDF_s) (see Section 5.5.3). Instead the DDF_s was calculated based on a comparison between the different reported DDFs of snow and ice worldwide (Appendix F.1). Typically a DDF_s is approximately 60% of a DDF_i (for Himalayan and European Alps glaciers) therefore at first the DDF_s for Brown Glacier was estimated as 7.0 mm w.e. $d^{-1}\,°C^{-1}$. Further analysis revealed that a higher DDF_s for Brown Glacier provided a better agreement with other mass balance parameters.

Summer ablation for Brown Glacier The summer ablation on Brown Glacier in 2001 was initially modelled from the AWS2 air temperature data at 550 m, a smoothed lapse rate ranging from $-0.003\,\mathrm{m}\,^{\circ}\,\mathrm{C}^{-1}$ for locations above 750 m and $-0.008\,\mathrm{m}\,^{\circ}\,\mathrm{C}^{-1}$ for location below 330 m (see Section 4.4.3), and a linear decrease in the DDF_i of 11.6 mm w.e. $\mathrm{d}^{-1}\,^{\circ}\mathrm{C}^{-1}$ at 80 m asl to a DDF_s of 7.0 mm w.e. $\mathrm{d}^{-1}\,^{\circ}\mathrm{C}^{-1}$ at 1100 m asl. The ablation was calculated for each of the stake elevations (Figure 7.3, pink line) for the period between 9 January and 14 February 2004 (36 days), the period when the best net balance stakes measurements and temperature data are available.

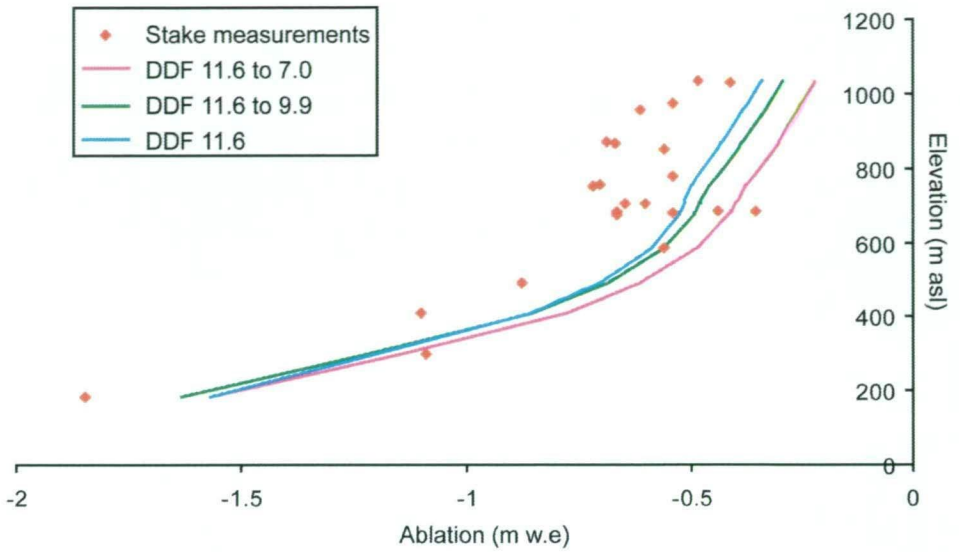

Figure 7.3.: The summer ablation (over 36 days) from different DDF compared to the measured net balance stake values.

These modelled values were then compared to the measurements at the net balance stakes. Figure 7.3 shows that the modelled ablation diverges from the measured values on the upper glacier. Yet on the lower glacier the difference between the modelled and measured values over the full period at BG50 are within 0.3 m. This is less then the difference between the sonic ranger and the net balance stake at BG50 of 0.4 m (see Section 5.5.3).

In an attempt to better match the measured ablation on the upper glacier, the DDF_s was increased to 9.9 mm w.e. $\mathrm{d}^{-1}\,^{\circ}\mathrm{C}^{-1}$ which is $\approx 85\%$ of the DDF_i. Figure 7.3 shows that this gives a better correlation on the lower glacier and a slightly better correlation on the upper glacier (green line). The DDF_s was also increased to its limit on Brown Glacier of 11.6 mm w.e. $\mathrm{d}^{-1}\,^{\circ}\mathrm{C}$. The DDF_s can not be higher than the DDF_i on the same glacier due to the relationship between higher energy fluxes and the snow or ice surface (Braithwaite, 1995). This constant DDF for Brown Glacier still did not provide the necessary increase in ablation on the upper glacier (Figure 7.3, blue line). To determine the best the DDFs for Brown Glacier several iterations of the summer and annual DDM were also compared to the measured and modelled mass flux values (see Sections 5.4.5 and 7.4). This analysis indicated that the bet fit DDFs for Brown Glacier are 11.6 mm w.e. $\mathrm{d}^{-1}\,^{\circ}\mathrm{C}^{-1}$ for ice and 9.9 mm w.e. $\mathrm{d}^{-1}\,^{\circ}\mathrm{C}^{-1}$ for snow.

There are several reasons why the Brown Glacier summer DDM does not compare well to the measured values on the upper glacier. These include the unquantified effects that föhn winds have on the glacier. It has already been shown that föhn winds occur with more frequency and intensity on the upper glacier then the lower glacier (see Section 4.4.4). These periods of high

temperature can occur over short periods of time resulting in short term high ablation periods. However this high temperature interval may not be reflected in the daily temperature average, resulting in an underestimation of ablation.

Another reason for the difference between modelled and measured ablation is due to the method of extrapolation of the air temperature (and therefore the PDD) from the AWS across the glacier surface. The lapse rates used are an average value for between 28 December 2003 and 16 February 2004. This averaging results in a smoothing of both the diurnal variation of the lapse rates and the bimodal distribution in the lapse rates between 550 m and 920 m, which as noted in Section 4.4.3 maybe due to föhn wind activity.

An annual ablation for Brown Glacier An annual ablation for Brown Glacier was modelled from the mean daily temperature measurements at BG AWS from 1 January to 31 December 2001, using the same lapse rates as the summer DDM, and a DDF_i of 11.6 mm w.e. $d^{-1}\,°C^{-1}$ and a DDF_s of 9.9 mm w.e. $d^{-1}\,°C^{-1}$. The ablation was calculated along the central flowline of the glacier at 0.25 km intervals, resulting in an annual ablation ranging from -13.3 m w.e. a^{-1} near the terminus to -1.6 m w.e. a^{-1} at 1100 m (Figure 7.4 and Appendix F.4.1). Similar high ablation measurements were recorded in 1999 near the terminus of the maritime glacier Nigardsbreen, Norway, which had a net balance of approximately -11.0 m (World Glacier Monitoring Service, 2001).

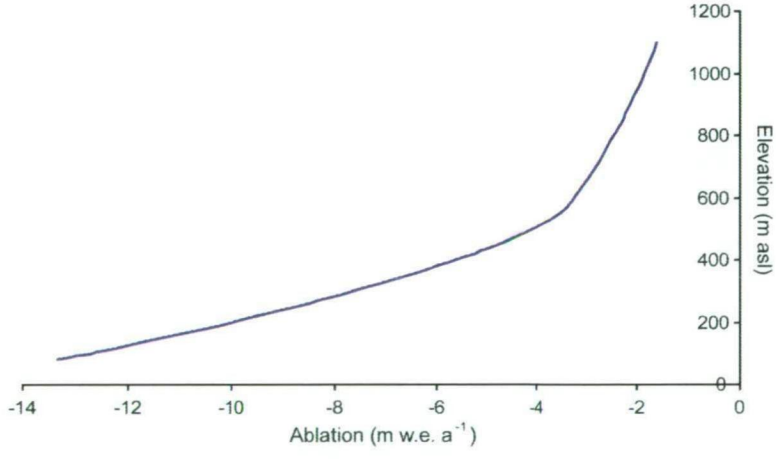

Figure 7.4.: Annual ablation of Brown Glacier in 2001 along the central flowline.

To summarise, the annual ablation estimate is based on the following assumptions:

- the DDF ratio between ice and snow is higher than is typically found on glaciers in the European Alps
- the annual temperature lapse rate values for the glacier are similar to measured summer lapse rates for these elevations
- AWS2 and BG AWS temperatures in conjunction with the lapse rates provide a good estimate of the temperature across the glacier
- the density values used to convert the stake measurements into water equivalent are a good representative of the surface (although it is acknowledged that they could be in some error).

It is considered that this DDM for Brown Glacier is the best possible model given the limited mass and energy balance measurements, estimated DDFs, and significant unknowns in the surface density values.

7.3.2. Brown Glacier accumulation

Accumulation on a glacier is spatially inhomogeneous. There can be large local variations in the deposition of snow due to altitude and wind speed and direction. The effect of altitude on the vertical distribution of precipitation in mountainous areas is highly variable for different geographical locations (Barry, 1992). Studies have demonstrated that the altitudinal increase in precipitation is due to the combined effect of higher intensities and greater duration of precipitation (Atkinsan and Smithson, 1976 as cited in Barry, 1992). In middle latitudes the general tendency for increased precipitation with height, typically to the highest observed levels, is modified considerably by a leeward or windward slope location (Barry, 1992).

The paucity of high altitude meteorological stations to record precipitation rates in mountainous regions means that to derive the accumulation on a glacier surface other methods are necessary. In most field studies snow pits are dug at multiple sites above the ELA to measure the depth of the previous year's accumulation (or net balance).

The *accumulation rate* (c_r) is the rate of mass gain at a given point on the glacier at a given time. The *ablation rate* (a_r) is the rate of mass loss at a given point on the glacier at a given time. The *balance* or *mass balance* (b) of a glacier is the sum of the accumulation (c) and ablation (a) over a time interval:

$$b = c + a = \int (c_r + a_r)\, dt \tag{7.11}$$

The *net balance* (b_n) is the mass balance at the end of a given year. The net balance is specific to a point but integrated over the balance year is defined as:

$$b_n = \int_{t_1}^{t_2} (c_r + a_r)\, dt = (b)_{t_2} - (b)_{t_1} \tag{7.12}$$

More recently ice cores have been drilled on temperate glaciers, which are analysed for ion chemistry and isotopes, to determine seasonal cycles in the glacier stratigraphy (see Chapter 6). But often direct accumulation measurements can not be made due to remoteness or logistical limitations encountered in the field, instead models are developed to estimate the changes in the accumulation with elevation.

Temperature effects on precipitation type In mountainous regions the type of precipitation that is deposited on a glacier's surface is dependent on the temperature. So, as well as calculating the annual accumulation, the amount of accumulation that falls as solid or liquid precipitation must be considered. A threshold temperature can be used to determine the type of precipitation on a statistical basis, for lowland stations in mid latitudes (Barry, 1992). The temperature records from nearby meteorological stations are projected to higher altitudes to ascertain the likelihood of solid precipitation deposited at a specific altitude and temperature.

There are no solid precipitation fraction observations for Brown Glacier, instead a polynomial function, derived for New Zealand glaciers (Ruddell, 1995), was used to calculate the solid precipitation factor, ψ (Ruddell, 1995; Williams, 1998):

$$\psi = a + b^2T + c^3T + d^4T + e^5T + f^6T + g^7T + h^8T + i^9T \quad (7.13)$$

the polynomial values are listed in Appendix F.2.

The mean solid precipitation factors for Brown Glacier in 2001 were determined from the lapse rate extrapolated temperatures from BG AWS. This resulted in the percent of the precipitation that fell at 1100 m being 97% snow and 3% rain whereas at 80 m it was 50% snow and 50% rain. The solid precipitation values for typical Brown Glacier temperatures are presented in Appendix F.3.

Sea level precipitation There has only been one annual record of precipitation measured on eastern Heard Island, at Spit Bay from March 1992 to February 1993 (see Section 4.3.2). Assuming that the annual accumulation on Heard Island has not changed significantly in the last 15 years, the total annual precipitation at sea level for Brown Glacier was derived from the difference between the January 1993 precipitation at Spit Bay and the January 2004 precipitation at Brown Hut. The difference between these two January values was then used to calculate the total annual precipitation at Brown Hut (2.80 m w.e.). This same process was used between the average Atlas Cove precipitation (1948 to 1954) and Brown Hut, resulting in a total annual precipitation of 2.50 m w.e. Brown Hut is located at 4 m asl whereas the terminus of the glacier is at ~ 80 m (in 2001). For the purpose of this model the annual precipitation at the terminus of Brown Glacier is assumed to be roughly equivalent to the annual precipitation at Brown Hut.

It is acknowledged that this estimate of the sea level precipitation on Heard Island does not account for the typically high inter-annual and local variability of precipitation, more so than temperature, that has been measured at Atlas Cove (see Section 4.3.2) and at field camps during the summer field season (see Section 3.3.2). However given the limited data that is available for Heard Island this is the best estimate possible.

Annual accumulation for Brown Glacier Precipitation is usually observed to increase with elevation (Barry, 1992) and the average precipitation over an entire catchment is greater than at sea level (see Section 5.5.4). Not all precipitation that falls on a glacier results in accumulation. Hence the temperature records and the solid precipitation factors, as defined by Ruddell (1995) in conjunction, with a trend in precipitation, derived from the precipitation records available from Heard Island, were used to provide the best estimate of annual accumulation on Brown Glacier.

For Brown Glacier, the precipitation was assumed to increase linearly from a sea level value to the top of the glacier. Initially the trend was assumed to be between a rate calculated from a trend line through three estimated precipitation values of $1.3\,m\,a^{-1}\,km^{-1}$ and the estimated trend of Budd and Allison (1975) for Heard Island of $0.6\,m\,a^{-1}\,km^{-1}$. The various accumulation trends were compared to three field based measurements (Figure 7.5).

The stratigraphic annual net balance was derived at 756 m and 920 m from two crevasses, which were analysed for trace ions, oxygen isotopes and visible stratigraphy (see Chapter 6). Despite the influence of meltwater percolation on the chemical constituents in the snow and ice on Brown Glacier an estimated range in net balance of 1.8 to 1.6 m w.e. at 756 m asl and 1.3 to 1.1 m w.e. at 920 m asl was found (see Section 6.7.10). These two net balance values were

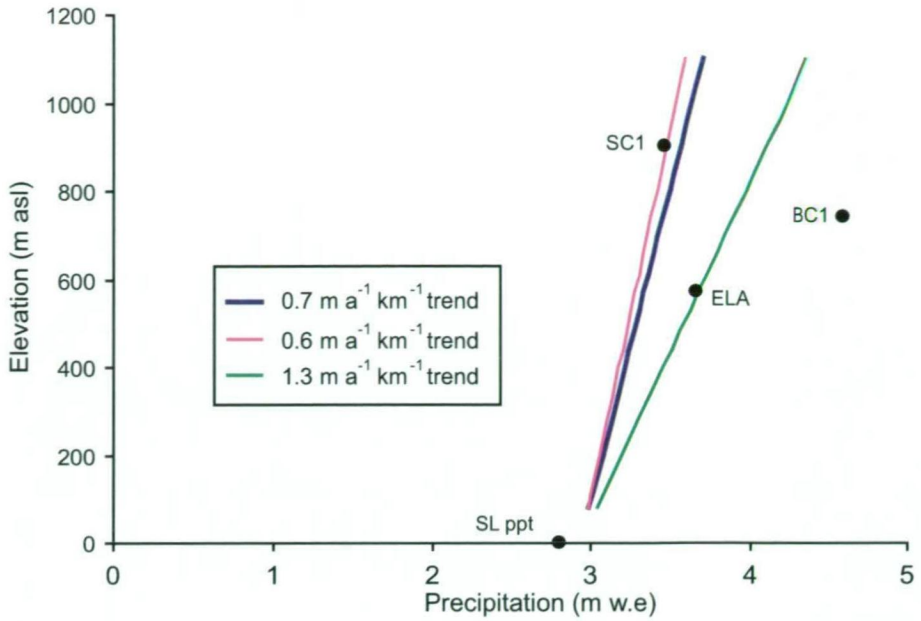

Figure 7.5.: Different total precipitation trends for Brown Glacier compared to the precipitation values derived from field measurements (refer to text for more details).

used in conjunction with ablation from the DDM and the solid precipitation factors to estimate the total precipitation at these two sites (SC1 and BC1) (Figure 7.5).

The precipitation at the ELA, which in 2001 was estimated at ~ 550 m asl, is equal to the ablation at the ELA. The DDM gives an ablation of -3.4 m w.e. at the ELA. The total annual precipitation at the ELA, assuming no snow redistribution, required to give a snow accumulation value of 3.4 m a^{-1} w.e. is 3.7 m a^{-1} w.e. (Figure 7.5).

The measured mass fluxes transported by ice motion were one further parameter used to check the accumulation estimate. The net balance profile selected must provide the right amount of mass flux to match the measured values. This is discussed further in Section 7.4, where several different mass flux sections were examined. As a result of these iterations an accumulation measured of 0.7 m a^{-1} km^{-1}, which together with the DDM ablation and comparison to the cumulative mass flux (see Section 7.4), gives the best net balance profile.

The resulting annual precipitation on Brown Glacier was estimated to range from 2.8 m near the terminus to 3.7 m at 1100 m asl and the annual snow accumulation profile to range from 1.5 m to 3.6 m (Figure 7.6 and Appendix F.4.1).

7.3.3. Net balance profile of Brown Glacier in 2001

The annual net balance profile of Brown Glacier was calculated from the accumulation and ablation (Equation 7.12). As mentioned in the ablation and accumulation sections the variability in the measured values required that the model be examined for various scenarios. After consideration of the spatial variability in accumulation on Heard Island (as discussed in Sections 3.3.2 and 6.10) and measurement uncertainty it was determined that the net balance values that gave the best fit to the measured mass flux values and the estimated ELA (between 500 and 600 m asl (see Section 5.5.1)) was from a DDM with DDFs of 11.6 mm w.e. d^{-1} $°C^{-1}$ and

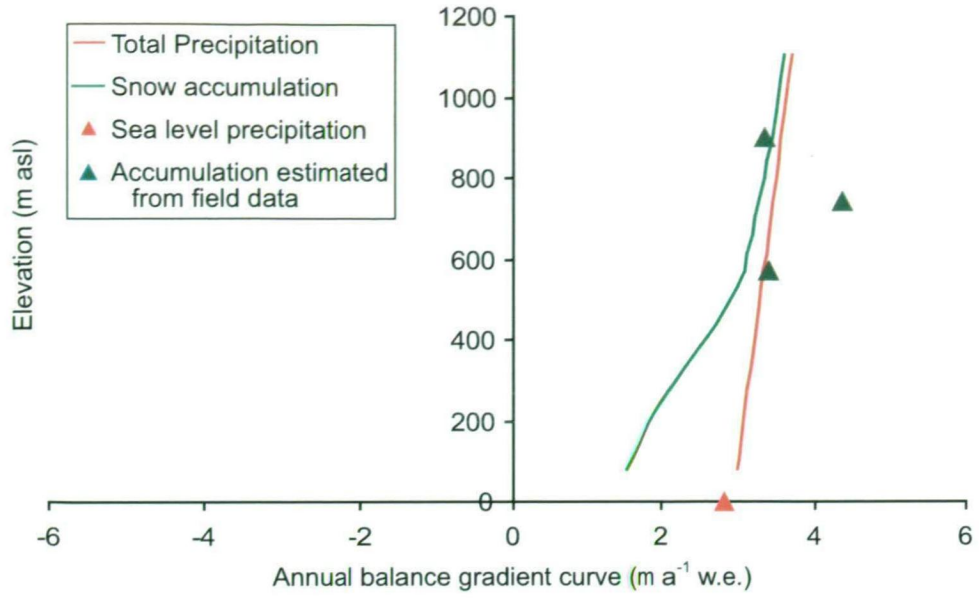

Figure 7.6.: The 2001 annual accumulation for Brown Glacier (green line) compared to the accumulation derived from the SC1 and BC1 crevasses, ELA, and sea level precipitation (SL ppt) estimates. Both the snow accumulation and the total precipitation profiles are shown.

a DDF_s of 9.9 mm w.e. d^{-1} $°C^{-1}$ and an accumulation trend of 0.7 m a^{-1} km^{-1} (Figure 7.7 and Appendix F.4.1).

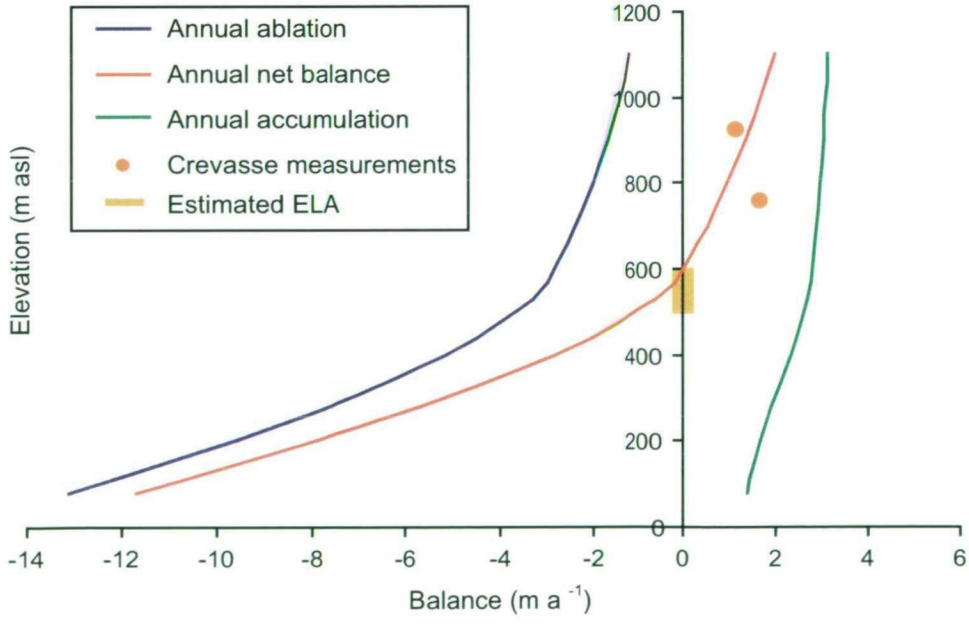

Figure 7.7.: The 2001 annual net balance of Brown Glacier compared to the net balance values derived from the stratigraphic analysis of crevasses.

These modelled annual ablation, accumulation and net balance profiles are the best estimate of the current mass balance of Brown Glacier given the limited available data, while giving consideration to the variability of precipitation on Heard Island (see Section 4.3.2), the density values used (see Section 5.5.2) and the derived lapse rates for Brown Glacier (see Section 4.4.3).

7.4. A steady state mass flux calculation

A glacier that is non-surging, or a calving tidewater and proglacial lake terminating glacier, is in steady state when its geometry and flow regime are unchanged over a long period of time and when its total net balance equals zero (Paterson, 1994). Steady state is a theoretical concept that rarely occurs in glaciers, though a relatively negligible volume change or redistribution can provide a satisfactory approximation (Paterson, 1994). A steady state glacier model is a useful tool in determining certain glacier and climatic characteristics.

Consider a sector of the glacier, between two arbitrary elevation contours and an average surface net balance of b_n. For steady state, the mass flux through a cross-section at the lower contour is equal to the mass influx through the upper section plus the surface net balance gain or loss over the area between the sections. Hence:

$$Q_b = b_n A + Q_{b-1}$$

where Q_b is the mass flux, A is the segment surface area and Q_{b-1} is the total mass flux of the glacier upstream of the grid point.

The area segments for Brown Glacier were determined from the 2001 contour map (see Section 5.3.1). The surface contours and the surface velocity measurements from the 2000/01 and 2003/04 surveys (see Section 5.4.5) were used to delineate the outline of the glacier (Figure 7.8) and to determine the central flowline. The central flowline was defined as the line that extends along the length of the glacier marking the highest surface velocities and is usually positioned near the middle of the glacier. Grid points every 0.25 km along the central flowline (Figure 7.8) were used to define the hypsometric sectors for mass flux calculations. The area of each grid segment was calculated using *Surfer 8.0*, a contour and surface mapping program, and are listed in Appendix F.5.

The morphology of Brown Glacier indicates that the glacier can be separated into two areas (southern and northern), that roughly bisect the upper glacier above 400 m asl (Figure 7.9). The southern area of the glacier terminates near the coast. The northern area seems to terminate in a stagnant ice field above a cliff (Figure 7.9). In order to compare the modelled and measured mass flux values only the southern area of the glacier is used. This is because the measured mass flux values do not extend across the total width of the glacier (see Section 5.4.5). The BG35 and BG25 mass fluxes were calculated only for the section of the ice thickness profile that extends across the southern area, whereas the BG20 mass flux was calculated from a profile that was partially estimated for the southern area.

The mass flux was also calculated for the smaller northern area of the glacier (not shown). The mass flux that terminates into the stagnant ice field was positive. Implying that as the glacier retreats there will be still some input into this region of the glacier.

Several net balance profiles were investigated based on different linear precipitation trends to find the net balance values that gave the best fit to the measured mass flux values (Figure 7.10). The cumulative mass flux for the southern area of Brown Glacier is derived from a precipitation trend of 0.7 m a^{-1} km^{-1} (see Section 7.3.2) and gives the best fit to the measured values (Figure 7.10).

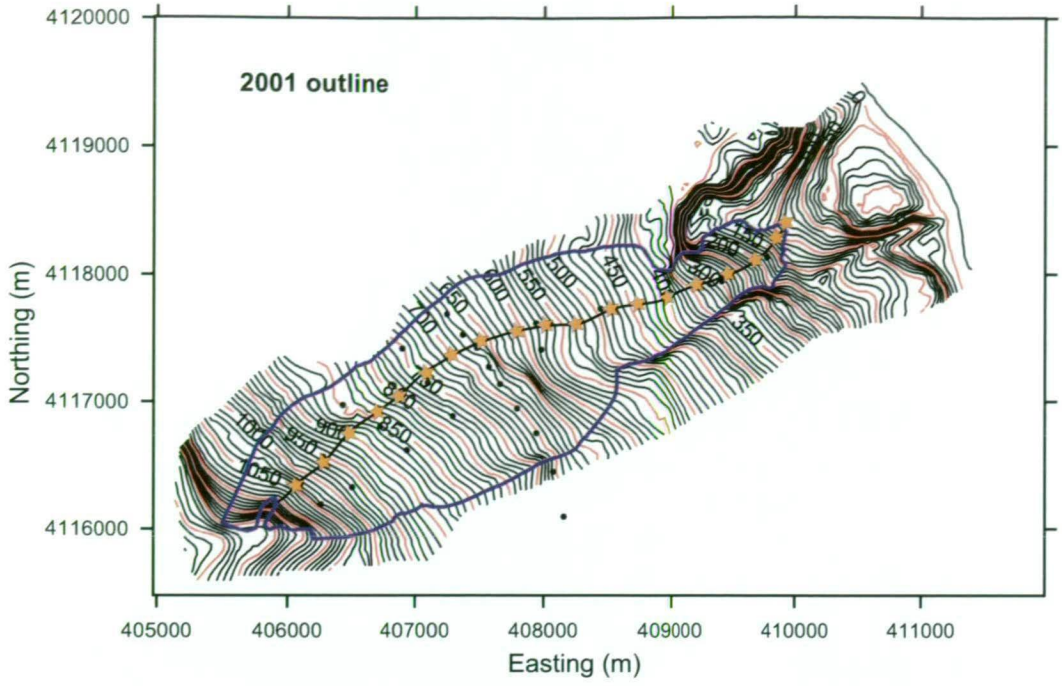

Figure 7.8.: The 2001 contour map for Brown Glacier. The contour intervals are 10 m with every 50 m interval highlighted in red. The 2001 glacier outline, the central flowline (blue) and the 0.25 km grid points (stars) are included.

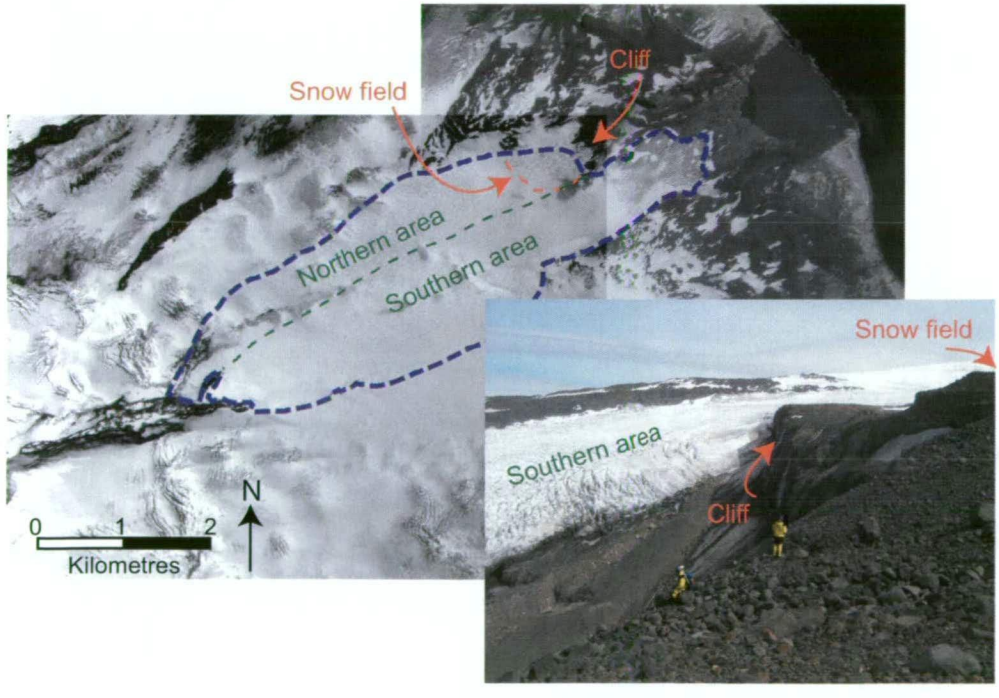

Figure 7.9.: The January 2001 Digital Globe satellite image of Brown Glacier showing the location of the northern cliff, snow field and the narrowing of the glacier around the northern cliff. The location of the approximate outline of the glacier is also indicated and a rough outline of the snow field. A photograph is also included to give another view of the the cliff and narrowing of the glacier.

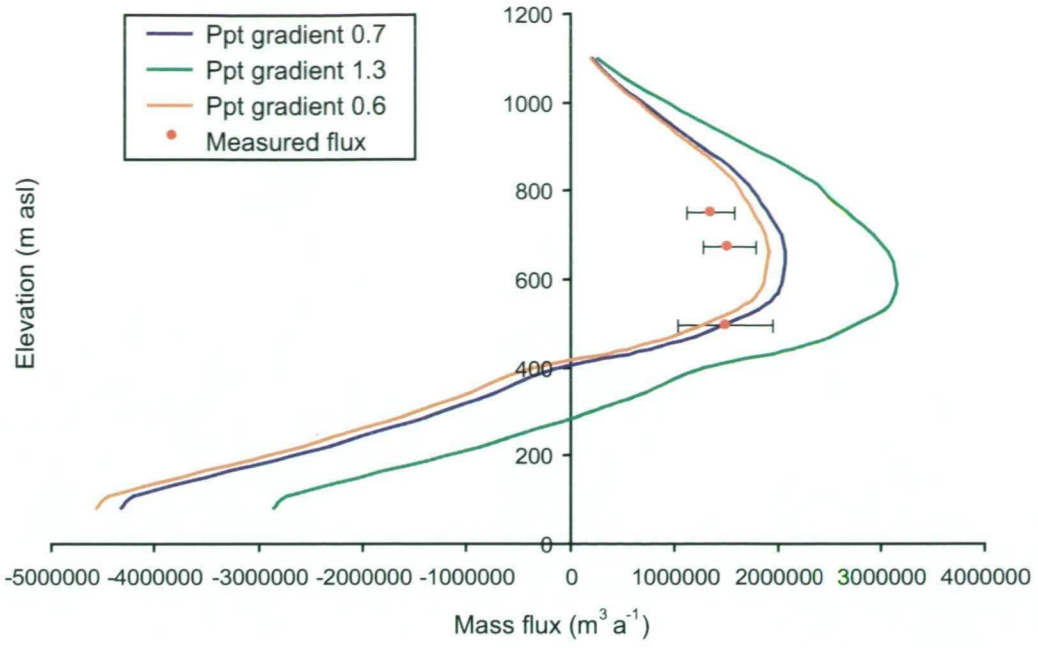

Figure 7.10.: The cumulative mass flux for the southern area of Brown Glacier compared to the mass flux values derived from field measurements (see Section 5.4.5).

Brown Glacier cumulative mass flux for 2001 The mass flux for the entire glacier area was also calculated. This mass flux value was necessary to compare with the dynamic model discussed in Section 7.5. The total mass flux of the glacier was also calculated from two different areas. The mass flux for the upper glacier was calculated from the total width of the glacier until an elevation of 400 m, below the BG35 net balance stake profile. For grid points between 400 m and 80 m asl the mass flux was calculated from the mass flux of the southern glacier area only. The combination of these two areas of the glacier gives the best estimate of the mass flux profile of Brown Glacier.

Figure 7.11 shows that the mass flux of Brown Glacier below 350 m asl is negative. This implies that if the current conditions persist, even with no further warming, then Brown Glacier will retreat to an elevation of 350 m asl. The negative mass flux also means that when modelling the steady state velocity and ice thickness there would be some instability in the lower glacier model.

7.5. A 2-D steady state dynamics model for Brown Glacier

Ruddell (1995) developed a steady state model of the dynamics for New Zealand glaciers, which was reconfigured in this study for Brown Glacier. This steady state model assumes that the glacier dynamics, which is the internal redistribution of mass by glacier motion according to mass conservation and the properties of ice, is stable.

7.5.1. Velocity

Glacier motion can be divided into two processes internal deformation and basal sliding. Internal deformation is movement within an ice mass due to gravity (Sugden and John, 1976). Basal sliding has several main processes, which have been derived from field and laboratory

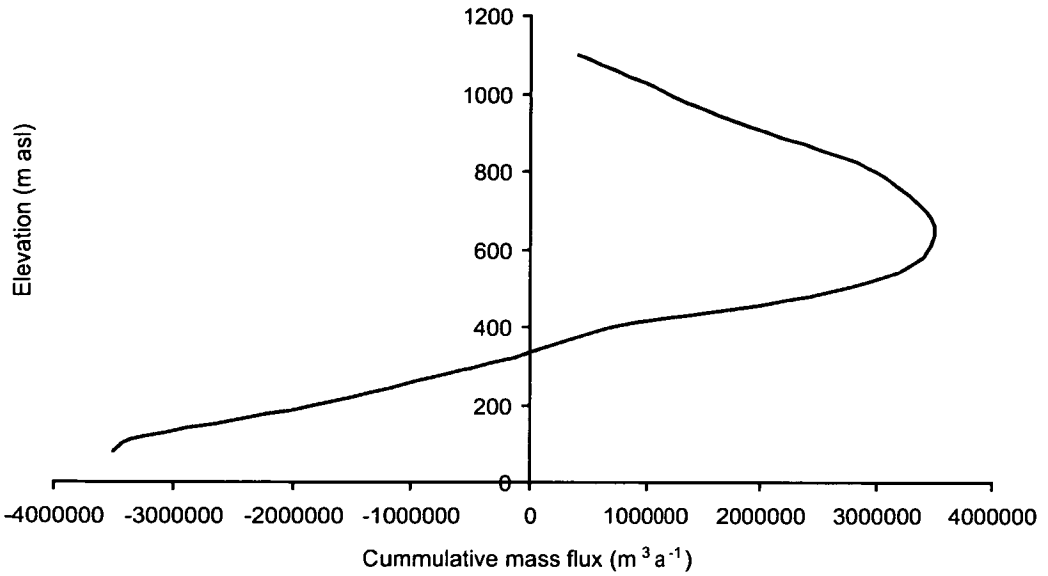

Figure 7.11.: The cumulative mass flux for northern and southern areas of Brown Glacier in 2001.

based experiments (Sugden and John, 1976). The sum of the internal deformation (U_i) and basal sliding (U_b) is the total velocity at the centre line of a glacier (U_s) (Aas and Bogen, 1988) and is given by:

$$U_s = U_i + U_b \tag{7.14}$$

Internal deformation velocity For internal deformation the relationship between ice velocity and stress is a function of the properties of ice that is given by the flow law (Glen, 1958). Basal shear stress is a direct result of the stress equation and momentum balance (with assumptions). The basal shear stress is given as:

$$\tau_b = f \rho_i g Z \sin \alpha \tag{7.15}$$

where,

$$f = \frac{\Omega}{PZ} \tag{7.16}$$

and α is the surface slope, ρ_i is the density of ice, g is the acceleration due to gravity, Z is the ice thickness, f is a stress shape factor, Ω is the cross sectional area perpendicular to the bed and P is the perimeter of the cross-section (Nye, 1965). The, f, stress shape factor of Nye (1965) was found by Smith (1984) to be very similar to the S_1 shape factor of Smith and Budd (1979):

$$\tau_b = S_1 \rho_i g \overline{Z \sin \alpha} \tag{7.17}$$

where $\overline{Z}$ is the centre line ice thickness normal to the surface and $\overline{\alpha}$ is the large scale surface slope normal to the surface. S_1 is a shape factor dependent on the shape and dimensions of the cross section and its estimated hydraulic radius for a rectangle of equivalent thickness:

$$S_1 = \frac{W}{W + (\eta Z)} \tag{7.18}$$

where W is the width of the glacier.

Bindschadler et al. (1977) suggests that the thickness coefficient (η) can be empirically derived from flow in a channel of known thickness. Ruddell (1995) uses this empirical method to derive a value of η =2.5. He found that when S_1 is calculated with η =2.5 it compares best with values from other glaciers.

The flow of glacial ice due to ice deformation (U_i) in this 2-D steady state, flowline model is expressed as:

$$U_i = k_1 \tau_b^n Z \tag{7.19}$$

The power law coefficient (k_1) in the deformation equation is defined by plotting the mean strain rate (U_i/Z) and the basal shear stress (τ_b) (Ruddell, 1995). Only glaciers with negligible basal sliding and no ice falls were used in the plot. A value of $k_1 = 0.1$ bar^{-n} a^{-1} is derived from this relationship based on a prescribed flow law exponent of n =3. These values are based on comparisons preformed by Ruddell (1995) between the calculated and observed deformation velocity for a wide range of temperate glaciers and laboratory experiments.

Basal sliding velocity The second component of the total centre line velocity of a glacier is the velocity due to basal sliding. Since temperate glaciers tend to be thin, steeply sloped and have low normal stress, basal sliding may compose a large component of the glacier's total motion. Glacier sliding is inversely proportional to friction and normal stress (Deeley and Parr, 1913). Many early studies (Lliboutry, 1968; Nye, 1969; Weertman, 1964) assumed that the sliding velocity is directly related to the basal shear stress and the irregularities and cavities in the bed.

Budd et al. (1979) and Ruddell (1995) proposed the relationship:

$$U_b = k_2 \frac{\tau_b^m}{N_s^{*q}} \tag{7.20}$$

where,

$$N_s^* = \rho_i g \cos\alpha Z^* \tag{7.21}$$

and,

$$Z^* = Z - \left(\frac{P_w}{\rho_i}\right) \tag{7.22}$$

where k_2 is a sliding factor, N_s^* is the effective normal stress, Z^* is the effective thickness, and m and q are empirically derived constants. Ruddell (1995) derived m and q values from fifteen glaciers. He found that a value of m =1 and q =2 gave the least scatter in results.

P_w is the water pressure at the bed of the glacier. There is a likely relation between water pressure and bed separation in low slope glaciers, polar ice sheets and outlet glaciers (Weertman, 1964; Bindschadler, 1983). Subglacial water is only important because of its lubricating effect as a thin film and when its thickness is sufficiently greater than that of the controlling obstacles (Weertman, 1957; Kamb, 1970). A small rise in water discharge can cause a large effect on water pressure even though the steady state water pressure will change very little (Bindschadler, 1983). A rise in the water pressure by a few bars is enough to increase the sliding velocity by an order of magnitude (Ruddell, 1995). If the water pressure is assumed to be negligible (as it is for this model of Brown Glacier) then the normal stress (N_s) is:

$$N_s = \rho_i g Z \cos\alpha \tag{7.23}$$

There are few direct measurements of the shear and normal stresses at the base of the glacier so the basal sliding velocity equation requires that there be adjustments in the k_2 (Budd and Smith, 1981). The k_2 values were empirically derived from the plot of the sliding velocity with τ_b/N_s^2 (Ruddell, 1995). It was found that the k_2 values vary between 3750 m a^{-1} bar for normal sliding to 30,000 m a^{-1} bar for rapid or accelerated sliding (Ruddell, 1995).

The basal sliding velocity can be given as:

$$U_b = k_2 \left(\frac{S_1 \tan\alpha}{\rho_i g Z \cos\alpha} \right) \tag{7.24}$$

Total velocity The total velocity can now be defined by combining Equations 7.17, 7.19 and 7.24 as:

$$U_s = k_1 (S_1 \rho_i g Z \sin\alpha)^3 Z + k_2 \left(\frac{S_1 \tan\alpha}{\rho_i g Z \cos\alpha} \right) \tag{7.25}$$

The modelled total velocity of Brown Glacier was calculated at the same grid points along the central flowline as the mass flux (see Section 7.4). To determine the total velocity the width of the glacier was measured from the 2001 contour map (Figure 7.8) midway between each grid point. This width was used to calculate the S_1 values (Appendix F.6.1). The S_1 values were further constrained by the measured ice thickness profiles (see Section 7.5.2).

The k_2 values for Brown Glacier were determined from several iterations of the model which were compared to the measured velocities and ice thickness values from the 2000/01 and 2003/04 surveys (Appendix F.6.1) and the modelled ice thickness values (see Section 7.5.2).

Total annual velocity profile on Brown Glacier in 2001 The final modelled velocities were in reasonable agreement with the measured velocities (Figure 7.12 and Appendix F.6.1). The peak in modelled velocity, at 4 km from the top of the glacier and at an elevation of 280 m, is similar to the measured velocities. To best match the measured values the k_2 values reached a peak at 3.5 km from the top of the glacier of 2000 m a^{-1} bar, which is below a normal sliding value of 3750 m a^{-1} bar (see Section 7.5.2). Williams (1998) found an even lower peak k_2 value for the Mary Powell Glacier of 600 m a^{-1} bar.

The total velocity profile has been split into two sections based on the two mass flux calculations used to determine the ice thickness profile of Brown Glacier (see Sections 7.4 and 7.5.2).

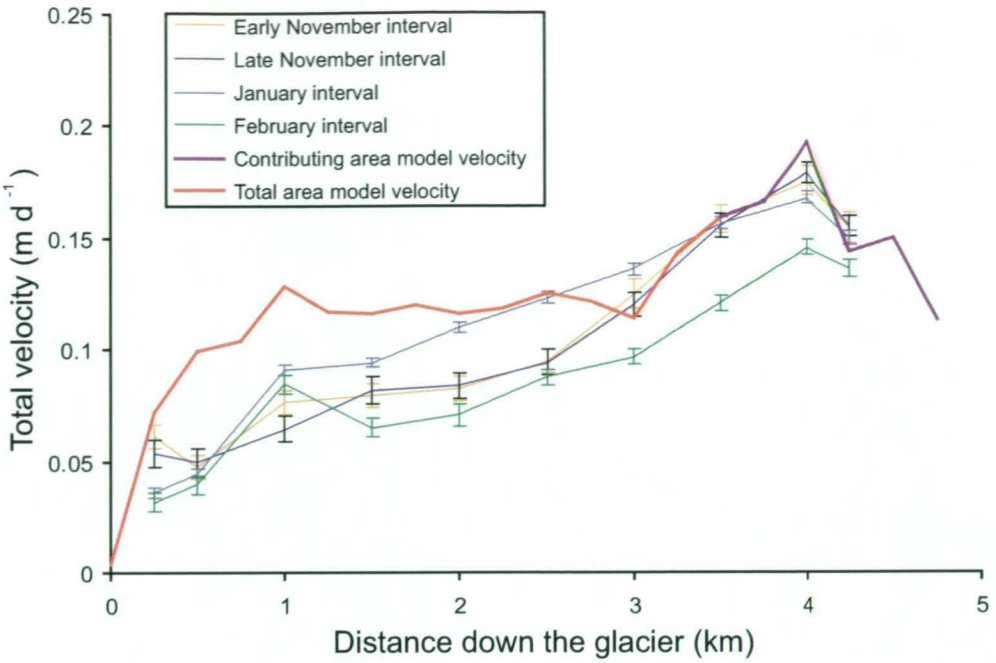

Figure 7.12.: The 2001 modelled and 2000/01 amd 2003/04 measured total velocities for Brown Glacier. The total velocity is split into two sections, based on the two mass flux values defined in Section 7.4, at 3.5 km along the glacier.

7.5.2. Ice thickness

The ice thickness of a steady state glacier can be determined from the net mass flux and the velocity (Ruddell, 1995). When the width and velocity of a cross-section is known then the ice thickness can be determined from the other cross-sections on the glacier. The dynamic flux (Q_d) across a section of the glacier is given by:

$$Q_d = WZU \tag{7.26}$$

where U is the mean velocity, W is the width of the glacier, and Z is the ice thickness.

Ruddell (1995) provided an alternate method for determining the ice thickness by comparing observations and measurements from a number of temperate glaciers. He showed that for glaciers with low slopes a basal shear stress of 1 bar is maintained but this increases with slope to 3 bar. The ice thickness decreases with increasing slope from several hundreds of metres to approximately seventy metres. Over this range the basal sliding increases from less than 25% of the total motion to 90% (Ruddell, 1995). At these higher stresses ice would be even thinner and basal sliding could increase to 100%. Despite all of these changes in glacier geometry, for a given slope, the width averaged balance flux remains roughly constant as U_b compensates for the changes.

For a glacier that is assumed to be in steady state and have insignificant water pressure, then the ice thickness can be determined from the dynamics flux (Equation 7.26). These steady state conditions also allow for the balance flux to be assumed to be equal to the dynamic flux ($Q_b = Q_d$) by:

$$Z = \frac{Q_b}{WU_s\varphi} \tag{7.27}$$

where φ is a dynamic mass flux shape factor (Ruddell, 1995).

Ruddell (1995) derived a φ value from thirty-two glaciers. The results indicated that the φ value does not vary much from the mean value of 0.49±12% and that despite the thinning of some of the thirty-two glaciers over time there has been little change in the φ value (Ruddell, 1995).

Then by rearranging Equations (7.18), (7.25) and (7.27) can determine Z without depending on velocity measurements. Assuming that q =2, m =1 and n =3:

$$Z = \frac{Q_b}{W\varphi\left(Zk_1\left(S_1\rho_i gZ\sin\alpha\right)^3 + k_2\left(\frac{S_1\tan\alpha}{(\rho_i gZ\cos\alpha)}\right)\right)}$$

then,

$$Q_b = Z^5 W\varphi k_1\left(S_1\rho g\sin\alpha\right)^3 + \frac{W\varphi Zk_2S_1\tan\alpha}{\rho gZ\cos\alpha}$$

and finally,

$$Z = \left[\frac{Q_b - \left(\frac{W\varphi k_2S_1\tan\alpha}{\rho g\cos\alpha}\right)}{W\varphi k_1\left(S_1\rho g\sin\alpha\right)^3}\right]^{\frac{1}{5}} \tag{7.28}$$

In this steady state model, S_1 is a function of Z therefore an iterative solution is necessary. To calculate S_1, the k_2 value is set to zero and an initial S_1 value is chosen between 0.6 to 0.99. This range was defined by studies on parabolic, rectangular, elliptical and triangular cross sections (Nye, 1965). The estimate of S_1 in this model is assisted by calculating the S_1 values for the grid points that have a measured ice thickness and width (six points in total).

Once the shape factor has converged the k_2 is increased by incremental amounts. The sliding factor ranges from 0 m a^{-1} bar for no sliding to 3750 m a^{-1} bar for normal sliding to 30,000 m a^{-1} bar for an ice fall. In this steady state model, the k_2 value is constrained by six radio echo profiles of Z obtained during the 2000/01 and 2003/04 surveys.

Brown Glacier ice thickness profile The modelled ice thickness on the upper glacier is dependent primarily on the k_2 values (Figure 7.13 and Appendix F.6.1). The Z is very sensitive to the k_2 values used therefore the k_2 values were increased at roughly equal intervals down the glacier, attempting to correlate the resulting Z with the measured values. Below 400 m (or 3.5 km down the glacier) this trend was reversed in order to maintain a stable model (Figure 7.13 and Appendix F.6.1). This is also where the change in mass flux from the total glacier to the southern glacier occurred.

The ice thickness values on the lower glacier could not be determined by the same methods as the upper glacier. The negative cumulative Q_b that occurs in a retreating glacier creates an unstable model (Figure 7.11). Instead the ice thickness was initially estimated to calculate the total velocity, which was then compared to the measured velocities (Figure 7.12). Several ice thickness and k_2 estimates were made before a reasonable estimate of the ice thickness was found for the lower glacier (Figure 7.13) (Appendix F.6.1).

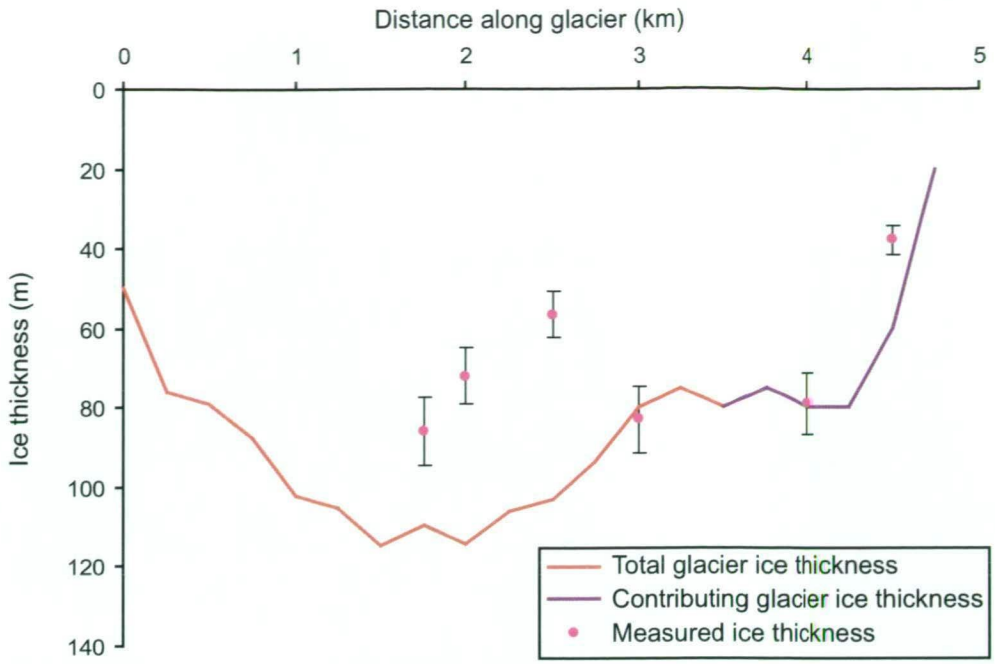

Figure 7.13.: The 2001 modelled and measured ice thickness measurements for Brown Glacier. The upper glacier uses a mass flux value that include the total width of the glacier, where as the lower glacier uses a mass flux that is representative of the contributing area of the glacier (see Section 7.4).

7.6. Past and future changes in Brown Glacier

The mass balance and steady state dynamics models were applied to two additional intervals. The first was 1950, when Brown Glacier was believed to be in equilibrium. The second was 2095, which represents the end of the recent IPCC report climate scenarios, to investigate what effect a further increase in temperature would have on Brown Glacier.

Initially the accumulation over these two epochs were assumed to be relatively unchanged from the 2001 value. This is based on studies that have shown that an increase of 1° C has a much greater effect on the glacier mass balance then a change in precipitation. For instance, Williams (1998) established a relationship between the change in temperature and a change in precipitation on the Mary Powell Glacier required to model the observed retreat. He estimated that a 32% decrease in precipitation would have the same effect as a 0.98° C warming. However, Williams (1998) did not take into the account the higher variability of precipitation over Heard Island, as indicated in Section 3.3.2, than temperature. Further investigations into the precipitation in 1950 indicates that there may be some differences between the 1950 and 2001 precipitation rates (see Section 7.6.1).

7.6.1. Past mass balance and dynamics (1950)

The 1950 glacier outline was determined from a combination of the GPS surveys and the 1947 DEM (Figure 7.8B). As discussed in Section 5.3.1 the upper glacier outline in 1950 is similar to the 2001 outline, based on the area of exposed rock outcrops. The 1950 lower glacier outline was defined by the height of the lateral moraines, observations made from the 1947 aerial photographs and the current seaward extent of the lagoon spit (Figure 7.14).

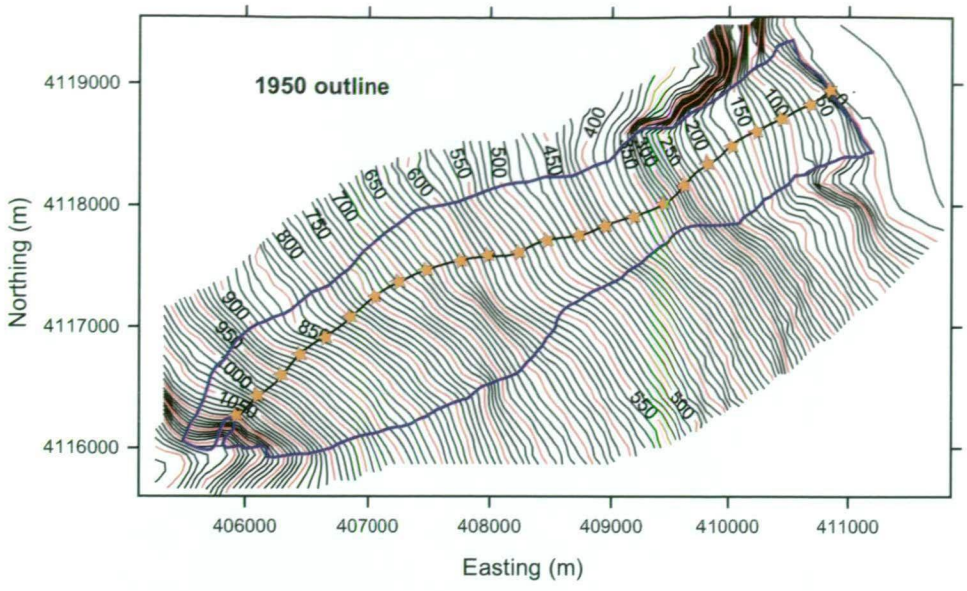

Figure 7.14.: The 1950 contour map of Brown Glacier. The contour intervals are 10 m with every 50 m interval highlighted in red. The 1950 glacier outline, the central flowline (blue) and the 0.25 km grid points (stars) are included.

Similar to the 2001 model, grid points were established every 0.25 km along the central flowline (Figure 7.14). The central flowline was assumed to be relatively unchanged between the two intervals. The width of the 1950 glacier was calculated as the width of the glacier at the midway point between two grid points (Appendix F.5).

The mass balance of Brown Glacier in 1950 was assumed to be in steady state based on historical observations that the glacier size did not fluctuate. To model the steady state mass balance for this period an estimate of the change in temperature and accumulation was necessary. The proxy temperatures were calculated from the difference between the 1948 to 1954 and the 1997 to 2006 Atlas Cove temperature records (−0.9 °C), which was then subtracted from the annual 2001 BG AWS temperature data. In estimating the ablation, the DDFs and lapse rates were assumed to be unchanged from 2001.

The annual ablation was found to range between $-1.1\,\mathrm{m\,a^{-1}}$ at 1100 m and $-11.6\,\mathrm{m\,a^{-1}}$ at sea level (Figure 7.15 and Appendix F.4.2). The 1950 annual ablation is less than the 2001 by about $0.5\,\mathrm{m\,a^{-1}}$ at 1100 m and approximately $3.0\,\mathrm{m\,a^{-1}}$ near the terminus. These differences illustrate the effects that a 0.9 °C warming has had on Brown Glacier.

Initially, the net accumulation for the 1950 glacier was assumed to be unchanged over the last 50 years, hence the same sea level precipitation values from the 2001 model were use to estimate the accumulation. This resulted in a glacier that was already retreating rather than in equilibrium. Instead, it was assumed that the sea level precipitation value was higher in 1950 then in 2001. This is supported by the precipitation records on the neighbouring sub-Antarctic islands. These records indicate that there has been a decrease in precipitation since the late 1960s (see Section 3.5.2).

To factor in an increase in accumulation between 1950 and 2001 the sea level precipitation value was increased until steady state conditions were achieved, i. e., when the mass flux near the terminus of the glacier is approximately zero (Figure 7.16). In this case the sea level

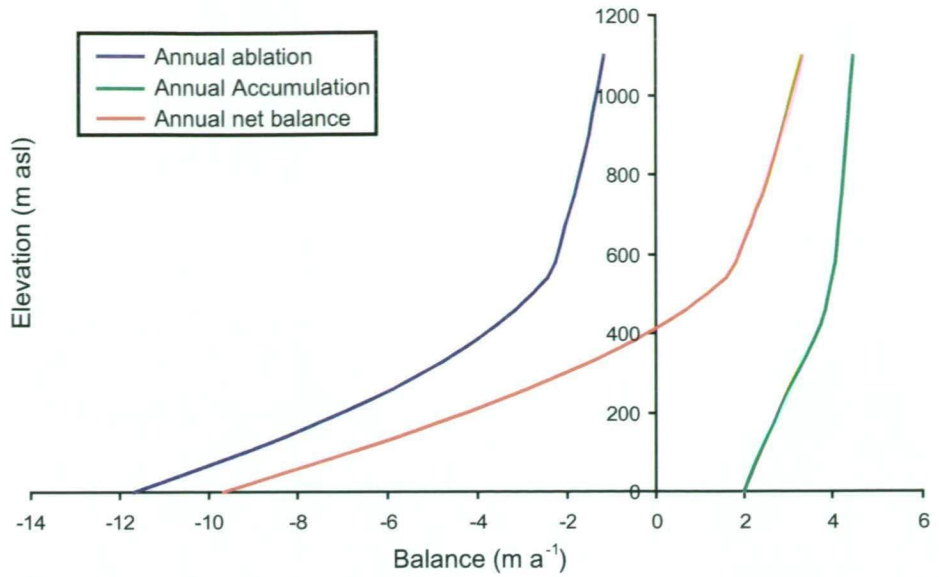

Figure 7.15.: The 1950 annual ablation, solid accumulation, and net balance for Brown Glacier.

precipitation was increased to 3.8 m (Figure 7.15). It is acknowledged that a 1 m decrease in sea level precipitation between 1950 and 2001 is unlikely. However in this model precipitation is a relative unknown compared to the temperature records. In fact, this iteration of the model may even be an indication that the sea level precipitation estimated for 2001 is too low.

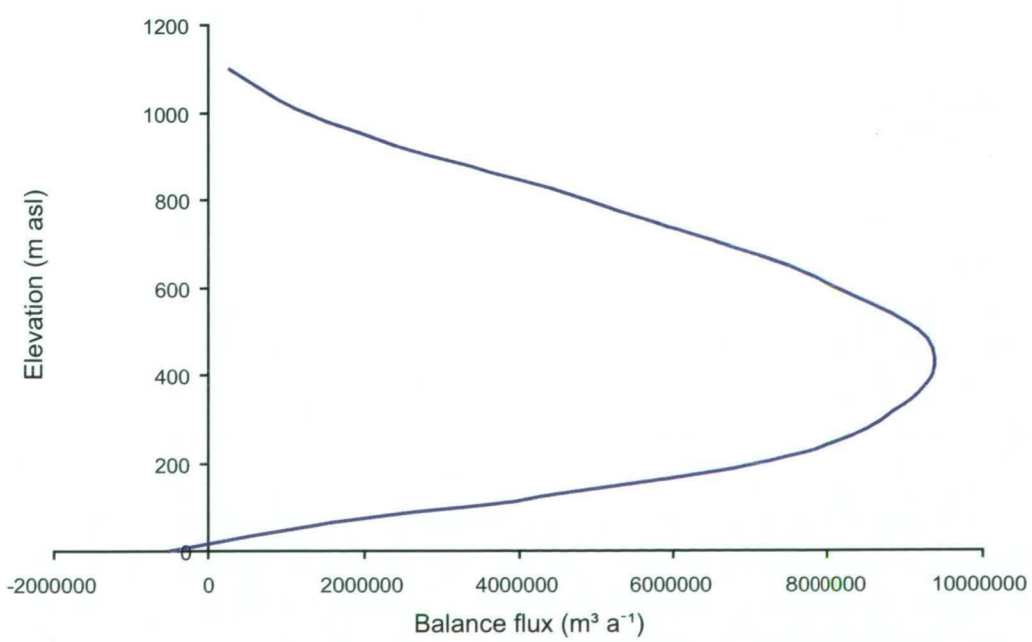

Figure 7.16.: The 1950 modelled cumulative mass flux.

Despite this increase in precipitation it was assumed that the same precipitation gradient ($0.7\,\mathrm{m\,a^{-1}\,km^{-1}}$) occurred over the glacier, resulting in an annual solid accumulation of $4.5\,\mathrm{m\,a^{-1}}$ at 1100 m and $2.0\,\mathrm{m\,a^{-1}}$ at the sea level terminus (Appendix F.3 and F.4.2).

The annual net balance that was derived from the 1950 ablation and accumulation suggests that the local ELA was near 400 m. This value is higher than the estimate from accumulation-area ratios, snowline height and contour analysis of 350 m (see Section 5.5.1).

The ice thickness and total velocity of the 1950 glacier were determined based on the steady state mass flux (Figure 7.16). The k_2 values were again increased in relatively equal intervals down the glacier, until below 400 m (3.75 km down the glacier) after which the k_2 values began to decrease again (Appendix F.6.2). The 1950 upper Brown Glacier ice thickness was found to be similar to the 2001 ice thickness (Figure 7.17). The two ice thickness profiles diverge about 2 km down the glacier. Below 2 km the 2001 glacier becomes thinner than the 1950 glacier, which extends to the sea, with its thickest point at 3.75 km down the glacier (400 m) near the ELA (Figure 7.15).

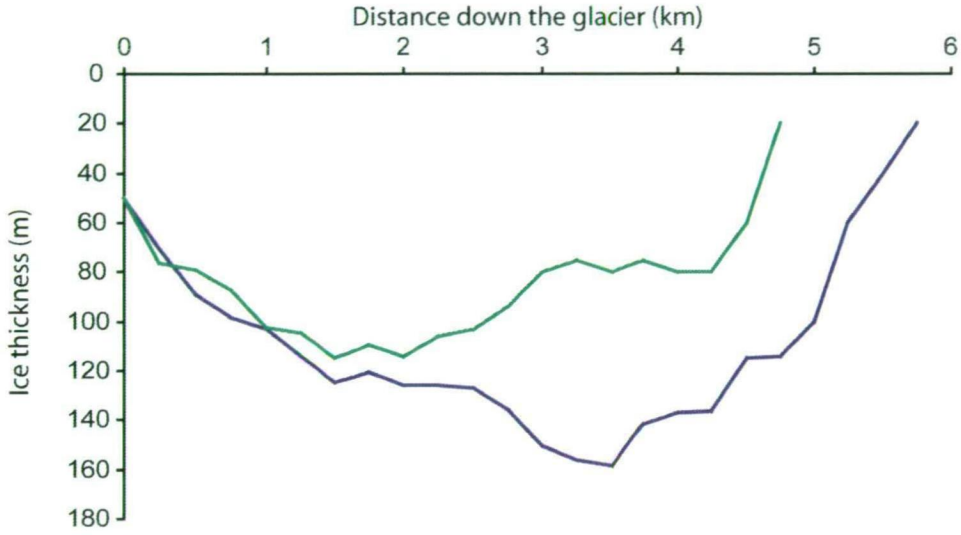

Figure 7.17.: The 1950 Brown Glacier modelled ice thickness (blue line) compared to the 2001 modelled values (green line).

When comparing the surface and bedrock elevations between the two epochs (Figure 7.18) the two bedrock profiles are similar except from 2.5 to 3.75 km from the head of the glacier. Along this ~1 km section, the 1950 glacier had a bedrock that was 20 to 50 m deeper than the 2001 glacier. This divergence in the estimation of bedrock elevation is along the same section of the glacier that the negative mass flux values for 2001 required several iterations of the dynamics model to determine an ice thickness that was a best fit to the measured data.

The total velocity in 1950 was higher then in 2001 (Figure 7.19). Near the terminus of the glacier, the modelled velocity decreased rapidly. There are no measured values at this elevation and this modelled decrease could be a true representation of the velocity at this grid point. A similar decrease in velocity at the terminus was measured by Mercanton (1916) on the Rhone Glacier and modelled by Ruddell (1995) for the same glacier using a similar model to the one used in this study.

7.6.2. Future mass balance estimates (2095)

Current climate change predictions do not bode well for temperate glaciers. The rising temperatures will continue to adversely effect the mass balance by lengthening the melt season

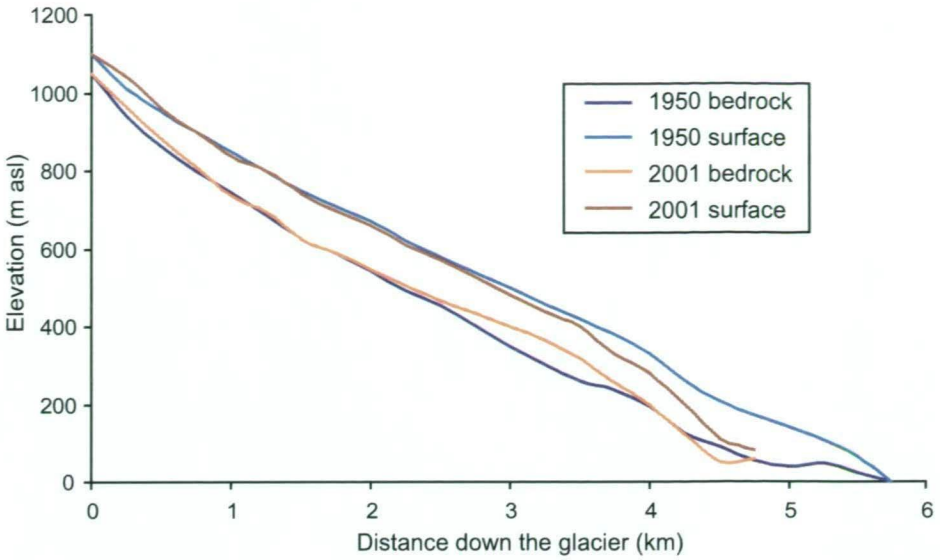

Figure 7.18.: The surface and modelled bedrock elevations for the 1950 and 2001 Brown Glacier.

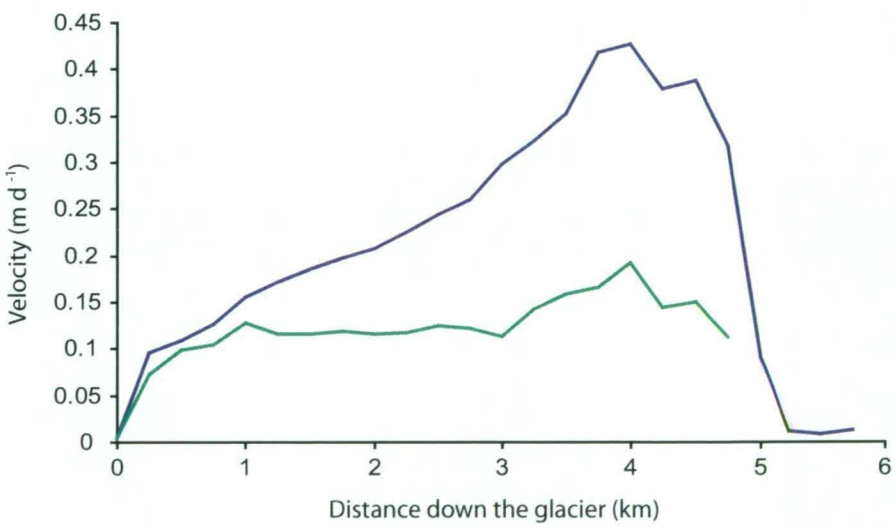

Figure 7.19.: The 1950 Brown Glacier modelled velocity (blue line) compared to the 2001 modelled values (green line).

and increasing the positive degree days. To predict the possible changes to Brown Glacier in the next 90 years the non-mitigation model scenarios for the mean temperature from the recent IPCC (Meehl et al., 2007) are applied to the 2001 BG AWS records.

The IPCC Fourth Assessment Report global warming temperature means were computed from multi-model results for future changes in the climate. The report focused on three emission scenarios, that represent a high (A2), medium (A1B) and low (B1) with respect to anthropogenic greenhouse gas emissions and the resulting radiative forcing, relative to the scenario range (Nakicenovic et al., 2001) (Figure 7.20).

To show how a warming on Heard Island would effect Brown Glacier the B1 and A2 scenario temperature warmings were applied. By 2090-2099 the multi-model mean surface air temperature and associated uncertainty ranges relative to 1980-1999 are +1.8° C (1.1° C to 2.9° C)

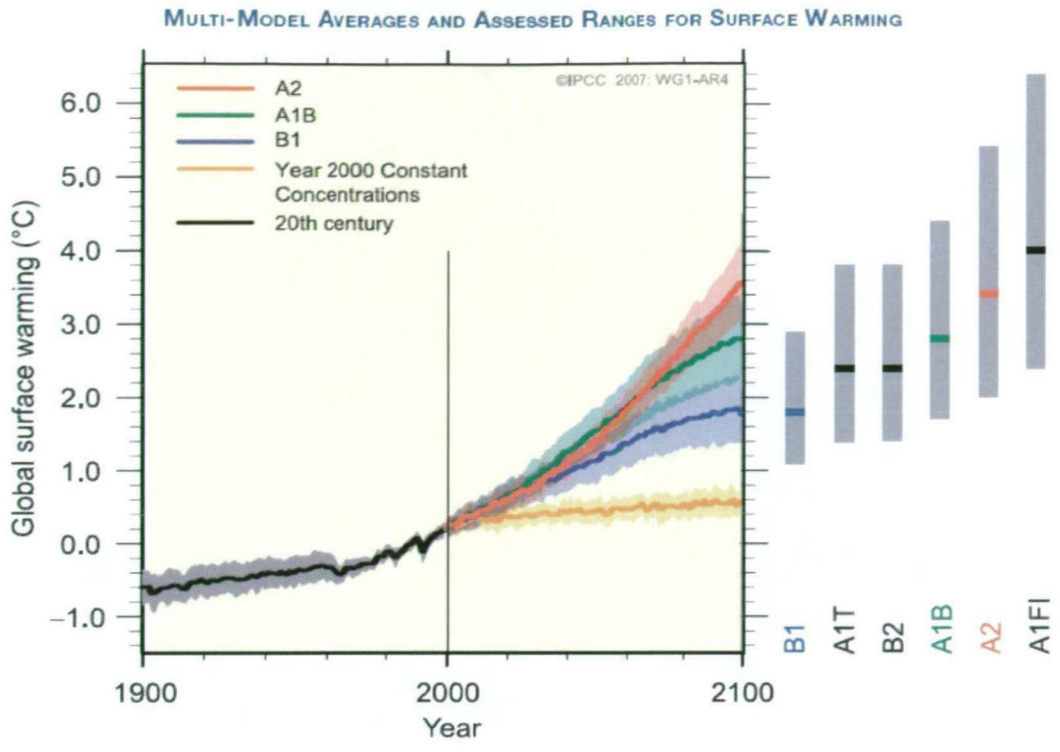

Figure 7.20.: The IPCC Fourth Assessment Report estimated global averages of surface warming. The solid lines are multi-model global averages of surface warming for each of the scenarios shown as continuation of the 20th century simulations. The orange line represents the changes if concentrations where kept at present levels. The grey bars at the right indicate the net estimate and likely range assessed for the six marker scenarios. This figure is from the IPCC (2007).

for the B1 scenario and +3.4° C (2.0° C to 5.4° C) for the A2 scenario. Both of these estimated increases in temperature were added to the BG AWS measurements to give an estimated temperature for the 2095 epoch near Brown Glacier.

Similar to the other two epochs of the model the precipitation gradient was assumed to increase at a rate of 0.7 m a^{-1} km^{-1}. It was also assumed in this model that the precipitation at sea level near Brown Glacier would not change between 2001 and 2095.

Both the B1 and A2 mass balance models suggest that, over the same elevation range as the 2001 model, that the 2095 ELA would be higher than the current head of the glacier (Figure 7.21A and B). Additionally the annual ablation would be very high, with a range of −3.3 m at 1100 m asl and −18.9 at 80 m asl for the B1 scenario and −5.9 m at 1100 m asl and −25.2 m at 80 m asl for the A2 scenario (Figure 7.21 and Appendix F.4.3). Both of these models suggest that Brown Glacier would cease to exist or be only a small patch of snow by 2095.

As mentioned above, the precipitation for this epoch was assumed to be unchanged from 2001. Given the current decrease in precipitation that has been reported for the SIO sub-Antarctic islands it is probable that there would be a decrease in precipitation on the Heard Island, which in conjunction with warmer temperatures may result in Brown Glacier disappearing even quicker.

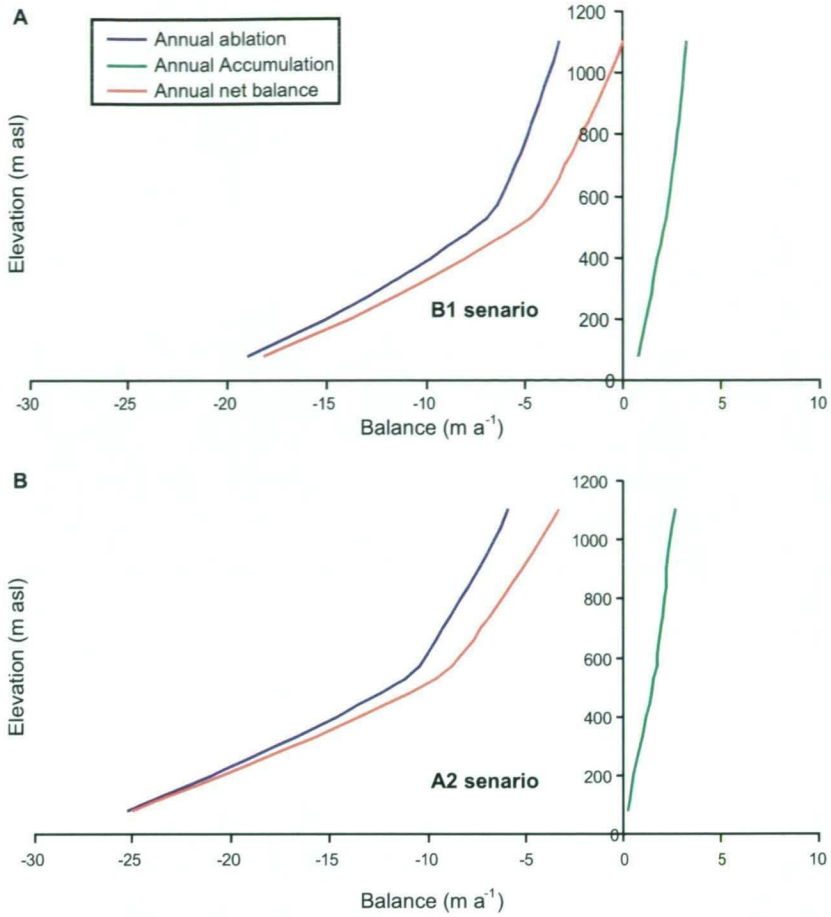

Figure 7.21.: The projected 2095 mass balance of Brown Glacier for **A**. the B1 scenario and **B**. the A2 scenario.

7.7. Conclusions

Climate has an immediate and direct effect on the annual accumulation and ablation of a temperate glacier. This change is propagated through the glacier over time before it becomes evident in the position of the glacier terminus. Air temperature and precipitation are often correlated to glacier fluctuations but other factors such as the mass balance, energy balance, glacier geometry and ice dynamics are also important.

The net balance stake measurements from 2003/04 were used to test the summer degree day model. The summer degree day model provided a good fit to the lower glacier net balance values but underestimated the upper glacier values. The föhn wind analysis from the temperature, wind and relative humidity measurements during 2003/04 indicated that föhn winds occurred for longer durations and at higher frequency on Brown Glacier, which may explain the higher measured net balance values on the upper glacier. It is acknowledged that the degree day model used in this study can not register the effects of föhn winds on the net balance.

The ice thickness and velocity measurements at the BG20, BG25 and BG35 profiles were used to derive a mass flux through these cross sections. These mass flux values were used to help determine a precipitation gradient on Brown Glacier after several iterations of the mass balance model.

The net balance values determined from the analysis of the two crevasses (BC1 and SC1) were compared to the 2001 annual net balance to ensure that the annual ablation and accumulation estimates on the upper glacier were within reason.

The ice thickness values were used to calculate an initial shape factor at six location in order to determine the central flowline ice thickness. The ice thickness and the velocities, measured at all of the net balance stakes during both 2000/01 and 2003/04 field seasons, were also used to constrain the sliding factor in both the central flowline ice thickness and velocity profiles. The measured surface velocities were also used to constrain the estimated ice thickness where the model was unstable, particularly near the terminus and headwall.

The mass balance model presented here provides a reasonable representation of the present Brown Glacier. The model suggests that in 1950 when the glacier was thought to be in steady state, both lower temperatures and higher precipitation would be required in order for the glacier to be in steady state. The model also predicts that if temperature continues to rise dramatically over the next 90 years, as predicted in the IPCC B1 and A2 scenarios, Brown Glacier will cease to exist.

If Brown Glacier was to disappear by 2090 it is reasonable to assume that many of the other lower glaciers on Heard Island, that do not descend from the summit of Big Ben such as the Mary Powell, AU1211, Nares and Fifty-one glaciers, will also disappear. The larger glaciers on the island will also be effected by the increase in temperature. Many of these glaciers may have retreated to higher elevations. This significant change to the environment on Heard Island would result in greater colonisation of plants and animals on the lower and mid-level slopes of Heard Island leaving only a snow capped peak above.

The steady state dynamics model presented in this study may not be the best indicator of the ice thickness and velocity on Brown Glacier, especially on the lower glacier. Several assumptions and estimates were necessary, especially in the modelled ice thickness values. Future work on the dynamics of Brown Glacier would suggest that further integrations of Ruddell's model or possibly a development of an alternate model would be a preferable option.

In the mean time Ruddell's model does give a first estimate of the 2001 upper glacier ice thickness and of the 1950 ice thickness and velocity when the glacier was closer to steady state as assumed in the model.

8. Overview and concluding remarks

8.1. Summary

The mass balance of glaciers globally have been studied with increased frequency in the last 50 years. Temperate glacier, in particular, make excellent climatic indicators because these warm, steep sloped, fast flowing glaciers have a quicker response time to climate change than larger, cooler ice masses such as those in Antarctica and Greenland. Observations of the fluctuation of temperate glaciers worldwide contribute important information for monitoring climate change. Changes in these permanent ice covered regions incorporate climatic variations over various time scales. Hence glaciers are among the clearest signals of ongoing warming trends existing in nature and good visible expressions of climate change (Lemke et al., 2007).

A combination of aerial photographic surveys, satellite imagery and historical photographs has provided information on the changes in the Heard Island glacier size, shape and extent over the past ~200 years. Due to infrequent visits to the island and incomplete surveys of all regions during each visit, the timing of the fluctuations may have some regional errors. The sealers and early scientific voyages provided the first observations of Heard Island glaciers. These observations indicate that there were only minor fluctuations of the glaciers until 1929. After 1929, there was a slight recession of the northern, eastern and Laurens Peninsula glaciers and a slight thinning of the southwestern glaciers. By the 1960s, the first widespread observations were made of the retreat of the northern, Laurens Peninsula and some of eastern glaciers. This retreat continued through the 1980s with some regional advances (e. g., Winston Glacier). Currently the eastern, northern and Laurens Peninsula glaciers are decreasing in size and now there is evidence of additional thinning of the larger glaciers across the island and the retreat of the smaller southwestern glaciers.

This mass balance change observed across the island has been studied in more detail on Brown Glacier, on the eastern coast. It is those glaciers on the eastern (leeward) side of the Big Ben massif that have been observed to have the most visually dramatic changes in their extent.

8.1.1. Mass balance surveys

The aim of this study was to use the results of two field surveys on Brown Glacier to integrate into mass balance and dynamics models. These two field surveys have provided more detail on the morphology, dynamics and mass balance of Brown Glacier than of any glacier on Heard Island. The benefit of having two field seasons means that we are finally getting an idea of the longer term changes on Brown Glacier and not just a snap shot of one season from a handful of sites.

The first survey, from the end of October 2000 to mid-January 2001, provided a baseline for the most recent changes on Brown Glacier, a glacier which had previously had only been observed from photographic evidence. The second survey, from the end of December 2003 to

mid-February 2004, provided evidence of the short term (approximately three years) changes that occurred between the two field season and increased the coverage of the first survey. Results from these two surveys include the following:

- The orographic variability caused by the Big Ben massif effects the distribution of temperature, precipitation, and winds across the island. This is highlighted by the differences between Atlas Cove and Spit Bay. Atlas Cove tends to have lower temperatures, lower measured precipitation, and no föhn wind events compared to Spit Bay
- Föhn winds play an important but as yet unquantified role in the mass balance of Heard Island glaciers. Föhn wind effects have been shown to occur more often at higher elevations on Brown Glacier then lower elevations
- Since 1947 the terminus of Brown Glacier has retreated a total of 1.7 km with an average retreat rate of 20 m a^{-1}
- Brown Glacier has thinned by up to −11.7 m on the lower glacier with an average of −9.9 m below the BG40 survey stake and −8.5 m on the upper glacier above the BG30 survey stake
- A series of net balance stakes and sonic rangers measurements have provided the most detailed summer ablation and net balance records on Heard Island
- A lower elevation lapse rate was calculated for Brown Glacier from the air temperature data at AWS1, AWS2 and AWS3. The average lapse rate between AWS1-AWS2 was −0.008°C m^{-1} and between AWS2-AWS3 was −0.003°C m^{-1}
- The collection of ice cores and crevasse samples on Brown Glacier has provided some of the first estimates of the accumulation on the upper glacier, and its variation with elevation. Previous precipitation records for sites above sea level have not been available on Heard Island
- The surface velocity survey found that there is a seasonal change in the surface velocity measurements. This suggests that geothermal heat, from the active Big Ben volcano, is not significant in smoothing the surface velocity
- Ice thickness measurements were made at six locations on the glaciers, including three detailed cross-section profiles
- DGPS surveys of the Brown Glacier basin and surrounding region and the increased availability of satellite imagery over the island, have been used to produce the most accurate digital elevation model (DEM) of the Brown Glacier basin
- The DEM, accumulation-area ratio, and snowline height observations were used to estimate an ELA. The ELA of Brown Glacier was estimated as being between 500 and 600 m in 2001 and at 350 m in 1950
- Based on a contour map and surface velocity profiles a more accurate outline of Brown Glacier could be mapped, although there are still some uncertainties in the upper margins
- Bathymetric surveys of all four major lagoon on the eastern coast provided a more detailed bedrock topography of these pro-glacial lagoons

8.1.2. Mass balance and dynamics models

The mass balance and dynamics models developed for Brown Glacier used these new data. The most valuable data in modelling Brown Glacier was the temperature records. BG AWS provides the only available annual temperature records above sea level of any of the sub-Antarctic islands in the southern Indian Ocean. This annual record is supplemented by the summer temperature records from AWS1, AWS2 and AWS3. These four AWS were used to derive a lapse rate for Brown Glacier and to estimate the ablation in a degree day model. In conjunction with the sonic ranger net balance measurements that were used to derive a degree day factor. Other records that were used included the January precipitation measurements at Brown Hut and the annual precipitation measurements at Spit Bay and Atlas Cove. The majority of the remaining results from the two field surveys were used to tune the model.

The mass balance models for Brown Glacier indicate that an increase in temperature of 0.9° C between 1950 and 2001, and possibly a decrease in precipitation, has resulted in the retreat of the glacier. The steady state mass flux for 2001 indicates that if all of the current parameters remained constant then the terminus of Brown Glacier will retreat to an elevation of 350 m.

IPCC for 2095 were used to predict the changes that would occur on Brown Glacier if there was a further increase of temperature of 1.8 and 3.4° C. In both of these models Brown Glacier would cease to exist or possibly retreat to a small, semi-permanent snow field.

This has similar implications for the other glaciers on Heard Island. Further increases in temperature and a continuation of the decreasing precipitation trends observed on the neighbouring sub-Antarctic islands implies that the smaller glaciers on Heard Island would also begin to retreat at a more rapid rate over the next 90 years. Glacier such as the Mary Powell, Nares, and Deacock that do not originate from the Big Ben Plateau are likely to retreat to elevation above ~1000 m asl and the glaciers on the Laurens Peninsula will have disappeared completely.

These higher temperatures across the islands would likely decrease the variable nature of the current observed mass balance for the different sectors of the island. Although based on current observations the smaller glaciers on the windward side of the island may not retreat as far as the glaciers on the leeward side. An additional mass balance survey of a glacier on one of the Southwestern glaciers would allow for a more detailed predication of the mass balance changes for this region.

The larger glacier on Heard Island would also be affected by these changes in climatic conditions. Without a mass balance model for one of these glaciers it is difficult to predict how far these glaciers would retreat but it can be assumed that if the smaller glacier have retreated to ~1000 m asl then the larger glacier will thin and may retreat to above 500 m asl or more.

This decrease in the glacier coverage on Heard Island would result in the further colonisation of bare rock and glacial till by vegetation, mammal and bird species. Thereby increasing the biological diversity and populations on the island.

8.1.3. Regional implications

Glacier have not only been retreating on Heard Island. More dramatic retreats have been observed on the other southern Indian Ocean sub-Antarctic islands (Crozet, Marion and Kerguelen),

while glaciers from the other sub-Antarctic islands (e. g., Bouvetøya, South Georgia, and South Sandwich islands) have been retreating at less dramatic rates.

The decrease in glacier extent on these sub-Antarctic islands is linked to the temperature and precipitation. The temperature and precipitation records from the meteorological stations in the southern Indian Ocean provide a good indication of the regional trends for the last 60 years. The increasing temperature measured at all of the stations and in the sea surface temperature data shows that, similar to the average global temperature, this region is warming. Measured precipitation at these southern Indian Ocean stations indicate that there is a decreasing trend in the annual precipitation, although only at Kerguelen and Marion was the trend significant (99%).

This changing climate has resulted in the retreat of the glaciers on all of the sub-Antarctic islands in the southern Indian Ocean with the northern-most islands being affected more dramatically then the southern islands. Marion, Crozet and Kerguelen, are located to the north of the Polar Front, whereas Heard, Bouvetøya, South Georgia and South Sandwich islands are south of the Polar Front. The influence of the Polar Front can been seen best by comparing the climate on Kerguelen and Heard islands. These two islands are only 440 km apart yet they are separated by the Polar Front, which results in a significant difference in the temperatures on the two islands, with Kerguelen annual temperatures typically being between 3.7 and 2.1° C warmer then Heard Island. The greater change in temperatures for latitude above the Polar Front are resulting in the more rapid decrease in glacier coverage than the lower temperatures found on islands located to the south of the Polar Front.

8.2. Conclusions

An understanding of the natural climate and glacier variability over the last 100 years on Heard Island has been hampered by the lack of continuous long term records. Glacier surveys and meteorological records for Heard Island are infrequent and sporadic yet they do provide data from which a broader understanding of the island's climate and glaciers can be inferred.

The increase in temperatures and decrease in precipitation on Heard Island has resulted in the dramatic retreat of the eastern glaciers. The mass balance of Brown Glacier, which has been examined in more detail, has indicated that a ~1° C warming since 1950 is likely to be the cause of this retreat. Predictions of further increases in temperature results in the glaciers on Heard island continuing to retreat to higher elevations. Leaving the island as a snow capped peak rather than a mountain that is 70% covered in glaciers.

Bibliography

Aas, E. and J. Bogen: 1988, 'Colors of glacier water'. *Water Resources Research* **24**(4), 561–565.

Allison, I.: 1980, 'A preliminary investigation of the physical characteristics of the Vahsel Glacier, Heard Island'. *ANARE Scientific Reports* **128**, 31.

Allison, I. and P. Keage: 1986, 'Recent changes in the glaciers of Heard Island'. *Polar Record* **23**(144), 255–271.

AMS: 2000, *Glossary of Meteorology*. American Meteorological Society.

Andrews, J.: 1975, *Glacial Systems: an approach to glaciers and their environments*. Massachusetts: Duxbury.

Aristarain, A.: 2002, *Argentine program on climatic and environmental studies by means of ice cores*, The Patagonian Icefields: A unique natural laboratory for environmental and climate change studies. New York: Kluwer Academic.

Aristarain, A. and R. Delmas: 1981, 'First glaciological studies on the James Ross Island ice cap, Antarctic Peninsula'. *Journal of Glaciology* **27**(97), 371–379.

Aristarain, A., R. Delmas, and M. Brait: 1982, 'Snow chemistry on James Ross Island (Antarctic Peninsula)'. *Journal of Geophysical Research* **87**(C13), 11004–11012.

Arnason, B.: 1969, 'The exchange of hydrogen isotopes between ice and water in temperate glaciers'. *Earth and Planetary Science Letters* **6**, 423–430.

Ashworth, A., W. Vestal, G. Hokanson, L. Joseph, M. Martin, K. McGlynn, M. Newbrey, N. Schlecht, J. Turnbull, A. White, and T. Zimmerman: 2000, 'Biota Australis Terrestris'. http://www.ndsu.edu/subantarctic/index.htm. accessed 14 July 2006.

Aubert de la Rue, E.: 1929, 'Un voyage d'exploration dans les mers Australes'. *Revue de Géographie Physique et de Géologie* **2**(3), 97–146.

Aubert de la Rue, E.: 1932, 'Étude géologique et géographique de L'Archipel de Kerguelen'. *Rvue de Géographie Physique et de Géologie Dynamique* **5**(1-2), 1–230.

Auzeneau, S.: 1994, 'Meteo-France: Catalogue of climatological data on French Stations in Antarctica and the sub-Antarctic region'. http://www.wmo.ch/pages/prog/www/OSY/Ant-cat-France.html. accessed 28 August 2007.

Baboukas, E., J. Sciare, and N. Mihalopoulos: 2004, 'Spatial, temporal and interannual variability of methanesulfonate and non-sea-salt sulfate in rainwater in the southern Indian Ocean (Amsterdam, Crozet and Kerguelen Islands)'. *Journal of Atmospheric Chemistry* **48**, 1–23.

Barry, R.: 1992, *Mountain Weather and Climate.* London: Routledge, 2nd edition.

Barry, R. and R. Chorley: 1976, *Atmosphere, Weather and Climate.* Methuen and Co. Ltd.

Bates, T., B. Lamb, A. Guenther, J. Dignon, and R. Stoiber: 1992, 'Sulfur emissions to the atmosphere from natural sources'. *Journal of Atmospheric Chemistry* **14**, 315–337.

Bauer, A.: 1963, 'Les glaciers de L'Ile de Kerguelen'. *Territoire des Terres Australes et Antarctiques Françaises* pp. 1–75, plus maps.

Beggs, P., P. Selkirk, and D. Kingdom: 2004, 'Identification of von Karman vortices in the surface winds of Heard Island'. *Boundary-Layer Meteorology* **113**, 287–297.

Belkin, I. and A. Gordon: 1996, 'Southern Ocean fronts from the Greenwich meridian to Tasmania'. *Journal of Geophysical Research* **101**, 3,675-3,696.

Bellair, P.: 1964, 'Recent data on the geology of Iles Crozet'. In: R. Adie (ed.): *Antarctic Geology.* North-Holland.

Benn, D. and D. Evans: 1998, *Glaciers and Glaciation.* Holder Aronld Publication.

Berresheim, H.: 1987, 'Biogenic sulfur emissions for the sub-Antarctic and Antarctic oceans'. *Journal of Geophysical Research* **92**, 13,245–13,262.

Bindschadler, R.: 1983, 'The importance of pressurized subglacial water in separation and sliding at the glacier bed'. *Journal of Glaciology* **29**(101), 3–19.

Bindschadler, R., W. Harrison, C. Raymond, and R. Crosson: 1977, 'Geometry and dynamics of a surge-type glacier'. *Journal of Glaciology* **18**(79), 181–194.

Bird, E.: 1994, *Physical setting and geomorphology of coastal lagoons*, Coastal Lagoon Processes. Amsterdam: Elsevier.

Boon, S. and M. Sharp: 2001, 'Impact of high-altitude chinook events on arctic glacier hydrology'. *Proceedings of the 58th Eastern Snow Conference.*

Bourgeois, O., O. Dauteuil, and B. Van Vliet-Lanoe: 2000, 'Geothermal control on flow patterns in the Last Glacial Maximum ice sheet of Iceland'. *Earth Surface Processes and Landforms* **25**, 59–76.

Bradley, R.: 1999, *Paleoclimatology: Reconstructing climates of the Quaternary*, Vol. 64. San Diego: Hardcourt Academic Press, 2nd edition.

Braithwaite, R.: 1995, 'Positive degree-day factors for ablation on the Greenland Ice Sheet studied by energy-balance modelling'. *Journal of Glaciology* **41**(137), 153–160.

Braithwaite, R.: 2002, 'Glacier mass balance: the first 50 years of international monitoring'. *Process in Physical Geography* **26**(1), 76–95.

Braithwaite, R. J.: 1981, 'On glacier energy balance, ablation, and air temperature'. *Journal of Glaciology* **27**(97), 381–391.

Braithwaite, R. J. and O. B. Olesen: 1989, 'Calculation of glacier ablation from air temperature, West Greenland'. In: *Glacier Fluctuations and Climatic Change.* Kluwer Academic Publishers, pp. 219–233.

Braithwaite, R. J. and O. B. Olesen: 1990, 'A simple energy-balance model to calculate ice ablation at the margin of the Greenland Ice Sheet'. *Journal of Glaciology* **36**(123), 222–228.

Braithwaite, R. J. and Y. Zhang: 1999, 'Modelling changes in glacier mass balance that may occur as a result of climate changes'. *Geografiska Annaler* **81**(A), 489–496.

Brinkmann, W.: 1971, 'What is a foehn?'. *Weather* **26**, 230–239.

Bruland, O., D. Maréchal, K. Sand, and A. Killingtveit: 2001, 'Energy and water balance studies of a snow cover during snowmelt period at a high arctic site'. *Theoretical and Applied Climatology* **70**, 53–63.

Budd, G.: 1964a, 'The ANARE 1963 Expedition to Heard Island'. *ANARE Reports* **1**(A).

Budd, G.: 1964b, 'The Southern Ocean Expedition to Heard Island, 1964-65'. *Polar Record* **12**(77), 193–95.

Budd, G.: 1965, 'South Indian Ocean expedition to Heard Island, 1964-65'. *Polar Record* **12**(81), 744.

Budd, G.: 1970, 'Heard Island Reconnaissance, 1969'. *Polar Record* **15**(96), 335–36.

Budd, G.: 1973, 'Fluctuations of Glaciers 1965-1970'. In: *IAHS (ICSI)-UNESCO*, Vol. 3. pp. 65–68, 163–164, IASH.

Budd, G.: 2000, 'Changes in Heard Island glaciers, King Penguins and Fur Seals since 1947'. *Papers and Proceedings of the Royal Society of Tasmania* **133**(2), 47–60.

Budd, G. and P. Stephenson: 1970, 'Recent glacier retreat on Heard Island'. In: *Proceedings of the International Symposium on Antarctic Glaciological Exploration (ISAGE)*, Vol. 86. pp. 449–458, IASH.

Budd, W. and I. Allison: 1975, 'An empirical scheme for estimating the dynamics of unmeasured glaciers'. In: *Snow and Ice - Symposium - Neiges et Glaces*, Vol. 104. Moscow, pp. 246–256, IASH-AISH.

Budd, W., P. Keage, and N. Blundy: 1979, 'Empirical studies of ice sliding'. *Journal of Glaciology* **23**(89), 157–169.

Budd, W. and I. Smith: 1981, 'The growth and retreat of ice sheets in response to orbital radiation changes'. *IAHS Publication* **131**, 369–409.

Burton, H. and D. Williams: 1985, 'Heard Island ANARE 1985 Report'. Australian Antarctic Division Report.

Caulkett, A. and J. Ellis-Evans: 1997, 'Chemistry of streams of Signy Island, maritime Antarctica: sources of major ions'. *Antarctic Science* **9**(1), 3–11.

Chen, X. and E. Zhang: 2002, 'Large and episodic decrease of water discharge from the Yangtze River to the sea during the dry season'. *Hydrological Sciences Journal* **47**(1), 41–48.

Chinn, T.: 1996, 'New Zealand glacier responses to climate change of the past century'. *New Zealand Journal of Geology and Geophysics* **39**, 415–428.

Chittleborough, R.: 1956, *Hydrology of Heard Island, 1949*, Vol. 30 of *Plankton, hydrology and marine fouling at Heard Island.* Melbourne: ANARE Publication.

Chown, S.: 2003, 'The probability of introduction of non-indigenous species to Heard and McDonald Islands: taxa, risk and mitigation'. Australian Antarctic Division Report.

Clapperton, C., D. Sugden, J. Birnie, and W. M.J.: 1989, 'Late-Glacial and Holocene glacier fluctuations and environmental change on South Georgia, Southern Ocean'. *Quaternary Research* **31**, 210–228.

Clifton, R.: 2004, 'Heard Island Expedition 2003/04: Field Leaders Report'. Australian Antarctic Division Report.

Cline, D., R. Bales, and J. Dozier: 1998, 'Estimating the spatial distribution of snow in mountain basins using remote sensing and energy balance modelling'. *Water Resources Research* **34**(5), 1275–1285.

Cogley, J.: 2005, 'Mass and energy balances of glaciers and ice sheets'. In: M. Anderson (ed.): *Encyclopaedia of Hydrological Sciences.* John Wiley & Sons.

Copeland, L. and M. Sharp: 2001, 'Mapping thermal and hydrological conditions beneath a polythermal glacier with radio-echo sounding'. *Journal of Glaciology* **47**(157), 232–242.

Crowther, W. E. L. H.: 1970, 'Captain J. W. Robinson's narrative of a sealing voyage to Heard Island. 1958-1960'. *Polar Record* **15**(96), 301–316.

Curran, M. and A. Palmer: 2001, 'Suppressed ion chromatography methods for the routine determination of ultra low level anions and cations in ice cores'. *Journal of Chromatography* **919**, 333–339.

Curran, M., T. van Ommen, and V. Morgan: 1998, 'Seasonal characteristics of the major ions in the high-accumulation Dome Summit South ice core, Law Dome, Antarctica'. *Annals of Glaciology* **27**, 385–390.

Dalzeil, K.: 1955, 'Rain measurements at Heard Island'. *Australian Meteorological Magazine* **10**, 47–56.

Deacon, G.: 1933, 'A general account of the hydrology of the Southern Atlantic Ocean'. *Discovery reports* **VII**, 177–238.

Deeley, R. and P. Parr: 1913, 'The viscosity of glacier ice'. *Philosophical Magazine* **26**(151), 85–111.

Downes, M.: 2002, 'First visitors to Heard Island'. *ANARE Research Notes* **104**, 1–70.

Drygalski, E. v.: 1905-1931, *Duetsche Südpolar Expedition.* Berlin: Georg Reimer. 20 Volumes, 2 Atlas.

Finsterwalder, S. and H. Schunk: 1887, 'Der Suldenferner'. *Zeitschrift des Duetschen und Oesterreichischen Alpenvereins* **18**, 72–89.

Fleagle, R.: 1946, 'A study of the effects of divergence and advection on lapse rate'. *Journal of the Atmospheric Sciences* **3**(1), 9–13.

French, G.: 1974, *The Antarctic Pilot: Comprising the coasts of Antarctica and all islands southward of the usual route of vessels.* Hydrographer of the Navy, 4th edition.

Frenot, Y., J. Gloaguen, G. Picot, J. Bougere, and D. Bengamin: 1993, '*Azorella selagro* Hook. used to estimate glacier fluctuations and climatic history in the Kerguelen Islands over the last two centuries'. *Oecologia* **95**(140-144).

Galloway, J., G. Likens, W. Keene, and J. Miller: 1982, 'The composition of precipitation in remote areas of the world'. *Journal of Geophysical Research* **87**(11), 8771–8786.

Garrick, A.: 1955, 'Cross section of Southern Ocean cyclone from observations at Kerguelen and Heard Islands'. *Australian Meteorological Magazine* **10**, 71–74.

Gat, J.: 1996, 'Oxygen and hydrogen isotopes in the hydrologic cycle'. *Annual Review of Earth and Planetary Sciences* **24**, 225–262.

Gibbs, W., A. Gotley, and A. Martin: 1950, 'ANARE Reports: Meteorology Heard and Macquarie islands, 1948'. Antarctic Division, Department of External Affairs.

Gibbs, W., A. Gotley, and A. Martin: 1952, 'ANARE Reports: Meteorology Heard and Macquarie islands, 1948'. Antarctic Division.

Glen, J.: 1955, 'The creep of polycrystalline ice'. *Proceedings of the Royal Society, London* **228**, 5199–538.

Glen, J.: 1958, 'THe flow law of ice: A discussion of the assumptions made in glacier theory, their experimental foundations and consequences'. *IAHS Publication* **47**, 171–183.

Godoi, M., T. Shiraiwa, S. Kohshima, and K. Kubota: 2002, *Firn-core drilling operation at Tyndall Glacier, Southern Patagonia Icefield*, The Patagonian Icefields: A unique natural laboratory for environmental and climate change studies. New York: Kluwer Academic.

Gordon, J., V. Haynes, and A. Hubbard: 2008, 'Recent glacier changes and climate trends on South Georgia'. *Global and Planetary Change* **60**, 72–84.

Gordon, J. and R. Timmis: 1992, 'Glacier fluctuations on South Georgia during the 1970s and early 1980s'. *Antarctic Science* **4**(2), 215–226.

Goto-Azuma, K., M. Nakawo, H. Jiankang, O. Watanabe, and N. Azuma: 1993, 'Melt-induced relocation of ions in glaciers and seasonal snowpack'. In: *Snow and Ice Covers: Interactions with the Atmosphere and Ecosystems*, Vol. 223. Yokohama Symposium: IAHS-AISH, pp. 287–298.

Gow, A.: 1970, *Deep core studies of the crystal structure and fabric of Antarctic glacier ice.* CRREL Report.

Gow, A., D. Meese, J. Alley, R.B. Fitzpatrick, S. Anandakrishnan, G. Woods, and B. Elder: 1997, 'Physical and structural properties of the Greenland Ice Sheet Project 2 ice core: a review'. *Journal of Geophysical Research* **102**(C12), 26,559–26,575.

Green, K.: 1990, 'Heard Island 1990 ANARE Report'. Australian Antarctic Division Report.

Green, K.: 1993a, 'Five on Heard Island'. *Aurora* **13**(1), 13–15.

Green, K.: 1993b, 'Heard Island 1992 ANARE Report'. Australian Antarctic Division Report.

Hall, K.: 1983, 'A reconstruction of the Quaternary ice cover on Marion Island'. In: R. Oliver, P. James, and J. Jago (eds.): *Antarctic Earth Science.* Australian Academy of Science, pp. 461–64.

Hall, K.: 1984, 'Evidence in favour of an extensive ice cover on sub-Antarctic Kerguelen Island during the last glacial'. *Palaeogeography, Palaeoclimatology, Palaeoecology* **47**, 225–232.

Hall, K.: 1990, 'Quaternary glaciation in the Southern Ocean: Sector 00 Long. -180 Long.'. *Quaternary Science Review* **9**, 217–228.

Harding, R.: 1978, 'The variation of the altitudinal gradient of temperature in the British Isles'. *Geografiska Annaler* **60A**(1/2), 43–49.

Hayward, R.: 1983, 'Glacier fluctuations in South Georgia, 1883-1974'. *British Antarctic Survey Bulletin* **52**, 47–61.

Headland, R.: 1989, *Chronological list of Antarctic expeditions and related events.* Cambridge: Cambridge University Press.

Heard Island Visitors logbook, 'Heard Island Atlas Cove Log Book'. Unpublished.

Helsen, M., R. Van de Wal, M. Van der Broeke, D. Van As, H. Meijer, and C. Reijmer: 2005, 'Oxygen isotope variability in snow from western Dronning Maud Land, Antarctica and its relations to temperature'. *Tellus* **57B**, 423–435.

Hendy, M.: 1983, 'Second ascent of Mawson's peak, Heard Island'. *Aurora* **9**, 14–16.

Herron, M.: 1982, 'Impurity sources of F^-, Cl^-, NO_3^-, and SO_4^{2-} in Greenland and Antarctic precipitation'. *Journal of Geophysical Research* **87**(C4), 3052–3060.

Hewson, J.: 1983, *A History of the Practice of Navigation.* Brown, Son and Ferguson, 2 edition.

Hock, R.: 1999, 'A distributed temperature-index ice and snowmelt model including potential solar radiation'. *Journal of Glaciology* **45**(149), 101–111.

Hock, R.: 2003, 'Temperature index modelling in mountain areas'. *Journal of Hydrology* **282**, 104–115.

Holdgate, M.: 1963, 'Observations in the South Sandwich Islands, 1962'. *Polar Record* **11**(73), 394–405.

Holdsworth, G. and H. Krouse: 2002, 'Altitudinal variation of the stable isotopes of snow in regions of high relief'. *Journal of Glaciology* **48**(160), 31–41.

Hollin, J. and D. Schilling: 1981, 'Late Wisconsin-Weichselian mountain glaciers and small ice caps'. In: G. Denton and T. Hughes (eds.): *The Last Great Ice Sheets*. J. Wiley and Sons.

Holtedahl, O.: 1929, 'On the geology and physiography of some Antarctic and sub-Antarctic islands'. *Scientific Research Norwegian Antarctic Expedition* **3**, 89–94.

Hooke, R. L.: 2005, *Principles of Glacier Mechanics*. Cambridge University Press.

Hooke, R. L., J. Brzozowski, and C. Bronge: 1983, 'Seasonal variations in surface velocity Storglaciren, Sweden'. *Geografiska Annaler* **65A**(3/4), 263–277.

Hooke, R. L., P. Calla, P. Holmlund, M. Nilsson, and A. Stroeven: 1989, 'A 3 year record of seasonal variations in surface velocity, Storglaciren, Sweden'. *Journal of Glaciology* **35**(120), 235–247.

Iken, A. and R. Bindschadler: 1986, 'Combined measurements of subglacial water pressure and surface velocity of Findelengletscher, Switzerland: conclusions about drainage system and sliding mechanism'. *Journal of Glaciology* **32**(110), 101–119.

Ilzuka, Y., M. Igarashi, K. Kamiyama, H. Motoyama, and O. Watanbe: 2002, 'Ratios of Mg^{2+}/Na^{+} in snowpack and an ice core at Austfonna ice cap, Svalbard, as an indicator of seasonal melt'. *Journal of Glaciology* **48**(162), 452–460.

IPCC: 2007, *Climate Change 2007: The Physical Science Basis. Contribution of Working Group 1 to the Fourth Assessment Report on the Intergovernmental Panel on Climate Change*, Chapt. Summary for Policymakers. Cambridge University Press, Cambridge, UK and New York, USA.

Irving, E., P. Stephenson, and A. Major: 1965, 'Magnetism in Heard Island Rocks'. *Journal of Geophysical Research* **70**(14), 3421–27.

Isaksson, E., M. Hermanson, S. Hicks, M. Igarashi, K. Kamiyama, J. Moore, H. Motoyama, D. Muir, V. Pohjola, R. Vaikme, R. van de Wal, and O. Watanabe: 2003, 'Ice cores from Svalbard - useful archives of past climate and pollution history'. *Physics and Chemistry of the Earth* **28**, 1217–1228.

Jacka, T., W. Budd, and A. Holder: 2004, 'A further assessment of surface temperature changes at stations in the Antarctic and Southern Ocean, 1949-2002'. *Annals of Glaciology* **39**, 331–338.

Jacka, T. and A. Ruddell: 1998, 'Construction of a temperature record for Heard Island, and comparison with glacier fluctuations'. Vol. F55 (Abstract U31E-04). San Francisco, California, USA, American Geophysical Union Fall Meeting.

Jansson, P.: 1996, 'Dynamics and hydrology of a small polythermal valley glacier'. *Geografiska Annaler* **78A**(2/3), 171–180.

Johnstone, G.: 1981, '1980 Expedition to Heard Island and McDonald Island'. *Aurora* pp. 10–13.

Kaczmarska, M., E. Isaksson, L. Karlöf, O. Brandt, J.-G. Winther, R. S. Van de Wal, M. Van den Broeke, and S. Johnsen: 2006, 'Ice core melt features in relation to Antarctic coastal climate'. *Antarctic Science* **18**(2), 271–278.

Kamb, W.: 1970, 'Sliding motion of glaciers: theory and observations'. *Reviews of Geophysics and Space Physics* **8**(4), 673–728.

Kaser, G., A. Fountain, and P. Jansson: 2003, 'A manual for monitoring the mass balance of mountain glaciers'. Paris.

Kayastha, R., Y. Ageta, and M. Nakawo: 2000a, 'Positive degree-day factors for ablation on glaciers in the Nepalese Himalayas: case study on Glacier AX010 in Shorong, Himal, Nepal'. *Bulletin of Glaciological Research* **17**, 1–10.

Kayastha, R., Y. Ageta, M. Nakawo, K. Fujita, A. Sakai, and Y. Matsuda: 2003, 'Positive degree-day factors for ice ablation on four glaciers in the Nepalese Himalayas and Qinghai-Tibetan Plateau'. *Bulletin of Glaciological Research* **20**, 7–14.

Kayastha, R., Y. Takeuchi, M. Nakawo, and Y. Ageta: 2000b, 'Practical prediction of ice melting beneath various thickness of debris cover on Khumbu Glacier, Nepal, using a positive degree-day factor'. In: M. Nakawo, C. Raymond, and A. Fountain (eds.): *Debris-covered Glaciers*, Vol. 264. IAHS Publication, pp. 71–81.

Keage, P.: 1981, 'The conservation status of Heard Island and the McDonald Islands'. Ph.D. thesis, Centre for Environmental Studies, University of Tasmania.

Kemp, S. and A. Nelson: 1932, 'The South Sandwich Islands'. *Discovery Reports* **3**, 135–198.

Kiernan, K. and A. McConnell: 2002, 'Glacier retreat and melt-lake expansion at Stephenson Glacier, Heard Island World Heritage Area'. *Polar Record* **38**(207), 297–308.

Kirkbride, M.: 1995, 'Relationship between temperature and ablation on the Tasman Glacier, Mount Cook National Park, New Zealand'. *New Zealand Journal of Geology and Geophysics* **38**, 17–27.

Kirkwood, R.: 1989, *The Heard Island Coastline*, Heard Island 1987/88 ANARE Report.

Kirkwood, R. and H. Burton: 1988, 'A bathymetric survey of Winston Lagoon'. *ANARE News* p. 8.

Kirkwood, R. and P. Mitchell: 1992, 'The status of the Black-browed Albatross *Diomedea melanophrys* at Heard Island'. *EMU* **92**(2), 111–114.

Kirkwood, R., E. Woehler, and H. Burton: 1989, 'Heard Island 1987/88 ANARE Report'. Australian Antarctic Division Report.

Koerner, R.: 1979, 'Accumulation, ablation and oxygen isotopes variations on the Queen Elizabeth Islands ice caps, Canada'. *Journal of Glaciology* **22**(86), 25–42.

Koerner, R.: 1997, 'Some comments on climatic reconstructions from ice cores drilled in areas of high melt'. *Journal of Glaciology* **43**(143), 90–97.

Kuhn, M.: 1981, 'Climate and glaciers'. In: *Sea level, Ice and Climatic Change*, Vol. 131. Canberra, IAHS.

Lambeth, A.: 1950, 'Heard Island. Geography and glaciology'. *Journal and Proceedings of the Royal Society of New South Wales* **84**, 92–98.

Lang, H.: 1968, 'Relations between glacier runoff and meteorological factors observed on and outside the glacier'. *IAHS/AISH* **79**, 429–439.

Lang, H.: 1986, 'Forecasting meltwater runoff from snow-covered areas and from glacier basins'. In: D. Kraijenhoff and J. Moll (eds.): *River Flow Modelling and Forecasting*. D. Reidel Publishing, pp. 99–127.

Lang, H. and L. Braun: 1990, 'On the information content of air temperature in the context of snow melt estimation'. In: *Hydrology of mountainous areas*, Vol. 190. Czechoslovakia, pp. 347–354, IAHS.

Laumann, T. and N. Reeh: 1993, 'Sensitivity to climate change of the mass balance of glaciers in southern Norway'. *Journal of Glaciology* **39**(133), 656–665.

Law, P. and T. Burnstall: 1953, 'Heard Island'. Australian Antarctic Division Reports.

Ledingham, R.: 1987a, 'Heard Island Expedition: 16 November 1986 to 21 January 1987'. *Aurora* **6**(4), 6–8.

Ledingham, R.: 1987b, 'Heard Island Expedition ANARE 1986-87'. Australian Antarctic Division Report.

Legrand, M. and S. Kirchner: 1990, 'Origins and variations of nitrate in South Polar precipitation'. *Journal of Geophysical Research* **95**(D4), 3493–3507.

Legrand, M. and P. Mayewski: 1997, 'Glaciochemistry of polar ice cores: a preview'. *Reviews of Geophysics* **35**(3), 219–243.

Lemke, P., J. Ren, R. Alley, I. Allison, J. Carrasco, G. Flato, Y. Fujii, G. Kaser, P. Mote, R. Thomas, and T. Zhang: 2007, *Climate Change 2007: The Physical Science Basis. Contribution of Working Group 1 to the Fourth Assessment Report on the Intergovernmental Panel on Climate Change*, Chapt. Observations: Changes in Snow, Ice and Frozen Ground. Cambridge University Press, Cambridge, United Kingdom and New York, NY, USA.

Lliboutry, L.: 1968, 'General theory of subglacial cavitation and sliding of temperate glaciers'. *Journal of Glaciology* **7**(49), 21–58.

Long, M.: 2004, 'Icebergs: Useful archives for climate information'. Honours Thesis.

Ludecke, C.: 2003, 'Scientific collaboration in Antarctica (1901-1904): a challenge in times of political rivalry'. *Polar Record* **39**(208), 35–48.

Manning, J.: 2002, 'Volcano doubles size of Australian island'. *AUSGEO News* **68**, 10.

Marshall, D. and S. Chown: 2002, 'The acarine fauna of Heard Island'. *Polar Biology* **25**, 688–695.

Matsuoka, K. and R. Naruse: 1999, 'Mass balance features derived from a firn core at Hielo Patagonico Norte, South America'. *Arctic, Antarctic and Alpine Research* **31**(4), 333–340.

Matthias, A.: 2004, 'Monitoring near surface air quality'. In: J. Artiola, I. Pepper, and M. Brusseau (eds.): *Environmental Monitoring and Characterization*. Elsevier Academic Press.

Maury, M. F.: 1851, *Explanations and sailing directions to accompany the wind and current charts*. U. S. Navy Department, Washington, DC.

McGowan, A.: 2000, 'On their own: towards an analysis of sealers' sites on Heard Island'. *Papers and Proceedings of the Royal Society of Tasmania* **133**(2), 61–70.

McGowan, H., A. Sturman, M. Kossmann, and P. Zawar-Reza: 2002, 'Observations of foehn onset in the Southern Alps, New Zealand'. *Meteorology and Atmospheric Physics* **79**, 215–230.

McMorrow, A., T. van Ommen, V. Morgan, and M. Curran: 2004, 'Ultra high resolution seasonality of trace ion species and oxygen isotope ratios in Antarctic firn over 4 annual cycles'. *Annals of Glaciology* **39**, 1–7.

Meehl, G., T. Stocker, W. Collins, P. Friedingstein, A. Gaye, J. Gregory, A. Kitoh, R. Knutti, J. Murphy, A. Noda, S. Raper, I. Watterson, A. Weaver, and Z.-C. Zhao: 2007, *Climate Change 2007: The Physical Science Basis. Contribution of Working Group 1 to the Fourth Assessment Report on the Intergovernmental Panel on Climate Change*, Chapt. Global Climate Projections. Cambridge University Press, Cambridge, UK and New York, USA.

Meier, M.: 1984, 'Contributions of small glaciers to global sea level'. *Science* **226**, 1418–1421.

Mercanton, P.: 1916, 'Vermessungen am Rhoneglatscher 1874 bis 1915'. *Neue Denkschr. d. Schweiz. Natf. Ges.* **52**.

Mercer, J.: 1967, *Southern Hemisphere Glacier Atlas*. New York, NY: American Geographical Society.

Millot, R., J. Gallardet, B. Dupré, and C. Allégre: 2003, 'Northern latitude chemical weathering rates: clues from the Mackenzie River Basin, Canada'. *Geochimica et Cosmochimica Acta* **67**(7), 1305–1329.

Moore, J., M. Abbott, and J. Richman: 1999, 'Location and dynamics of the Antarctic Polar Front from satellite sea surface temperature data'. *Journal of Geophysical Research* **104**(C2), 3,059–3,073.

Morgan, V.: 1982, 'Antarctic Ice Sheet surface oxygen isotope values'. *Journal of Glaciology* **28**(99), 315–323.

Moser, H. and W. Stichler: 1975, 'Deuterium and oxygen-18 contents as an index of the properties of snow covers'. In: *Snow Mechanics*, Vol. 114. Grindelwald, pp. 122–135, IAHS-AISH.

Mosley, H.: 1877, *Report on the scientific results of the Voyage of HMS Challenger during the years 1873-1876: Botany*, Vol. 1, p. 216.

Mosley, H.: 1885, *Report on the botany of the Bermudas and various other islands of the Atlantic and Southern Ocean*, Vol. 1 of *Report on the scientific results of the Voyage of the HMS Challenger during the years 1873-1876, Botany*. London: HM Stationary.

Motoyama, H., K. Kamiyama, M. Igarashi, F. Nishio, and O. Watanbe: 2000, 'Distribution of chemical constituents in superimposed ice from Austre Broggerbreen, Spitsbergen'. *Geografiska Annaler* **82**(A), 33–38.

Munro, D.: 2005, 'A revised Canadian perspective: progress in glacier hydrology'. *Hydrological Processes* **19**, 231–245.

Nakicenovic, N., J. Alcamo, G. Davis, B. de Vries, J. Fenhann, S. Gaffin, K. Gregory, A. Grubler, T. Jung, T. Kram, E. Lebre la Rovere, L. Michaelis, S. Mori, T. Morita, W. Pepper, H. Pitcher, L. Price, K. Riahi, A. Roehrl, H.-H. Rogner, A. Sankovski, M. Schlesinger, P. Shukla, S. Smith, R. Swart, S. van Rooijen, N. Vistor, and D. Zhou: 2001, *Special Report on the Emission Scenarios*. Intergovernmental Panel on Climate Change. http://www.grida.no/climate/ipcc/emission/.

Nguyen, B., B. Bonsang, and G. Lambert: 1974, 'The atmospheric concentration of sulfur dioxide and sulfate aerosols over Antarctic, Subantarctic areas and oceans'. *Tellus* **16**(1-2), 241–249.

Nye, J.: 1965, 'The flow of a glacier in a channel of rectangular, elliptic or parabolic cross-sections'. *Journal of Glaciology* **5**(41), 661–690.

Nye, J.: 1969, 'A calculation on the sliding of ice over a wavy surface using Newtonian viscous approximation'. *Proceedings of the Royal Society of London* **A311**(1506), 445–467.

O'Dwyer, J., E. Isaksson, T. Vinje, T. Jauhiainen, J. Moore, V. Pohjola, R. Vaikmäe, and S. van de Wal: 2000, 'Methanesulfonic acid in a Svalbard ice core as an indicator of ocean climate'. *Geophysical Research Letters* **27**(8), 1159–1162.

Oerlemans, J.: 1994, 'Quantifying global warming from the retreat of glaciers'. *Science* **264**, 243–245.

Oerlemans, J.: 2001, *Glaciers and Climate Change*. Lisse: A.A. Balkema.

Oerlemans, J.: 2005, 'Extracting a climate signal from 169 glacier records'. *Science* **308**, 675–677.

Oerlemans, J., B. Anderson, A. Hubbard, P. Huybrechts, T. Jóhannesson, W. Knap, M. Schmeits, A. Stroeven, R. van de Wal, J. Wallinga, and Z. Zuo: 1998, 'Modelling the response of glaciers to climate warming'. *Climate Dynamics* **14**, 267–274.

Oerlemans, J. and J. Fortuin: 1992, 'Sensitivity of glaciers and small ice caps to greenhouse warming'. *Science* **258**(5079), 115–117.

Oerter, H., D. Baker, W. Stichler, and W. Rauert: 1985, 'Isotope studies of ice cores from a temperate alpine glacier (Vernagtferner, Austria) with respect to the meltwater flow'. *Annals of Glaciology* **7**, 90–93.

Ohmura, A., P. Kasser, and M. Funk: 1992, 'Climate at the equilibrium line of glaciers'. *Journal of Glaciology* **38**(130), 397–411.

Orheim, O.: 1981, 'Glaciers of Bouvetøya'. *Norsk Polarinstitutt Skrifer* **175**, 79–84. Abstract only.

Orsi, A., T. Whitworth, III, and W. Nowlin, Jr.: 1995, 'On the meridional extent and fronts of the Antarctic Circumpolar Current'. *Deep-Sea Research* **42**(5), 641–673.

Palmer, A.: 2002, 'Environmental signals from chemical measurements on Law Dome ice cores'. Ph.D. thesis, University of Tasmania, Hobart.

Palmer, A., T. van Ommen, M. Curran, V. Morgan, J. Souney, and P. Mayewski: 2001, 'High-precision dating of volcanic events (A.D. 1301-1995) using ice cores from Law Dome, Antarctica'. *Journal of Geophysical Research* **106**(D22), 28,089–28,095.

Park, Y.-H., L. Gamberoni, and E. Charriaud: 1993, 'Frontal structure, water masses and circulation in the Crozet Basin'. *Journal of Geophysical Research* **98**(C7), 12,361–12,385.

Pasteur, E. and R. Mulvaney: 1999, 'Laboratory study of the migration of methane sulphonate in firn'. *Journal of Glaciology* **45**(150), 214–218.

Paterson, W.: 1994, *Physics of Glaciers*. Tarrytown, NY: Elsevier Science.

Pepin, N.: 2001, 'Lapse rate changes in northern England'. *Theoretical and Applied Climatology* **68**(1-2), 1–16.

Pepin, N., D. Benham, and K. Taylor: 1999, 'Modeling lapse rates in the maritime uplands of northern England: implications for climate change'. *Arctic, Antarctic, and Alpine Research* **31**(2), 151–164.

Pepin, N. and M. Losleben: 2002, 'Climate change in the Colorado Rocky Mountains: free air versus surface temperature trends'. *International Journal of Climatology* **22**, 311–329.

Pielke, R. and P. Mehring: 1977, 'Use of mesoscale climatology in mountainous terrain to improve the spatial representation of mean monthly temperatures'. *Monthly Weather Review* **105**(1), 108–112.

Poage, M. and C. Chamberlain: 2001, 'Empirical relationships between elevation and the stable isotope composition of precipitation and surface waters: considerations for studies of paleoelevation change'. *American Journal of Science* **301**, 1–15.

Podlech, S., C. Mayer, and C. Boggild: 2004, 'Glacier retreat, mass-balance and thinning: Sermilik Glacier, South Greenland'. *Geografiska Annaler* **86**(A), 305–317.

Pohjola, V., T. Martma, H. Meijer, J. Moore, E. Isaksson, R. Vaikmäe, and S. van de Wal: 2002a, 'Reconstruction of 300 years annual accumulation rates based on the record of stable isotopes of water from Lomonosovfonna, Svalbard'. *Annals of Glaciology* **35**, 57–62.

Pohjola, V., J. Moore, E. Isaksson, T. Jauhiainen, R. van de Wal, T. Martma, H. Meijer, and R. Vaikmäe: 2002b, 'Effect of periodic melting on geochemical and isotopic signals in an ice core from Lomonosovfonna, Svalbard'. *Journal of Geophysical Research* **107**(D4), 4036–49.

Quilty, P. and G. Wheller: 2000, 'Heard Island and the McDonald Islands: a window into the Kerguelen Plateau'. *Papers and Proceedings of the Royal Society of Tasmania* **133**(2), 1–12.

Raben, P. and W. Theakstone: 1994, 'Isotropic and ionic changes in a snow cover at different altitudes: observations at Austre Okstindbreen in 1991'. *Annals of Glaciology* **19**, 85–91.

Ridal, M.: 2001, 'Water vapour isotopes in the stratosphere'. Department of Meteorology, Stockholm University Report.

Rintoul, S., C. Hughes, and D. Olbers: 2001, 'The Antarctic Circumpolar Current System'. In: G. Siedler, J. Church, and J. Gould (eds.): *Ocean Circulation and Climate: observing and modelling the global oceans*, Vol. 77. pp. 271–302, Academic Press.

Roberts, B.: 1950, 'Historical notes on Heard and McDonald islands'. *Polar Record* **5**(40), 580–584.

Roe, G., D. Montgomery, and B. Hallet: 2003, 'Orographic precipitation and the relief of mountain ranges'. *Journal of Geophysical Research* **108**(B6), 2315.

Rolland, C.: 2003, 'Spatial and seasonal variation of air temperature lapse rates in alpine regions'. *Journal of Climate* **16**, 1032–1046.

Ruddell, A.: 1995, 'Recent glacier and climate change in the New Zealand Alps'. Ph.D. thesis, University of Melbourne, Melbourne.

Ruddell, A.: 2006, *Heard Island: Southern Ocean Sentinel*, Chapt. An Inventory of present glaciers on Heard Island and their historical variation. Surrey Beatty & Sons, Chipping Norton.

Ruddell, A. and W. Budd: 1990, 'An investigation into the feasibility of using a New Zealand ice core for paleo-climate interpretation'.

Ryan, U.: 2004, 'Heard Island RADARSAT (1997) DEM'. Australian Antarctic Data Centre - SnoWhite Metadata http://www.aad.gov.au/default.asp?casid=3802.

Saltzman, E. S., D. Savioe, J. M. Prospero, and R. G. Zika: 1986, 'Methanesulfonic acid and non-sea-salt sulfate in Pacific air: regional and seasonal variations'. *Journal of Atmospheric Chemistry* **4**, 227–240.

Savoie, D., J. Prospero, R. Larsen, F. Huang, M. Izaguirre, T. Huang, T. Snowdon, L. Custals, and C. Sanderson: 1993, 'Nitrogen and sulfur species in Antarctic aerosols at Mawson, Palmer Station and Marsh (King George Island)'. *Journal of Atmospheric Chemistry* **17**, 95–122.

Scaire, J., N. Mihalopoulos, and B. Nguyen: 1999, 'Summertime seawater concentrations of Dimethylsulfide in the western Indian Ocean: reconciliation of fluxes and spatial variability with long-term atmospheric observations'. *Journal of Atmospheric Chemistry* **32**, 357–373.

Schaper, J., J. Martinec, and K. Seidel: 1999, 'Distributed mapping of snow and glaciers for improved runoff modelling'. *Hydrological Processes* **13**, 2023–2031.

Schotterer, U., K. Fröhlich, H. Gäggler, S. Sandjordj, and W. Stichler: 1997, 'Isotope records from Mongolian and alpine ice cores as climate indicators'. *Climatic Change* **36**(3-4), 519–530.

Schotterer, U., W. Stichler, and P. Ginot: 2004, *Earth Paleoenvironments: Records Preserved in Mid- and Low-Latitude Glaciers*, Chapt. The influences of post-depositional effects on ice core studies: Examples from the Alps, Andes and Altai, pp. 39–59. Kluwer Academic Publishers.

Schotterer, U., W. Stichler, W. Graf, H.-U. Bürki, L. Gourcy, P. Ginot, and T. Huber: 2002, 'Stable isotopes in alpine ice cores: Do they record climate variability?'. In: *Proceedings of an International Symposium on the Study of Environmental Change using Isotope Techniques*. Vienna, pp. 292–300, IAEA.

Schytt, V.: 1964, 'Scientific results of the Swedish Glaciological Expedition to Nordaustlandet, Spitsbergen, 1957 and 1958'. *Geografiska Annaler* **46**(3), 242–281.

Scott, J.: 1987, 'A sample of Heard Island, 1986'. *Aurora* **6**(4), 13–15.

Scott, J.: 1990, *Changes in vegetation on Heard Island 1947-1987*, Antarctic Ecosystems: Ecological Change and Conservation. Springer-Verlag.

Shaw, P.: 1955, 'Some effects of topography on weather observations at Heard Island'. *Australian Meteorological Magazine* **10**, 34.

Short, S. and G. Holdsworth: 1985, 'Pollen, oxygen isotope content and seasonality in an ice core from the Penny Ice Cap, Baffin Island'. *Arctic* **38**(3), 214–218.

Shuman, C., R. Alley, M. Fahnestock, P. Fawcett, R. Bindschadler, J. White, P. Grootes, S. Anandakrishnan, and C. Stearns: 1997, 'Detecting and monitoring of stratigraphic markers and temperature trends at the Greenland Ice Sheet Project 2 using passive-microwave remote-sensing data'. *Journal of Geophysical Research* **102**(C12), 26,877–27,750.

Singh, P. and N. Kumar: 1996, 'Determination of snowmelt factor in the Himalayan region'. *Hydrological Sciences Journal* **41**(3), 301–310.

Singh, P., N. Kumar, and M. Arora: 2000, 'Degree-day factors for snow and ice for Dokriani Glacier, Garhwal Himalayas'. *Journal of Hydrology* **235**, 1–11.

Singh, P. and V. Singh: 2001, *Snow and Glacier Hydrology*. Kluwer Academic Publishers.

Smith, I.: 1984, 'Numerical modelling of ice masses'. Ph.D. thesis, University of Melbourne, Melbourne.

Smith, I. and W. Budd: 1979, 'The derivation of past climate changes from observed changes of glaciers'. In: *Sea level, Ice and Climate Change*, Vol. 131. Canberra, pp. 31–51, IAHS.

Smith, J.: 1960, 'Glacier problems in South Georgia'. *Journal of Glaciology* **3**, 705–714.

Sparrow, M., K. Heywood, J. Brown, and D. Stevens: 1996, 'Current structure of the south Indian Ocean'. *Journal of Geophysical Research* **101**(C3), 6,377–6,391.

Spencer, M., P. Mayewski, and W. Lyons: 1985, 'A preliminary assessment of the potential application of glaciochemical investigations on Heard Island, South Indian Ocean'. *Journal of Glaciology* **31**(109), 233–236.

Staubes, R. and H.-W. Georgii: 1993, 'Biogenic sulfur compounds in seawater and the atmosphere of the Antarctic region'. *Tellus* **45B**(2), 127–137.

Stephenson, J., G. Budd, J. Manning, and P. Hansbro: 2005, 'Major eruption-induced changes to the McDonald Islands, southern Indian Ocean'. *Antarctic Science* **17**(2), 259–266.

Stramma, L.: 1992, 'The South Indian Ocean Current'. *Journal of Physical Oceanography* **22**(4), 421–430.

Sturm, M.: 1995, 'Short-period velocity fluctuations of two glaciers on Mt. Wrangell, Alaska'. *Physical Geography* **16**(1), 42–58.

Sturman, A. and N. Tapper: 1996, *The Weather and Climate of Australia and New Zealand.* Oxford University Press.

Sugden, D. and B. John: 1976, *Glaciers and Landscape: A Geomorphological Approach.* John Wiley and Sons.

Sumner, P.D. ad Meiklejohn, K., J. Boelhouwers, and D. Hedding: 2004, 'Climate change melts Marion Island's snow and ice'. *South African Journal of Science* **100**, 395–398.

Szafraniec, J.: 2002, 'Influence of positive degree-day and sunshine duration on the surface ablation of Hansbreen, Spitsbergen Glacier'. *Polish Polar Research* **23**(3-4), 227–240.

Taljaard, J. and H. Van Loon: 1984, *Climate of the Indian Ocean South of 35° S*, Vol. 15 of *World Survey of Climatology: Climates of the Oceans.* Elsevier.

Taylor, S., X. Feng, J. Kirchner, R. Osterhuber, B. Klaue, and C. Renshaw: 2001, 'Isotopic evolution of a seasonal snowpack and its melt'. *Water Resources Research* **37**(3), 759–769.

The Bureau of Meteorology: 1955a, 'ANARE Reports: Meteorology Heard and Macquarie islands, 1952'. Antarctic Division, Department of External Affairs.

The Bureau of Meteorology: 1955b, 'ANARE Reports: Meteorology Heard and Macquarie islands, 1953'. Antarctic Division, Department of External Affairs.

The Bureau of Meteorology: 1957, 'ANARE Reports: Meteorology Heard and Macquarie islands, 1954'. Antarctic Division, Department of External Affairs.

The Central Office, Meteorological Branch: 1953a, 'ANARE Reports: Meteorology Heard and Macquarie islands, 1949'. Antarctic Division, Department of External Affairs.

The Central Office, Meteorological Branch: 1953b, 'ANARE Reports: Meteorology Heard and Macquarie islands, 1950'. Antarctic Division, Department of External Affairs.

The Central Office, Meteorological Branch: 1953c, 'ANARE Reports: Meteorology Heard and Macquarie islands, 1951'. Antarctic Division, Department of External Affairs.

Thompson, L.: 1979, 'Ice core studies from Mt Kenya, Africa, and their relationship to other tropical ice core studies'. In: *Sea Level, Ice, and Climate Change*, Vol. 131.

Thompson, L.: 2000, 'Ice core evidence for climate change in the Tropics: implications for our future'. *Quaternary Science Reviews* **19**, 19–35.

Thompson, L.: 2001, 'Stable isotopes and their relationship to temperature as recorded in low-latitude ice cores'. In: L. Gerhard, W. Harrrison, and B. Hanson (eds.): *Geological Perspectives of global climate change*. pp. 99–109.

Thompson, L., M. Davis, E. Mosley-Thompson, T. Sowers, K. Henderson, V. Zagorodnov, P.-N. Lin, V. Mikhalenko, R. Campen, J. Bolzan, J. Cole-Dai, and B. Francou: 1998, 'A 25,000-year tropical climate history from Bolivian ice cores'. *Science* **282**, 1858–1864.

Thompson, L., E. Mosley-Thompson, M. Davis, P.-N. Lin, K. Henderson, and T. Mashiotta: 2003, 'Tropical glacier and ice core evidence of climate change on annual to millennial time scales'. *Climatic Change* **59**, 137–155.

Thompson, L., T. Yao, E. Mosley-Thompson, M. Davis, K. Henderson, and P.-N. Lin: 2000, 'A high-resolution millennial record of the South Asian Monsoon from Himalayan ice cores'. *Science* **289**, 1916–1919.

Thomson, C. and J. Murrary: 1885, *Report on the scientific results of the voyage of the HMS Challenger during the years 1873-76, Narrative*, Vol. 1. London: HM Stationery.

Thost, D. and I. Allison: 2006, *Heard Island: Southern Ocean Sentinel*, Chapt. The Climate of Heard Island, pp. 52–68. Surrey Beatty & Sons, Chipping Norton.

Thost, D. and M. Truffer: 2008, 'Glacier recession on Heard Island, southern Indian Ocean'. *Arctic, Antarctic and Alpine Research* **40**(1), 199–214.

Thost, D., M. Truffer, and S. Donoghue: 2004, 'The Heard Island Glaciology Program 2003-04'. Australian Antarctic Division Report.

Tilbury, L.: 1981, 'The 1980 Heard Island expedition: Marine geophysical operations and preliminary results'. *Bureau of Mineral Resources, Geology and Geophysics Record* **16**, 16p.

Tomczak, M. and J. Godfrey: 1994, *Regional oceanography: An Introduction*. Elsevier.

Trenberth, K.: 1990, 'Recent observed interdecadal climate changes in the Northern Hemisphere'. *Bulletin of the American Meteorological Society* **71**, 988–993.

Trenberth, K., P. Jones, P. Ambenje, D. Bojariu, D. Easterling, A. Klein Tank, D. Parker, F. Rahimzadeh, J. Renwick, M. Rusticucci, B. Soden, and P. Zhai: 2007, *Climate Change 2007: The Physical Science Basis. Contribution of Working Group 1 to the Fourth Assessment Report on the Intergovernmental Panel on Climate Change*, Chapt. Observations: Surface and Atmospheric Climate Change. Cambridge and New York: Cambridge University Press.

Truffer, M., D. Thost, and A. Ruddell: 2001, 'The Brown Glacier, Heard Island: its morphology, dynamics, mass balance and climate setting'. Antarctic CRC Report.

Tsiouris, S., C. Vincent, T. Davies, and P. Brimblecombe: 1985, 'The elution of ions through field and laboratory snowpacks'. *Annals of Glaciology* **7**, 196–201.

Turner, J. and S. Pendlebury: 2004, *The International Antarctic Weather Forecasting Handbook*. British Antarctic Survey.

Vallon, M.: 1977, 'Topographie sous-glaciaire du Glacier Ampere (Iles Kerguelen, TAAF)'. *Zeitschrift fur Gletscherkunde und Glazialgeologie* **13**, 37–55.

Van de Wal, R.: 1992, 'Ice and climate'. Ph.D. thesis, Utrecht University.

Van Ommen, T. and V. Morgan: 1997, 'Calibrating the ice core paleothermometer using seasonality'. *Journal of Geophysical Research* **102**(D8), 9351–9357.

Veenstra, C. and J. Manning: 1982, 'Expedition to the Australian Territory of Heard Island and McDonald Islands 1980'.

Verwoerd, W.: 1971, 'Geology'. In: E. Van Zinderen Bakker Sr., J. Winterbottom, and R. Dyer (eds.): *Marion and Prince Edward Islands: Report on the South African biological and geological expedition 1965-1966*. A. A. Balkema.

Vining, R.: 1983, 'Heard Island Expedition 1983 Scientific Reports: a summary of the field work carried out'.

Vrana, A. and A. Ruddell: unpub, 'Data from a 1992 net balance stake network on Brown Glacier'. Australian Antarctic Division, Unpublished Data.

Wagenbach, D., F. Ducroz, R. Mulvaney, L. Keck, A. Minikin, M. Legrand, J. Hall, and E. Wolff: 1998, 'Sea-salt aerosol in coastal Antarctic regions'. *Journal of Geophysical Research* **103**(D9), 10961–10974.

Weertman, J.: 1957, 'On the sliding of glaciers'. *Journal of Glaciology* **5**, 33–38.

Weertman, J.: 1964, 'The theory of glacier sliding'. *Journal of Glaciology* **5**(39), 287–303.

Welch, B., W. Pfeffer, J. Harper, and N. Humphrey: 1998, 'Mapping subglacial surfaces of temperate valley glaciers by two-pass migration of a radio-echosounding survey'. *Journal of Glaciology* **44**(146), 164–170.

Werth, D.: 1921, 'Aufbau und Gestaltung von Kerguelen'. In: *Deutsche Südpolar Expedition*, Vol. 2. Georg Reimer, pp. 93–183. In German.

Williams, G.: 1998, *The response of Heard Island Glaciers to climate change*. Hobart: University of Tasmania. Honours Thesis.

Wilson, T.: 1975, *Salinity and the major elements of sea water*, Vol. 1 of *Chemical Oceanography*. London: Academic Press, 2nd edition.

World Glacier Monitoring Service: 2001, 'Glacier Mass Balance Bulletin (1998-1999)'. IAHS (ICSI), UNEP, UNESCO, WMO Report.

Xie, S.-P., H. Annamalai, F. Schott, and J. McCreary Jr: 2002, 'Structure and mechanism of South Indian Ocean climate variability'. *Journal of Climate* **15**, 864–878.

Xie, Z., J. Han, C. Liu, and S. Liu: 1999, 'Measurement and estimative models of glacier mass balance in China'. *Geografiska Annaler* **81**(A), 791–796.

Yoshino, M.: 1966, 'Some aspects of air temperature climate of the high mountains in Japan'. Japanese Progr. Climat. Report.

Young, I.: 1999, 'Seasonal variability of the global ocean wind and wave climate'. *International Journal of Climatology* **19**, 931–950.

Yuanqing, H., Y. Tandong, W. Theakstone, and Y. Meixue: 2000, 'Isotropic and chemical analyses of a temperate firn core from a Chinese alpine glacier and its regional climatic significance'. *Chinese Journal of Polar Science* **11**(2), 97–106.

Yuanqing, H. and W. Theakstone: 1994, 'Climatic influence on the composition of snow cover at Austre Okstindbreen, Norway, 1989 and 1990'. *Annals of Glaciology* **19**, 1–6.

A. Heard Island and its setting

A.1. Discovery of Heard Island

Heard Island's isolation and persistent cloud cover, together with somewhat primitive 18th and 19th century navigation and sailing techniques, resulted in the island being discovered by happenstance. In the 1800s, navigation methods included using magnetic compasses, chronometers, quadrants or sextants and leadlines (Hewson, 1983). The use of the sextant was limited by the weather. Either the stars, sun or moon must be visible at a known time of the day for the calculations to be made. Therefore sailing in the persistent cloud-covered regions of the southern Indian Ocean made exact navigation difficult. Despite these limitations to navigation methods, it was the winds that were the biggest concern to sailors (Maury, 1851).

Many early explorers passed near Heard Island without sighting land (e. g., Cook's voyage on the HMS *Resolution* in 1773) (Downes, 2002). On 27 November, 1833 the British sealer, Peter Kemp on *Magnet* marked on his charts 'saw land' and 'sounded in 55 fathoms'. It is unclear if this was Heard Island as he did not investigate his sighting any further but continued south to the Antarctic Coast (Downes, 2002). In 1849, Thomas Long on the *Charles Carroll*, a sealing vessel (note the difference in spelling from Charles Carol Bluff, a steep bluff on the south coast), reported having 'seen land' but again there are no record of the sealers exploiting this new, large population of fur and elephant seals. In fact E.D. Rogers, first mate of the *Charles Carroll*, made no mention of seeing the island before following Captain Heard's logs to locate the island in 1855 (Downes, 2002).

Captain John Heard on the *Oriental* made the first conclusive report of Heard Island's existence, sighting the island on 25 November, 1853. The first public announcement of Captain Heard's discovery was in the Melbourne *Argus* on 25 December, 1853. The reason that Captain Heard discovered land where others before him had sailed past was because he was sailing from Boston to Melbourne on the newly-promoted 'Composite Great Circle Route' of Matthew Maury. Matthew Maury, known as the 'Pathfinder of the Seas' because of his contributions to navigation and meteorological charts, proposed that vessels that were heading westward would travel more efficiently if they were to sail along 50° S as the winds were stronger and more persistent then the 'Calms of the Capricorn' (Maury, 1851). Vessels that followed Maury's route were to pass more often and closer to Heard Island than any vessels before them (e. g., *Samarang*, which discovered the McDonald Islands in January 1854, *Earl of Eglinton* heading towards Melbourne in 1854, and *Herald of the Morning* heading for Port Phillip, Australia in 1854) on their way to Australia (coinciding with the discovery of gold in Australia).

Once discovery was announced, sealers soon began to exploit the island. On February 15, 1855, E.D. Rogers, the captain of an American sealer, the *Corinthian*, was the first to land on Heard Island, at Try Pot Beach (near Atlas Cove) (Downes, 2002). Rogers had become aware of Captain Heard's report of Heard Island's existence while working on Kerguelen Island.

Captain Rogers returned in March of 1855 to begin sealing operations. Henry Rogers, mate of the brig *Zoe*, lead the first wintering party of 25 men to Heard Island, and was based there from the March to October 1856 (Downes, 2002).

A.2. A history of exploration

Heard Island has been intermittently occupied by sealers, whalers and scientists for the past 150 years (Table A.1). American sealers occupied the island through a peak sealing period between 1855 and 1880 (Figure A.1A). By 1880, most of the elephant and Antarctic fur seal population had been depleted, resulting in sealing operations becoming sporadic until ending completely in 1927. As the sealers were beginning to leave, whalers made an attempt to use Heard Island, starting in 1900, as a base for operations. After little success they also abandoned the island by 1927.

The first scientific expedition to reach Heard Island arrived on the HMS *Challenger* in 1873. This scientific voyage landed at Corinthian Bay, on 6 February, for one day of observations on the northwestern end of the island and to collect geological and botanical samples (Mosley, 1885; Thomson and Murrary, 1885). The *Challenger* visit to the island was short due to an incoming storm. The ship set sail on 7 February.

The Deutsche Südpolar-Expedition aboard the *Gauss* visited Atlas Cove in 1902 (Downes, 2002). Ten men went ashore at Corinthian Bay to collect and archive the western Heard Island's geology, flora and fauna (Drygalski, 1931). The men stayed ashore for one day and returned to the ship with the falling light to set sail the next day due to deteriorating weather conditions.

In 1929, Edgar and Andrée Aubert de la Rue (believed to be the first woman ashore) visited the island, via the whaling ship *Kildalkey*. On 15 January they arrived at Heard Island from Kerguelen Island. They found that the seas were too rough to land at Spit Bay therefore disembarked on a beach on the eastern shores of Atlas Cove. From 15 to 22 January 1929 they engaged in eight days traversing the Atlas Cove region making geologic observations and collecting rock samples (Aubert de la Rue, 1929) while the *Kildalkey* harvested the near by waters.

In November 1929, the RRS *Discovery* under the leadership of Sir Douglas Mawson called into Heard Island, from Cape Town en route to Antarctica (Figure A.1B). Mawson was the leader of BANZARE (the British, Australian, and New Zealand Antarctic Research Expedition), and spent seven days making geological and biological observations and temperature measurements (Veenstra and Manning, 1982) with eight other scientific staff. A hut was built during this time as a refuge for stranded sailors, the remains of which are still being battered by the winds and sand at Atlas Cove (Figure A.1C).

Table A.1.: A list of the sealing, science and climbing expeditions and voyages to Heard Island over the past 150 years that are referred to in this study (for a full list see Appendix A.3) (Chown, 2003)

Expedition/Visitor	Period of visit	Date and purpose of visit
American Sealers	variable	1855-1880, peak period of operations; 1880-1927, sporadic operations continued
Whalers	variable	Early 1900's until 1927
HMS *Challenger* voyage	1 day	1873, collected geologic and botanical samples
Deutsche Südpolar-Expedition	1 day	1902, comprehensive collection of geology, flora and fauna
Kildalkey	8 days	1929, geologic sampling
BANZARE	7 days	1929, geological and biological observations and temperature measurements
ANARE	7 years	1947-55, seven years uninterrupted meteorological, geophysical observations, topographical, geological, glaciological and biological sampling
ANARE	1 day	1956, vessel stopped homeward bound from Mawson
ANARE	1 day	1958, vessel stopped homeward bound from Mawson
ANARE	1 day	1960, vessel stopped homeward bound from Mawson
ANARE	6 weeks	1963, first attempt to climb Mawson Peak; geophysical observations
South Indian Ocean Expedition	1 month	1965, first successful attempt of Mawson Peak, first observations of summit
ANARE	7 days	1969, glaciological and biological survey from Spit Bay to Red Island
US Satellite Triangulation Team	2 months	1969, photograph satellites
USCOC, US Coast and Geodetic Survey Team	1 year	1969-70, mapping, glaciological and biological survey from Spit Bay to Red Island
French-Australian Expedition	42 days	1971, coupled magnetic phenomena research, aurora and geophysical observations and glaciology
Damien	3 days	1972, French yacht
1980 Heard Island Expedition (National Mapping Expedition)	17 days	1980, bathymetric, aerial photography, mapping, magnetic, botanical, zoological and geological surveying
1983 Heard Island Expedition (Project Blizzard)	1 month	1983, glaciological, geological, meteorological, botanical and zoological surveys, amateur radio contacts and a successful summit attempt
The Heard Island DX Association Expedition (*Cheynes II*)	10 days	1983, biological, geological, and botanical surveys, amateur radio contacts and an unsuccessful summit attempt
Nella Dan	1 day	1983, vessel stopped en route to Mawson and Davis Stations
ANARE	2 months	1985, biological, meteorological, geophysical, glaciological and mapping surveys
ANARE	2 months	1986, geological, glaciological, botanical, ornithological, seismological, upper atmosphere and archaeological surveys
ANARE	6 months	1987, biological, glaciological, hydrological and meteorological surveys
ANARE	2 months	1990, glaciological, biological and archaeological surveys
ANARE	1 year	1992, glaciological, geological, biological, meteorological observations and mapping surveys (winter season)
Cordell Heard Island Expedition	1 month	1997, setting an amateur radio operation record and vegetation distribution observations
Aurora Australis	1 day	1997, deploying tide gauge and an automatic weather station
Army Alpine Association	16 days	2000, Mawson Peak climbing party
ANARE	5 months	2000, zoological, botanical, glaciological and archaeological surveys
ANARE	2 months	2004, zoological, botanical and glaciological surveys

On 11 December 1947, the HMAS *Labuan* arrived at Heard Island and established the first research station at Atlas Cove by ANARE (Australian National Antarctic Research Expeditions) (Figure A.1D). This expedition was initially intended to establish sovereignty and maintain requirements pertinent to the 'exchange of note' through which Australia assumed responsibility for Heard Island in 1950 from the British (Keage, 1981). The Atlas Cove station was continuously occupied until March 1955 (Figure A.1E). During this period, ANARE recorded seven years of uninterrupted observations in meteorology and geophysics and provided the first comprehensive record of most of the island's topography, geology, glaciology and biology (e.g., Shaw, 1955; Dalzeil, 1955; Garrick, 1955; Chittleborough, 1956) (Figure A.1F). Eventually it was necessary to close the station due to funding constraints when an Australian continental Antarctic station, Mawson, was constructed. Between 1955 and 1963, several visits of a few hours duration were made to the Atlas Cove station by ANARE vessels returning from the Australian Antarctic stations of Davis and Mawson (Table A.1).

In 1963, six ANARE expeditioners spent six weeks on the island (Budd, 1964a) (Table A.1). A first attempt was made to climb Big Ben by a three man party from Long Beach (Budd, 1964a). The attempt was unsuccessful, with the climbing party abandoning their tent on the summit plateau. Once the summit party returned to Long Beach they traversed the southern coast towards Spit Bay. After a few days of observations the party continued along the north coast to Atlas Cove recording changes in the glaciers. Members of the party that were not involved in the summit attempt were occupied with geophysical research (Irving et al., 1965) and penguin, sheathbill, giant petrel, and elephant seal population surveys.

In 1965, a private expedition (the South Indian Ocean Expedition) visited the island, landing at Gilchrist Beach (Table A.1). The five man shore party completed the first successful climbing attempt of Mawson Peak. Storms prevented them from making summit observations as planned. Instead the team retreated back down the mountain to survey South Barrier, collect soil, plant and insect samples, census fur and elephant seal and king penguin populations and photograph the glaciers (Budd, 1965).

Between March 1969 and April 1970, the United States Coast and Geodetic Survey (USCGS) TOPOCOM expedition, spent a year at Atlas Cove (Table A.1). During deployment of the Americans, three ANARE expeditioners recorded changes in the glaciers and fur seals and king penguins population since 1965. The ANARE party landed on 11 March and walked from Saddle Point to Spit Bay returning to disembark from the island on the 17 March (Budd, 1970). The Americans established a survey station at Atlas Cove, which operated until 19 April 1970 as part of the PAGEOS programme of satellite observations to determine the geodetic shape of the Earth (Headland, 1989). In November 1969, the six man wintering party was relieved by a summer party of USCGS expeditioners on the MV *Nella Dan*. They then attempted a survey of the northern coast from Red Island to Spit Bay (Heard Island Visitors logbook).

25 January to 9 March 1971, a French-Australian expedition conducted research at Atlas Cove concentrating on coupled magnetic phenomena, geophysical, and auroral observations in conjunction with studies at Kerguelen Island and stations in the USSR and Antarctica (Table A.1). In addition to the geophysical investigations, mass balance measurements of one of the Heard Island glaciers (Vahsel Glacier) were made (Allison, 1980) and biological surveys were undertaken (Veenstra and Manning, 1982). In 1972 the first record of a purely tourist visit was made to the island by the French yacht *Damien* (Table A.1).

Figure A.1.: Historical photos from the Atlas Cove region. **A**) Sealers grave, **B**) "Battlefields of mist", *Discovery* about to drop anchor in Corinthian Bay, National Library of Australia (NLA) #an10932811-11, **C**) BANZARE established this Norwegian designed hut on Heard Island in 1929, NLA #an10932811-9, **D**) "First party ashore at Atlas Cove, Heard Island, Antarctica 1947", NLA #vn3765860-v, **E**) "A young red polled bull" bought ashore for stores, NLA #vn3765888-v, **F**) "Chief surveyor Bob Dovers views a cold morning after a night on the Jacka Glacier, Heard Island, 1948", **G**) Atlas Cove station 1955, NLA #vn3765989, and **H**) Remains of Atlas Cove station, 2004. *Photo credits*: G. Newman, F. Hurley 1929, F. Hurley 1929, D. Eastman 1948, G. Lowe 1955, A. Campbell-Drury 1948, G. Lowe 1955, and S. Donoghue, 2004.

In the 1980s there was an increasing number of visits. In 1980 the Australian Division of National Mapping, the Bureau of Mineral Resources, Geology and Geophysics and Australian Antarctic Division (AAD) expeditioners conducted programs on McDonald Island Group and Heard Island (Table A.1). The expedition recorded the first landing by sea on McDonald Island and the first landing by helicopter on Flat Island. The main goal of the National Mapping program was to carry out topographic surveys of the islands and bathymetric surveys of the surrounding offshore areas (Johnstone, 1981). The Bureau of Mineral Resources, Geology and Geophysics undertook magnetic surveys to define the extent and thickness of any sedimentary basins in order to determine the magnetic anomaly pattern over the deep ocean basins adjacent to the Kerguelen Plateau (Tilbury, 1981). Helicopters were used to complete a four day aerial photographic survey of the entire Heard Island coastline, which in combination with the topographical surveys greatly improved the maps of the island. The Expedition collected rocks, for geochemical strontium (Sr) isotope and potassium-argon (K-Ar) dating (Tilbury, 1981; Quilty and Wheller, 2000), plants (including mosses and lichens), dead birds and bones. They also erected an automatic weather station (AWS) at Atlas Cove and completed the first comprehensive biological and geological surveys of McDonald Island (Johnstone, 1981; Heard Island Visitors logbook).

In January 1983, the *Anaconda II*-based private Heard Island Expedition (Project Blizzard) spent one month on Heard Island attempting to summit Mawson Peak (Hendy, 1983) (Table

A.1). In addition to their successful summit ascent, the members of the expedition collected geological samples of isotopic and petrological data, made volcanic observations (Quilty and Wheller, 2000) and conducted glaciological, meteorological, botanical and zoological studies (Vining, 1983; Hendy, 1983; Heard Island Visitors logbook). They also made radio contact with over 30,000 radio stations around the world from Atlas Cove. While Project Blizzard was on the island another ship the *Cheynes II* (The Heard Island DX Association Expedition) arrived at Atlas Cove for 10 days of biological, geological, and botanical sampling, and whom also made amateur radio contacts to stations around the world. The Heard Island DX Association Expedition also landed four mountaineers on the southern coast for an attempt to climb Mawson Peak, which was unsuccessful due to inclement weather.

The summer of 1985 was the first of three consecutive years of summer research on Heard Island. In September 1985, ANARE landed on Heard Island from the MV *Nella Dan* with the goal of completing an elephant seal census (Table A.1). In addition to the seal survey, the four expeditioners at Spit, and ten expeditioners at Atlas Cove recorded fauna and flora community distribution, engaged in meteorological observations, geophysics, surveying and glaciology (Burton and Williams, 1985). The 1986/87 summer season's initial objective was geological (due to the recent eruption on Big Ben in January of 1985) but this was later expanded to include biological and archaeological studies (Ledingham, 1987b) (Table A.1). Geological mapping was completed of the whole island where access was not too dangerous (Ledingham, 1987b). Vegetation mapping of mosses and succession studies of coastal botany were conducted (Scott, 1987). A resurvey was carried out of the elephant seals that were tagged during the 1985 season. Biological studies also predominated in the study's final summer of 1987/88 with a focus on bird and seal populations, a continuing vegetation survey and the installation of an AWS (Kirkwood et al., 1989) (Table A.1).

In May/June 1990, an ANARE marine science voyage (*R/V Aurora Australis*) stopped by Heard Island, at Atlas Cove and Spit Bay to complete some glaciological, biological, archaeological work and deploy a meteorological buoy ashore (Green, 1990) (Table A.1). The ANARE winter expedition of 1992 was the first wintering party based at Spit Bay. During the 13 months that the five men were stationed at Spit Bay, glaciological, geological, biological, meteorological observations and mapping surveys were accomplished (Green, 1993a,b). In 1997, the Cordell Heard Island Expedition spent a summer attempting to set a radio operating record and also reporting on vegetation distribution (`www.cordell.org/htdocs/HI/`, 20 May 2004) (Table A.1). The *Aurora Australis* visited Heard again in March, 1997 to deploy a tide gauge and AWSs at Spit Bay and Atlas Cove (Table A.1).

At the beginning of 2000, an Australian Army Alpine Association climbing party successfully climbed Mawson Peak from Atlas Cove (Table A.1). The following November to March ANARE conducted glaciological, biological and archaeological studies and an initial clean up of the historical Atlas Cove station (Truffer et al., 2001; Marshall and Chown, 2002; Beggs et al., 2004) (Table A.1). From December 2003 to February 2004, predator-prey surveys were made of fur seals, penguins and albatrosses, in addition to vegetation and glaciological surveys (Clifton, 2004) (Table A.1).

A.3. List of scientific expeditions to Heard Island

Expedition	Year	Date	Ship	Objective	Area	Resident time	Source
	1874		*Arkona*	Explore Heard Island establish station at Iles Kerguelen			(Chown, 2003)
	1874	Feb	HMS *Challenger*	Geological and biological collections	Corinthian Bay	1 day	(Mosley, 1877)
Deutsche Südpolar-Expedition	1902	Feb	Gauss	E. von Drygalski stopped by Heard Island on way to Antarctica from Kerguelen arriving on the 3 February and completing the first comprehensive observations of geology, flora and fauna		1 day	(Drygalski, 1931; Ludecke, 2003; Law and Burnstall, 1953)
	1929	Jan	*Kildalky*	E. Aubert de la Rue, geology of island, first woman to land on island	Atlas Cove	8 days	(Aubert de la Rue, 1929)
BANZARE	1929	Nov	RRS *Discovery*	D. Mawson collected geological and meteorological observations		7 days	(Law and Burnstall, 1953)
ANARE	1947-55		HMSAS *Labuan* and others	Building and continuous occupation of the Atlas Cove station. Provided the most complete record of topography, geology, biology, glaciology, meteorology and geophysics to date.	Atlas Cove	7 years 3 months	(Law and Burnstall, 1953; Shaw, 1955; Dalzeil, 1955)
	1947		Commandant Charcot	Short visit by the French en route to Antarctica.	Atlas Cove		(Chown, 2003)
ANARE	1963	Jan- Feb	MV *Nella Dan*	Five-man summit attempt on Mawson Peak. Geological, biological and meteorological studies undertaken.	Spit Bay, Long Beach, Atlas Cove	6 weeks	(Budd, 1964b,a)

Expedition	Year	Date	Ship	Objective	Area	Resident time	Source
South Indian Ocean Expedition	1965	Jan	*Patanela*	Private expedition. First successful attempt of Mawson Peak. Biological and glaciological investigations. Visited McDonald Island but did not land.	Atlas Cove, Spit Bay, Capsize Beach	1 month	(Headland, 1989)
ANARE	1968	Nov	MV *Nella Dan*	Science	Atlas Cove		(Chown, 2003)
ANARE	1969	Mar	USCG *Southwind*	Recorded changes in glaciers and populations of fur seals and king penguins.	Spit Bay, Atlas Cove	7 days	(Budd, 1970)
US Coast and Geodetic Survey	1969-70		USCG *Southwind*, MV *Nella Dan*, USS *Columbia Hawk*	Wintering expedition established a survey stations as part of the Pageos satellite geodetic programme.	Atlas Cove	13 months	(Headland, 1989; Heard Island Visitors logbook)
French and Australian Expedition	1971		MV *Nella Dan*, MV *Gallieni*	Conducted geophysical and glaciological investigations. Landing made on McDonald Island	Atlas Cove, McDonald Is	6 weeks	(Allison, 1980; Headland, 1989)
–	1972	Jan	Damien	Private yacht	Atlas Cove	3 days	(Heard Island Visitors logbook)
1980 expedition to Heard and McDonald Is.	1980	Mar	MV *Cape Pillar*	First landing of McDonald Is. by sea, first helicopter landing on Flat Is, hydrography survey of Atlas Cove, mapping of the island	McDonald Is., Atlas Cove	16 days	(Johnstone, 1981; Tilbury, 1981; Veenstra and Manning, 1982)
Heard Island Expedition	1983	Jan	*Anaconda II*	Private expedition. Second ascent of Mawson Peak, Ham radio operations at Atlas Cove, first recorded landing on Shag Island, glaciological and biological observations	Atlas Cove, Skua Beach	1 month	(Hendy, 1983; Headland, 1989)
1983 Heard Island DX Association Expedition	1983	Feb	*Cheynes II*	Private expedition. Unsuccessful attempt on Mawson Peak, amateur radio operations and biological collections	Atlas Cove	11 days	(Headland, 1989)

Expedition	Year	Date	Ship	Objective	Area	Resident time	Source
ANARE	1985	Sept	MV *Nella Dan*, MV *Icebird*	Elephant seal census, mapping and distribution of plants, meteorological measurements, and measurements of absolute magnetic values.	Spit Bay, Atlas Cove	8 weeks	(Heard Island Visitors logbook)
ANARE	1986-87	Nov-Jan	MV *Nella Dan*	Geological, biological, glaciological, geophysical and archaeological studies.	Atlas Cove, Spit Bay	10 weeks	(Ledingham, 1987a,b; Scott, 1987)
ANARE	1987	Oct-Mar	MV *Nella Dan*, MV *Icebird*, MV *Lady Franklin*	Emphasis on biological studies.	Spit Bay, Atlas Cove	7 months	(Kirkwood, 1989)
ANARE	1990	May-Jun	RSV *Aurora Australis*	Conducted some glaciological, biological and archaeological work and deployed a meteorological buoy ashore.	Atlas Cove, Spit Bay	1 month	(Green, 1990)
ANARE	1992-93		MV *Icebird*	Wintering expedition. Biological, meteorological and glaciolical work was conducted	Spit Bay	14 months	(Green, 1993a,b)
ANARE	1997	Mar	RSV *Aurora Australis*	Deployment of AWS buoys	Atlas Cove, Spit Bay	1 day	(Heard Island Visitors logbook; Chown, 2003)
ANARE	2000-01	Oct-Mar	MV *Polar Bird*, RSV *Aurora Australis*, FV *Southern Champion*	Biological, glaciological, vegetation and archaeological surveys	Atlas Cove, Spit Bay, Sooty Valley, Brown Glacier	5 months	(Truffer et al., 2001)
ANARE	2003-04	Dec-Feb	*Southern Supporter*	Predator-prey, vegetation and glaciological surveys	Jacka Valley, Spit Bay, Capsize Beach, Sooty Valley, Brown Glacier	2 months	(Clifton, 2004)

A.4. Heard Island glaciers

Ruddell (2006) provides an inventory of all of 32 glacier basins on Heard Island, including three that no longer contain a glacier (non-glacierised basin (NGB)). Ruddell (2006) used the World Glacier Monitoring Service (WGMS) nomenclature to label all of the Heard Island glaciers. The prefix 'AU' refers to Australian territory. The first digit refers to the mountain massif (i. e., 1 for Big Ben and 2 for Laurens Peninsula). The second and third numbers refer to the basin (or glacier) number. The fourth digit refers to the glacier terminus number. The larger glaciers are still referred to by their official name (the majority of which are named after early ANARE expeditioners) rather than a WGMS number, whereas the more recently labelled glaciers are referred to by their WGMS number. There are several glacier basins that have two termini. In the past these has been assumed to be two separate glaciers but Ruddell (2006) shows that these have accumulation areas that are indistinguishable from each other. Examples include the Baudissin and Schmidt glaciers and the Allison and Vahsel glaciers. In these cases the glacier basin should be referred to by the name of the glacier that has the highest elevation in the inventory. But in this study these divergent terminating glaciers are still referred to separately due to the variable nature of their individual termini.

WGMS No.	No.	Glacier name	Orientation		Elevations (m asl)		Length	Area	Volume
			Accum. area	Ablation area	Max.	Min.	(km)	(km^2)	(km^3)
BIG BEN									
AU1011	1	Schmidt	NW	NW	2300	200	7.90		
AU1012		Baudissin	NW	NW	2300	0	8.42	**15.80**	**0.874**
AU1021	2	Nares	NNW	NNW	850	150	2.76	1.80	0.076
AU1032	3	Challenger	N	NNW	2300	0	7.19	7.39	0.372
AU1041	4	Un-named	N	NNW	850	350	1.69	0.40	0.014
AU1051	5	Mary Powell	N	N	1075	65	3.71	2.42	0.106
AU1061	6	Downes	NNE	NNW	2360	0	8.46	**16.66**	**0.928**
AU1062		"	NNE	NNE	2360	0	8.13		
AU1071	7	Ealey	NNE	NNW	2320	0	8.12	**21.37**	**1.228**
AU1072		"	NNE	NE	2320	0	8.03		
AU108	8	NGB	NE	NE					
AU1091	9	Compton	NE	NE	2320	0	6.21	**14.84**	**0.82**
AU1092		"	NE	NE	2320	0	6.79		
AU1093		"	NE	NE	2320	0	2.02		
AU110	10	NGB	ENE	ENE					
AU1111	11	Brown	NE	NE	1250	10	5.54	4.27	0.201
AU1121	12	un-named	ENE	E	1200	150	4.73	3.02	0.136
AU1131	13	Stephenson	E	ENE	2270	0	10.19	**20.41**	**1.166**
AU1132		"	E	SE	2270	0	12.02		
AU1141	14	un-named	SE	SE	1550	5	6.35	6.86	0.342
AU1151	15	Winston	SE	SE	2270	0	8.01	**15.86**	**0.878**
AU1152		"	SE	SE	2270	0	8.08		
AU116	16	NGB	SE	SE					
AU1171	17	Fiftyone	SSE	S	2270	5	9.21	**23.68**	**1.378**

WGMS No.	No.	Glacier name	Orientation		Elevations (m asl)		Length	Area	Volume
			Accum. area	Ablation area	Max.	Min.	(km)	(km^2)	(km^3)
AU1172		un-named	SE	SSW	1100	150	3.77		
AU1181	18	Deacock	S	S	1110	160	2.90	2.77	0.124
AU1191	19	un-named	SW	SSW	1110	290	2.83	1.33	0.054
AU1201	20	Gotley	SW	SW	2750	0	13.20	27.43	1.625
AU1211	21	un-named	SSW	SW	2750	5	7.93	7.51	0.379
AU1221	22	Lied	SW	WSW	2750	0	8.18	15.49	0.855
AU1231	23	Abbotsmith	WSW	WSW	2750	0	8.48	**22.67**	**1.312**
AU1232		"	WSW	W	2750	0	8.44		
AU1241	24	Allison	WNW	WSW	2360	5	8.23		
AU1242		Vahsel	WNW	WNW	2360	5	8.99	**18.39**	**1.037**
		Sub-total for Big Ben						**250.4**	**13.9**
LAURENS PENIN-SULA									
AU201	1	un-named	NE	NE	500	250	1.20	0.71	0.027
AU2021	2	Jacka	NE	NE	500	150	2.24	2.53	0.112
AU2031	3	un-named	N	N	550	300	0.70	**0.18**	0.006
AU2032		un-named	N	NE	550	230	0.94		
AU2041	4	un-named	NE	NE	450	220	0.60	**0.26**	0.008
AU2042		un-named	NE	NE	450	220	0.60		
AU205	5	un-named	S	S	550	250	0.60	0.70	0.026
AU2061	6	un-named	S	S	500	200	1.20	0.86	0.033
AU2071	7	un-named	NE	NE	500	250	0.72	0.51	0.018
AU2081	8	un-named	N	N	500	250	0.97	0.77	0.029
		Sub-total for Lauren's Peninsula						**6.5**	**0.3**
		Total for Heard Island						**256.9**	**14.2**

B. Glacier coverage of the sub-Antarctic islands

B.1. Photographic sequence of the retreat of Heard Island's glaciers

A sequence of several Heard Island glaciers (Jacka, Stephenson and Compton) were compiled to illustrate the changes in the glaciers from the early 1900s to 2004. It should be noted that many of these photographs were taken on an opportunistic basis therefore are not from the same vantage point. Prominent features are highlighted in most sequence to help with orientation and identification of changes in the glacier front or outline.

B.1.1. Compton Glacier

A photographic sequence of the retreat of Compton Glacier (*3*). The yellow outline in each picture shows that change in an exposed rock outcrop that initially was in the accumulation area of the glacier and eventually acted as a topographic barrier around which the two termini of Compton Glacier flowed. Photo credits: 1947-Photo 629 by RAAF, 1971-AAD Photo 21775, 2004 by M. Truffer.

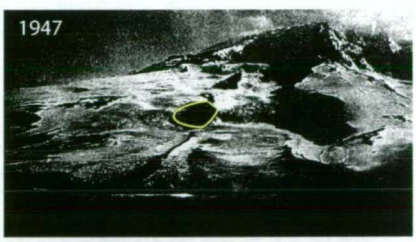

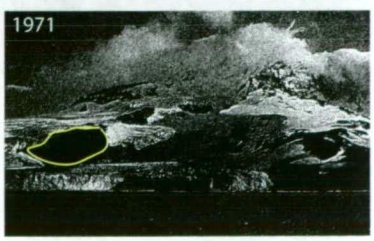

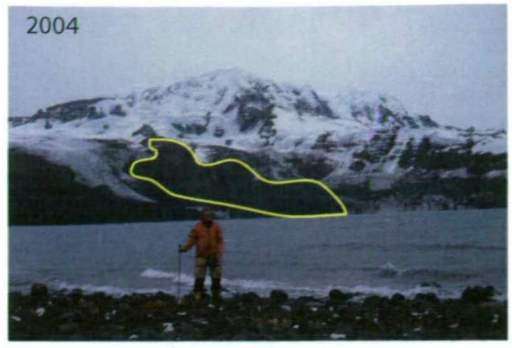

B.1.2. Jacka Glacier

A photo sequence of the retreat of Jacka Glacier (*5*), located on the northeast coast of the Laurens Peninsula, from 1929-2004. These photos show that Jacka Glacier until 1963 reached the the coast. By 1971 the glacier had begun to retreat up the slope. This retreat was observed to continue to 1986 and by 2004 the glacier had retreated back to the ice cap that it had originated from. Photo credits: 1929, de la Rue; 1963, P. Law; 1971, AAD photo collection; 1986, J. Scott; and 2004, S. Donoghue.

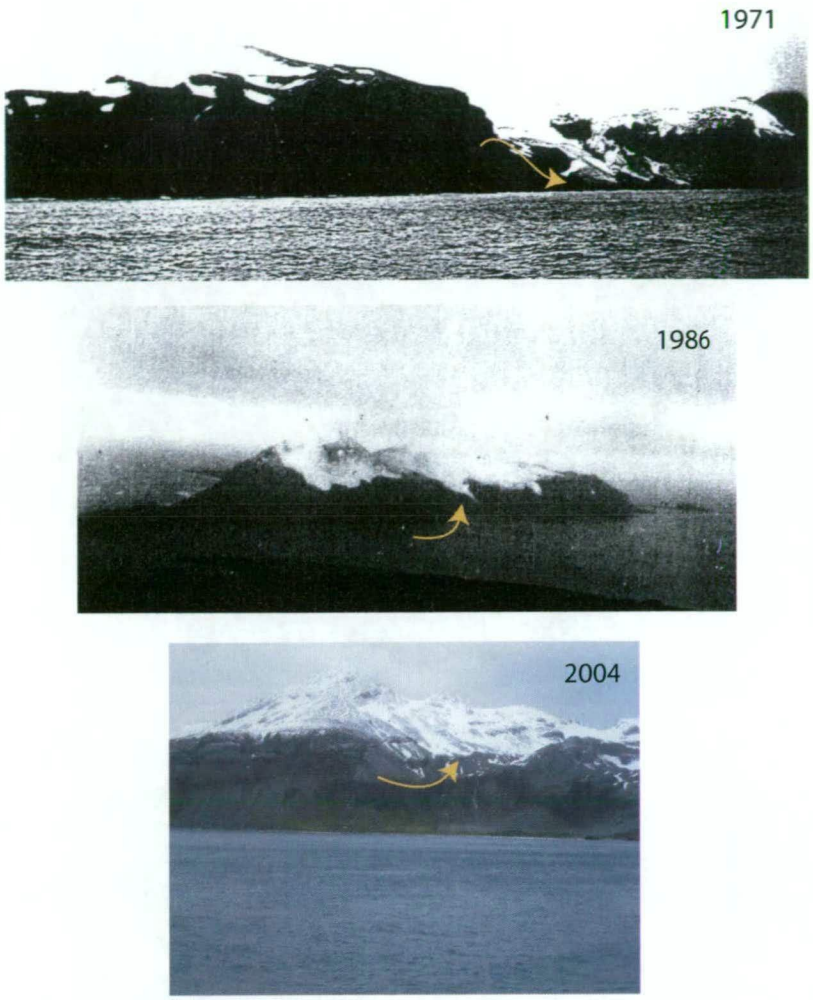

B.1.3. Stephenson Glacier

A photographic sequence of the retreat of Stephenson Glacier from 1947 to 2004 (*6*). The changes in lagoon size are highlighted in yellow. In 1947 both the northern and southern termini reached the sea in ice cliffs. By 1963 a lagoon had begun to form as the northern terminus began to retreat. In 1980 the glacier became more debris covered and retreat continued of the northern and southern (not pictured) termini. In 1986 the glacier had continued to retreat and large ice bergs can be seen in the lagoon. In 2004 the glacier termini had retreated further and the glacier had thinned (2004-A this photo is a better comparison with the 1947 aerial photograph with 'A' marking the same rock outcrop in both images). Now the lagoons are connected by a narrow waterway (2004-B). Photo credits: 1947-Photo 631, RAAF; 1963-ANARE Photo 12594, P.J. Stephenson; 1980-AAD Photo 9495-14; 1986, J. Scott; and 2004A and B, S. Donoghue.

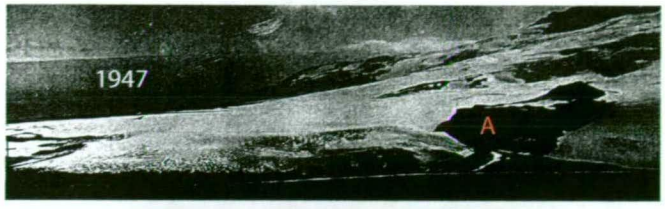
1947
A

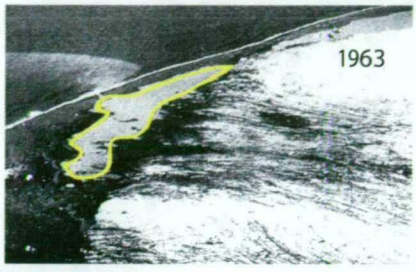
1963


1980

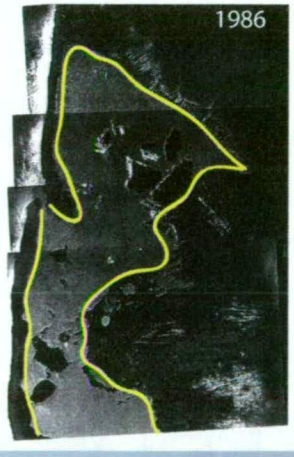
1986

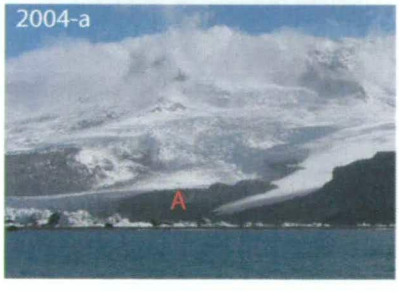
2004-a
A

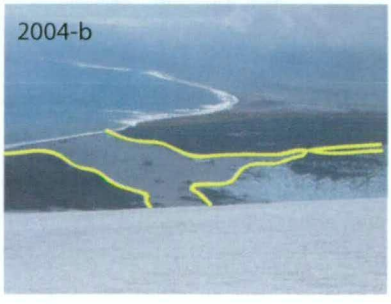
2004-b

B.2. Satellite images of eastern Heard Island

Two satellite images, first is a Digital Globe Multi Spectral (or Quickbird) Image acquired in January 2003 and second is a Digital Globe Multi Spectral (or Quickbird) Image acquired in January 2006 (AAD Data Centre map numbers 13275 and 13029), showing the changes in Brown, Compton, Stephenson and Winston glaciers. The third image highlights the Compton, Brown, Stephenson and Winston glacier's front changes between 2003 and 2006, as determined from a comparison between the two images.

The change in glacer area was calculated by overlaying the two satellite images, then tracing the outline of the terminus in both images, and finally, the number of pixels contained within the outline was converted to metres providing an estimate of the area change in the terminus.

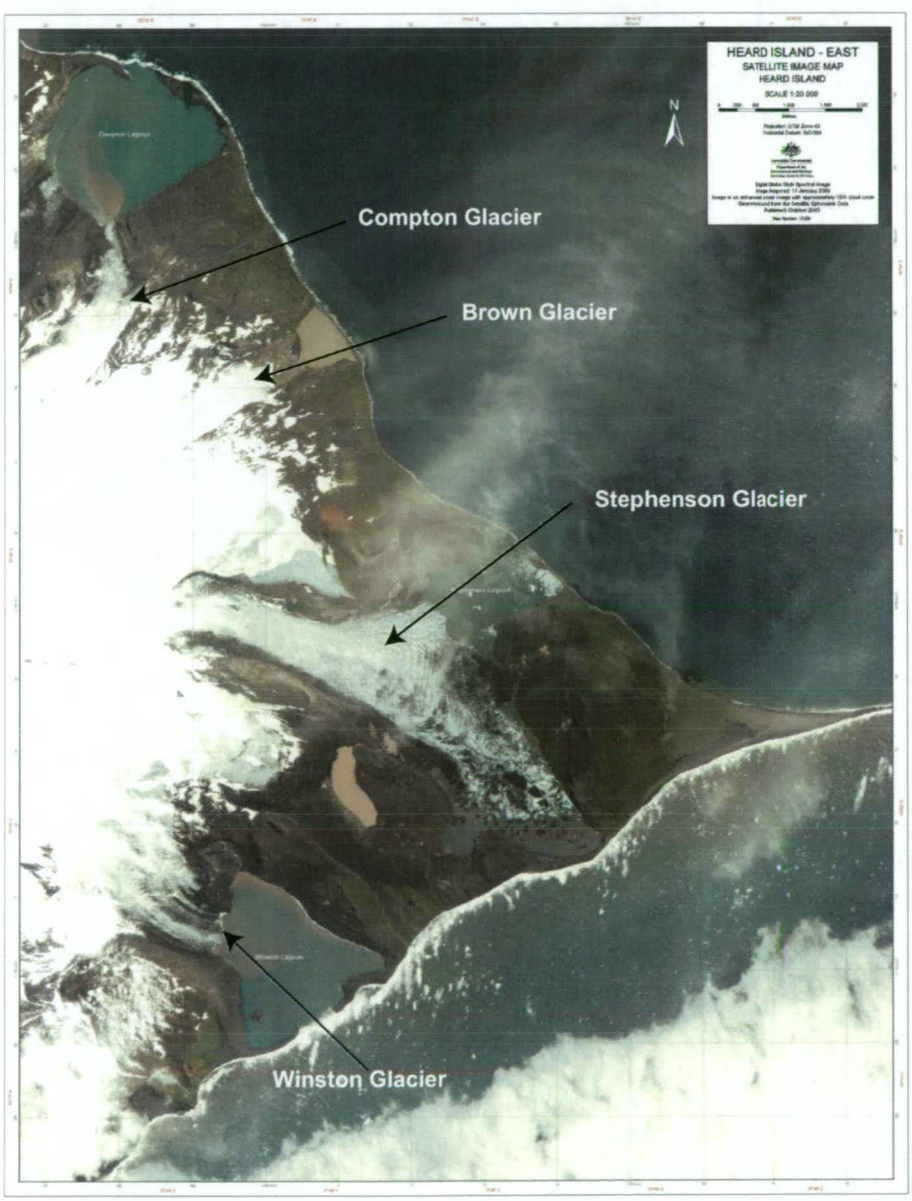

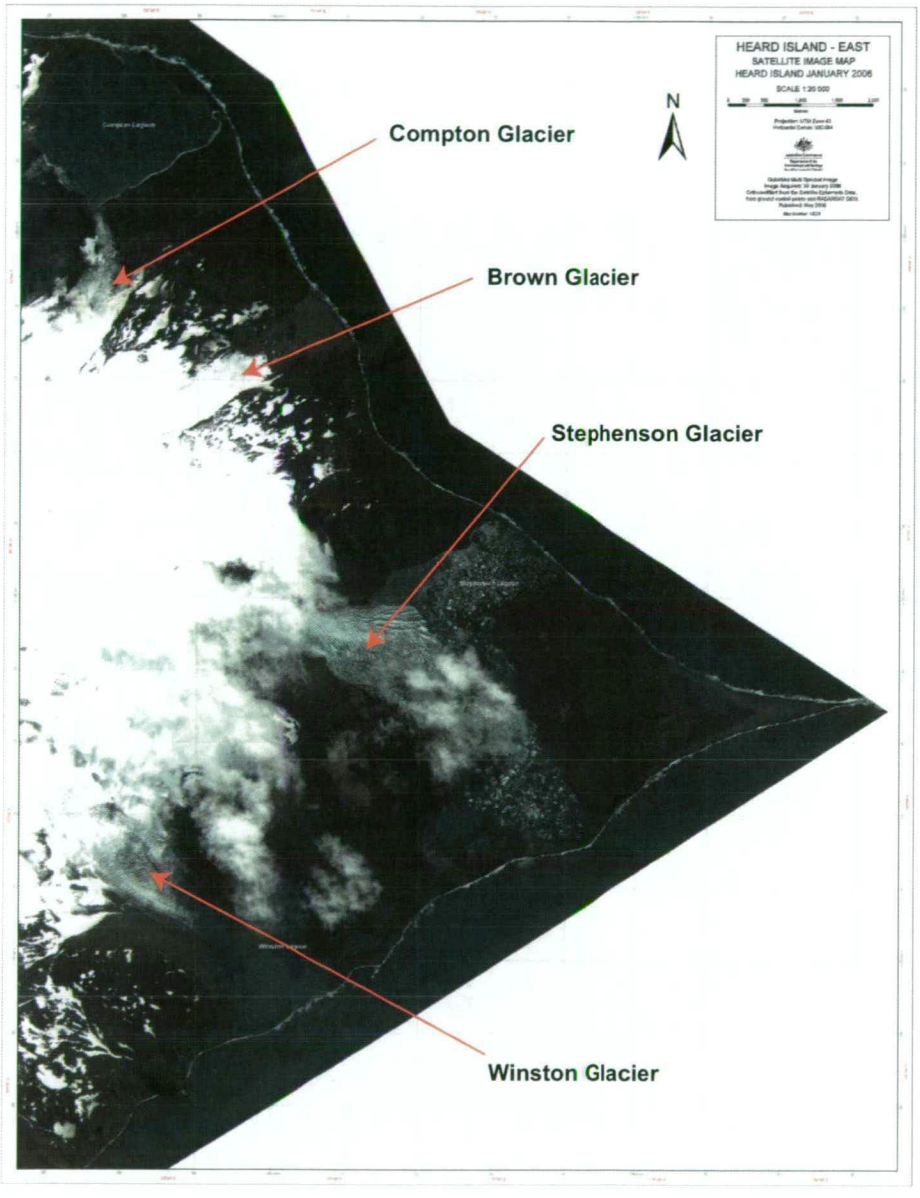
HEARD ISLAND - EAST
SATELLITE IMAGE MAP
HEARD ISLAND JANUARY 2006
SCALE 1:20 000
N
Compton Glacier
Brown Glacier
Stephenson Glacier
Winston Glacier


Compton Lagoon
Compton Glacier
Brown Glacier
Stephenson Lagoon
Stephenson Glacier (northern)
Stephenson Glacier (southern)
Winston Glacier
Winston Lagoon

C. Sub-Antarctic meteorological records

C.1. Marion Island precipitation and temperature records

A digital copy of the monthly temperature and precipitation data for Marion Island is provided on the CD attached to the back cover. Meteorological records were supplied by the South African Weather Service.

C.2. Heard Island meteorological records

A digital copy of all of the meteorological records for Heard Island that are used in this study can be found on the CD attached to the back cover.

C.3. New Amsterdam precipitation and temperature records

A digital copy of the monthly temperature and precipitation data for New Amsterdam Island is provided on the CD attached to the back cover. Meteorological records were supplied by the Antarctic READER website, LEGOS, and Météo-France.

C.4. Crozet Island precipitation and temperature records

A digital copy of the monthly temperature and precipitation data for Crozet Island is provided on the CD attached to the back cover. Meteorological records were supplied by the Antarctic READER website, LEGOS, and Météo-France.

C.5. Kerguelen Island precipitation and temperature records

A digital copy of the monthly temperature and precipitation data for Kerguelen Island is provided on the CD attached to the back cover. Meteorological records were supplied by the Antarctic READER website, LEGOS, Y. Frenot (pers.com.) and Météo-France.

C.6. Location of AWS and coastal meteorological stations

Photographs of the location of the mobile AWSs near Brown Glacier during 2003/04 and the BG AWS (current and following page). Followed by photographs of the setup at the individual 2003/04 field camp temperature and precipitation instruments (next page). Photo credits: AWS1, D. Thost; AWS2 and AWS3 S. Donoghue; Doppler Hill, Jacka Valley and Capsize beach, D. Thost; Brown Hut, S. Donoghue.

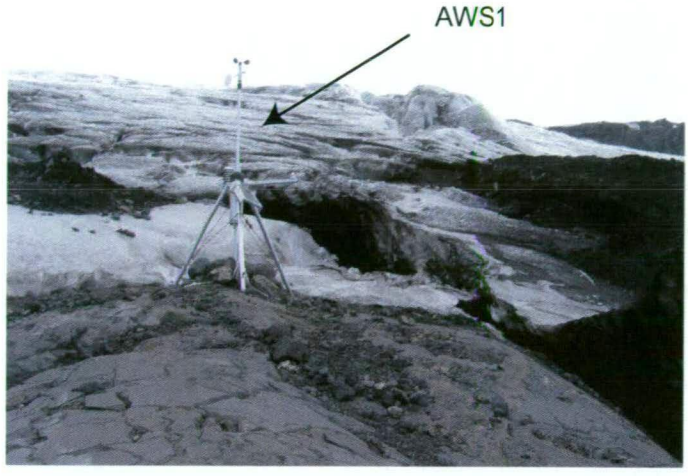

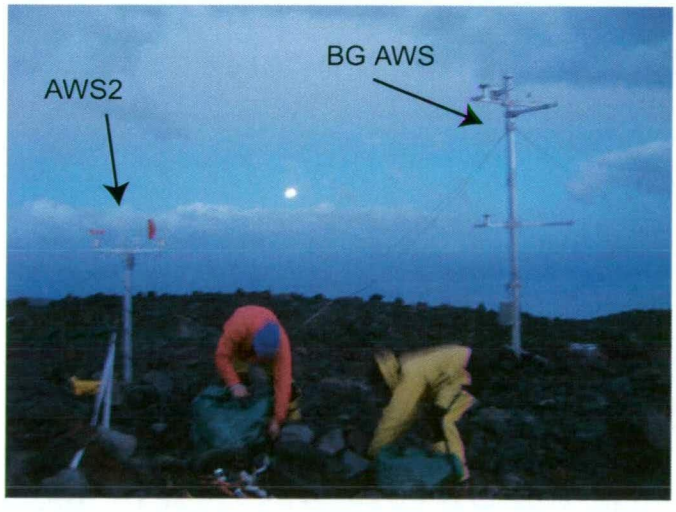

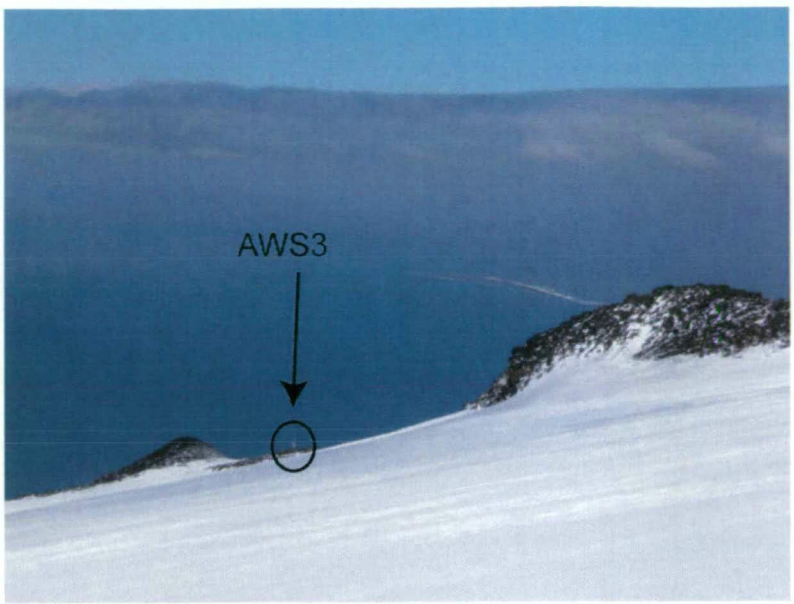
AWS3

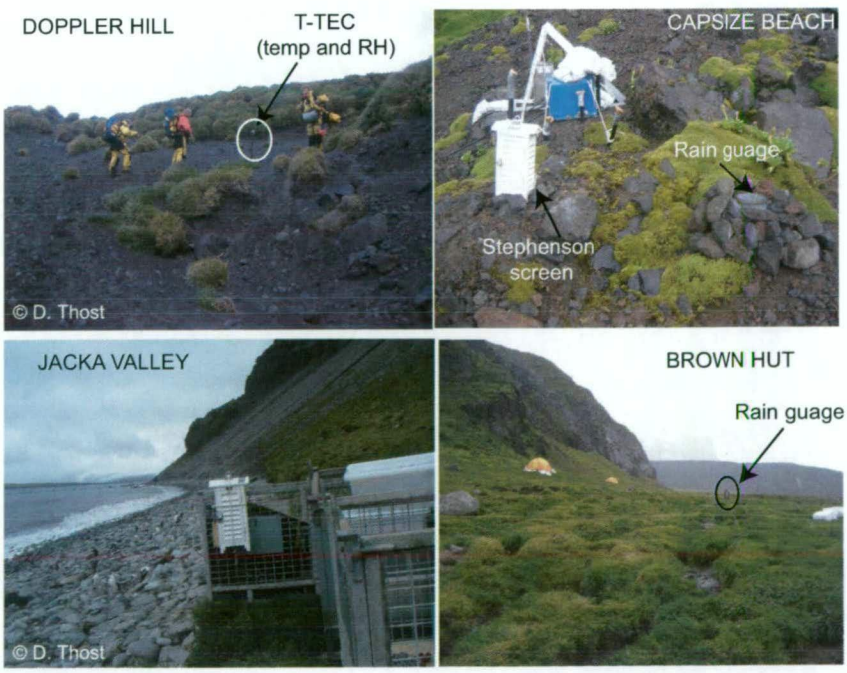
DOPPLER HILL
T-TEC
(temp and RH)
© D. Thost
CAPSIZE BEACH
Rain guage
Stephenson
screen
JACKA VALLEY
© D. Thost
BROWN HUT
Rain guage

D. Morphology, dynamics and mass balance

D.1. Net balance stake measurements

D.1.1. Net balance data for both field seasons

All net balance data is presented in metres. The first two pages are the 2000/01 data. The following three pages are the 2003/04 data (horizontal tables).

Elevation (m asl)	1063	966	867	867	755	678	588	496	412	302	188
Date/ Site	BG05	BG10	BG15	BG15	BG20	BG25	BG30	BG35	BG40	BG45	BG50
23-Oct-00						0	0				
24-Oct-00											
25-Oct-00							0.055	0	0	0	0
26-Oct-00											
27-Oct-00	0	0	0		0	-0.086	-0.025	0.006	-0.058	0	-0.009
28-Oct-00											-0.049
29-Oct-00								0.006			
30-Oct-00								0.001			
31-Oct-00								0.048			
1-Nov-00											
2-Nov-00								0.166			
3-Nov-00			0.375	0.375							
4-Nov-00											
5-Nov-00											
6-Nov-00								0.368			
7-Nov-00								0.226	-0.158	0.275	0.009
8-Nov-00											
9-Nov-00	0.38	0.06	0.3	0.277	-0.055	-0.161	0.065	0.201			
10-Nov-00											
11-Nov-00											
12-Nov-00											
13-Nov-00											
14-Nov-00											
15-Nov-00											
16-Nov-00											

Elevation (m asl)	1063	966	867	867	755	678	588	496	412	302	188
17-Nov-00											
18-Nov-00											
19-Nov-00										0.37	
20-Nov-00		0.395	0.63	0.502	0.225	0.154	0.54	0.526			
21-Nov-00	0.375	0.325		0.452			0.5	0.521	0.152		
22-Nov-00										0.358	0.094
23-Nov-00											
24-Nov-00											
25-Nov-00								0.431			
12-Jan-01	0.15	0.28	0.38	0.182	0.04	-0.071	0.305	0.361	-0.378	-0.87	
Total net balance (m)	**0.905**	**1.06**	**1.685**	**1.788**	**0.21**	**-0.164**	**1.44**	**2.861**	**-0.442**	**0.133**	**0.045**

Date	BG05	BG052	BG101	BG10	BG151	BG15	BG152	BG201	BG20	BG202	BG251	BG252	BG25	BG253	BG254	BG255	BG256	BG257	BG258	BG301	BG30	BG35	BG40	BG45	BG50
Elevation (m asl)	1030	1034	972	955	851	866	871	756	752	779	682	684	673	678	682	703	705	715	715	580	582	492	407	296	179
21-Dec-03																									
22-Dec-03																									
23-Dec-03																				0.03	-0.03	-0.02	-0.03	-0.02	-0.03
24-Dec-03																									
25-Dec-03																									
26-Dec-03		-0.005	0.16																						
27-Dec-03													-0.13		-0.15	0	-0.135								
28-Dec-03																						-0.125	-0.36	-0.19	-0.33
29-Dec-03																									
30-Dec-03																									-0.03
31-Dec-03																									
1-Jan-04																									
2-Jan-04																							-0.19	-0.21	-0.21
3-Jan-04																									
4-Jan-04																									
5-Jan-04																									-0.2
6-Jan-04																									
7-Jan-04																									
8-Jan-04																									
9-Jan-04	-0.665	-0.97	-1.095	-1.04	-1.075	-1.15		-1.15	-1.075				-0.96	-0.69	-1.065	-0.73	-1.105								
10-Jan-04																				-1.11	-1.37	-1.165	-1.195	-0.77	-0.46
11-Jan-04																									
12-Jan-04																									

Date	BG05	BG052	BG101	BG10	BG151	BG15	BG152	BG201	BG20	BG202	BG251	BG252	BG25	BG253	BG254	BG255	BG256	BG257	BG258	BG301	BG30	BG35	BG40	BG45	BG50
13-Jan-04	-0.34	-0.25	-0.3	-0.33	-0.4	-0.37	-0.49	-0.37	-0.33	-0.265			-0.42	-0.035	-0.44	-0.31	-0.41			-0.165	-0.245	-0.175	-0.135	-0.07	
14-Jan-04							-0.04				0	0		-0.02		-0.06								-0.02	
15-Jan-04																									
16-Jan-04																									
17-Jan-04																									
18-Jan-04																									-0.67
19-Jan-04																									
20-Jan-04																				-0.72	-0.965	-0.94	-0.64	-0.61	-0.265
21-Jan-04																									
22-Jan-04																				0.205	0.305	0.085	0.01	0.04	-0.065
23-Jan-04																									
24-Jan-04																									
25-Jan-04							-0.77										-0.67	-0.87	-0.84						
26-Jan-04	-0.56	-0.375	-0.595	-0.72	-0.685	-0.74	-0.005	-0.75	-0.81	-0.68	-0.52	-0.65	-0.783	-0.58	-0.71	-0.59	0.04								-0.42
27-Jan-04																									
28-Jan-04								0.01	0	-0.01	0.08	0.06	0.2	0.03	0.24	0	0.12	0.13							
29-Jan-04																									
30-Jan-04																									
31-Jan-04																						-0.12			
1-Feb-04	0.15	0.033	0.045	-0.01	-0.03	-0.07	0.2		0.01	-0.11			-0.055				-0.07			0.115	0.03				
2-Feb-04																						-0.05	-0.475		
3-Feb-04																									
4-Feb-04																						-0.155			
5-Feb-04																	-0.19								
6-Feb-04																						-0.075	-0.215	-0.6	-0.5

Date	BG05	BG052	BG101	BG10	BG151	BG15	BG152	BG201	BG20	BG202	BG251	BG252	BG25	BG253	BG254	BG255	BG256	BG257	BG258	BG301	BG30	BG35	BG40	BG45	BG50
7-Feb-04																									
8-Feb-04																									
9-Feb-04							-0.435				-0.44	-0.365	-0.465	-0.49	-0.515	-0.53	-0.25	-0.42	-0.455	-0.43	-0.365				-0.11
10-Feb-04																									
11-Feb-04							0.14															-0.01	-0.12	-0.02	
12-Feb-04	-0.065	-0.39	-0.215	-0.165		-0.135	0.055	-0.28	-0.27	0.01							0.26					-0.02	-0.01		
13-Feb-04	-0.01	0.015	-0.015	0		-0.02	-0.03	-0.01	-0.03	-0.025	0.165	0.08	0.195	0.016	0.1	0.2	-0.03	0.11	0.18						-0.14
14-Feb-04																				0.18	0.125	0	0.015		
15-Feb-04																									
16-Feb-04																									
17-Feb-04																									
18-Feb-04																									-0.21
Total net balance (m)	**-1.49**	**-1.94**	**-2.02**	**-2.27**	**-2.19**	**-2.49**	**-1.38**	**-2.55**	**-2.51**	**-1.08**	**-0.72**	**-0.88**	**-2.42**	**-1.77**	**-2.54**	**-2.02**	**-2.44**	**-1.05**	**-1.12**	**-1.90**	**-2.52**	**-2.77**	**-3.35**	**-2.47**	**-3.64**

D.2. Bathymetry Heard Island's lagoons

D.2.1. Stephenson lagoon

Bathymetric survey of Stephenson Lagoon from the several traverse lines that were surveyed then plotted over the 17 January 2003 Digital Globe satellite image.

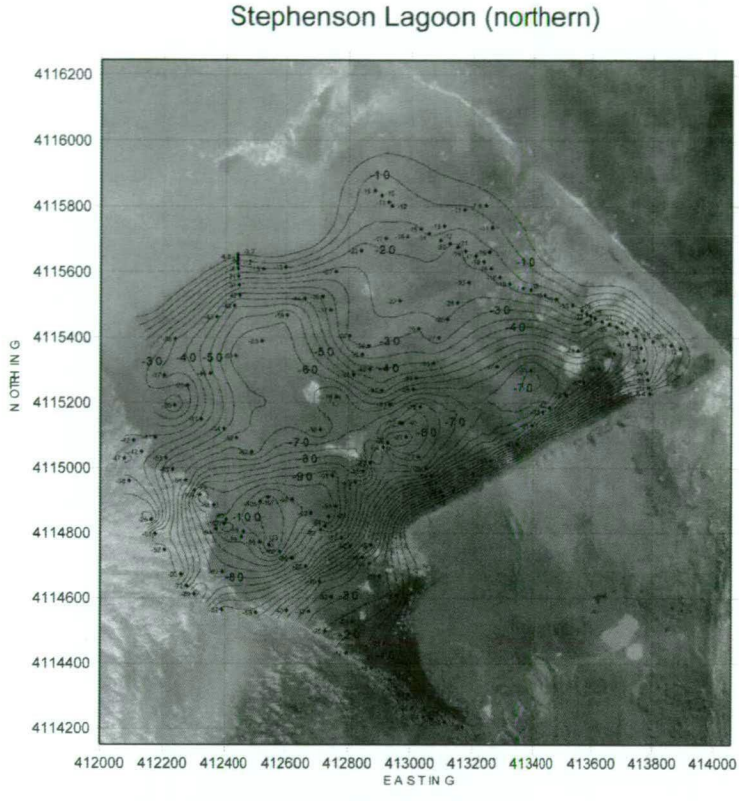

D.2.2. Brown Lagoon

Bathymetric survey of Compton Lagoon from the several traverse lines that were surveyed then plotted over the 17 January 2003 Digital Globe satellite image.

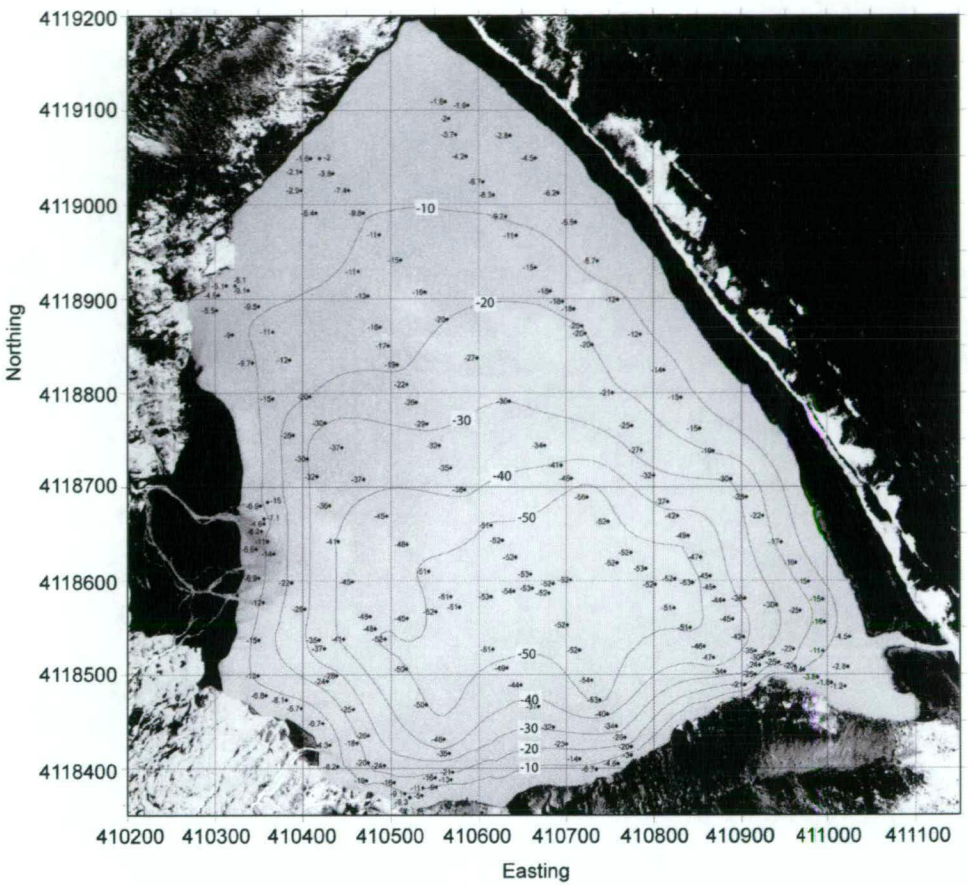

Bathymetric survey 3 Feb 2004 by M. Truffer, S. Donoghue, D. Thost
Depths relative to lagoon surface, which is apprximately 1 m asl.
Positional error: ± 5 m. Depth error: ± 1 m where shallower than -30m;
± 5 m where deeper than -30m.
Horizontal datum WGS84. Map projection UTM Zone 43
Bachground image Quickbird Satellite image acquired 12 Jan 2003

Map compilation by D. Thost, Australian Antarctic Division

D.2.3. Compton lagoon

Bathymetric survey of Compton Lagoon from the several traverse lines that were surveyed then plotted over the 17 January 2003 Digital Globe satellite image.

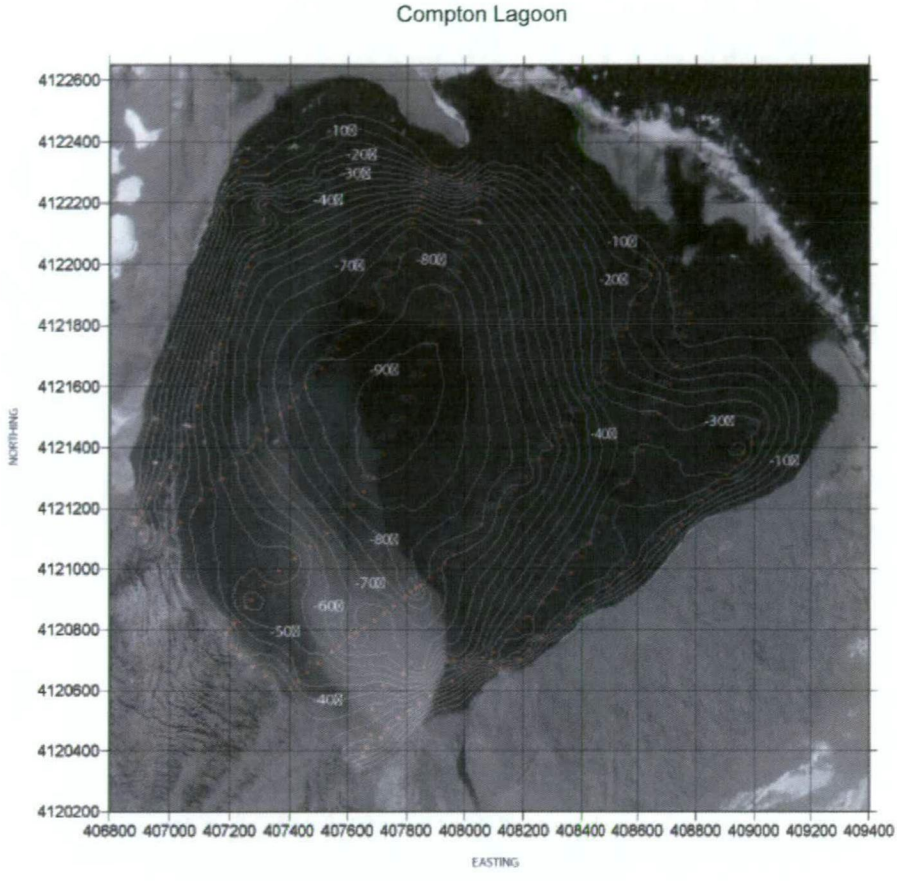

Bathymetric survey 3 Feb, 2004 by M. Truffer, S. Donoghue, C. Stephenson.
Deapths relative to sea level.
Positional error ±5 m. Depth error ±1 m where shallower than -30m;
±5 m where deeper than -30m.
Horizontal datum WGS84. Map projection UTM Zone 43
Map compilation D. Thost

D.2.4. Winston lagoon

Bathymetric survey of Winston Lagoon from the several traverse lines that were surveyed then plotted over the 17 January 2003 Digital Globe satellite image.

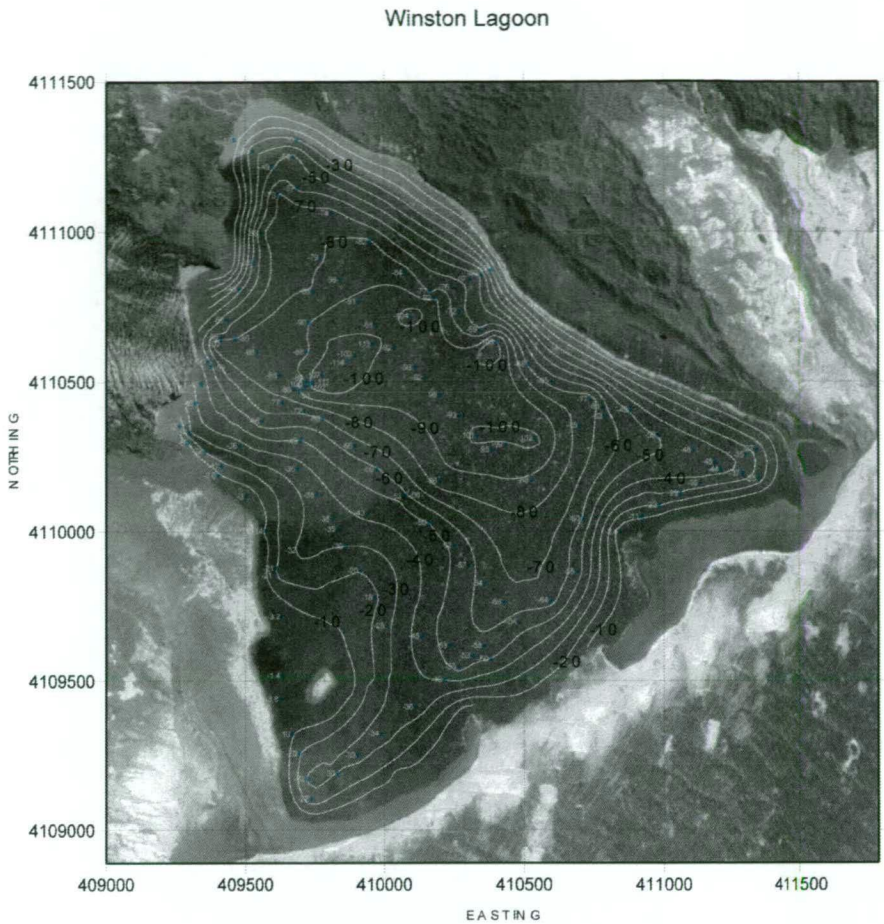

Bathymetric survey 21 Jan. and 15 Feb 2004 by H. Kirkpatrick, R. Clifton, K. Rollings
D. Thost, M. Truffer, S. Donoghue
Depths relative to lagoon surface, which is approximately at sea level.
Positional error ±5 m. Depth error: ±1 m where shallower than -30 m;
±5 m where deper than -30 m.
Horizontal datum WGS84. Map projection UTL Zone 43
Map complied by D. Thost.

E. Isotopes and glaciochemistry

E.1. Isotopes in Precipitation

Isotopes in Precipitation at latitudes south of 30° S. Table from the International Atomic Energy Agency (IAEA), the WMO (2004), and Global Network of Isotope in Precipitation (GNIP) website: `http://isohis.iaea.org`. This site provides further information on data collection and statical analysis. This table is shows the range in δ^{18} O for the southern hemisphere for comparison with the Heard Island δ^{18} O values.

Station	Latitude and Longitude	Elevation (m)	Weighted annual δ^{18} O (‰)	Weighted monthly range in δ^{18} O (‰)
Adelaide, Aus	34.93° S; 138.53° E	43	-4.47	-7.64 to -2.53
Cape Grim, Aus	40.68° S; 144.69° E	90	-4.30	-5.63 to -2.64
Melbourne, Aus	37.82° S; 144.97° E	28	1-5.06	-6.37 to -3.30
Perth, Aus	31.95° S; 115.97° E	17	-3.89	-4.13 to -1.43
Marion Island, South Indian Ocean	46.88° S; 37.87° E	26	-4.84	-5.53 to -3.79
Gough Island	40.35° S; 9.88° W	54	-3.75	-4.18 to -3.16
Invercargill, NZ	46.42° S; 168.32° E	2	-7.16	-7.83 to -6.47
Kaitaia Island	35.07° S; 173.28° E	76	-5.00	-5.91 to -4.12
Buenos Aires, Arg	34.58° S; 58.48° W	24	-4.30	-5.83 to -1.88
Ciudad, Arg	34.38° S; 58.28° W	0	-5.17	-7.58 to -3.35
Conception, Chile	36.46° S; 73.03° W	11	-3.58	-5.93 to -1.89
Cöyhaique, Chile	45.35° S; 72.07° W	310	-11.96	-14.14 to -10.99
Juan Fernandez Islands, Chile	33.62° S; 78.83° W	6	-3.26	-4.28 to -1.10
La Suela, Arg	30.58° S; 64.58° W	900	-5.58	-12.27 to -4.12
Mendoza, Arg	32.88° S; 68.85° W	827	-5.44	-19.70 to -2.73
Nancuna, Arg	34.03° S; 67.97° W	572	-6.54	-14.70 to -2.40
Pôrto Alegre, Brazil	30.08° S; 51.18° W	7	-4.84	-7.02 to -2.53
Puerto Montt, Chile	42.48° S; 65.05° W	100	-7.59	-10.72 to -4.43
Puerto Montt, Chile	41.47° S; 72.93° W	13	-6.28	-7.79 to -4.06
Punta Arenas, Chile	53.00° S; 70.51° W	37	-10.06	-12.71 to -6.44
Santiago, Chile	33.45° S; 70.70° W	520	-9.84	-12.93 to -6.84
Temuco, Chile	38.46° S; 72.38° W	114	-7.41	-8.08 to -5.30
Ushuaia, Arg	54.78° S; 68.28° W	10	-11.02	-12.45 to -9.96

Station	Latitude and Longitude	Elevation (m)	Weighted annual $\delta^{18}O$ (‰)	Weighted monthly range in $\delta^{18}O$ (‰)
Fort Malan, South Africa	33.97° S; 18.60° E	44	-3.58	-4.00 to -1.67
Vernads, Ant	65.25° S; 64.27° W	-	-10.71	-13.13 to -8.72
Rothera, Ant	67.57° S; 68.13° W	5	-13.76	-17.44 to -6.44
Stanley, Falkland Islands	51.70° S; 57.87° W	51	-8.06	-9.74 to -6.30
Halley, Ant	75.50° S; 26.65° W	-	-20.16	-26.44 to -11.67

F. Mass balance modelling

F.1. Degree Day Factors

Published degree day factors for snow and ice in mm d^{-1} $°C^{-1}$.

Site	Latitude	Altitude (m asl)	DDF snow	DDF ice	Dates	References
Northern Europe						
Vestfonna, Spitsbergen	~80° N	310-410		13.8	26 Jun. - 5 Aug. 1958	(Schytt, 1964)
Aletschgletscher, Switz.	46°27' N	2200		11.7	2 Aug. - 27 Aug 1965	(Lang, 1986)
		3366	5.3		3 Aug. - 19 Aug. 1973	(Lang, 1986)
Basin Massa-Blatten, Switz.	46° N	1447-4191	4 to 6	7 to 7.2	Apr. - Oct. 1985	(Schaper et al., 1999)
Alfotbreen, Norway	61°45' N	850-1400	4.5	6.0	1961 - 1990	(Laumann and Reeh, 1993)
Hellstugubreen, Norway	61°34'N	1450-2200	3.5	5.5	1961 - 1990	(Laumann and Reeh, 1993)
Nigardsbreen, Norway	61°41'N	300-2000	4.0	5.5	1961 - 1990	(Laumann and Reeh, 1993)
Storglaciären, Sweden	67°55'N	1550	3.2		5 Jul. - 7 Sept. 1993	(Hock, 1999)
				5.4 to 6.4	5 Aug. 1993 - 4 Sept. 1994	(Hock, 1999)
near Ny-Ålesund, Svalbard	76°N	1250-1370	7.0		1992 - 1996	(Bruland et al., 2001)
Himalaya						
Doriani Glacier	31°45'N	4000	5.9		4 Jun. - 6 Jun. 1995	(Singh and Kumar, 1996)
		4000	5.7	7.4	4 days on 1997-98	(Singh et al., 2000)
Glacier AX010	27°45'N	4956	7.3	8.1	Jun. - Aug. 1978	(Kayastha et al., 2000a)
		5072	8.7	8.8	Jun. - Aug. 1978	(Kayastha et al., 2000a)
		5245	11.6		1 Jun. - 31 Aug. 1978	(Kayastha et al., 2000a)
Khumbu Glacier	28°00'N	5350		16.9	21 May - 1 Jun. 1999	(Kayastha et al., 2000b)
Rakhiot Glacier	35°22'N	3350		6.6	18 Jul. - 6 Aug. 1986	(Kayastha et al., 2000b)
Yala Glacier	28°14'N	5120		9.3	1 Jun. - 31 Jul. 1996	(Kayastha et al., 2003)
		5270		10.1	1 Jun. - 31 Jul. 1996	(Kayastha et al., 2003)

Site	Latitude	Altitude (m asl)	DDF snow	DDF ice	Dates	References
Greenland						
Qamanâraaûp	64°28'N	790		8.4 to 7.1	1980 - 1986 summers	(Braithwaite and Olesen, 1989)
		790		8.2	512 days (1980 - 86)	(Braithwaite, 1995)
Nordboglacier	61°28'N	880		7.5	415 days (1979 - 83)	(Braithwaite, 1995)
Sermilik Glacier	60°55'N	520 - 1015		3.5 to 9.5	Jan. 1961 - Dec 2002	(Podlech et al., 2004)
Greenland Ice Margin Project	67°06'N	341		8.7	10 Jun. - 31 Jul. 1991	(Van de Wal, 1992)
		519		9.2	15 Jun. - 6 Aug. 1991	(Van de Wal, 1992)
	67°04'N	1028		20.0	15 Jun. - 6 Aug. 1991	(Van de Wal, 1992)
New Zealand						
Tasman Glacier	44°S	960		1.8 to 6.5	26 Sept. 1985 - 13 Sept. 1986	(Kirkbride, 1995)
	44°S	960		2.4 to 7.4	13 Sept. 1986 - 9 May 1987	(Kirkbride, 1995)
	44°S	1360		2.8 to 5.6	11 Nov. 1985 - 14 Sept. 1986	(Kirkbride, 1995)
	44°S	1360		1.8 to 6.3	14 Sept. 1986 - 8 May 1987	(Kirkbride, 1995)
sub-Antarctic						
Vahsel Glacier, Heard Is.		200	16.6 to 10.7	4 Feb. - 28 Feb. 1971	this study	

F.2. Solid Precipitation factors (ψ) variables

Variable	value
a	0.932042026
b	-0.02944942
c	-0.031293831
d	-0.01657173
e	0.00047051
f	0.001237987
g	-0.0000315007
h	-0.0000332135
i	0.00000269469

F.3. Percent solid precipitation for each interval

F.3.1. Percent solid precipitation

Elevation (m)	1950 annual mean		Elevation (m)	2001 annual mean	2090 annual mean
1100	98%		1100	97%	73%
1010	98%		1040	97%	70%
950	98%		960	97%	67%
900	98%		900	96%	65%
850	97%		840	96%	63%
800	97%		800	96%	62%
750	97%		740	95%	60%
710	97%		700	94%	58%
670	97%		660	94%	57%
620	97%		610	93%	54%
580	96%		570	93%	54%
540	96%		530	90%	50%
500	95%		480	87%	47%
460	93%		440	83%	43%
420	91%		400	79%	38%
380	88%		330	72%	33%
330	84%		280	67%	26%
260	77%		200	59%	18%
205	71%		110	52%	11%
170	67%		80	50%	10%
140	64%				
105	61%				
65	57%				
0	52%				

F.4. Mass balance summary

F.4.1. 2001 mass balance

Elevation (m)	b_a (m a^{-1} w e)	b_c (m a^{-1} w e)	b_c (m a^{-1} w e) (snow)	b_n (m a^{-1} w e)
1100	-1.62	3.70	3.60	2.08
1040	-1.76	3.66	3.56	1.90
960	-1.97	3.60	3.49	1.64
900	-2.14	3.56	3.44	1.42
840	-2.32	3.52	3.38	1.20
800	-2.46	3.49	3.34	1.03
740	-2.67	3.45	3.27	0.78
700	-2.82	3.42	3.23	0.60
660	-2.99	3.39	3.18	0.41
610	-3.20	3.36	3.12	0.16
570	-3.39	3.33	3.09	-0.06
530	-3.72	3.30	2.99	-0.42
480	-4.38	3.27	2.83	-1.12
440	-4.99	3.24	2.69	-1.75
400	-5.66	3.21	2.54	-2.45
330	-6.99	3.16	2.27	-3.83
280	-8.06	3.13	2.08	-4.94
200	-10.00	3.07	1.81	-6.93
110	-12.43	3.01	1.56	-9.42
80	-13.31	2.99	1.48	-10.32

F.4.2. 1950 steady state mass balance

Elevation (m)	b_a (m a^{-1} w e)	b_c (m a^{-1} w e)	b_c (m a^{-1} w e) (snow)	b_n (m a^{-1} w e)
1100	-1.15	4.57	4.48	3.34
1010	-1.29	4.51	4.41	3.12
950	-1.40	4.47	4.36	2.96
900	-1.49	4.43	4.32	2.83
850	-1.60	4.40	4.28	2.69
800	-1.71	4.36	4.25	2.54
750	-1.82	4.33	4.21	2.39
710	-1.92	4.30	4.17	2.26
670	-2.02	4.27	4.14	2.12
620	-2.15	4.23	4.09	1.94
580	-2.26	4.21	4.05	1.79
540	-2.43	4.18	4.01	1.58
500	-2.77	4.15	3.93	1.17
460	-3.15	4.12	3.84	0.69
420	-3.59	4.09	3.72	0.13
380	-4.08	4.07	3.58	-0.50
330	-4.77	4.03	3.38	-1.40
260	-5.91	3.98	3.06	-2.85
205	-6.93	3.94	2.80	-4.13
170	-7.63	3.92	2.64	-5.00
140	-8.27	3.90	2.51	-5.77
105	-9.07	3.87	2.36	-6.71
65	-10.01	3.85	2.21	-7.80

F.4.3. 2090 mass balance

The 2090 mass balance predicted by the IPCC B1 scenario.

Elevation (m)	b_a (m a^{-1} w e)	b_c (m a^{-1} w e)	b_c (m a^{-1} w e) (snow)	b_n (m a^{-1} w e)
1100	-3.28	3.57	3.23	-0.04
1040	-3.55	3.53	3.14	-0.41
960	-3.94	3.47	3.01	-0.93
900	-4.25	3.43	2.90	-1.35
840	-4.60	3.39	2.80	-1.80
800	-4.83	3.36	2.73	-2.11
740	-5.21	3.32	2.62	-2.60
700	-5.48	3.29	2.54	-2.94
660	-5.75	3.26	2.47	-3.28
610	-6.11	3.23	2.38	-3.73
570	-6.40	3.20	2.31	-4.10
530	-6.94	3.17	2.20	-4.74
480	-7.95	3.14	2.01	-5.94
440	-8.84	3.11	1.88	-6.96
400	-9.76	3.08	1.75	-8.01
330	-11.49	3.03	1.56	-9.93
280	-12.82	3.00	1.43	-11.39
200	-15.12	2.94	1.19	-13.92
110	-17.95	2.88	0.88	-17.07
80	-18.93	2.86	0.77	-18.15

The 2090 mass balance predicted by the IPCC A2 scenario.

Elevation (m)	b_a (m a^{-1} w e)	b_c (m a^{-1} w e)	b_c (m a^{-1} w e) (snow)	b_n (m a^{-1} w e)
1100	-5.89	3.57	2.60	-3.29
1040	-6.32	3.53	2.46	-3.86
960	-6.93	3.47	2.31	-4.62
900	-7.41	3.43	2.22	-5.19
840	-7.92	3.39	2.15	-5.77
800	-8.27	3.36	2.08	-6.20
740	-8.81	3.32	2.00	-6.81
700	-9.18	3.29	1.92	-7.26
660	-9.55	3.26	1.85	-7.70
610	-10.04	3.23	1.76	-8.28
570	-10.44	3.20	1.71	-8.72
530	-11.14	3.17	1.58	-9.56
480	-12.43	3.14	1.47	-10.96
440	-13.52	3.11	1.35	-12.17
400	-14.67	3.08	1.17	-13.50
330	-16.79	3.03	1.00	-15.79
280	-18.37	3.00	0.78	-17.59
200	-21.00	2.94	0.53	-20.47
110	-24.13	2.88	0.31	-23.82
80	-25.21	2.86	0.27	-24.94

F.5. Brown Glacier grid point area and width

F.5.1. The model area and width for the 1950 interval

Length (km)	Grid elevation (m)	Area (m^2)	Secondary grid elevation (m)	Width (m)
0	1100	73915.77559		
0.25	1010	244624.7664	1050	920
0.5	950	259420.7432	980	1140
0.75	900	281588.5891	925	1280
1	850	346890.1022	875	1360
1.25	800	340918.7363	528	1380
1.5	750	331009.9494	775	1380
1.75	710	280927.3289	730	1500
2	670	290290.5004	690	1520
2.25	620	339986.426	645	1540
2.5	580	250707.8868	600	1500
2.75	540	269375.6607	560	1400
3	500	265612.9808	520	1140
3.25	460	266279.1669	480	1040
3.5	420	177938.1117	440	940
3.75	380	185627.9365	400	880
4	330	203650.0718	355	860
4.25	260	207065.7974	295	900
4.5	205	223475.0357	235	920
4.75	170	193557.0249	190	960
5	140	199272.4839	155	920
5.25	105	185298.5281	122	920
5.5	65	221915.9126	95	960
5.75	0	200140.2061	32	1100

F.5.2. The model grid points, area and width for the 2001 and 2090 intervals

The model grid points, area and width for the 2001 interval and grid points for the 2090 interval.

Length (km)	Grid elevation (m)	Area (m^2)	Secondary grid elevation (m)	Width (m)
0	1100	188169		
0.25	1040	215361	1070	860
0.5	960	398864	1000	1080
0.75	900	372453	930	1260
1	840	533066	870	1140
1.25	800	314773	820	1360
1.5	740	440383	770	1380
1.75	700	319010	720	1460
2	660	333928	680	1480
2.25	610	372062	635	1540
2.5	570	299990	590	1460
2.75	530	328152	550	1520
3	480	395105	505	1000
3.25	440	319125	460	940
3.5	400	262541	420	840
3.75	330	142873	365	520
4	280	95352	305	540
4.25	200	125333	240	540
4.5	110	127585	155	380
4.75	80	9795	95	100

F.6. Dynamics summary

F.6.1. 2001 dynamics

The cumulative mass flux, S_1, k_2, ice thickness and total velocity values for the 2001 Brown Glacier. The values in italics are estimates based on field measurements and model results.

Elevation (m)	Q_b ($m^3\,a^{-1}$)	Q_b ice ($m^3\,a^{-1}$)	S_1	k_2	Ice thickness (m)	Total velocity ($m\,d^{-1}$)
1100	373678	415197	*0.6*	0	*50*	0.00
1040	760645	845160	0.82	0	76	0.07
960	1366902	1518779	0.85	0	79	0.10
900	1850397	2055995	0.85	100	87	0.10
840	2413618	2681796	0.82	100	102	0.13
800	2691135	2990146	0.84	100	105	0.12
740	2956037	3284482	0.83	100	115	0.12
700	3085225	3428024	0.84	100	110	0.12
660	3150853	3500944	0.84	500	114	0.12
610	3120775	3467524	0.85	1000	106	0.12
570	3031568	3368406	0.85	1000	103	0.13
530	2789644	3099602	0.87	1500	94	0.12
480	2176857	2418727	0.88	1500	*80*	0.11
440	1444921	1605466	*0.8*	1750	*75*	0.14
400	627462	697179	*0.8*	2000	*80*	0.16
330	-46491	-51656	*0.8*	1500	*75*	0.17
280	-616619	-685131	*0.8*	1000	*80*	0.19
200	-1642587	-1825095	*0.8*	1000	*80*	0.14
110	-3029980	-3366641	*0.8*	1000	*60*	0.15
80	-3145875	-3495413	*0.6*	500	*20*	0.11

F.6.2. 1950 dynamics

The cumulative mass flux, S_1, k_2, ice thickness and total velocity values for the 1950 Brown Glacier. The values in italics are estimates based on field measurements and model results.

Elevation (m)	Q_b ($m^3 a^{-1}$)	Q_b ice ($m^3 a^{-1}$)	S_1	k_2	Ice thickness (m)	Total velocity ($m d^{-1}$)
1100	246512	273902	*0.60*	0	*50*	0.00
1010	1008609	1120676	0.84	250	70	0.10
950	1776720	1974132	0.84	500	89	0.11
900	2573382	2859311	0.84	500	98	0.13
850	3505933	3895477	0.84	1000	103	0.16
800	4371557	4857281	0.83	1000	114	0.17
750	5161280	5734749	0.82	1000	125	0.19
710	5794806	6438667	0.83	1500	121	0.20
670	6409546	7121711	0.83	2000	126	0.21
620	7069065	7854509	0.83	2500	126	0.23
580	7517901	8353215	0.83	3000	127	0.24
540	7943390	8825980	0.81	4000	136	0.26
500	8252840	9169813	0.75	5000	150	0.30
460	8436481	9373859	0.73	6000	156	0.32
420	8459875.	9399852	0.70	6000	158	0.35
380	8367282	9296971	0.71	6000	141	0.42
330	8083101	8981214	0.72	5000	137	0.43
260	7492800	8325325	0.73	4000	136	0.38
205	6570395	7300432	0.76	2000	115	0.39
170	5603498	6226103	0.77	1000	114	0.32
140	4454267	4949181	0.73	100	135	0.22
105	3211412	3568233	0.72	100	60	0.01
65	1479410	1643787	0.74	100	40	0.01
0	-454055	-504505	*0.70*	100	*20*	0.01